



**HELLENIC REPUBLIC**  
**UNIVERSITY OF IOANNINA**  
**SCHOOL OF ENGINEERING**  
**DEPARTMENT OF MATERIALS SCIENCE AND ENGINEERING**

“Study of structural behavior and damage mechanisms appearing in composite materials with the use of numerical simulations”

**Eleftherios Tsivolas**

Civil Engineer, MSc

**Thesis for the degree of Doctor of Philosophy**

**Ioannina-Greece, 2022**







**ΕΛΛΗΝΙΚΗ ΔΗΜΟΚΡΑΤΙΑ  
ΠΑΝΕΠΙΣΤΗΜΙΟ ΙΩΑΝΝΙΝΩΝ  
ΠΟΛΥΤΕΧΝΙΚΗ ΣΧΟΛΗ  
ΤΜΗΜΑ ΜΗΧΑΝΙΚΩΝ ΕΠΙΣΤΗΜΗΣ ΥΛΙΚΩΝ**

«Μελέτη δομικής συμπεριφοράς και μηχανισμών αστοχίας σύνθετων υλικών με χρήση αριθμητικών προσομοιώσεων»

**Ελευθέριος Τσιβόλας**  
Πολιτικός Μηχανικός, ΜΔΕ

**Διδακτορική Διατριβή**

**Ιωάννινα-Ελλάδα, 2022**



**«The acceptance of Doctoral Dissertation from the Department of Materials Science and Engineering of University of Ioannina, Greece, does not imply the acceptance of the author's opinion». (Law 5343/1932, article 202)**



*«Η έγκριση της διδακτορικής διατριβής από το Τμήμα Μηχανικών Επιστήμης Υλικών της Πολυτεχνικής Σχολής του Πανεπιστημίου Ιωαννίνων δεν υποδηλώνει αποδοχή των γνώμων του συγγραφέα Ν. 5343/32, άρθρο 202, παράγραφος 2».*



**Application date of MSc Eleftherios Tsivolas:** 29/01/2019

**Appointment date for the three-membered advisory committee:** 27/02/2019

**Members of the three-membered advisory committee:**

Supervisor:

**Leonidas N. Gergidis**, Associate Professor at the Dept. of Materials Science and Engineering, School of Engineering, University of Ioannina

Members:

**Alkiviadis S. Paipetis**, Professor at the Dept. of Materials Science and Engineering, School of Engineering, University of Ioannina

**Antonios Charalambopoulos**, Professor at the School of Applied Mathematical and Physical Sciences, National Technical University of Athens

**Subject appointment date:** 27/02/2019

“Study of structural behavior and damage mechanisms appearing in composite materials with the use of numerical simulations”

**Appointment date for the seven-membered committee:** 09.11.2022

1. **Leonidas N. Gergidis**, Associate Professor at the Dept. of Materials Science and Engineering, School of Engineering, University of Ioannina
2. **Alkiviadis S. Paipetis**, Professor at the Dept. of Materials Science and Engineering, School of Engineering, University of Ioannina
3. **Antonios Charalambopoulos**, Professor at the School of Applied Mathematical and Physical Sciences, National Technical University of Athens
4. **Dimitrios I. Fotiadis**, Professor at the Dept. of Materials Science and Engineering, School of Engineering, University of Ioannina
5. **Theodoros Matikas**, Professor at the Dept. of Materials Science and Engineering, School of Engineering, University of Ioannina
6. **Nektaria-Marianthi Barkoula**, Professor at the Dept. of Materials Science and Engineering, School of Engineering, University of Ioannina
7. **Christina Lekka**, Associate Professor at the Dept. of Materials Science and Engineering, School of Engineering, University of Ioannina

**The Head of the Department**

**The Secretary of the Department**

**Apostolos Avgeropoulos**  
Professor

**Maria Kontou**



Ημερομηνία αίτησης του κ. Ελευθερίου Τσιβόλα: 29/1/2019

Ημερομηνία ορισμού Τριμελούς Συμβουλευτικής Επιτροπής: 27/2/2019

Μέλη Τριμελούς Συμβουλευτικής Επιτροπής:

Επιβλέπων

**Λεωνίδας Γεργίδης**, Αναπληρωτής Καθηγητής του Τμήματος Μηχανικών Επιστήμης Υλικών της Πολυτεχνικής Σχολής του Πανεπιστημίου Ιωαννίνων

Μέλη

**Αλκιβιάδης Παϊπέτης**, Καθηγητής του Τμήματος Μηχανικών Επιστήμης Υλικών της Πολυτεχνικής Σχολής του Πανεπιστημίου Ιωαννίνων,

**Αντώνιος Χαραλαμπόπουλος**, Καθηγητής της Σχολής Εφαρμοσμένων Μαθηματικών και Φυσικών Επιστημών (Σ.Ε.Μ.Φ.Ε.) του Ε.Μ.Π.

Ημερομηνία ορισμού θέματος: 27/2/2019

Μελέτη δομικής συμπεριφοράς και μηχανισμών αστοχίας σύνθετων υλικών με χρήση αριθμητικών προσομοιώσεων

ΔΙΟΡΙΣΜΟΣ ΕΠΤΑΜΕΛΟΥΣ ΕΞΕΤΑΣΤΙΚΗΣ ΕΠΙΤΡΟΠΗΣ : 9/11/2022

1. **Λεωνίδας Γεργίδης**, Αναπληρωτής Καθηγητής του Τμήματος Μηχανικών Επιστήμης Υλικών της Πολυτεχνικής Σχολής του Πανεπιστημίου Ιωαννίνων,
2. **Αλκιβιάδης Παϊπέτης**, Καθηγητής του Τμήματος Μηχανικών Επιστήμης Υλικών της Πολυτεχνικής Σχολής του Πανεπιστημίου Ιωαννίνων,
3. **Αντώνιος Χαραλαμπόπουλος**, Καθηγητής της Σχολής Εφαρμοσμένων Μαθηματικών και Φυσικών Επιστημών (Σ.Ε.Μ.Φ.Ε.) του Ε.Μ.Π.,
4. **Δημήτριος Φωτιάδης**, Καθηγητής του Τμήματος Μηχανικών Επιστήμης Υλικών της Πολυτεχνικής Σχολής του Πανεπιστημίου Ιωαννίνων,
5. **Νεκταρία-Μαριάνθη Μπάρκουλα**, Καθηγήτρια του Τμήματος Μηχανικών Επιστήμης Υλικών της Πολυτεχνικής Σχολής του Πανεπιστημίου Ιωαννίνων,
6. **Θεόδωρος Ματίκας**, Καθηγητής του Τμήματος Μηχανικών Επιστήμης Υλικών της Πολυτεχνικής Σχολής του Πανεπιστημίου Ιωαννίνων,
7. **Χριστίνα Λέκκα**, Αναπληρώτρια Καθηγήτρια του Τμήματος Μηχανικών Επιστήμης Υλικών της Πολυτεχνικής Σχολής του Πανεπιστημίου Ιωαννίνων.

Έγκριση Διδακτορικής Διατριβής με βαθμό «**ΑΡΙΣΤΑ**» στις 8/12/2022

Ο Πρόεδρος του Τμήματος



**Απόστολος Αυγερόπουλος**  
Καθηγητής



Η Γραμματέας του Τμήματος



**Μαρία Κόντου**

## **Abstract**

Over the years, the design of sophisticated structural materials has become an important engineering task. The development of composite materials partially solves this growing need because their behavior is tailor made for the desired application. For that reason, efforts in materials science and engineering has been focused in the design and manufacturing of new materials by changing their composition at multiple scales. This need for new materials has lead to the development of the continuum micromechanics field, which is a subdomain of the mechanics of solids. This field introduces new concepts for the prediction of the macroscopic properties of a composite material knowing the properties of its individual constituents. Concepts like Representative Volume Element (RVE), micromechanics and mean-field material homogenization are vital for the separation of scales in the process of material characterization.

Furthermore, the rapid increase of computer power is followed by the increasing need for simulation of complicated systems and materials. The study of heterogeneous materials necessitates a detailed description of the microstructure to accurately capture changes in micro or nano scales. The increase of computational memory and processor speed has not only permitted the simulation of large structures but also to perform analyses in multiple scales in order to predict complex material behaviors.

This work focuses on the numerical simulation of structures consisted by heterogeneous materials, and in the prediction of progressive damage and failure under mechanical loading using multiscale methodologies. Special attention was given in the comprehension and implementation of the state of the art homogenization methods, prior to their modification in order to capture more complex phenomena. In the context of this research, several methods have been developed to predict the structural response in both macro and micro scales and all these methods are integrated under an inhouse multidisciplinary software for multiscale analysis.

Mean-field homogenization strategies, which are widely used in this thesis, provide an efficient way to simulate the behavior of non homogeneous materials. In this category be-

long several homogenization solutions with varying accuracy and complexity. Generally, they are analytical or semi analytical solutions of the boundary value problem defined in the microstructure of the heterogeneous material and can be very accurate in predicting the mean response of the RVE. The most of the aforementioned homogenization strategies are based on Eshelby's single inclusion solution, and initially designed for the prediction of the elastic behavior of composites. Some approaches extend their applicability to non-linear regimes such as elasto-plasticity and rate dependent plasticity. Since these methods are semianalytical, the comparison with finite element approaches allows not only the validation of such methods, but also assists the discovery of limitations that can be overcome by future research and development.

In this thesis the theoretical aspects and concepts of mechanics of composite materials along with their novel numerical simulation campaigns are presented. In the first chapter, the state of the art of the multiscale methods is presented. In the second chapter, a comparison between numerical and mean-field homogenization methods is conducted regarding linear isotropic, transversely isotropic and orthotropic composite materials to understand the impact of the assumptions and simplifications that are made in the mean-field methods. In the sequel, this comparison is extended for nonlinear composite materials. In the third chapter, the aim is to predict the transverse cracking of a cross-ply composite material loaded in uniaxial tension. The properties of each ply were predicted by performing visco-elastic mean-field homogenization using a modified Mori-Tanaka homogenization scheme. The transverse cracking was predicted using the cohesive zone modelling technique. Finally, a cross ply microstructure was generated for the simulation of the cracking propagation in microscale with the eXtended Finite Element Method (XFEM) and the correlation of the stress concentration between the micro and macro scale. In the fourth chapter, the mean-field homogenization scheme was extended to take into account nonlinear effects such as microplasticity and progressive damage with failure criteria in both the homogeneous and constituent levels to control the element deletion. This multiscale method produced results closer to the available experimental measurements. It is also

capable to predict successfully the matrix softening and the total failure of the composite specimen. Finally, in the fifth chapter, the aforementioned mean-field methodology is extended once more to take into account healing effects in a self healing mechanism coupled with damage. Based on this phenomenon, the increasing damage rate can be reduced, resulting either in partial damage restoration or in full retrieval of the material's structural integrity. Furthermore, a methodology in microscale is proposed to predict the healing efficiency of a composite material embedded with healing microcapsules.

## Περίληψη

Τα τελευταία χρόνια, ένα πολύ σημαντικό μέρος της ερευνητικής δραστηριότητας στον τομέα της μηχανικής, είναι ο σχεδιασμός εξελιγμένων υλικών για την επίλυση δομικών προβλημάτων. Η ανάπτυξη των σύνθετων υλικών συνιστά ένα μεγάλο μέρος της λύσης αυτών των προβλημάτων, καθώς τα υλικά αυτά είναι σχεδιασμένα με γνώμονα τις ανάγκες της εκάστοτε εφαρμογής. Για το λόγο αυτό, οι προσπάθειες στον τομέα της επιστήμης υλικών επικεντρώνονται στο σχεδιασμό και την κατασκευή νέων υλικών αλλάζοντας τη σύσταση υπάρχοντων υλικών σε πολλαπλές κλίμακες. Η ανάγκη για νέα υλικά, έχει οδηγήσει στην ανάπτυξη μοντέλων στο πεδίο της μικρομηχανικής συνεχούς μέσου, η οποία συνιστά μια υποκατηγορία της κλασικής μηχανικής στερεού σώματος. Αυτό το πεδίο εισάγει νέες έννοιες για την πρόβλεψη των μακροσκοπικών ιδιοτήτων ενός σύνθετου υλικού, γνωρίζοντας τις ιδιότητες των επιμέρους συστατικών. Έννοιες όπως το στοιχείο αντιπροσωπευτικού όγκου, μικρομηχανική και ομογενοποίηση υλικού είναι ζωτικής σημασίας για τον διαχωρισμό και τη συσχέτιση μεταξύ διαφορετικών κλιμάκων στη διαδικασία χαρακτηρισμού των υλικών.

Με τις συνεχείς βελτιώσεις των υπολογιστικών συστημάτων αυξάνεται και η ανάγκη για μοντελοποίηση πολύπλοκων δομικών συστημάτων και υλικών. Η έρευνα ανομοιογενών υλικών απαιτεί λεπτομερή περιγραφή της μικροδομής ώστε να προβλεφθεί η μηχανική συμπεριφορά τους σε μικροκλίμακα ή σε νανοκλίμακα. Επίσης, η αύξηση της μνήμης των ηλεκτρονικών υπολογιστών, εκτός από την προσομοίωση μεγάλων δομικών συστημάτων, έχει επιτρέψει και την ανάλυσή τους σε πολλαπλές κλίμακες, λαμβάνοντας περισσότερες πληροφορίες σχετικά με τη σύστασή τους και το πώς αυτή επηρεάζει τα μακρομηχανικά συστήματα.

Η παρούσα διατριβή επικεντρώνεται στην αριθμητική προσομοίωση δομικών συστημάτων που αποτελούνται από ανομοιογενή υλικά, και στην πρόβλεψη της εμφάνισης και ανάπτυξης βλάβης και αστοχίας υπό συνθήκες μηχανικής φόρτισης, αναπτύσσοντας μεθοδολογίες πολλαπλών κλιμάκων. Προηγήθηκε η κατανόηση, εμβάθυνση και υλοποίηση των τελευταίων και πιο εξελιγμένων μεθόδων ομογενοποίησης υλικών, και ακο-

λούθησε η επέκταση των μεθόδων αυτών ώστε να λαμβάνουν υπόψη και να προβλέπουν ακόμα πιο σύνθετα φαινόμενα. Στο πλαίσιο αυτής της έρευνας, αναπτύχθηκαν διάφορες μέθοδοι που προβλέπουν τη δομική συμπεριφορά τόσο σε μικροκλίμακα όσο και σε μακροκλίμακα, ενώ όλες αυτές οι μέθοδοι ενσωματώθηκαν σε ένα ενιαίο υπολογιστικό πρόγραμμα.

Οι μεθοδολογίες ομογενοποίησης μέσου πεδίου, οι οποίες χρησιμοποιούνται εκτενώς σε αυτή τη διατριβή, παρέχουν έναν αποτελεσματικό τρόπο πρόβλεψης της δομικής συμπεριφοράς μη ομογενών υλικών. Σε αυτή την κατηγορία μεθοδολογιών, ανήκουν αρκετές μέθοδοι, των οποίων η πολυπλοκότητα και κατ' επέκταση η ακρίβεια, ποικίλει. Γενικά, οι μέθοδοι αυτές, αποτελούν αναλυτικές ή ημιαναλυτικές λύσεις του προβλήματος συνοριακών τιμών που επιβάλλεται σε μια μικροδομή ενός μη ομογενούς υλικού και μπορεί να είναι αρκετά ακριβείς στην πρόβλεψη της μέσης απόκρισης ενός στοιχείου αντιπροσωπευτικού όγκου. Βασίζονται κυρίως στη θεωρία του **Eshelby**, και αρχικά αναπτύχθηκαν για την πρόβλεψη της ελαστικής συμπεριφοράς των σύνθετων υλικών. Κάποιες προσεγγίσεις, επεκτείνουν την εφαρμοσιμότητα τέτοιων μεθοδολογιών σε μη γραμμικά υλικά, όπως η ελαστο-πλαστικότητα. Η σύγκρισή τους με προσεγγίσεις τύπου πεπερασμένων στοιχείων όχι μόνο επιτρέπει την αξιολόγησή τους, αλλά βοηθά και στον εντοπισμό περιορισμών που μπορεί να υπάρχουν, ώστε μελλοντικά να ξεπεραστούν με περαιτέρω έρευνα και ανάπτυξη.

Στη διατριβή αυτή, παρουσιάζονται σημαντικές θεωρίες και έννοιες για την επίλυση μηχανικών προβλημάτων με σύνθετα υλικά. Αποτελείται από μια σειρά επιστημονικών πρωτότυπων ερευνητικών εργασιών που έλαβαν χώρα κατά τη διάρκεια εκπόνησης της διδακτορικής έρευνας, ενώ περιέχονται και λεπτομερείς επεξηγήσεις των διαδικασιών και των ευρημάτων-ερευνητικών αποτελεσμάτων.

Στην πρώτη ερευνητική εργασία (Κεφ.2), πραγματοποιήθηκε μια λεπτομερής σύγκριση μεταξύ των ημιαναλυτικών και αριθμητικών μεθόδων ομογενοποίησης που πραγματοποιήθηκε για ισότροπα, εγχαρσίως ισότροπα και ορθότροπα υλικά τονίζοντας τις απλοποιήσεις και υποθέσεις που λαμβάνουν χώρα στις ημιαναλυτικές μεθόδους και

πως αυτές επηρεάζουν την αποτελεσματικότητά τους. Στη συνέχεια, η σύγκριση επεκτείνεται και σε μη γραμμικά μοντέλα υλικών.

Στη δεύτερη ερευνητική εργασία (Κεφ.3), στόχος είναι η πρόβλεψη της εγκάρσιας ρηγματώσεως σύνθετων υλικών διασταυρούμενων στρώσεων υπό αξονική εφελκυστική φόρτιση. Το υλικό κάθε στρώσης προκύπτει από την εφαρμογή της μεθόδου ομογενοποίησης των **Mori-Tanaka**, λαμβάνοντας υπόψη φαινόμενα ιξώδους. Η εγκάρσια ρηγματώση προβλέφθηκε επιτυχώς με χρήση της τεχνικής μοντελοποίησης συνεκτικής ζώνης. Επίσης, κατασκευάστηκε ένα αντιπροσωπευτικό στοιχείο όγκου διασταυρούμενων στρώσεων και πραγματοποιήθηκε η ρηγματώσή του με στόχο την συσχέτιση των συγκεντρώσεων τάσεων στην αιχμή των ρωγμών μεταξύ μικροσκοπικής και μακροσκοπικής προσέγγισης.

Στην τρίτη ερευνητική εργασία (Κεφ.4), η προαναφερθείσα τεχνική ομογενοποίησης επεκτάθηκε και στη μη γραμμική περιοχή ώστε να λαμβάνει υπόψη πλαστικότητα και θεωρίες βλάβης στο υλικό του υλικού της μήτρας, καθώς και την τροποποίησή τους ώστε να μπορούν να ελέγχονται διάφορα κριτήρια αστοχίας κατά την επίλυση του μοντέλου, η επαλήθευση των οποίων προκαλεί ρηγματώση, διαγράφοντας πεπερασμένα στοιχεία. Η νέα αυτή μέθοδος, που λαμβάνει υπόψη περισσότερα φαινόμενα όπως η υποβάθμιση των ιδιοτήτων του υλικού της μήτρας, παράγει αποτελέσματα πιο κοντά στις πειραματικές μετρήσεις σε σχέση με την προηγούμενη μεθοδολογία.

Τέλος, η προαναφερθείσα μεθοδολογία επεκτείνεται για ακόμη μια φορά, με στόχο μια τέταρτη ερευνητική εργασία, όπου αυτή τη φορά εκτός από πλαστικότητα και βλάβη λαμβάνεται υπόψη και η ικανότητα αυτοίσσης. Με το φαινόμενο αυτό η ποσότητα βλάβης που έχει υποστεί ένα υλικό μπορεί να μειωθεί, ανακτώντας μερικώς ή πλήρως τη δομική του ακεραιότητα. Επιπλέον, προτείνεται μια μεθοδολογία σε μικροσκοπική κλίμακα για την πρόβλεψη της ικανότητας ίσσης ενός υλικού που περιέχει μικροκάψουλες για την επίτευξη της ίσσης.

## Acknowledgements

With this preface the author would like to express his gratitude to the people that contributed during the dissertation process.

First of all, I would like to thank with heartfull gratitude my advisor, Associate Professor of the Department of Materials Science and Engineering of University of Ioannina, Dr. Leonidas N. Gergidis for the continuous scientific guidance, mentorship, and moral support that he offered me during the whole dissertation process. He helped me overcome any difficulties I encountered during the past years and trusted me from the beginning of our collaboration. I would also like to thank Professor Alkiviadis S. Paipetis for sharing his valuable expertise and guidance in the field of materials science and engineering. His invaluable contribution in this work is of great importance in order to achieve this goal. I would like to thank Professor Antonios Charalambopoulos of the School of Applied Mathematical and Physical Sciences, National Technical University of Athens for honoring me with his participation in the advisory committee.

Furthermore, I would like to thank the rest of the members of this seven-member examination committee for the honor they gave me to participate in the judgment of the doctoral dissertation, and specifically Dr. Dimitrios I. Fotiadis, Professor of the Department in Materials Science and Engineering of University of Ioannina, Dr. Theodoros Matikas, Professor of the Department in Materials Science and Engineering of University of Ioannina, Dr. Nektaria-Marianthi Barkoula, Professor of the Department in Materials Science and Engineering of University of Ioannina and Dr. Christina Lekka, Associate Professor of the Department of Materials Science and Engineering of University of Ioannina.

I would also like to thank Dr. George Mokios, senior supervisor of BETA CAE Systems SA, for his guidance and for offering me technical knowledge in the field of computational mechanics and software engineering from the beginning of my professional career.

I would like to thank my parents for their support. Finally, I would like to thank my future wife, Marianna, for the unwavering support and continuous encouragement that

she provided me throughout this fruitful journey. Without her support, the completion of my dissertation would have been impossible.

# Contents

<b>1</b>	<b>Introduction to Multiscale Simulation of Inhomogeneous Materials</b>	<b>1</b>
1.1	Introduction . . . . .	1
1.2	Motivation . . . . .	3
1.3	State of the art of multiscale methods . . . . .	5
1.3.1	Finite element method . . . . .	7
1.3.2	Method of cells (MOC) . . . . .	11
1.3.3	Fast Fourier Transform (FFT) method . . . . .	14
1.3.4	Mean-Field homogenization method . . . . .	16
1.3.5	Machine learning in multiscale modeling . . . . .	20
1.4	Transition between scales . . . . .	23
1.4.1	The Eshelby Tensor . . . . .	23
1.4.2	Transition from macro to microscale . . . . .	24
1.4.3	Transition from micro to macroscale . . . . .	25
<b>2</b>	<b>Computational Multi-Scale Modelling of Fiber-Reinforced Composite Materials</b>	<b>39</b>
2.1	Introduction . . . . .	40
2.2	Mean-field Homogenization . . . . .	41
2.3	Numerical homogenization . . . . .	42
2.3.1	Microstructure generation method . . . . .	43
2.3.2	Isotropic materials . . . . .	46

2.3.3	Transversely isotropic and orthotropic materials . . . . .	48
2.4	Types of boundary conditions . . . . .	48
2.5	Mean-field homogenization vs. numerical homogenization . . . . .	49
2.5.1	Linear elastic case . . . . .	49
2.5.2	Nonlinear case . . . . .	50
2.6	Crack profile on mesoscale and microscale model . . . . .	55
2.7	Conclusions . . . . .	57
<b>3</b>	<b>Crack Growth and Delamination Analysis in GFRP Composite Materials</b>	<b>61</b>
3.1	Introduction . . . . .	62
3.2	Homogenization Procedure . . . . .	64
3.2.1	Homogenization method for elastic materials . . . . .	64
3.2.2	Homogenization of viscoelastic materials . . . . .	67
3.3	Modeling a cross ply composite material (0/90)s . . . . .	68
3.4	Results and Discussion . . . . .	70
3.4.1	Delaminations and shear lag zone . . . . .	71
3.4.2	Comparison with Experiments . . . . .	73
3.4.3	Mesh sensitivity analysis . . . . .	73
3.5	Crack growth in microscale using fracture mechanics . . . . .	76
3.6	Conclusions . . . . .	80
<b>4</b>	<b>Prediction of Damage Mechanisms of Cross-ply Composite Materials Using Novel Nonlinear Multiscale Methodologies</b>	<b>87</b>
4.1	Introduction . . . . .	88
4.2	Multiscale analysis algorithm . . . . .	91
4.3	Material modelling . . . . .	94
4.3.1	Matrix material . . . . .	94
4.3.2	Homogenization of viscoelastic materials . . . . .	94
4.3.3	Homogenization of materials in plastic region . . . . .	96

4.3.4	Chaboche ductile damage model . . . . .	98
4.3.5	Algorithm for calculation of matrix stress increment . . . . .	99
4.4	Fiber material . . . . .	100
4.5	Composite material . . . . .	100
4.6	Cohesive zone modelling . . . . .	101
4.7	Finite Element Model description . . . . .	103
4.7.1	Geometry . . . . .	106
4.7.2	Boundary conditions . . . . .	107
4.8	Results . . . . .	107
4.8.1	Mesh Dependency-Sensitivity Analysis . . . . .	111
4.9	Conclusions . . . . .	113
<b>5</b>	<b>Multiscale Modelling of Extrinsic Self Healing GFRP Materials</b>	<b>121</b>
5.1	Introduction . . . . .	122
5.2	Proposed multiscale algorithm . . . . .	124
5.3	Matrix material . . . . .	127
5.3.1	Homogenization of materials in plastic region . . . . .	128
5.3.2	Continuum damage mechanics . . . . .	130
5.3.3	Healing . . . . .	131
5.4	Composite material . . . . .	132
5.5	Results . . . . .	133
5.5.1	Three point bending test . . . . .	133
5.5.2	Parametric study . . . . .	138
5.5.3	Parametric study of $g$ parameter . . . . .	138
5.5.4	Time dependency analysis . . . . .	141
5.6	Microscale modelling . . . . .	142
5.7	Conclusions . . . . .	147

<b>6</b>	<b>General Conclusions and Future Work</b>	<b>155</b>
6.1	General Conclusions . . . . .	155
6.2	Future work . . . . .	158
	<b>Appendices</b>	<b>161</b>
A	Multiscale material model verification . . . . .	163
B	Periodic Boundary Conditions . . . . .	167
B.1	PBC formulation . . . . .	167
B.2	Implementation in the FE model . . . . .	168
C	The GUI of Multiscale Modeller . . . . .	171
C.1	User Inteface . . . . .	171
	<b>Curriculum vitae</b>	<b>179</b>

# List of Figures

1.1	Engineering fields which heavily rely on computer simulation methods . . .	2
1.2	Representative length scales in Materials Science and Engineering . . . .	3
1.3	Transition between scales . . . . .	6
1.4	Boundary value problem definition, where the macroscopic strain is imposed as displacements in the boundary of the RVE . . . . .	8
1.5	Solution of boundary value problem of RVE with FEM . . . . .	9
1.6	FE2 method description . . . . .	11
1.7	Generalized MOC . . . . .	12
1.8	Voxel based microstructure appropriate for FFT homogenization (61) . .	15
1.9	Multiscale modelling using mean-field approaches . . . . .	17
1.10	Multiscale modelling with Neural Networks . . . . .	21
2.1	Method for RVE generation with periodically placed inclusions . . . . .	44
2.2	Three cases of intersection between the inclusion and the RVE boundaries in periodic microstructures. <b>Top Left</b> : Intersection with one of the RVE faces. <b>Top Right</b> : Intersection with one of the RVE edges. <b>Bottom</b> : Intersection with one of the RVE vertices . . . . .	45
2.3	RVE generation for : unidirectional long fibers <b>Top Left</b> , random fiber orientation tensor $(1/3, 1/3, 1/3, 0, 0, 0)$ <b>Top Right</b> , almost aligned fibers with orientation tensor $(0.9, 0.05, 0.05, 0, 0, 0)$ <b>Middle Left</b> , continuous fiber laminated composite <b>Middle Right</b> , multiple phases <b>Bottom Left</b> , multiple layers $[0, 90]_s$ <b>Bottom Right</b> . . . . .	47

2.4	RVEs for the studied cases from left to right: Isotropic, Transversely isotropic, Orthotropic . . . . .	49
2.5	<b>Top:</b> Representation of mean-field result with uniform fields in the RVE <b>Bottom:</b> Representation of FE RVE result that can predict non-uniform fields in the RVE. Colorbars depict stresses in MPa . . . . .	52
2.6	FE vs MF for RVE with spherical inclusions with 20% volume fraction . . . . .	53
2.7	FE vs MF for RVE with short aligned fibers with 30% volume fraction . . . . .	54
2.8	FE vs MF for RVE with short fibers with 20% volume fraction and random orientation of (0.7,0.15,0.15,0,0,0) . . . . .	54
2.9	FE vs MF for continuous fiber RVE with 30% volume fraction . . . . .	55
2.10	Plane strain 2-Dimensional RVE model . . . . .	56
2.11	Colorbars represent stress values (MPa) around the crack . . . . .	57
3.1	Steps used during homogenization procedure: i. pseudo-grain discretization, ii. homogenization of each pseudo-grain, iii. homogenization of all pseudo-grains with Voigt approach . . . . .	65
3.2	Time dependent homogenized axial Young's modulus $E_{11}$ from viscoelastic homogenization . . . . .	69
3.3	Geometry of the cross-ply composite model. . . . .	70
3.4	Modeling of the possible transverse cracks with cohesive interface . . . . .	70
3.5	Modeling of the possible transverse cracks with cohesive interface. The existence of the shear lag zone is apparent. The upper layer is hidden to get a more clear image of the cracks and the delamination area. Values of <i>CSQUADSCRT</i> quantity are given in the colorbar . . . . .	72
3.6	Middle layer transverse cracks at different time steps . . . . .	74
3.7	Crack density as a function of strain for experiment data (reproduced with permission from (32)) and simulation model data for quasi-static loading and for total loading time about 270 sec . . . . .	74

3.8	Final cracking at the model material geometry for five different meshes for quasi-static loading. At the right corner a magnified local domain encapsulating crack is also given for each of the five different meshes . . .	75
3.9	Mean delamination length as a function of the number of finite elements .	76
3.10	Crack growth in a cross-ply RVE using XFEM . . . . .	78
3.11	Stress concentration comparison between micro and macro models. Colorbars depict stresses in MPa . . . . .	79
4.1	Flow chart of multiscale material implementation . . . . .	93
4.2	Axial stress vs. axial strain of elastic glass fibers, visco-elasto-plastic with damage matrix and of the homogenized response (Not enabled failure). The inset figure represents the values of axial stress in logarithmic scale for clarity . . . . .	101
4.3	Crack and delamination using cohesive zone modeling. Color bar represents contact failure . . . . .	103
4.4	Experimental (45) vs. calibrated response of a visco-elasto-plastic with damage non-linear material . . . . .	105
4.5	Geometry of cross-ply composite material model . . . . .	106
4.6	Progressive failure of the composite material. The colored lines represent the potential cracks. Blue color represents fully bonded parts and red color total debonding, i.e the satisfaction of the failure criterion. The axial strain is also depicted . . . . .	108
4.7	Stress vs. strain plot of a solid above the crack tip that fails due to fiber failure at strain around 0.013 . . . . .	109
4.8	Stress vs. strain plot for the whole composite material . . . . .	110
4.9	Comparison of multiscale algorithm with simple visco-elastic model and experimental results . . . . .	110

4.10	Cracking saturation state for the different discretizations used: a. 8000, b. 45144, c. 96000 and d. 208306 elements. Colorbar represents contact failure value . . . . .	112
4.11	Crack density as a function of the total number of elements . . . . .	112
5.1	A.Damaged (nominal) configuration B.Healing Configuration C.Effective (undamaged) configuration . . . . .	124
5.2	Flow chart of multiscale material implementation . . . . .	125
5.3	Three point bending setup . . . . .	134
5.4	Virtual three point bending experiment. <b>Top Left:</b> Matrix stress without healing. <b>Top right:</b> Matrix damage parameter without healing. <b>Middle left:</b> Matrix stress with 200 s healing. <b>Middle right:</b> Matrix damage parameter with 200 s healing. <b>Bottom left:</b> Matrix stress with 600 s healing. <b>Bottom right:</b> Matrix damage parameter with 600 s healing. Stress values depicted in the left colorbars are in MPa while the right side colorbars represent the dimensionless matrix damage parameter values . . . . .	135
5.5	Matrix response for variable healing times . . . . .	136
5.6	Fiber response for variable healing times . . . . .	136
5.7	Homogenized response for variable healing times . . . . .	137
5.8	Effect of parameter $g$ in matrix axial stress vs. axial strain in tensile test at 4000 s ) . . . . .	139
5.9	Healing variable evolution vs analysis time . . . . .	140
5.10	Effective damage evolution vs analysis time . . . . .	140
5.11	Time dependency analysis . . . . .	141
5.12	Loading scale factor vs analysis time . . . . .	143
5.13	Algorithm for failure and heal of materials around failed capsules . . . . .	144
5.14	<b>a:</b> Failed capsules in red <b>b:</b> Microcracks in RVE <b>c:</b> Isolated failed elements, while in green color are the healed elements . . . . .	145

5.15	Average stresses - average strains relation obtained from the RVE tensile test for the undamaged epoxy material at the first loading cycle, and healed material at the second loading cycle. . . . .	146
A.1	Representation of 1-layer RVE with volume fraction $V_f \approx 0.4$ . . . . .	163
A.2	von Mises stress distribution in RVE . . . . .	164
A.3	Fiber stress-strain diagram for direct comparison between the micro model (RVE) and the developed multiscale model (Umat) . . . . .	165
A.4	Matrix stress-strain diagram for direct comparison between the micro model (RVE) and the developed multiscale model (Umat) . . . . .	165
A.5	Homogenized stress-strain diagram for direct comparison between the micro model (RVE) and the developed multiscale model (Umat) . . . . .	166
B.1	RVE and corresponding node numbering . . . . .	169
C.1	Multiscale Modeller modes . . . . .	171
C.2	Examples of definition of multiscale material model parameteres. <b>a</b> : Elasticity <b>b</b> : Elasto-plasticity <b>c</b> :Elasto-plasticity with damage <b>d</b> : Visco-elasticity <b>e</b> : Assignment of failure indicator . . . . .	172
C.3	Micromechanics mode with stress/strain curves of each constituent, the homogenized response and the representation of the fictitious RVE . . . . .	173
C.4	Finite element mode example with boundary condition application of shear in yz and numerical homogenization of RVE . . . . .	174
C.5	Finite element mode example with mean-field homogenization for each integration point . . . . .	174
C.6	Setting up control points to visualize the microstructures' response for specified material points, after the completion of FE2 method . . . . .	175
C.7	Finite element mode example with FE2 method and visualization of failure status . . . . .	176



# List of Tables

2.1	Isotropic Elastic Properties after MF and FE Homogenization . . . . .	49
2.2	Transversely isotropic Elastic Properties after MF and FE Homogenization	50
2.3	Orthotropic Elastic Properties after MF and FE Homogenization . . . . .	50
2.4	Properties of matrix and inclusions . . . . .	51
3.1	Elastic Properties after elastic and viscoelastic Homogenization . . . . .	68
4.1	Elastic Properties . . . . .	104
4.2	Relaxation modulus prony series relaxation times $\tau_i$ and weights $w_i$ obtained from (44) . . . . .	104
4.3	Plastic and damage properties of matrix . . . . .	105
4.4	Strength values from literature (46) . . . . .	106
5.1	Matrix and fiber material properties, for elasticity, plasticity, damage and healing . . . . .	133



# Chapter 1

## Introduction to Multiscale Simulation of Inhomogeneous Materials

### 1.1 Introduction

In the last decades, simulation has become an integral part of the industry. The discovery of the finite element method was the beginning in the establishment of simulation as an initial stage for the design of a structure or a product. Initially, simulations were used in the field of structural engineering, but with the improvement and evolution of computing systems, the needs for the application of simulations in more scientific fields also increased as shown in **Figure 1.1**. Thus, models for heat transfer, computational fluid dynamics, electromagnetism, acoustics, injection molding, and biomechanics among others were developed and adopted in the industry.

Multiscale modeling and hierarchical simulation approaches starting from the nanoscale and progressing through different time and length scales provide detailed and accurate information at the macroscale. With the emergence of new lightweight structural parts, several industries use inhomogeneous materials with two or more phases making this way the research in composite materials mechanics more imperative and more relevant than ever. The mechanical behaviour of such materials depend largely on the microstructure,

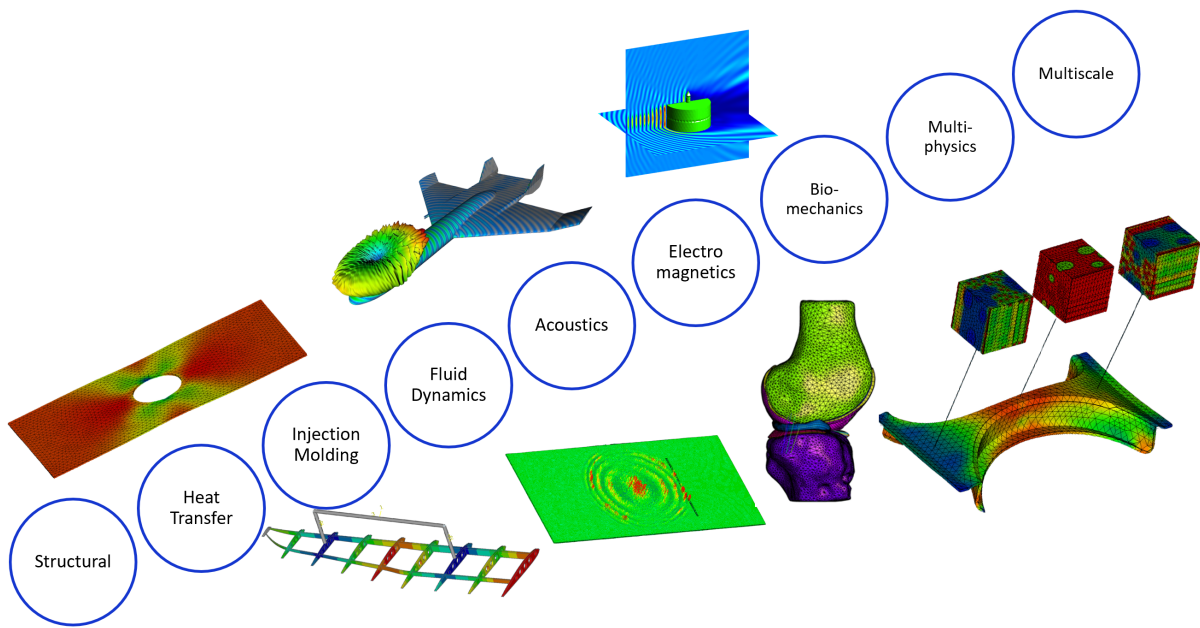


Figure 1.1: Engineering fields which heavily rely on computer simulation methods

meaning the topology, geometry and the properties of each phase. Due to their nature of inhomogeneity, different observations can be made, depending on the scale under consideration. On one hand, in the macroscale the material can be considered homogeneous with effective homogenized properties to represent the mechanical behaviour and on the other hand the microscale, where all the constituents of the microstructure are distinguishable. In order to be able to predict the material properties it is imperative to understand in depth the relationship between the microstructure of the material and physics of its underlying molecular mechanics (**Figure 1.2**). In other words, the modern engineering applications, lead the materials science field to extend the research to lower scales.

One of the most important theories when examining inhomogeneous materials, is the mathematical model that defines the scale transition from micro to macro and vice versa. This model takes into account the contribution of each constituent in the microscale and the role it plays when the macroscale predictions are made. This contribution is expressed in terms of variables that describe the phase, such as the volume fraction, the aspect ratio of the fiber and the orientation among others.

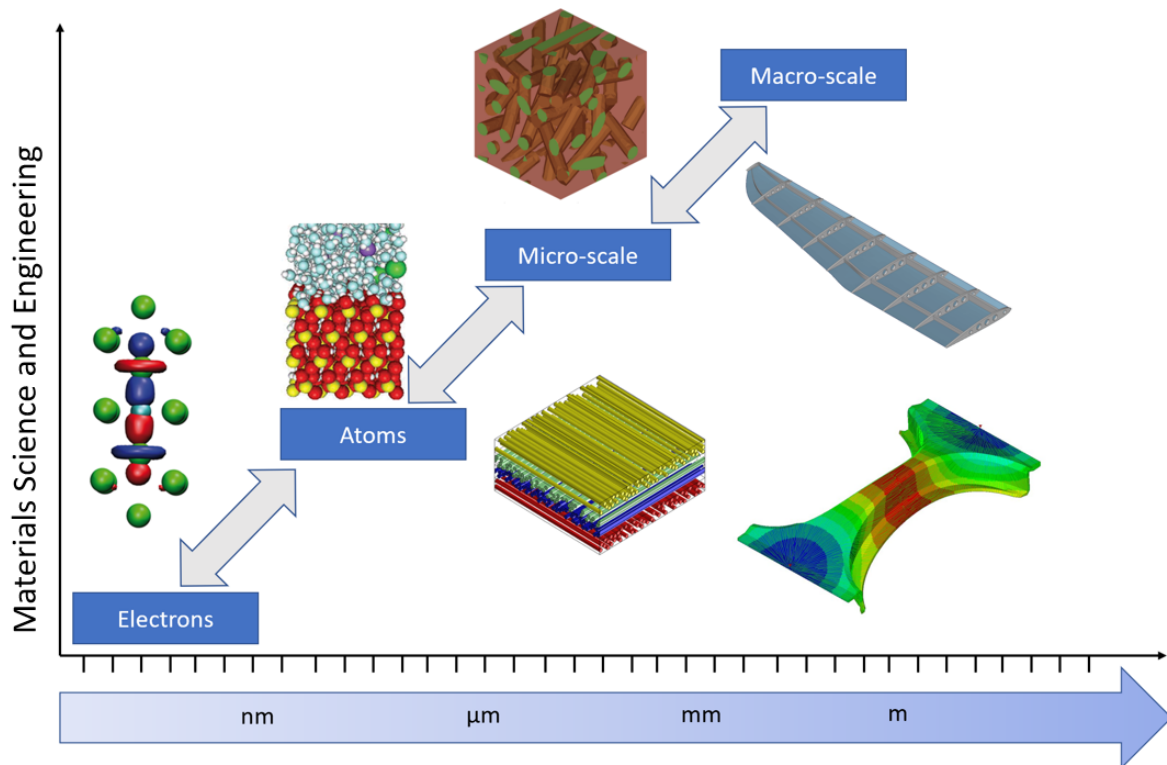


Figure 1.2: Representative length scales in Materials Science and Engineering

## 1.2 Motivation

The response of composite materials under mechanical loading can be quite unpredictable due to different damage mechanisms that can appear prior to their failure. For this reason it is not always possible to use classical constitutive formulations to model composite materials. Therefore, the main objective is the development of material models that describe accurately the damage and failure behaviour of such materials. However, treating composite materials as homogeneous in the constitutive equations often hides inconsistencies and problems. For instance the inhomogeneities in the microstructures usually cause local stress concentration that is responsible for inelastic material behaviours, damage in the matrix material around them or even debonding between the matrix and the fibers. Subsequently, it is essential to take into account these phenomena and evaluate their effect on the macroscopic behaviour. This can be achieved by adopting and extending multiscale methodologies. Physics and mechanics in the microstructure drive various phenomena that occur in the macroscopic level. Those multiscale methodologies consist the so called

homogenization methods that describe the scale transition from micro to macro level.

The purpose of these methods is to provide information that can be used to find a material model to predict the effective response, and also to identify the parameters that are introduced in this effective material model that is supposed to represent the macroscopic properties of the heterogeneous material. In general, the produced material model cannot be of the same type as the model used for the constituents, a fact that complicates the search for an effective material model. Until some decades ago, the identification of the homogeneous response could be performed experimentally, or by physical assumptions such as the rule of mixtures. All of the homogenization strategies can be categorized to the following groups:

a) Phenomenological methods. The methods primary attempts to predict a homogeneous behaviour of an heterogeneous material (Voigt, Reuss, Nemat Nasser and Hori (1), Ponte Castaneda (2) (3)). Those methods are the simplest, purely analytical with the least accuracy and take into account only the volume fraction and the properties of each constituent. They are mostly used to obtain a lower and upper limit of the overall homogenized properties.

b) Mean-Field homogenization methods. They are semi-analytical and are based mostly on Eshelby's (4) single inclusion problem. The formulation of such methods takes into account the fiber's geometry and orientation, the volume fraction of the inclusions and can be also adopted for composite materials with multiple phases. They are computationally fast with good accuracy and can be extended to describe nonlinear materials. Mori-Tanaka method is one of the most common mean-field methods with enough research around the extension of this method to predict not only the elastic properties but also, viscous effects, plasticity etc.

c) Representative Volume Element (RVE) based homogenization methods. They rely on studying the discretized microstructures in order to evaluate the microscale fields and subsequently the macroscale properties. These methods fully account for the interactions of the constituents and overcome some simplifications made in the phenomenological and

mean-field methods. RVE based methods are the most accurate but the most computationally expensive.

During this research, all of the above methods have been applied both separately in some cases and combined in others, to either achieve a high level of accuracy or to verify the novel developed methods.

### **1.3 State of the art of multiscale methods**

The intention of continuum mechanics is to determine the constitutive law that describes best the stress/strain relations in order to match the real behaviour of the material. In case of nonlinear materials such as plasticity and damage, the constitutive law can be quite complex and in many cases a single scale approach cannot produce the required level of accuracy. Multiscale methods can overcome such limitations where each constituent can follow a different constitutive law and with the appropriate scale transition methods the nonlinear macroscale behaviour can be predicted accurately.

Considering a composite material at the macroscopic level, the material is seen as homogeneous. By applying loads on the structure induce strain and stress fields in the material. The relation that links macroscopic strain and stress depends on the microstructure of the heterogeneous material, which can be examined only at the microscale. In order for the microstructure to be taken into consideration, a RVE can be defined at each point of the macroscopic model. When transitioning between these scales many problems may occur. For example, a way to transfer the macroscopic strain or stress to the RVE must be defined in order to solve the boundary value problem and compute the total macroscopic response taking into account the microstructure (**Figure 1.3**).

The first step is to localize the solution variables such as strains and strain rates to transform from the homogeneous level to the microscale level. In this way, each constituent can be taken into account separately. The second step, after predicting the response of each constituent, is to combine the individual responses and produce a homog-

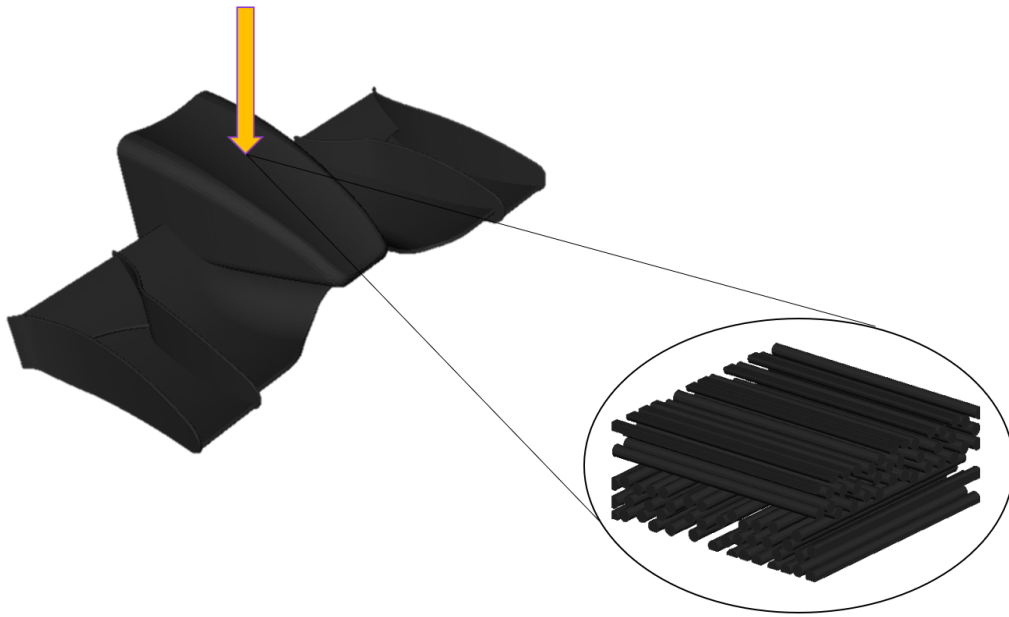


Figure 1.3: Transition between scales

enized prediction, moving from microscale to macroscale.

During the past years, many multiscale methods have been developed. Most of them focus on the computational efficiency and are mainly semi analytic, in order to offer a valuable tool for simulating complex structures taking into account the heterogeneous nature of the materials. These methods are extended from their initial form of simulating linear behaviours to sophisticated nonlinear regimes, such as plasticity and damage. Others, mainly based on discretized models, focus on the accuracy of the produced results and used to be adopted mostly for material characterization rather than for full multiscale analyses. However, as the computational systems are updated offering fast CPUs and enormous amounts of memory they are adopted for full analyses where for each point of the model the boundary value problem of a discretized domain is solved, overcoming several simplifications and assumptions that the semi-analytical techniques adopt.

With the progress of machine learning and neural networks, many methods have been combined to generate training data of abstract microstructures in arbitrary loadings in order for the system to be able to predict the solution of a microstructure without fully solving the discretized domain, saving valuable computational time with increased accu-

racy. However, at the time being, the mean-field methods are the most computationally efficient methods that can be used to describe any microstructure geometry with any material model under arbitrary loading.

In the following subsections, the state of the art of the multiscale techniques and homogenization methods will be presented, highlighting their applicability for solving structural engineering problems.

### 1.3.1 Finite element method

In order to solve the boundary value problem (BVP) for an elastic solid  $R$  with a given geometry, the displacement, stress and strain fields that correspond to the prescribed sets of body forces  $b^o$ , surface tractions  $t^o$  or displacements  $u^o$  are sought. For displacement boundary value problems, three components of  $u^o$  are specified on the surface boundary  $\partial R$ . The displacement, stress and strain fields are calculated from the equation of motion

$$\frac{\partial \sigma_{ij}}{\partial x_i} + b_j^o = \rho \frac{d^2 u_i}{dt^2} \quad (1.1)$$

combined with Hooke's law  $\sigma_{ij} = C_{ijkl} \varepsilon_{kl}$  and the strain-displacement relation

$$\varepsilon_{ij} = \frac{1}{2} \left( \frac{\partial u_j}{\partial x_i} + \frac{\partial u_i}{\partial x_j} \right) \quad (1.2)$$

where the term  $\frac{\partial \sigma_{ij}}{\partial x_i}$  is the derivative of the Cauchy stress,  $b_i^o$  is the body force per unit volume,  $\rho$  is the density, and  $\frac{d^2 u_i}{dt^2}$  is the acceleration. For static or quasi-static problems the right hand side of the equation is zero.

The concept of RVE in micromechanics as defined in (5) is used to estimate the material properties and constitutive relations at a material point considering the microstructure. These constitutive relations are then used in balance equations to predict the overall response of a continuum material. The balance equations include mass and energy conservation equations, linear and angular momenta. These equations often contain the body forces representing the effect of the materials not in contact with the considered contin-

uum and the inertia forces due to the motion of the continuum itself. They also contain the associated force and displacement boundary data which represent the effect of the other continua in contact with the considered continuum. Therefore, when formulating BVPs associated with an RVE, it is not necessary to include the body forces, especially in static or quasi-static conditions. The main goal is to obtain the overall average properties of the RVE when particular boundary conditions apply. The BVP as defined in **Figure 1.4** on a RVE can be solved with the finite element approach by applying displacements in the boundaries of a discretized RVE domain (**Figure 1.5**). Its weak form in 3D (6) is defined in terms of finding the unknown displacement field  $u^T = [u \ v \ w]$  from the momentum equilibrium relation

$$\int_{\Omega_0} \sigma : [\delta u \otimes \nabla] d\Omega_0 = \int_{\Gamma_0} u_d \cdot \delta u \ d\Gamma_0 \quad (1.3)$$

with suitable boundary conditions and pertinent test functions  $\delta u$ . In this relation, the RVE is defined within the region  $\Omega_0$  and is subjected to tractions  $u_d$  on its boundary  $d\Omega_0 = \Gamma_0$ . The outer product (also referred to as the dyadic product) is defined as  $a \otimes b = a_i b_j$  and  $\nabla$  is the spatial gradient with respect to coordinates  $\mathbf{x}$ . The boundary conditions on the surface of the RVE are imposed using the equation  $u_d = \varepsilon_{ij} x$ .

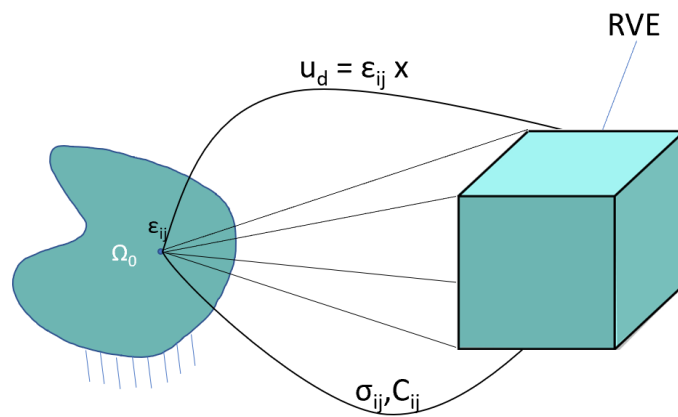


Figure 1.4: Boundary value problem definition, where the macroscopic strain is imposed as displacements in the boundary of the RVE

The finite element solution provides very accurate results for both the local (micro)

and global (macro) fields making this method attractive when the accuracy of results is of high importance. One of the most known and widely adopted by the individual researchers multiscale methodologies based on the solution of discretized RVEs is the FE2 method.

The FE2 multiscale approach (7) is based on FE homogenization of a microstructure that corresponds to a point of the macroscale model. This method solves nested finite element problems successively, one for the macroscale model and one for the microstructure. The solution data of the microstructure are then used in order for the solver of the macro model to converge and proceed to the next time step. The main advantages of this method, except from the fact that it is the most accurate between all the multiscale methods, is the ability to incorporate any microstructure geometry, and consider the interactions between the inclusions.

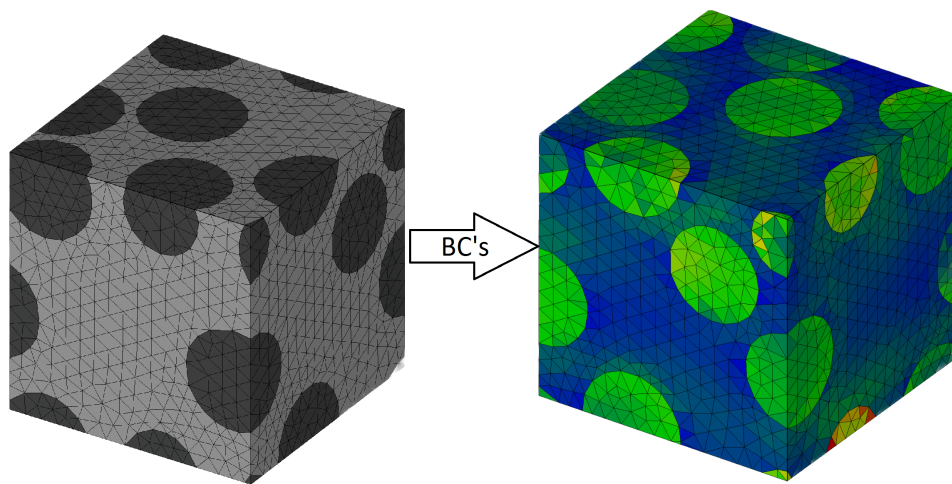


Figure 1.5: Solution of boundary value problem of RVE with FEM

Feyel and Chaboche (8) proposed the first-order FE2 multiscale method to predict the behaviour of composite materials with continuous fibers (**Figure 1.6**). They proved that this method can simulate the composite structures with detailed microscopic information. The information between the macroscopic and microscopic finite element models is correlated based on the homogenization theory, where the macroscopic deformation gradient  $F^-$  is transferred to the microscopic level and macroscopic tangent and stress  $P^-$  averaged over the RVE are transferred to macroscopic level.

Kouznetsova et al. (9) proposed the second-order FE2 multiscale method that takes

into account macroscopic localization and size effects. This method extends the first-order FE2 framework by deriving the higher-order macroscopic constitutive tangents through static perturbations among microscopic overall response. Both the macroscopic deformation gradient  $F^-$  and its gradient  $\nabla_0 F^-$  are transferred to the microscopic scale, while the tangents, averaged stress  $P^-$  and the higher order stress tensor  $Q^-$  coupled with  $\nabla_0 F^-$ , are transferred to macroscopic scale.

Nezamabadi et al. (10) suggested a nonlinear multiscale formulation based on the FE2 method to study the instability phenomenon of fiber reinforced composites while Cong et al. (11) proposed a multiscale approach that can be used to simulate heterogeneous shell structures using finite strain theory.

Since the FE2 method uses a bidirectional real-time exchange of macroscopic and microscopic information (the macroscopic level transmits the strain to the microscopic RVE, and the RVE transmits the stress to the macroscopic level after converting the strain to boundary conditions and solving the boundary value problem), a RVE at each integration point of the macroscopic finite element model is required resulting in a large amount of computations. For this reason, efforts for the improvement of computational efficiency were made by Praster et al. (12). The same path was followed by Tuijl et al. (13) and Hernandez et al. (14) with the empirical interpolation method and later Hernandez et al. (15) the empirical cubature method.

More attempts to improve the efficiency of computational multiscale methods were made by using model order reduction techniques, such as POD (proper orthogonal decomposition) (13) (16) (17) and the Fourier-related envelope model (18) (19). Efforts to ensure algorithmic convergence are presented in (20) (21) and a methodology that requires the solution of the micro problem for the minimum amount of times possible (22) (23).

Even though this method proved to be the most accurate between the multiscale methods, it has two main disadvantages that limit its applicability. The first one has to do with the microstructure generation. Several RVE generation methods have been proposed

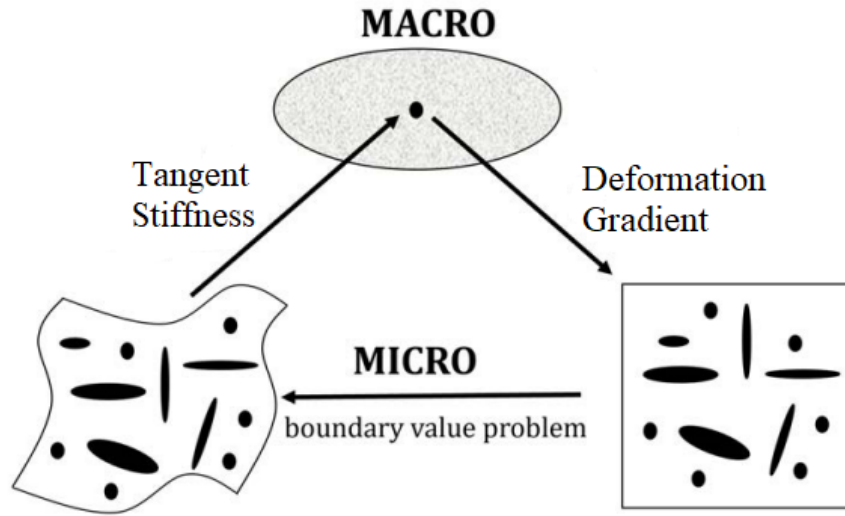


Figure 1.6: FE2 method description

but all of them seem to show difficulty in achieving high volume fractions of fibers or do not successfully cope with the production of fine mesh for complex microstructures with various inclusion sizes. The second disadvantage has to do with the computational cost associated with the solution of the boundary value problem for RVEs with millions of elements, a fact that makes this method the most cost ineffective. Even when reducing the dimensionality of the problem to 2D with plane strain or axisymmetric conditions the computational cost is not reduced drastically. The FE homogenization and FE2 method are only used in this work for verification purposes for the newly developed multiscale models (Appendix C).

### 1.3.2 Method of cells (MOC)

The method of cells relies on the fundamental assumption that the composite has a periodic microstructure where the fibers are arranged in periodic manner. This assumption allows to analyze just a single repeating unit cell (RUC) rather than the whole composite. The RUC is defined as a representative building block where the composite can be constructed by the unit cell repetition. In order to analyze the RUC, imposition of the dis-

placement and traction continuity conditions at the interfaces within the unit cell as well as at the interfaces between neighboring unit cells, in conjunction with the equilibrium conditions, is needed. For composites consisted of linear elastic phases, the analysis should provide the relations between the average effective stresses and strains and determine the effective modulus in a closed form solution. In the work of Aboudi (24) the MOC was used to predict the overall behaviour of a viscoplastic composite material. The maximum number of different composite phases that the MOC could take into account was limited to four, but an extension of this model, the Generalized Method of Cells (GMC), allowed any number of phases (25) (26).

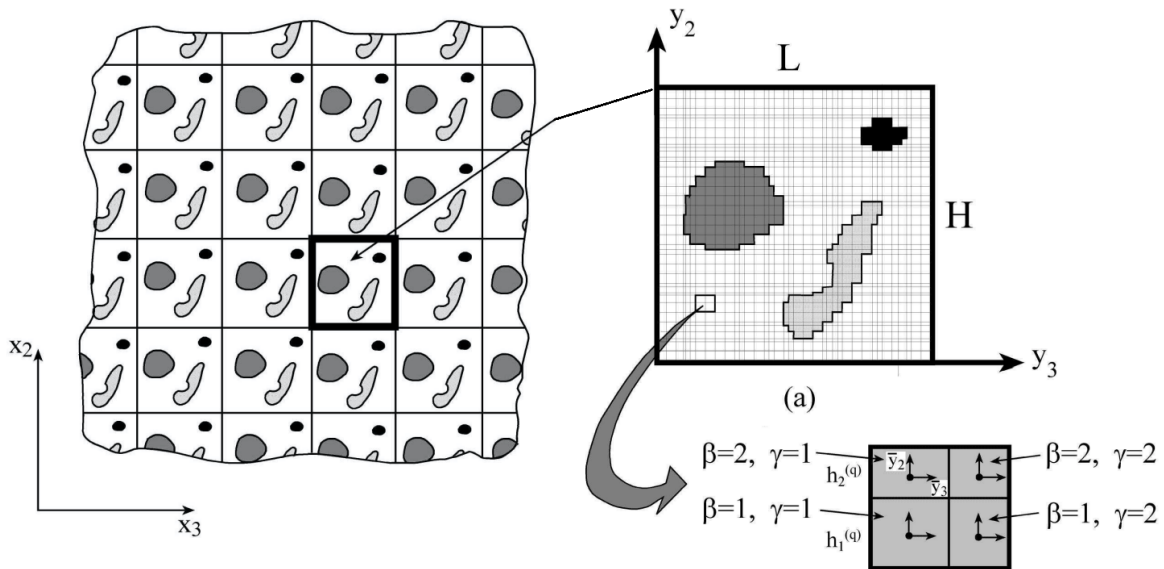


Figure 1.7: Generalized MOC

The generalized method of cells computes both microscopic and macroscopic properties of linear and nonlinear heterogeneous materials under mechanical or thermal loading. This method was initially introduced by Aboudi (27), Paley and Aboudi (25) and Dvorak (28) (called the transformation field analysis) and divides a repeating unit cell into an arbitrary number of generic cells, being divided into subcells that each one may contain a distinct homogeneous material (**Figure 1.7**). The basic assumption of this method is that the displacement vector in each subcell varies linearly with the local subcell coordinates. The global response is calculated by the classical volume averaging technique.

Algorithmically, this method shows high efficiency and good accuracy. However, due to the assumption of linear displacement fields, the produced results regarding the local fields are not very accurate. This method was extended in order to better capture the nonlinearities of the materials and the High Fidelity Generalized Method of Cells (HFGMC) (29) (30) has been developed. Higher order displacement fields are used so that additional equations are needed to solve the system. This requires a much higher computational cost than the original method of cells but it is still more efficient than the corresponding finite element simulation method. However, because of the rectangular shape of the generated subcells, the finite element methods can produce much more accurate predictions for the micro-fields.

Voyadjis and Deliktas (31) incorporated continuum damage into the GMC and applied the method to metal matrix composites. The local incremental damage model developed by Voyadjis and Guelzim (32) can take into account the damage in each subcell separately establishing elastoplastic constitutive equations that govern the behaviour of the composite with damage evolution.

Most of the applications of GMC regard continuous fiber composites because the study of short fiber composites require a three dimensional analysis that can be highly intensive computationally and complicated. Pahr and Arnold (33) present a model based on GMC for the study of short fiber composites, and showed that the GMC can be successfully used for such cases with some modifications of the initial method.

Despite the demonstrated efficiency and accuracy of the GMC to perform linear and nonlinear homogenization of composite materials with periodic microstructures, the accuracy in predicting local fields inside the microstructure was not as good as in the prediction of macroscopic (global) fields. Most recently, a new model developed to overcome the shortcoming of the GMC, termed as High Fidelity Generalized Method of Cells (HFGMC). The framework of the HFGMC was motivated by a higher order theory that has been developed for the analysis of graded materials, and is capable of simulating the micro stress and micro strain fields of materials under 3D loading (29)(34). This method

appears to predict both the global and local field with high accuracy.

Since all the aforementioned methods are based on the method of cells use a discretized domain in micro level to solve the constitutive equations and retrieve the local and global fields, not only makes them mesh dependent and limited to periodic structures, but are much more computationally expensive than the mean-field methods.

### **1.3.3 Fast Fourier Transform (FFT) method**

This approach, introduced by Moulinec and Suquet (35), build upon the Lippmann-Schwinger equation (36) that is solved iteratively in the Fourier space. It operates directly on pixels or voxel data (**Figure 1.8**) and was formulated for nonlinear material behaviour from the very beginning. For that reason this method is suitable for analyses of digital images or tomography scans of the real microstructure taking into account clustering and percolation phenomena. Due to its inherently matrix-free formulation and the associated low memory footprint, the method ensures applicability to large-scale microstructures, is comparatively simple to implement and produces impressive results in short time, due to the efficient numerical implementations of the FFT available (37) (38).

In the 2000s, the Moulinec–Suquet method was accelerated and applied to a wider range of materials and constitutive behaviours such as damage and fracture mechanics, conductivity and emissivity, polycrystalline materials and composite materials among others. In the beginning of the 2010s, the number of corresponding articles started to increase significantly, but there was still a lack of deeper understanding of the numerical method, obstructing further developments. The strategy presented by Moulinec and Suquet provides a solution method for a discretized system of equations. By separating the discretization step from the solver, the FFT approach was re-integrated into the conventional canon of contemporary computational methods. Thus, around 2015, the previous obstructions were removed and it became possible to change the discretization while preserving the salient features of the solver, or to use faster solution methods for the same discretization.

Regarding the prediction of damage and fracture using FFT approaches, Herrmann et al. (39) first considered linear and elastoplastic fracture mechanics and subsequently more FFT-based approaches are reported for isotropic local damage (40) (41) (42) , and anisotropic local damage (43). Non local damage models, that remove the mesh dependence that local models introduce upon failure, are considered in (44) (45) (46) where the non locality is handled by a convolution-type integral which is computed in Fourier space. A semi explicit FFT solver was introduced by Chen et al. (47) while Ernesti et al. (48) discussed a fully implicit solver based on a fast gradient method. Extensions were made to account for finite strains for hyperelastic (49) and hypoelastic (50) constitutive formulations. FFT-based methods were reported to be effective for aluminum (51), concrete (52) and ceramic foams (53). Applications to cellular alumina ceramics (54), sintered alumina ceramics (55), alumina and zirconia ceramics (56), ferroelectric ceramics (57) and for auxetic ceramics (58) were reported. Besides, applications to cubic-cell (59) and porous metamaterials (60) were provided.

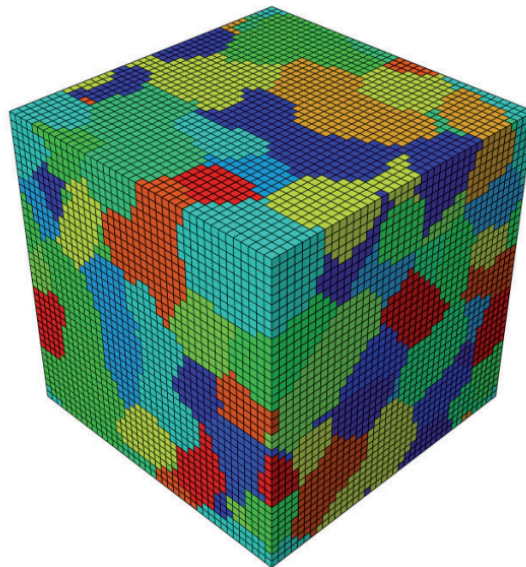


Figure 1.8: Voxel based microstructure appropriate for FFT homogenization (61)

Computational homogenization methods utilizing the FFT are developed into a mature state and can treat complex microstructures with constituents following sophisticated material behaviours within reasonable time. These methods make use of the specific struc-

ture of regular grids and utilize the FFT for constructing general-purpose pre-conditioners for the discretized systems that can be solved with dedicated solvers.

However, despite the progress that was made, there are still some hurdles that need to be overcome. In order for this technique to be an efficient multiscale method, it is necessary to go beyond the solution of a specific homogenization problem of a single microstructure. For instance, for short fiber composite materials after injection molding, the fiber orientation may be locally varying and single microstructure cannot predict accurately the behaviour of the whole continuum. In conjunction with the increased computational cost the FFT-based methods are not suitable to solve a microscale problem for each material point of the macroscale model.

### **1.3.4 Mean-Field homogenization method**

As mentioned earlier, RVE based homogenization methods present difficulties to generate a finite element mesh in order to simulate accurately the microstructure and to achieve a numerical solution on the macroscopic scale within a reasonable time interval. Besides, the finite element procedure bears a geometric restriction for composites reinforced with high aspect ratio fibers and large volume fractions (62). To overcome these obstacles, micromechanical models turn out to be very useful. These methods can predict the macroscale behavior of composite materials while taking into account the microstructural parameters of each phase.

Analytical and semi-analytical homogenization methods started several decades ago when computational resources were very limited. They are based on observations of the interactions between the phases, and they produce a prediction for both the macroscopic response and the deformation for each phase. One of the limitations of such methods are that they cannot predict localization of stresses or strains. Most of these homogenization methods are based on the Eshelby's theory (4) for ellipsoidal inclusions that assumes that the matrix and inclusions are bonded perfectly. They were initially developed to predict linear homogenized response and later extended for the prediction of nonlinear materials

by linearizing their behaviour in an incremental formulation scheme. Mean-field methods are very computationally efficient with good accuracy and can be used to predict the response of large composite structures while producing results at multiple scales for both the macro model and constituent-wise (**Figure 1.9**). One of the most common mean-field methods is the Mori-Tanaka (63) and is used extensively in this work for elastic, visco-elastic, elasto-plastic, visco-elasto-plastic with damage, and elasto-plastic with coupled damage-healing composite materials.

Regarding the study of heterogeneous materials, many multiscale methods have been proposed (review from Kanouté et al. (64), Geers et al. (65)) for the calculation of the effective behaviour based on the local behaviour of each phase and on the morphology of the microstructure. The homogenization methods can be separated into two main categories according to the way the information is transferred between scales. Those are the sequential and the integrated multiscale methods.

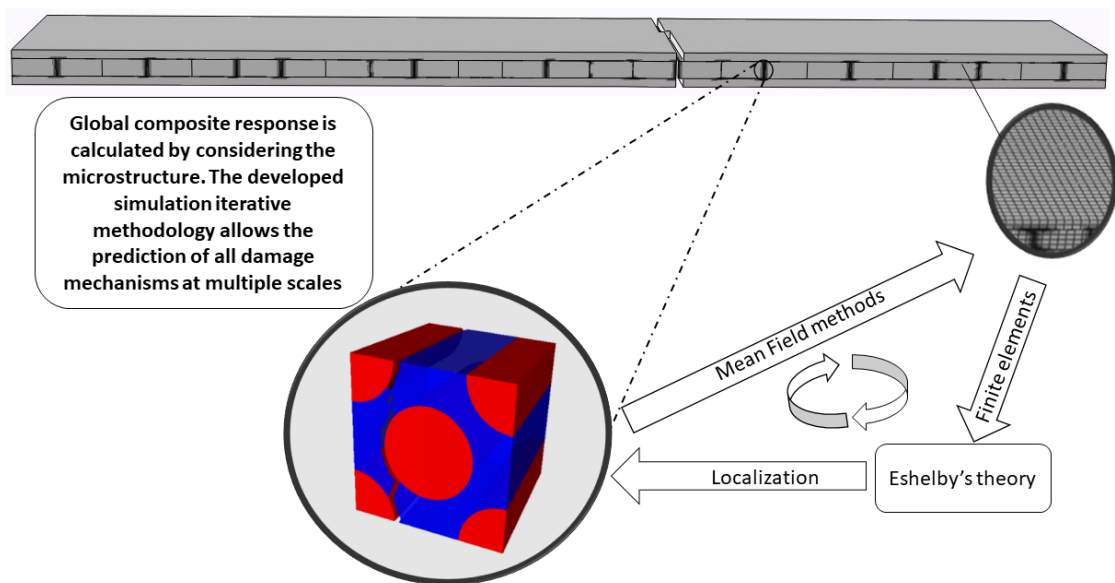


Figure 1.9: Multiscale modelling using mean-field approaches

The methods that belong to the first category, handle the problems on different scales sequentially and independently and are best applied to linear behaviour. To elaborate, an overall effective response on the microscopic level under a specific loading history

is calculated firstly on the microscopic level, and afterwards is used as the constitutive law of the macroscopic structure. Mori-Tanaka and self-consistent methods are some of the most accurate methods that predict the homogeneous behaviour and can be used as constitutive equations for the macroscale model. These methods instead of computing in detail the fields for all the material points of the microstructure, it computes only the variables' average values for each phase resulting in high computational efficiency. Assuming that the averaged variables among each phase sub-domain still follows its continuum material behaviour, the microscopic problem is described by formulating the averaged stress-strain relation of each phase sub-domain and the interaction effect between different sub-domains :

$$f = \begin{cases} \langle \sigma \rangle_{\omega_r} = C_r : \langle \varepsilon \rangle_{\omega_r} \\ \langle \sigma \rangle_{\omega_r} = A_{rk} : \langle \sigma \rangle_{\omega_k} \\ \langle \varepsilon \rangle_{\omega_r} = B_{rk} : \langle \varepsilon \rangle_{\omega_k} \end{cases} \quad (1.4)$$

where  $\langle \dots \rangle$  is the volume averaging operator,  $\sigma$  and  $\varepsilon$  is the stress and strain,  $C_r$  is the stiffness tensor of constituent family  $r$ , and  $A_{rk}$ ,  $B_{rk}$  are the fourth order stress and strain concentration tensors between sub-domain  $\omega_r$  and  $\omega_k$  respectively. After the calculation of the concentration tensors, an analytical solution of the microscale problem can be obtained. The average response of the microstructure can be also computed to define the macroscopic behaviour of the heterogeneous material. The way these concentration tensors are calculated differ from method to method consisting the main difference between variants of mean-field homogenization methods.

Most of the mean-field methods can be extended to describe constitutive relations for nonlinear behaviours too. In order for this to happen, the sequential application of the formulations is not enough. Nonlinear material are always dependent on the loading history, and can be rate dependent. This means that a pre-computation of the effective properties of the material is not effective. The mean-field methods have to be applied for all the material points of the microstructure, each one having its own loading path, using lin-

earizing methods such as incremental formulation. Although the incremental formulation can capture with good accuracy the nonlinear behaviour of heterogeneous materials, it leads to a stiffer overall response resulting from the assumption of uniform properties in the matrix (66) (67) (68). This assumption has led to high interactions between the matrix and the inclusions, and consequently higher flow stresses. Many attempts have been made to overcome this limitation and improve the accuracy of the predictions (69) (70) by using isotropization methods on the Eshelby's tensor when calculating iteratively the effective tangent stiffness on the composite material. Besides the numerous isotropization procedures such as general isotropization and spectral decomposition techniques, more methods have been proposed to deal with the anisotropy of the tangent modulus in order to soften the composite response (71) (72). However, the method using the isotropization of the estimation of Eshelby tensor seems to lead to better predictions of the elastoplastic behaviour of composite materials.

Furthermore, Mori-Tanaka approach has been successfully extended to use the secant approach within a small strain formulation, to predict the behaviour of elastoplastic composites (73) (74) (75) (76). However, the non incremental nature of the secant procedure may prompt slight waviness for the stress-strain curve (74). In attempts to account for these fluctuations Qiu and Weng (77) use the shear energy in the matrix to define the homogeneous response of composite materials based on the incompressible behaviour hypothesis and Suquet (78) defines the linear comparison composite using a second-moment reference state to describe more general cases.

The restrictions of the secant approach, renewed the interest of the researchers on the incremental approaches. Brenner et al. (79) (80) and Gonzalez et al. (81) developed one of the first implementations of the affine formulation concept for the second-order homogenization. The good accuracy of these methods motivated Doghri et al. (82) to enhance the incremental linearization scheme by including second-order moment of the per-phase strain based on the Mori-Tanaka scheme. Even though the second-order approaches exhibit great accuracy, they are still very complex to implement.

Finally, integration of damage mechanics with mean-field homogenization approaches has been successfully implemented for local (83) and nonlocal (84) damage models and extended for anisotropic damage models (85) where the damage variable is represented by a tensor instead of a scalar variable.

In order to successfully implement nonlinear mean-field homogenization methods, a communication channel between the solver of the macro model and the system that performs the mean-field analysis should exist. This can be achieved by utilizing the user material subroutines feature that most of the commercial solvers offer.

### **1.3.5 Machine learning in multiscale modeling**

As mentioned earlier, most of the full field homogenization methods such as FE2 are time consuming because they are based on constitutive relations rather than phenomenological models (i.e. no parameters calibration is required) . This fact led the composites researchers to integrate machine learning methodologies in multiscale modeling. Deep learning network (DLN) model is an ideal tool to simulate nonlinear composite materials (**Figure 1.10**) and solve the homogenization problem, especially for two-phase composites such as fiber reinforced polymers.

The reasons for the successful integration of the machine learning methods to multiscale modelling can be summarized as follows:

- Machine learning methods can reduce effectively the computational time compared to conventional full field multiscale models
- Setting up surrogate models enables parallel computations
- Due to complete physics free modeling, machine learning models can link the input design parameters to the output parameters rather than conducting time consuming numerical computations in order to calculate them, such as in finite element analysis.

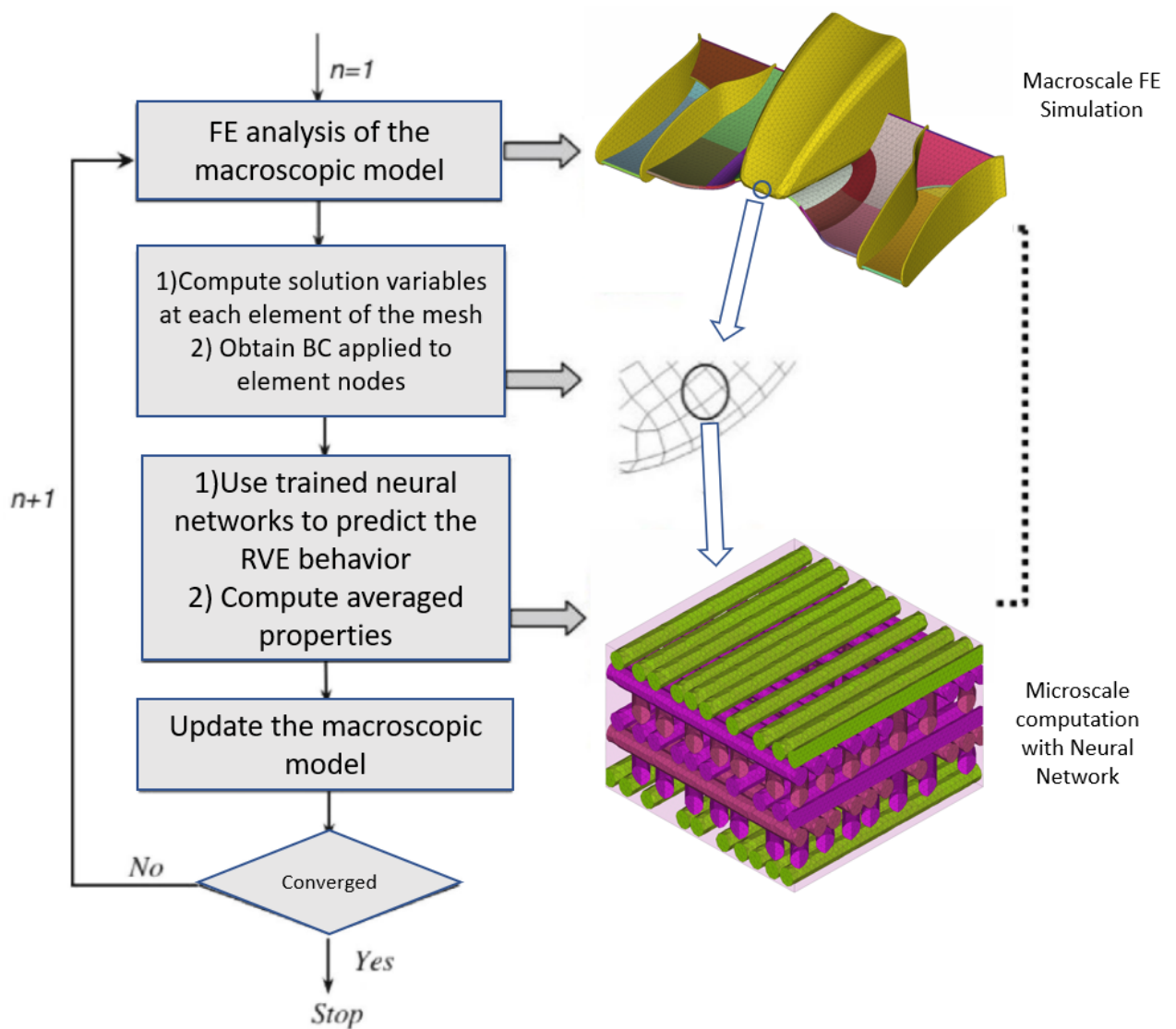


Figure 1.10: Multiscale modelling with Neural Networks

From structural perspective, DLN share some similarities with the FE2 homogenization method and specifically, the elements that have representative constitutive relations can be used as input layer in DLN, some parameters in the homogenization such as fiber aspect ratio, volume fraction and orientation can be chosen as fitting parameters and finally the homogenized macroscopic values such as stress and stiffness can be considered as output layer. Artificial neural network (ANN) models have been used successfully to simulate the homogenized material properties of biphasic composite materials (86). In (23) the ANN is firstly trained by data from a microscale model and then used to ap-

proximate the relation of macroscopic stress. In (87) the use of ANN was proposed to approximate a surface response that represents the corresponding effective (homogenized) stress and tangent stiffness modulus. Lu in (88) proposed the use of ANN trained by a series of nonlinear RVE simulation data to act as a role of nonlinear effective electric constitutive model. Wang and Sun (89) combined supervised machine learning models with classic constitutive models to simulate porous media coupled with various pore sizes and showed higher computation efficiency than the conventional FE2 method.

Liu et al. (90) (91) proposed an advanced data driven multiscale modeling technique which is termed as Deep Material Network (DMN) algorithm. This method is based on machine learning and RVE homogenization theories. For multiscale modelling the basic procedures are the same regardless the machine learning algorithm that is applied. The main three steps that it consists of are:

1. The sampling phase, that includes the design of experiment and the generation of the set of training data, such as for different cases of loading conditions. A huge dataset generated from a lot of preliminary analysis (e.g RVE analysis) is needed to assemble the data and construct the training database.
2. The training phase, where the sampling data were applied for the training of the deep material network to obtain the optimal fitting parameters. In this step, read-in data of database and preprocess of the data to remove noise, smooth and normalize the set may be needed. Also testing of database may be performed to test the condition of the trained network. Plotting of errors may be applied to visualize the fitting condition of the trained model.
3. The prediction phase, where the trained deep material network was used to extrapolate some nonlinear cases in material design such as plasticity and failure. Comparison between the produced results of the trained model and other conventional methods to decide the efficiency and accuracy of the machine learning method.

The sampling and the training step are considered an offline stage that it needs to be

completed only once but will be applicable to many cases, while the prediction step is termed as online stage.

For multiscale modelling the basic procedures are the same regardless the machine learning algorithm that is applied.

In the recent years many researchers have already applied machine learning methods for computational homogenization methods to several material models such as hyperelastic (92), elasto-plastic (93), visco-plastic (94) among others. It is worth mentioning that several studies are concerned about utilizing the machine learning methods to speed up the conventional finite element methods not only for the prediction of mechanical properties but also for electrical and thermodynamics properties.

## 1.4 Transition between scales

### 1.4.1 The Eshelby Tensor

In 1957, Eshelby introduced the solution of the single inclusion problem, that is considered to be one of the major achievements in the analytical approach for predicting the effective material properties of heterogeneous microstructures. Most of the mean-field homogenization models are based on this analysis that offers a general solution for one ellipsoidal particle embedded in an infinite matrix in linear elasticity. Eshelby found that for a homogeneous isotropic infinite body which contains a single ellipsoidal inclusion subjected to a uniform eigenstrain  $\varepsilon^*$ , the resulting strain field within the inclusion is uniform. He suggested a tensor that relates the strain the ellipsoidal subregion would possess if it was unconstrained by the rest of the medium to the elastic strain  $\varepsilon_{ij}^{el}$  of the constrained subregion, and it can be easily extended to cases where the infinite matrix and the inclusion has different material properties. The total strain can be expressed as:

$$\varepsilon_{ij} = \varepsilon_{ij}^{el} + \varepsilon_{ij}^* \quad (1.5)$$

and can be rewritten including Eshelby's fourth order tensor as :

$$\varepsilon_{ij} = S_{ijkl}^* \varepsilon_{kl}^* \quad (1.6)$$

The tensor  $S^*$  is a function of the Poisson's ratio of the infinite matrix and the semi-axes of the ellipsoid. Analytical presentation of the calculation of Eshelby's tensor can be seen in chapter 3.1. The strain and stress fields inside the ellipsoid are uniform and outside the ellipsoid subregion are nonuniform but it is possible to reduce the results to a form that involves only three elliptic integrals (95). The stress field using Hooke's law can be calculated by :

$$\sigma_{ij} = C_{ijkl} \varepsilon_{kl}^{el} \quad (1.7)$$

and by using the Eshelby's tensor can obtain the form:

$$\sigma_{ij} = C_{ijkl} (S_{klpq}^* \varepsilon_{pq}^* - \varepsilon_{kl}^*) \quad (1.8)$$

## 1.4.2 Transition from macro to microscale

The starting point of the multiscale algorithms is to distribute the strain (for elasticity) or strain rate tensor (for nonlinear materials) to the individual constituents. This problem, for most of the mean-field approaches, is solved by adopting the single inclusion problem solution of Eshelby. After calculating the Eshelby's tensor, which demands integral calculations containing the fiber's aspect ratio and the Poisson's ratio of the matrix material, it is trivial to calculate the strain concentration tensors, as defined by the method each time. Using the strain concentration tensors, one is able to distribute the strains (and strain increments) to each constituent as shown in the following equations:

$$\Delta \varepsilon_m = [V_f \mathbf{B}^\varepsilon + (1 - V_f) \mathbf{I}]^{-1} : \Delta \varepsilon \quad (1.9)$$

$$\Delta\varepsilon_f = \mathbf{B}^\varepsilon : \Delta\varepsilon_m = \mathbf{B}^\varepsilon : [V_f\mathbf{B}^\varepsilon + (1 - V_f)\mathbf{I}]^{-1} : \Delta\varepsilon \quad (1.10)$$

with  $\mathbf{B}^\varepsilon$  given by

$$\mathbf{B}^\varepsilon = [\mathbf{I} + \mathbf{E} : (\mathbf{C}_m^{-1} : \mathbf{C}_f - \mathbf{I})]^{-1}, \quad (1.11)$$

where  $\mathbf{I}$  is the fourth order unit tensor,  $\mathbf{E}$  is the Eshelby's tensor,  $\mathbf{C}_m$ ,  $\mathbf{C}_f$  the stiffness tensor for matrix and fiber respectively and  $V_f$  the fiber's volume fraction.

Finally, knowing the strain (or strain increment) and the properties of each constituent, the stress (or stress increment) for the matrix and fiber can be calculated by adopting the constitutive laws that each phase follows.

### 1.4.3 Transition from micro to macroscale

In order to consider the microstructure influence on the composite material's macroscale response, a link between the macro and micro levels is made through the RVE. Since the RVE is a statistical representation of microstructure, it is independent of the fluctuations on the structural scale. In other words, the RVE represents all the elementary volumes that correspond to any point of the macro model. Using a strain driven problem as an example, the macroscopic strain is known, while the effective material stiffness and the macroscopic stress are computed from a microscale boundary condition.

The result of this transition is to obtain a homogenized stress response after applying the appropriate material model for each of the constituents

$$\hat{\sigma}_{ij} = \frac{1}{V} \int_V \sigma_{ij} dV. \quad (1.12)$$

As eq. (1.12) indicates, the homogenized macroscopic stress tensor  $\hat{\sigma}_{ij}$  is obtained as the volume average of the microscopic stress fields  $\sigma_{ij}$  inside the RVE.

## References

- [1] S. Nemat-Nasser, M. Lori, and S. K. Datta, “Micromechanics: Overall Properties of Heterogeneous Materials,” *Journal of Applied Mechanics*, vol. 63, no. 2, pp. 561–561, 1996.
- [2] P. Castañeda, “The effective mechanical properties of nonlinear isotropic composites,” *Journal of the Mechanics and Physics of Solids*, vol. 39, no. 1, pp. 45–71, 1991.
- [3] P. Ponte Castañeda, “Second-order homogenization estimates for nonlinear composites incorporating field fluctuations: I—theory,” *Journal of the Mechanics and Physics of Solids*, vol. 50, no. 4, pp. 737–757, 2002.
- [4] J. D. Eshelby, “The Determination of the Elastic Field of an Ellipsoidal Inclusion, and Related Problems,” *Proceedings of the Royal Society of London Series A*, vol. 241, pp. 376–396, 1957.
- [5] S. Nemat-Nasser, M. Lori, and S. K. Datta, “Micromechanics: Overall Properties of Heterogeneous Materials,” *Journal of Applied Mechanics*, vol. 63, 1996.
- [6] A. Sciegaj, P. Grassl, K. Lundgren, F. Larsson, and K. Runesson, “On periodic boundary conditions in variationally consistent homogenisation of beams and plates,” in *32nd Nordic Seminar on Computational Mechanics*, pp. 150–153, 2019.
- [7] J. Schröder, *A numerical two-scale homogenization scheme: the FE2-method*, pp. 1–64. Vienna: Springer Vienna, 2014.
- [8] F. Feyel and J.-L. Chaboche, “Fe2 multiscale approach for modelling the elastoviscoplastic behaviour of long fibre sic/ti composite materials,” *Computer Methods in Applied Mechanics and Engineering*, vol. 183, no. 3, pp. 309–330, 2000.
- [9] V. Kouznetsova, M. Geers, and W. Brekelmans, “Multi-scale second-order computational homogenization of multi-phase materials: a nested finite element solu-

- tion strategy,” *Computer Methods in Applied Mechanics and Engineering*, vol. 193, no. 48, pp. 5525–5550, 2004.
- [10] S. Nezamabadi, M. Potier-Ferry, H. Zahrouni, and J. Yvonnet, “Compressive failure of composites: A computational homogenization approach,” *Composite Structures*, vol. 127, pp. 60–68, 2015.
- [11] Y. Cong, S. Nezamabadi, H. Zahrouni, and J. Yvonnet, “Multiscale computational homogenization of heterogeneous shells at small strains with extensions to finite displacements and buckling,” *International Journal for Numerical Methods in Engineering*, vol. 104, no. 4, pp. 235–259, 2015.
- [12] M. Praster, M. Klassen, and S. Klinkel, “An adaptive fe2 approach for fiber–matrix composites,” *Computational Mechanics*, vol. 63, pp. 1333–1350, 2018.
- [13] R. van Tuijl, J. Remmers, and M. Geers, “Integration efficiency for model reduction in micro-mechanical analyses,” *Computational Mechanics*, vol. 62, pp. 151–169, 2018.
- [14] J. Hernandez, J. Oliver, A. Huespe, M. Caicedo-Silva, and J. Cante, “High-performance model reduction techniques in computational multiscale homogenization,” *Computer Methods in Applied Mechanics and Engineering*, vol. 276, pp. 149–189, 2014.
- [15] J. Hernandez, M. Caicedo-Silva, and A. Ferrer Ferre, “Dimensional hyper-reduction of nonlinear finite element models via empirical cubature,” *Computer Methods in Applied Mechanics and Engineering*, vol. 313, pp. 687–722, 2016.
- [16] J. Yvonnet, H. Zahrouni, and M. Potier-Ferry, “A model reduction method for the post-buckling analysis of cellular microstructures,” *Computer Methods in Applied Mechanics and Engineering*, vol. 197, no. 1, pp. 265–280, 2007.

- [17] E. Monteiro, J. Yvonnet, and Q. He, “Computational homogenization for nonlinear conduction in heterogeneous materials using model reduction,” *Computational Materials Science*, vol. 42, no. 4, pp. 704–712, 2008.
- [18] N. Damil and M. Potier-Ferry, “A generalized continuum approach to predict local buckling patterns of thin structures,” *European Journal of Computational Mechanics*, vol. 17, no. 5-7, pp. 945–956, 2008.
- [19] N. Damil and M. Potier-Ferry, “Influence of local wrinkling on membrane behaviour: A new approach by the technique of slowly variable fourier coefficients,” *Journal of the Mechanics and Physics of Solids*, vol. 58, no. 8, pp. 1139–1153, 2010.
- [20] D. Somer, E. de Souza Neto, W. Dettmer, and D. Perić, “A sub-stepping scheme for multi-scale analysis of solids,” *Computer Methods in Applied Mechanics and Engineering*, vol. 198, no. 9, pp. 1006–1016, 2009.
- [21] F. Reis and F. Andrade Pires, “An adaptive sub-incremental strategy for the solution of homogenization-based multi-scale problems,” *Computer Methods in Applied Mechanics and Engineering*, vol. 257, pp. 164–182, 2013.
- [22] F. Otero, X. Martinez, S. Oller, and O. Salomon, “An efficient multi-scale method for non-linear analysis of composite structures,” *Composite Structures*, vol. 131, pp. 707–719, 2015.
- [23] J. Unger, “An fe<sup>2</sup>-x1 approach for multiscale localization phenomena,” *Journal of the Mechanics and Physics of Solids*, vol. 61, pp. 928–948, 2012.
- [24] J. Aboudi, “A continuum theory for fiber-reinforced elastic-viscoplastic composites,” *International Journal of Engineering Science*, vol. 20, no. 5, pp. 605–621, 1982.
- [25] M. Paley and J. Aboudi, “Micromechanical analysis of composites by the generalized cells model,” *Mechanics of Materials*, vol. 14, no. 2, pp. 127–139, 1992.

- [26] J. Aboudi, “Micromechanical analysis of thermo-inelastic multiphase short-fiber composites,” *Composites Engineering*, vol. 5, no. 7, pp. 839–850, 1995.
- [27] J. Aboudi, “Micromechanical Analysis of Composites by the Method of Cells,” *Applied Mechanics Reviews*, vol. 42, no. 7, pp. 193–221, 1989.
- [28] G. J. Dvorak, “Transformation field analysis of inelastic composite materials,” *Proceedings: Mathematical and Physical Sciences*, vol. 437, no. 1900, pp. 311–327, 1992.
- [29] J. Aboudi, M.-J. Pindera, and S. M. Arnold, “Linear thermoelastic higher-order theory for periodic multiphase materials,” *Journal of Applied Mechanics*, vol. 68, no. 5, pp. 697–707, 2001.
- [30] J. Aboudi, M.-J. Pindera, and S. M. Arnold, “Higher-order theory for periodic multiphase materials with inelastic phases,” *International Journal of Plasticity*, vol. 19, pp. 805–847, 2003.
- [31] G. Z. Voyiadjis and B. Deliktas, “Damage in mmcs using the gmc: theoretical formulation,” *Composites Part B: Engineering*, vol. 28, no. 5, pp. 597–611, 1997.
- [32] G. Voyiadjis and Z. Guelzim, “A coupled incremental damage and plasticity theory for metal matrix composites,” *Journal of the Mechanical Behavior of Materials*, vol. 6, no. 3, pp. 193–220, 1996.
- [33] D. Pahr and S. Arnold, “The applicability of the generalized method of cells for analyzing discontinuously reinforced composites,” *Composites Part B: Engineering*, vol. 33, pp. 153–170, 2001.
- [34] J. Aboudi, M.-J. Pindera, and S. Arnold, “High-fidelity generalization method of cells for inelastic periodic multiphase materials,” *NASA TM-2002-211469*, 2002.
- [35] H. Moulinec and P. Suquet, “A fast numerical method for computing the linear and

nonlinear mechanical properties of composites,” *Comptes Rendus de l’Académie des sciences. Série II. Mécanique, physique, chimie, astronomie*, 1994.

- [36] B. A. Lippmann and J. Schwinger, “Variational principles for scattering processes. i,” *Phys. Rev.*, vol. 79, pp. 469–480, 1950.
- [37] M. Frigo and S. Johnson, “The design and implementation of FFTW3,” *Proceedings of the IEEE*, vol. 93, pp. 216 – 231, 2005.
- [38] L. Dalcin, M. Mortensen, and D. E. Keyes, “Fast parallel multidimensional FFT using advanced mpi,” *Journal of Parallel and Distributed Computing*, vol. 128, pp. 137–150, 2019.
- [39] K. Herrmann, W. Müller, and S. Neumann, “Linear and elastic–plastic fracture mechanics revisited by use of fourier transforms – theory and application,” *Computational Materials Science*, vol. 16, no. 1, pp. 186–196, 1999.
- [40] C. Moos, *An algorithm for damage mechanics based on the fast fourier transform*. doctoralthesis, Ruhr-Universität Bochum, Universitätsbibliothek, 2013.
- [41] J. Spahn, H. Andrä, M. Kabel, and R. Müller, “A multiscale approach for modeling progressive damage of composite materials using fast fourier transforms,” *Computer Methods in Applied Mechanics and Engineering*, vol. 268, pp. 871–883, 2014.
- [42] Q. Zhu and J. Yvonnet, “An incremental–iterative method for modeling damage evolution in voxel-based microstructure models,” *Computational Mechanics*, vol. 55, pp. 371–382, 2014.
- [43] F. Bernachy-Barbe, L. Gélébart, M. Bornert, J. Crépin, and C. Sauder, “Anisotropic damage behavior of sic/sic composite tubes: Multiaxial testing and damage characterization,” *Composites Part A: Applied Science and Manufacturing*, vol. 76, pp. 281–288, 2015.

- [44] J. Li, S. Meng, X. Tian, F. Song, and C. Jiang, “A non-local fracture model for composite laminates and numerical simulations by using the FFT method,” *Composites Part B: Engineering*, vol. 43, no. 3, pp. 961–971, 2012.
- [45] M. Boeff, F. Gutknecht, P. S. Engels, A. Ma, and A. Hartmaier, “Formulation of nonlocal damage models based on spectral methods for application to complex microstructures,” *Engineering Fracture Mechanics*, vol. 147, pp. 373–387, 2015.
- [46] Y. Chen, D. Vasiukov, L. Gélébart, and C. H. Park, “Fast fourier transform solver for damage modeling of composite materials,” *JMST Advances*, vol. 1, pp. 49–55, 2019.
- [47] Y. Chen, D. Vasiukov, L. Gélébart, and C. H. Park, “A FFT solver for variational phase-field modeling of brittle fracture,” *Computer Methods in Applied Mechanics and Engineering*, vol. 349, pp. 167–190, 2019.
- [48] F. Ernesti, M. Schneider, and T. Böhlke, “Fast implicit solvers for phase-field fracture problems on heterogeneous microstructures,” *Computer Methods in Applied Mechanics and Engineering*, vol. 363, pp. 112–793, 2020.
- [49] N. Lahellec, J. C. Michel, H. Moulinec, and P. Suquet, “Analysis of inhomogeneous materials at large strains using fast fourier transforms,” in *IUTAM Symposium on Computational Mechanics of Solid Materials at Large Strains* (C. Miehe, ed.), (Dordrecht), pp. 247–258, Springer Netherlands, 2003.
- [50] R. Ma and T. J. Truster, “FFT-based homogenization of hypoelastic plasticity at finite strains,” *Computer Methods in Applied Mechanics and Engineering*, vol. 349, pp. 499–521, 2019.
- [51] J. Nmeček, V. Králík, and J. Vondřejc, “A two-scale micromechanical model for aluminium foam based on results from nanoindentation,” *Computers and Structures*, vol. 128, pp. 136–145, 2013.

- [52] M. B. Youssef, F. Lavergne, K. Sab, K. Miled, and J. Neji, “Upscaling the elastic stiffness of foam concrete as a three-phase composite material,” *Cement and Concrete Research*, vol. 110, pp. 13–23, 2018.
- [53] W. Pabst, T. Uhlířová, E. Gregorová, and A. Wiegmann, “Young’s modulus and thermal conductivity of closed-cell, open-cell and inverse ceramic foams – model-based predictions, cross-property predictions and numerical calculations,” *Journal of the European Ceramic Society*, vol. 38, pp. 2570–2578, 2018.
- [54] W. Pabst, T. Uhlířová, and E. Gregorová, “Shear and bulk moduli of isotropic porous and cellular alumina ceramics predicted from thermal conductivity via cross-property relations,” *Ceramics International*, vol. 44, no. 7, pp. 8100–8108, 2018.
- [55] T. Uhlířová, V. Necina, and W. Pabst, “Modeling of young’s modulus and thermal conductivity evolution of partially sintered alumina ceramics with pore shape changes from concave to convex,” *Journal of the European Ceramic Society*, vol. 38, no. 8, pp. 3004–3011, 2018.
- [56] T. Uhlířová and W. Pabst, “Phase mixture modeling of the grain size dependence of young’s modulus and thermal conductivity of alumina and zirconia ceramics,” *Journal of the European Ceramic Society*, vol. 40, no. 8, pp. 3181–3190, 2020.
- [57] A. Vidyasagar, W. Tan, and D. Kochmann, “Predicting the effective response of bulk polycrystalline ferroelectric ceramics via improved spectral phase field methods,” *Journal of the Mechanics and Physics of Solids*, vol. 106, pp. 133–151, 2017.
- [58] T. Uhlířová and W. Pabst, “Poisson’s ratio of porous and cellular materials with randomly distributed isometric pores or cells,” *Journal of the American Ceramic Society*, vol. 103, pp. 6961–6977, 2020.
- [59] T. Uhlířová and W. Pabst, “Thermal conductivity and young’s modulus of cubic-cell metamaterials,” *Ceramics International*, vol. 45, no. 1, pp. 954–962, 2019.

- [60] T. Uhlířová and W. Pabst, “Conductivity and young’s modulus of porous metamaterials based on gibson-ashby cells,” *Scripta Materialia*, vol. 159, pp. 1–4, 2019.
- [61] S. Lucarini, *Micromechanics based fatigue modeling using Fast Fourier Transform based homogenization*. PhD thesis, Higher Technical School of Civil Engineers, 2020.
- [62] W. Tian, L. Qi, J. Liang, X. Chao, and J. Zhou, “Evaluation for elastic properties of metal matrix composites with randomly distributed fibers: Two-step mean-field homogenization procedure versus fe homogenization method,” *Journal of Alloys and Compounds*, vol. 658, pp. 241–247, 2015.
- [63] T. Mori and K. Tanaka, “Average stress in matrix and average elastic energy of materials with misfitting inclusions,” *Acta Metallurgica*, vol. 21, no. 5, pp. 571 – 574, 1973.
- [64] P. Kanouté, D. Boso, J. Chaboche, and B. Schrefler, “Multiscale methods for composites: A review,” *Archives of Computational Methods in Engineering*, vol. 16, pp. 31–75, 2009.
- [65] M. Geers, V. Kouznetsova, and W. Brekelmans, “Multi-scale computational homogenization: Trends and challenges,” *Journal of Computational and Applied Mathematics*, vol. 234, no. 7, pp. 2175–2182, 2010. Fourth International Conference on Advanced Computational Methods in Engineering (ACOMEN 2008).
- [66] P. Lipinski, A. Naddari, and M. Berveiller, “Recent results concerning the modelling of polycrystalline plasticity at large strains,” *International Journal of Solids and Structures*, vol. 29, no. 14, pp. 1873–1881, 1992.
- [67] P. Suquet, “Overall properties of nonlinear composites,” in *IUTAM Symposium on Micromechanics of Plasticity and Damage of Multiphase Materials* (A. Pineau and A. Zaoui, eds.), (Dordrecht), pp. 149–156, Springer Netherlands, 1996.

- [68] P. Suquet, “Effective properties of nonlinear composites,” in *Continuum Micromechanics*, (Vienna), Springer Vienna, 1997.
- [69] T. Jiang and J. Shao, “On the incremental approach for nonlinear homogenization of composite and influence of isotropization,” *Computational Materials Science*, vol. 46, no. 2, pp. 447–451, 2009.
- [70] I. Doghri and A. Ouair, “Homogenization of two-phase elasto-plastic composite materials and structures: Study of tangent operators, cyclic plasticity and numerical algorithms,” *International Journal of Solids and Structures*, vol. 40, no. 7, pp. 1681 – 1712, 2003.
- [71] O. Pierard and I. Doghri, “Study of various estimates of the macroscopic tangent operator in the incremental homogenization of elastoplastic composites,” *International Journal for Multiscale Computational Engineering*, vol. 4, pp. 521–543, 2006.
- [72] A. Zaoui, “Continuum micromechanics: Survey,” *Journal of Engineering Mechanics*, vol. 128, no. 8, pp. 808–816, 2002.
- [73] G. Tandon and G. Weng, “A theory of particle-reinforced plasticity,” *Journal of Applied Mechanics*, vol. 54, pp. 822–827, 1988.
- [74] W. Yanchao and Z. Huang, “A review of analytical micromechanics models on composite elastoplastic behaviour,” *Procedia Engineering*, vol. 173, pp. 1283–1290, 2017.
- [75] L. Wu, L. Noels, L. Adam, and I. Doghri, “A combined incremental-secant mean-field homogenization scheme with per-phase residual strains for elasto-plastic composites,” *International Journal of Plasticity*, vol. 51, pp. 80–102, 2013.
- [76] L. Wu, L. Noels, L. Adam, and I. Doghri, “An implicit-gradient-enhanced incremental-secant mean-field homogenization scheme for elasto-plastic compos-

- ites with damage,” *International Journal of Solids and Structures*, vol. 50, no. 24, pp. 3843–3860, 2013.
- [77] Y. P. Qiu and G. J. Weng, “A Theory of Plasticity for Porous Materials and Particle-Reinforced Composites,” *Journal of Applied Mechanics*, vol. 59, no. 2, pp. 261–268, 1992.
- [78] P. Suquet, “Overall properties of nonlinear composites,” in *IUTAM Symposium on Micromechanics of Plasticity and Damage of Multiphase Materials*, pp. 149–156, Springer Netherlands, 1996.
- [79] R. Brenner, O. Castelnau, and P. Gilormini, “A modified affine theory for the overall properties of nonlinear composites,” *Comptes Rendus de l’Académie des Sciences - Series IIB - Mechanics*, vol. 329, no. 9, pp. 649–654, 2001.
- [80] R. Brenner, O. Castelnau, and L. Badea, “Mechanical field fluctuations in polycrystals estimated by homogenization techniques,” *Proceedings of The Royal Society A: Mathematical, Physical and Engineering Sciences*, vol. 460, pp. 3589–3612, 2004.
- [81] C. González, J. Segurado, and J. Llorca, “Numerical simulation of elasto-plastic deformation of composites: Evolution of stress microfields and implications for homogenization models,” *Journal of the Mechanics and Physics of Solids*, vol. 52, pp. 1573–1593, 2004.
- [82] I. Doghri, L. Brassart, L. Adam, and J.-S. Gérard, “A second-moment incremental formulation for the mean-field homogenization of elasto-plastic composites,” *International Journal of Plasticity*, vol. 27, pp. 352–371, 2011.
- [83] S. Kammoun, L. Brassart, I. Doghri, L. Delannay, and G. Robert, “Micromechanical modeling of short glass-fiber reinforced thermoplastics-isotropic damage of pseudo-grains,” *AIP Conference Proceedings*, vol. 1353, 2011.

- [84] L. Wu, L. Noels, L. Adam, and I. Doghri, “Non-local damage-enhanced mfh for multiscale simulations of composites,” in *Composite Materials and Joining Technologies for Composites, Volume 7* (E. Patterson, D. Backman, and G. Cloud, eds.), (New York, NY), pp. 115–121, Springer New York, 2013.
- [85] L. Wu, F. Sket, J. Molina-Aldareguia, A. Makradi, L. Adam, I. Doghri, and L. Noels, “A study of composite laminates failure using an anisotropic gradient-enhanced damage mean-field homogenization model,” *Composite Structures*, vol. 126, pp. 246–264, 2015.
- [86] N. Huber and C. Tsakmakis, “A neural network tool for identifying the material parameters of a finite deformation viscoplasticity model with static recovery,” *Computer Methods in Applied Mechanics and Engineering*, vol. 191, no. 3, pp. 353–384, 2001.
- [87] B. A. Le, J. Yvonnet, and Q.-C. He, “Computational homogenization of nonlinear elastic materials using neural networks,” *International Journal for Numerical Methods in Engineering*, vol. 104, no. 12, pp. 1061–1084, 2015.
- [88] X. Lu, D. G. Giovanis, J. Yvonnet, V. Papadopoulos, F. Detrez, and J. Bai, “A data-driven computational homogenization method based on neural networks for the nonlinear anisotropic electrical response of graphene/polymer nanocomposites,” *Computational Mechanics*, vol. 64, p. 307, 2019.
- [89] K. Wang and W. Sun, “A multiscale multi-permeability poroplasticity model linked by recursive homogenizations and deep learning,” *Computer Methods in Applied Mechanics and Engineering*, vol. 334, pp. 337–380, 2018.
- [90] X. Liu, F. Tao, H. Du, W. Yu, and K. Xu, “Learning nonlinear constitutive laws using neural network models based on indirectly measurable data,” *Journal of Applied Mechanics*, vol. 87, pp. 1–10, 2020.

- [91] X. Liu, F. Tao, and W. Yu, “A neural network enhanced system for learning non-linear constitutive law and failure initiation criterion of composites using indirectly measurable data,” *Composite Structures*, vol. 252, pp. 112–658, 2020.
- [92] V. M. Nguyen-Thanh, X. Zhuang, and T. Rabczuk, “A deep energy method for finite deformation hyperelasticity,” *European Journal of Mechanics - A/Solids*, vol. 80, pp. 103874–, 2020.
- [93] L. Wu, K. Zulueta, Z. Major, A. Arriaga, and L. Noels, “Bayesian inference of non-linear multiscale model parameters accelerated by a deep neural network,” *Computer Methods in Applied Mechanics and Engineering*, vol. 360, p. 112693, 2020.
- [94] M. Stoffel, F. Bamer, and B. Markert, “Artificial neural networks and intelligent finite elements in non-linear structural mechanics,” *Thin-Walled Structures*, vol. 131, pp. 102–106, 2018.
- [95] T. Mura, *Micromechanics of Defects in Solids*. Martinus Nijhoff Publishers, 1988.



## **Chapter 2**

# **Computational Multi-Scale Modelling of Fiber-Reinforced Composite Materials**

As mentioned in the previous chapter, there are many multiscale methods that can predict the homogeneous behavior of non homogeneous materials. The most accurate between the homogenization methods is by solving the RVE boundary value problem with the finite element method. Then by averaging the stress and strain fields the macroscopic properties can be predicted. However, this method is the least computationally efficient and cannot be easily applied to large scale problems. In such cases, different homogenization methods are preferred that are mainly analytical or semi- analytical and can predict the homogenized properties of a material point instantly, knowing the properties of the microstructure constituents. Furthermore, there are many difficulties when generating and discretizing a statistically representative volume element which is a prerequisite in order for numerical homogenization to be applied.

The main purpose of this chapter is to compare the widely used mean-field homogenization method of Mori-Tanaka with the FE homogenization method. Initially, the results are compared for the linear elastic case and three different material symmetry

cases (isotropic, transversely isotropic, orthotropic). In the second part of this chapter, the mean-field method has been extended to work for elasto-plastic matrix and elastic fibers, and compared again with the results of the nonlinear FE homogenization method. This time, the stress strain curves of the materials are compared as opposed to the elastic case where the homogenized elastic properties calculated by each method are compared. Moreover, an algorithm for generating microstructures is presented, based on the Random Sequential Adsorption method (RSA), extended to account for periodicity.

In the sequence, a cross-ply fiber-reinforced composite in uniaxial tension is modelled using a mesoscale and a microscale approach comparing the results from both the analyses. The use of multiscale modelling gives directly the macroscopic constitutive behaviour of the structures based on its microscopically heterogeneous representative volume element (RVE). In the meso-scale approach the material of each layer is modelled as a homogeneous transversely isotropic material whose properties resulted from a numerical homogenization analysis. One of the main advantages of microscale modelling is the ability to simulate damage mechanisms such as matrix cracking, delaminations of the matrix-fiber interface and fiber-damage. A comparison of the results between the simulations of both scales is performed. In the meso-scale model stochasticity has been introduced, by assigning interfacial strength which follows a normal distribution, in order to predict cracking initiation, propagation and saturation at the matrix material. The stresses at the crack tips are compared with the stress fields around the cracks from the microscale analysis and the results are in good agreement.

## **2.1 Introduction**

In order to reduce time consuming and expensive experimental efforts, analytical and numerical modelling approaches have been developed to simulate real phenomena that occur in the microscale of composite materials. Homogenization methods are powerful tools helping the engineer towards the design and calculation of homogeneous mechani-

cal, thermal expansion, conductivity and other properties considering the microstructure response of each constituent. There are three categories of methods in the relevant literature. The phenomenological-empirical models (Voigt, Reuss, Rule of mixtures, Halpin-Tsai, Chamis), the mean-field (semi-analytical) methods based on Eshelby's single inclusion solution (1) (Mori-Tanaka, dilute approximation, self-consistent) and the numerical homogenization method (2). The first category, is the least computationally expensive but with poor accuracy, ignoring microstructure information such as the geometry of fillers and the orientation. The second category, is the most explored category, firstly applied for linear elasticity and has been extended to several material models such as elasto-plasticity, thermo-elasto-plasticity, viscoelasticity, viscoplasticity, coupling plasticity with damage, combining computational efficiency, good accuracy of macroscopic response, but with low accuracy regarding the prediction of the micro-fields through strain concentration tensors. The numerical homogenization is the most accurate method in both the microscale and the macroscale but has its own disadvantages. It is the most computationally expensive methodology, and there are some complications regarding the model generation and discretization of the whole RVE. It should be mentioned that numerical homogenization can potentially be used in the elastic region of materials but research work is still ongoing for more complicated material models.

## **2.2 Mean-field Homogenization**

The most commonly used mean-field approach is the Mori-Tanaka (3). It assumes that each inclusion behaves like an isolated inclusion and the strain in the matrix is considered as the far-field strain and can be used for multiple inclusions of variable shape and orientation. The results from the Mori-Tanaka approach are in good agreement with experimental measurements especially for low volume fraction of inclusions.

In case of composite material with multiple inclusions and random orientations the Mori-Tanaka scheme can produce unphysical results. In such cases a multi-step formula-

tion is adopted. The microstructure is discretized in pseudo-grains and each pseudo-grain contains only the matrix material and one family of inclusions. Each pseudo-grain is homogenized following the Mori-Tanaka formulation. In the next step all pseudo-grains are homogenized to a single material using Voigt scheme. This method ensures physical results, symmetric stiffness and thermal expansion matrices.

Mean-field homogenization methods are extremely efficient and are used with molding simulations, bridging the gap between process simulation and structural analysis. This can be done by using the fiber orientations resulted from the simulation of the manufacturing process and use homogenization techniques to account for the composite material's response in elastic and plastic regions and also to predict damage in multiple scales. Those homogenization procedures can only be applied in elasticity. In order to avoid this constraint and apply this formulation in elasto-plasticity a linear comparison composite is identified by linearizing stress-strain behaviour of the plastic region (4). In this case instead of  $\sigma = C \epsilon$ , where  $\sigma$  and  $\epsilon$  are the elastic stresses and strains,  $C$  is the stiffness matrix, from incremental formulation of plasticity one has  $\sigma' = C_{tang} \epsilon'$ , where  $\sigma'$  and  $\epsilon'$  are stress and strain rates and  $C_{tang}$  is the tangent stiffness matrix of the material. Discretising this relation over a time interval  $[t_n, t_{n+1}]$ , the rate form can be converted to the following incremental form  $\Delta\sigma = C_{tang} \Delta\epsilon$ . Finally, using the incremental form, the homogenization procedure can be applied for each time increment.

## 2.3 Numerical homogenization

In a numerical simulation, it is not efficient to simulate everything as far as the structure is concerned, especially when there are fast analytical models that can sufficiently describe and solve the task. Generally, we choose an area of interest in which we conduct a numerical simulation where limitations of analytical models exist. There are cases where mean-field homogenization methods may face significant limitations, thus numerical simulations become necessary to calculate homogeneous properties of a composite material.

Most of the numerical methods invoke only linear material laws with small deformation theory. However, during the last years more complicated numerical methods have been developed for nonlinear elasticity (hyper or visco – elasticity) and generally nonlinear material behaviour.

### 2.3.1 Microstructure generation method

One of the most important and difficult tasks of numerical homogenization is the construction of the microstructure. In order to be representative of the total composite structure the size of the Representative Volume Element (RVE) is of great importance and the RVE itself must contain enough information about the microstructure. The most common method to create microstructure models with stochasticity about the fillers' position and orientation is the RSA (Random Sequential Adsorption) method (5) which is used extensively in this study. According to this method fibers are inserted into the RVEs space sequentially at random positions (using a random number generator), and are checked for intersection with the already placed fibers. If any kind of intersection exists, then the placing of inclusion fails and the inclusion is discarded. The procedure stops when the number of failed attempts reach a maximum attempts threshold or when the required volume fraction is achieved. A flow chart of the RVE generation method with periodically placed inclusions is shown in **Figure 2.1**.

In order to ensure periodicity in the RVE generation algorithm intersection between the newly placed inclusion and the RVE faces, edges and vertices must be checked. In the first case of intersection with a face, assuming that the cubic RVE has length  $L$  and volume  $L^3$ , an identical inclusion must be placed in the opposite face translated by  $L$  (**Figure 2.2**, Top Left). In case of edge intersection, three more identical inclusions must be placed in the other three parallel edges. One inclusion will be translated by  $L$  in x-direction, the other will be translated by  $L$  in the y-direction, and the last one will be translated by  $L$  in both the x- and y-directions as shown in **Figure 2.2** top right. In case where the inclusion volume contains one of the RVE vertices, then seven more identical inclusions

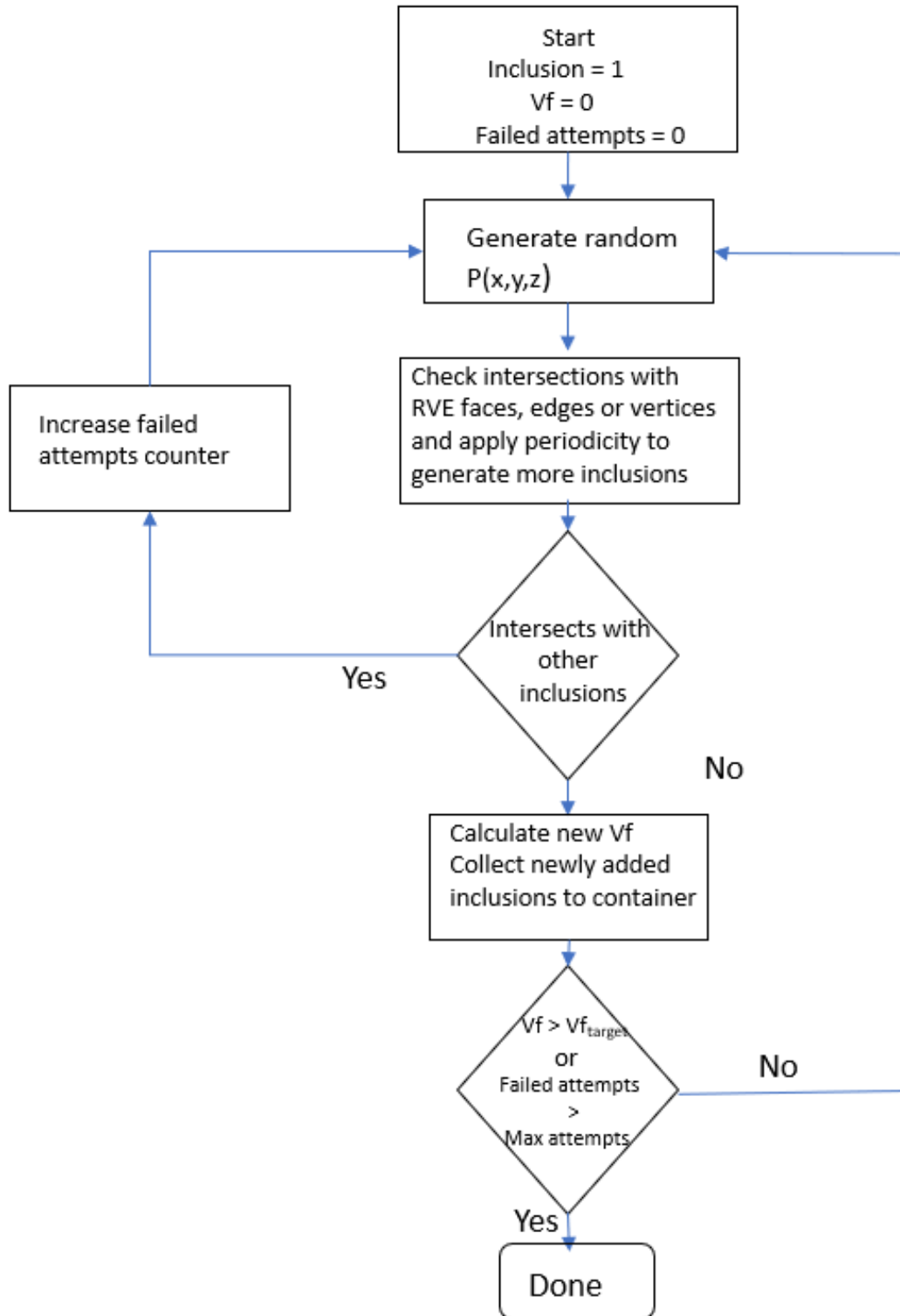


Figure 2.1: Method for RVE generation with periodically placed inclusions

must be placed in the rest of the vertices respectively (**Figure 2.2**, Bottom). All of the aforementioned cases, for coding efficiency can be handled in a recursive manner, and all

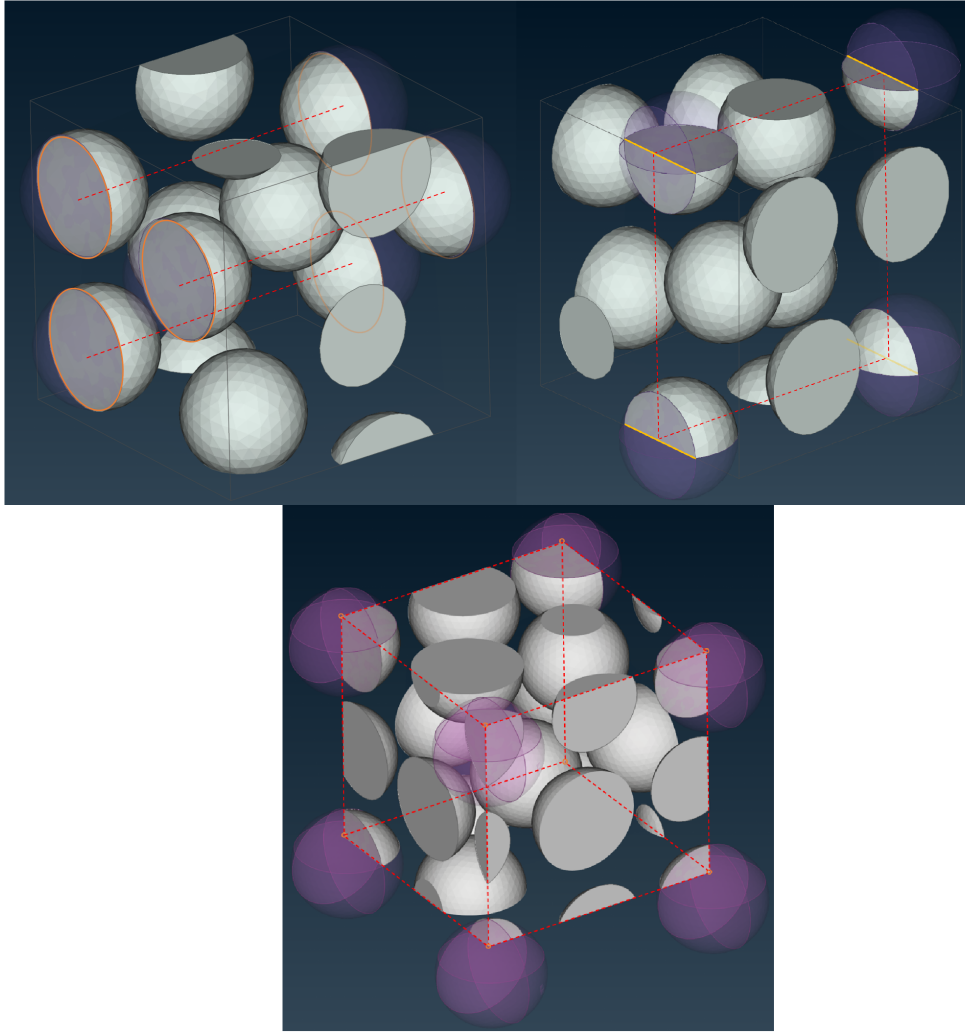


Figure 2.2: Three cases of intersection between the inclusion and the RVE boundaries in periodic microstructures. **Top Left** : Intersection with one of the RVE faces. **Top Right** : Intersection with one of the RVE edges. **Bottom** : Intersection with one of the RVE vertices

of the periodically generated inclusions must be checked for intersections with already positioned inclusions. The volume of all the periodically placed parts of the inclusion is equal to the volume of a whole inclusion.

Many constrains can be considered such as volume fraction, minimum distance between inclusions, fibers geometry etc. Also, fiber orientation tensors (6) can be used to place the inclusions orientation with stochasticity. The orientation distribution function (ODF) is reconstructed, which describes two Gaussian distributions for each angular coordinate  $\phi$ ,  $\theta$  of the spherical coordinates system and the fibers are placed according to

these two distributions. Afterwards, a meshing procedure follows to create the final RVEs, as can be seen in **Figure 2.3**.

After creating the RVEs, numerical homogenization is the next task to be completed. In this procedure the aim is to find constitutive equations for the effective material properties using a simple direct volume averaging equation (2). In the present approach, the effective material property is calculated in the main direction of the stresses. For this reason, it is necessary to have a uniaxial stress state in the direction of the perturbation when applying compressive or tensile loadings on the RVE. So, one has to decide what kind of material will be created. The type of material e.g. isotropic or orthotropic, defines the boundary conditions of the RVE. For example, in case of an isotropic material, the microstructures response of a simple uniaxial tension is enough. On the other hand, for transversely isotropic materials where the symmetry exists with respect to the plane normal to the strong axis of the material, 4 simulation tests have to be performed. Two tensile and two shear tests at directions 1 and 2 (3 direction is the same as 2 due to material symmetry). In case of orthotropic materials the total number of virtual experiments would be six (1 tensile and 1 shear for each direction) as presented below.

### 2.3.2 Isotropic materials

RVEs with spherical inclusions or with random fiber orientation tensor exhibit this kind of symmetry. Random orientation tensor  $(1/3, 1/3, 1/3, 0, 0, 0)$  in Voigt notation denotes an equal probability of the fiber to be aligned in each direction resulting in a pseudo-isotropic material. The homogenization procedure for isotropic materials is the fastest because a tensile loading is enough to define all material constants using the equations (2.1 - 2.4) where  $\langle \sigma_{ij} \rangle$  and  $\langle \varepsilon_{ij} \rangle$  are the volume average stress and strain tensor fields within an RVE of volume  $\Omega_0$ .

$$E^{eff} = E_{11}^{Eff} = \frac{\langle \sigma_{11} \rangle_{\Omega_0}}{\langle \varepsilon_{11} \rangle_{\Omega_0}} \quad (2.1)$$

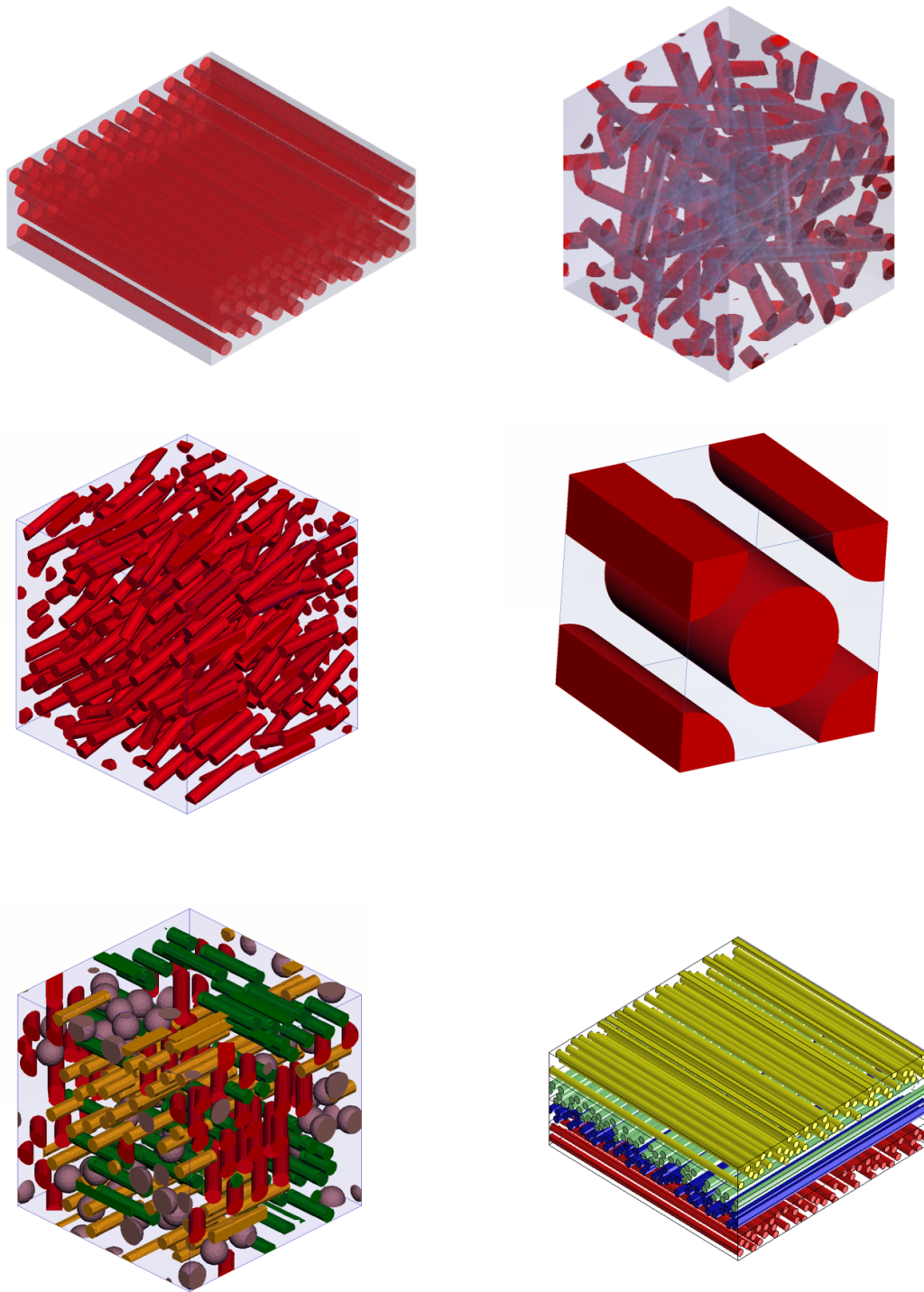


Figure 2.3: RVE generation for : unidirectional long fibers **Top Left**, random fiber orientation tensor  $(1/3, 1/3, 1/3, 0, 0, 0)$  **Top Right**, almost aligned fibers with orientation tensor  $(0.9, 0.05, 0.05, 0, 0, 0)$  **Middle Left**, continuous fiber laminated composite **Middle Right**, multiple phases **Bottom Left**, multiple layers  $[0, 90]_s$  **Bottom Right**

$$\nu_{12}^{eff} = -\frac{\langle \epsilon_{22} \rangle_{\Omega_0}}{\langle \epsilon_{11} \rangle_{\Omega_0}} \quad (2.2)$$

$$\nu_{13}^{eff} = -\frac{\langle \epsilon_{33} \rangle_{\Omega_0}}{\langle \epsilon_{11} \rangle_{\Omega_0}} \quad (2.3)$$

$$\nu^{eff} = (\nu_{12}^{eff} + \nu_{13}^{eff})/2 \quad (2.4)$$

Another approach is to load the RVE at all directions and average between the moduli of all directions. For well defined RVEs this will have very small effect at the results and large effect at the computational time.

### 2.3.3 Transversely isotropic and orthotropic materials

Composites with aligned fibers whose material is isotropic exhibit transverse isotropy with the plane of isotropy being transverse to the fibers axis. An orthotropic material can occur with more than one families of inclusions or with a family of inclusions with random orientations with diagonal orientation tensor e.g. (0.7, 0.2, 0.1, 0, 0, 0) . In the general case, to perform numerical homogenization of an orthotropic material, six boundary value problems have to be solved. Three tensile loading tests and three shear tests, one for each direction. The equations that need to be solved for those cases are similar to the isotropic case, and should be solved for all three principal directions.

## 2.4 Types of boundary conditions

The boundary conditions describe the behavior of the microstructure in the simulation. There are two types of boundary conditions, the homogeneous and the periodic boundary conditions. Choosing the periodic boundary conditions (**Appendix B**), the generated results would represent a macrostructure with periodically repeated cells while in case of the homogeneous boundary conditions the results would represent the RVE as a macrostruc-

ture with micro-constituents. This case is simpler when applying the boundary conditions but the first case is recommended when periodic microstructures are generated.

## 2.5 Mean-field homogenization vs. numerical homogenization

### 2.5.1 Linear elastic case

The RVEs of the studied examples can be seen in **Figure 2.4**. The models are solved with homogeneous boundary conditions even though the generated microstructures are periodic.

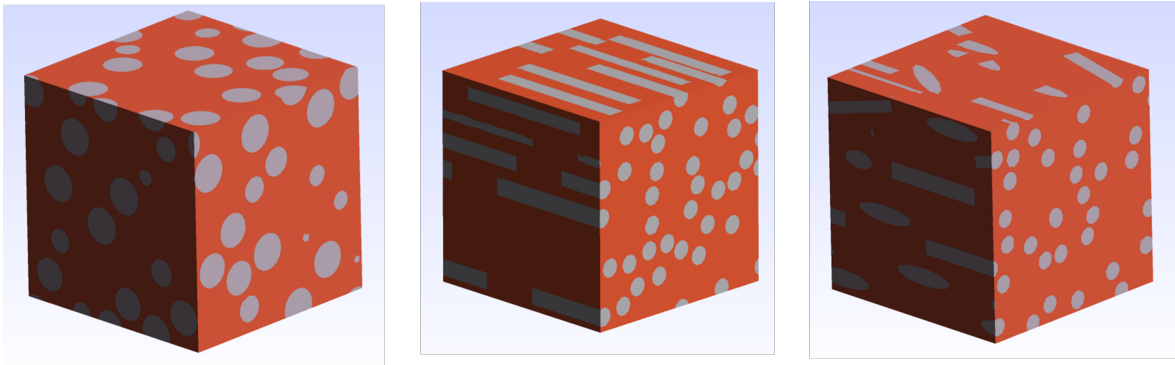


Figure 2.4: RVEs for the studied cases from left to right: Isotropic, Transversely isotropic, Orthotropic

The microstructure properties is an epoxy matrix material with  $E = 5500$  MPa ,  $\nu = 0.395$  and glass spherical inclusions with properties  $E = 73100$  MPa and  $\nu = 0.18$  and volume fraction of inclusions 0.238. The results comparing these two methods can be seen in Table 1.

Table 2.1: Isotropic Elastic Properties after MF and FE Homogenization

	$E$ (MPa)	$\nu$
mean-field	8559.95	0.371272
FE-RVE	9415.89	0.3633

For the transversely isotropic case, a microstructure with the same materials was created with volume fraction 0.22 and fibers aspect ratio 15.63 (Table 2).

Table 2.2: Transversely isotropic Elastic Properties after MF and FE Homogenization

	$E_1$ (MPa)	$E_2$ (MPa)	$\nu_1$	$\nu_2$	$G$ (MPa)
mean-field	17681.2	8499.2	0.3517	0.47	2931
FE-RVE	16577.31	9761.84	0.344	0.453	3358.06

Finally, for the orthotropic case (Table 3), a RVE with the same materials but with random orientations (0.8, 0.15, 0.05, 0, 0, 0) was created. Fiber aspect ratio 12 and volume fraction 0.188.

Table 2.3: Orthotropic Elastic Properties after MF and FE Homogenization

	$E_1$ (MPa)	$E_2$ (MPa)	$E_3$ (MPa)	$\nu_{12}$	$\nu_{13}$	$\nu_{23}$	$G_{xy}$ (MPa)	$G_{yz}$ (MPa)	$G_{xz}$ (MPa)
MF	11320.9	7671.4	7891.4	0.43	0.354	0.44	2892.6	2864.1	2678.9
FE	12063.3	8330.1	8481.4	0.42	0.364	0.44	3377.1	3468.3	3038.1

It is worth mentioning the important role of stochasticity in the RVE generation and how much it affects the results of the numerical homogenization procedure. The size of the RVE, the number of the generated inclusions and the proximity between them, are some of the parameters that are not taken into account in the mean-field homogenization approach, but in the numerical analysis those parameters affect greatly the homogenization results. The mean-field approaches best work for low volume fractions due to the constraint that the strain in the matrix is considered as the far field strain and in addition there is no interference between the inclusions.

## 2.5.2 Nonlinear case

In this section, the results of the analytical and numerical methods are compared in the nonlinear regime. In the numerical homogenization case, the strain was applied in the boundary of the RVE and solved incrementally, using homogeneous material properties

for the fibers and the matrix. In the mean-field approach the strain is also applied incrementally in a fictitious RVE, and by using strain concentration tensors the strain increment is separated to fiber strain increment and matrix strain increment, allowing the application of different material models for the constituents. Finally, after getting the response of each constituent separately, homogenization is performed for each time increment to acquire the homogenized stress response. The comparison will be performed directly on the produced stress strain curves instead of comparing the engineering properties. An in-house FE solver was developed and implemented for the purpose of the FE homogenization and direct comparison with the implemented mean-field methods took place. In all of the following cases the matrix follows an elastic plastic material with isotropic hardening while the fibers remain elastic. The properties of matrix and inclusion can be seen in Table 2.4.

Table 2.4: Properties of matrix and inclusions

	Matrix	Inclusions
Young's Modulus (MPa)	5500	73100
Poisson's Ratio	0.395	0.18
Hardening Modulus(MPa)	100	-
Hardening Exponent	0.4	-
Yield Stress (MPa)	30	-

Mean-field homogenization methods calculate the mean-field response of the composite assuming that the strain field inside the RVE is uniform as shown in **Figure (2.5)**.

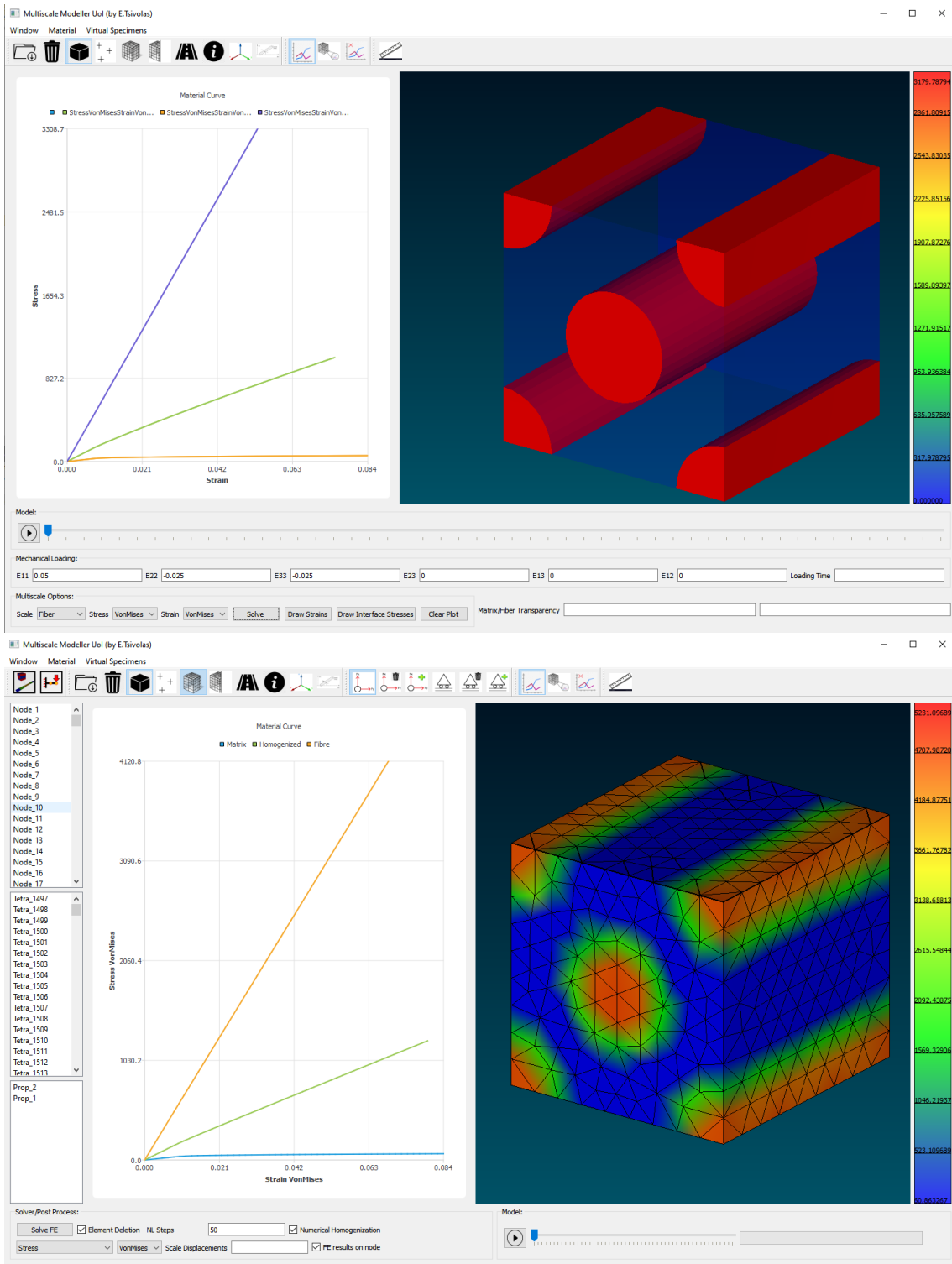


Figure 2.5: **Top:** Representation of mean-field result with uniform fields in the RVE  
**Bottom:** Representation of FE RVE result that can predict non-uniform fields in the RVE.  
 Colorbars depict stresses in MPa

It is clear in **Figure 2.5**, that it is impossible using mean-field methods to predict the actual, non-uniform micromechanical fields inside the RVE as in the full field methods or the FE RVE method. However, the produced homogeneous results can be considered quite accurate. This can be attributed to the fact that the stress and strain fields inside the inclusions are indeed uniform and can be predicted with good accuracy by adopting Eshelby-based methodologies. In the volume out of the ellipsoid inclusion, the fields are more complex, but their calculation formulations can still be reduced to expressions involving a small number of elliptic integrals (7).

In **Figures 2.6 - 2.9** the results between the mean-field homogenization method and the FE RVE method are compared for the displayed microstructures. Since the comparison concerns nonlinear analysis the microfields of the individual constituents and the homogenized fields as calculated by the two methods are compared in place of effective engineering properties as in the case of elasticity.

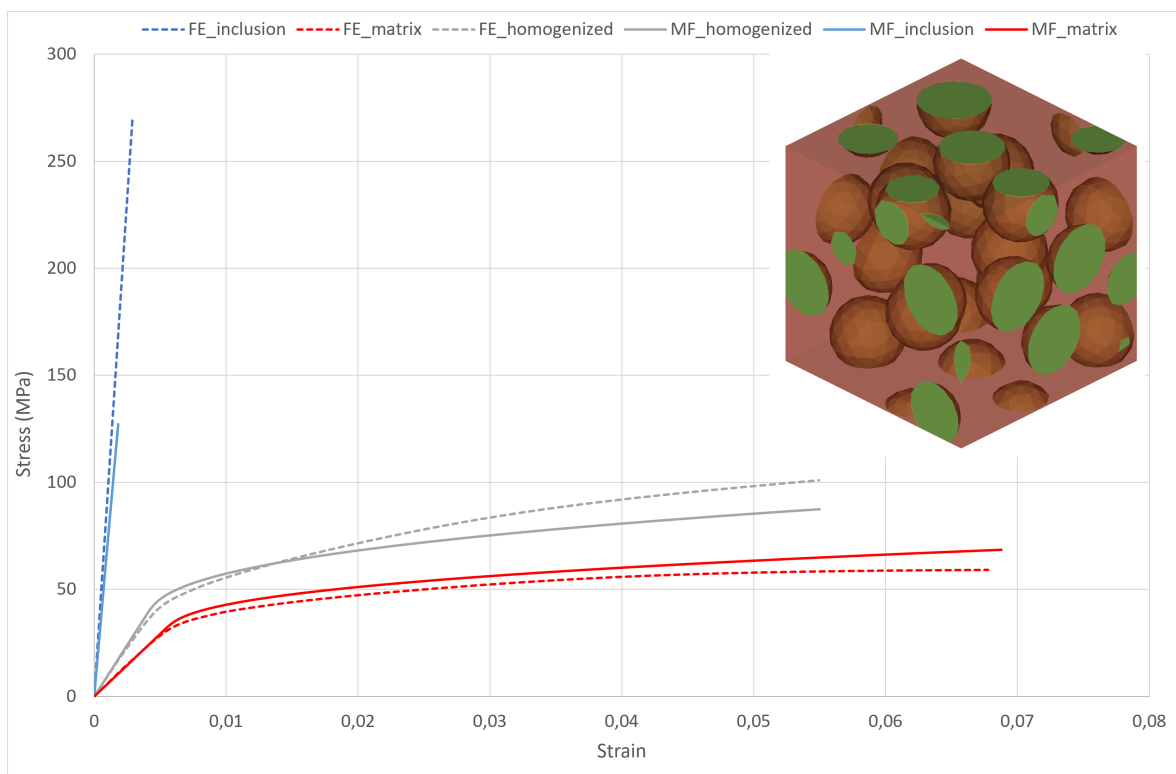


Figure 2.6: FE vs MF for RVE with spherical inclusions with 20% volume fraction

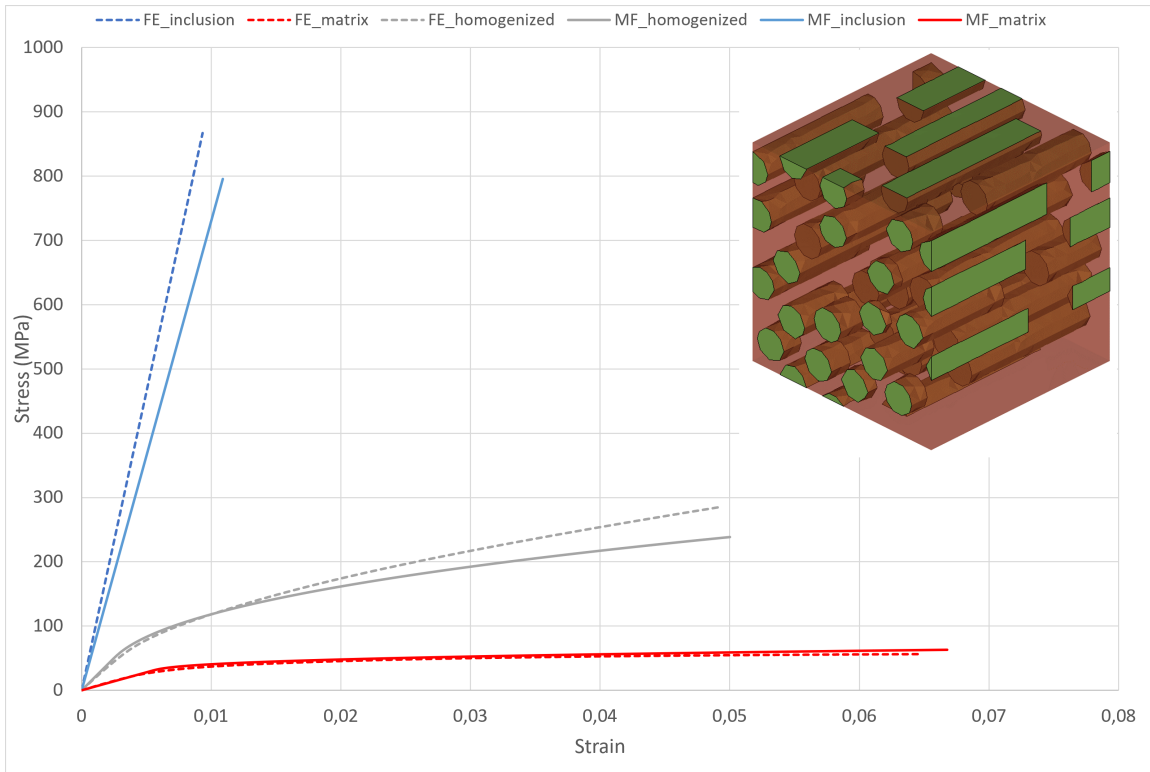


Figure 2.7: FE vs MF for RVE with short aligned fibers with 30% volume fraction

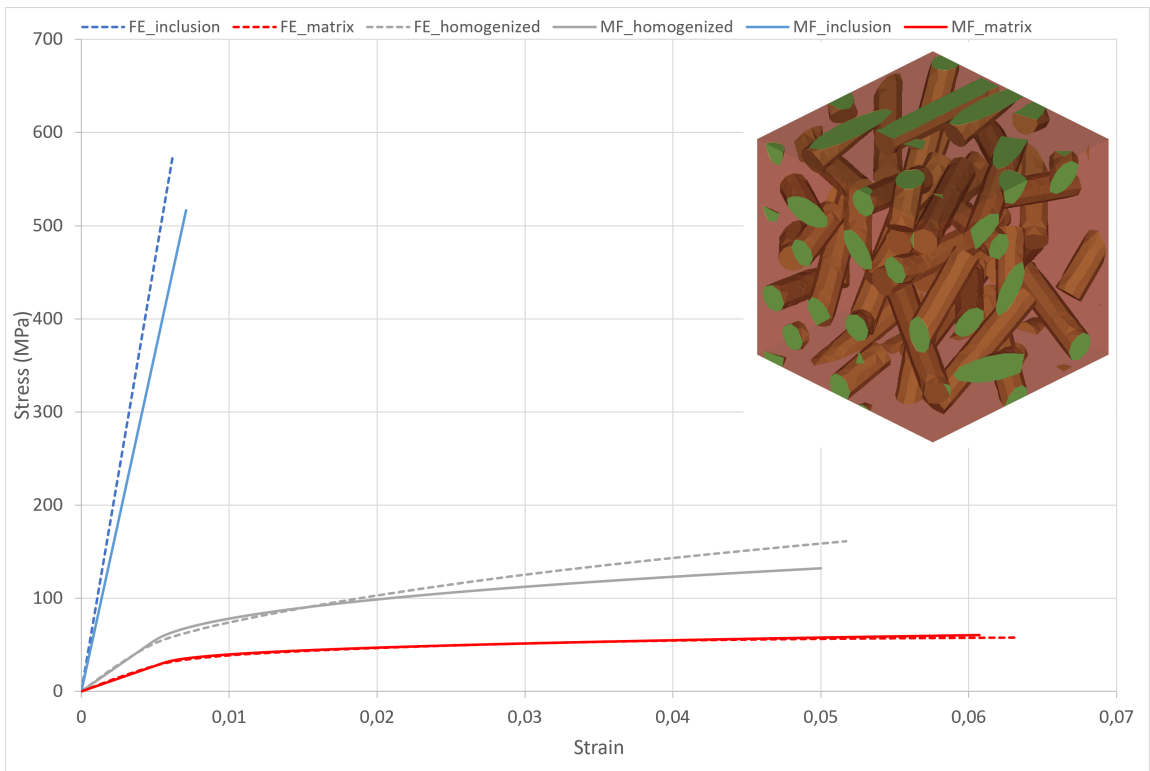


Figure 2.8: FE vs MF for RVE with short fibers with 20% volume fraction and random orientation of  $(0.7, 0.15, 0.15, 0, 0, 0)$

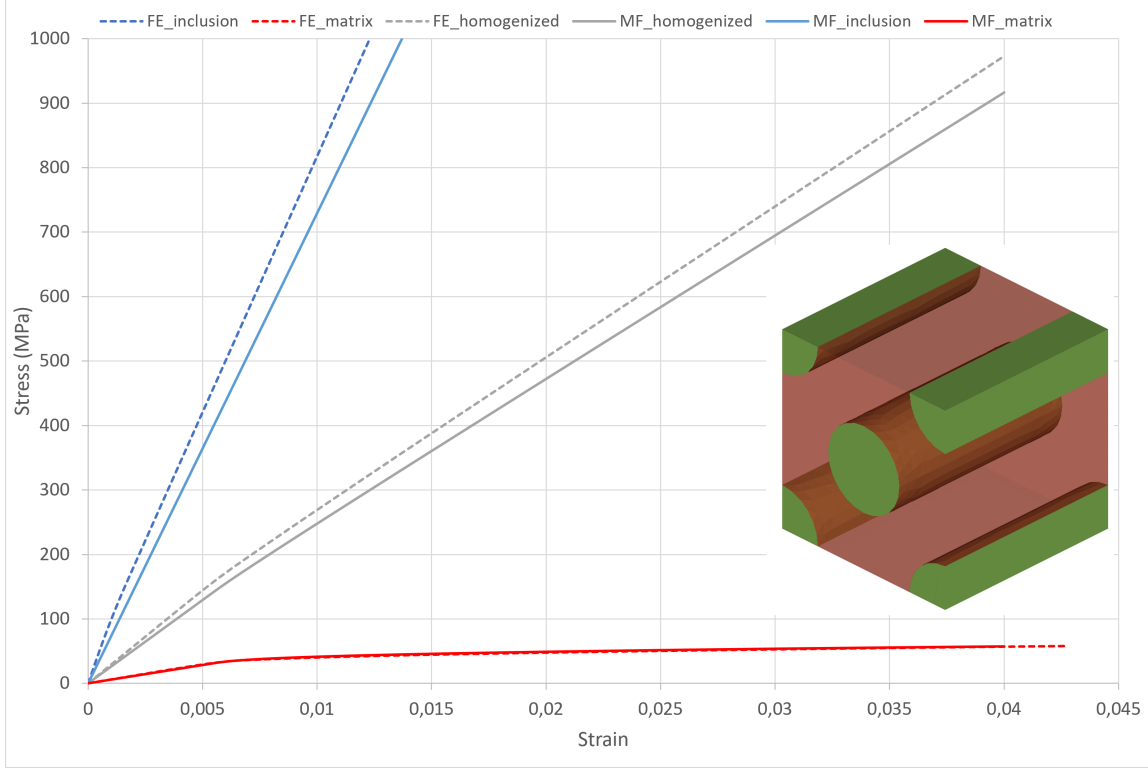


Figure 2.9: FE vs MF for continuous fiber RVE with 30% volume fraction

## 2.6 Crack profile on mesoscale and microscale model

The numerical model used in this analysis calculates one stress intensity factor for each of the three modes of fracture and eventually the stress concentration near the crack tip, analytical from micromechanics formulas considering the cracks position and geometry. For this specific model which is a 2D plain strain model the mode 3 fracture is not considered since it is the fracture due to out of plane shear, and only two intensity factors are calculated. Considering Griffith's and Irwin's works (8), (9), the stress due to fracture after the calculation of stress intensity factors is calculated according to the following relation

$$\sigma_{ij} = \frac{KI}{\sqrt{2\pi r}} f_{ij}(\theta) \quad (2.5)$$

where  $\sigma_{ij}$  is the Cauchy stress,  $r$  is the distance from the crack tip,  $\theta$  is the angle to the plane of the crack,  $KI$  is the stress intensity factor and  $f_{ij}(\theta)$  are functions that depend

on the crack geometry and loading conditions. It is worth mentioning that for uniaxial tension the contribution of the stress intensity factors other than  $KI$  can be ignored. The crack path is predefined and from the fracture mechanics model the stress intensity factors are calculated at the crack tips. A dynamic crack propagation can also be modeled easily with adopted mesh and XFEM method but this study aims to compare the stress fields around a predefined crack in multiple scales.

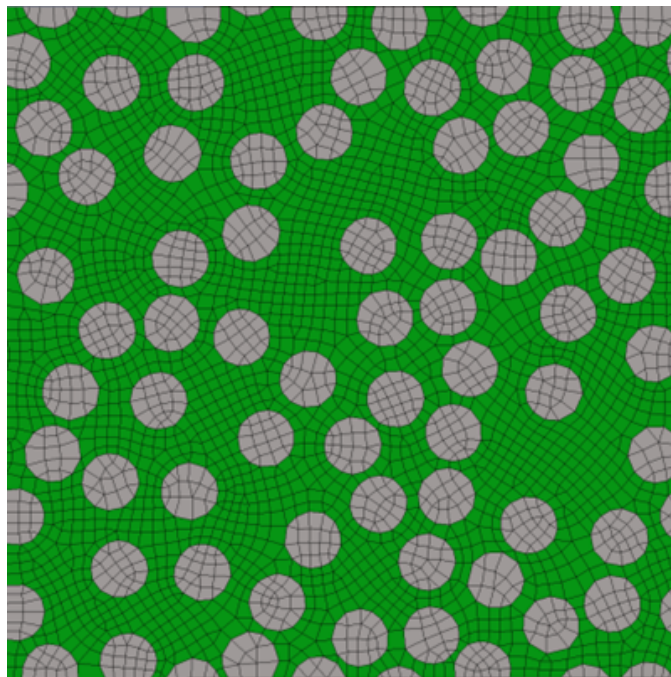


Figure 2.10: Plane strain 2-Dimensional RVE model

A 2D plain strain RVE model (**Figure 2.10**) with epoxy resin and glass fibers has been created to predict the stress distribution around the crack and compare with the 3D mesoscale solution with transverse cracking shown in **Figure 2.11**. The RVE is loaded in tension at y-axis with the same boundary conditions as in the mesoscale model in the 90 degrees layer around the crack. Good correlation of the stress fields around the cracks between the meso-scale and the microscale model can be seen in **Figure 2.11**.

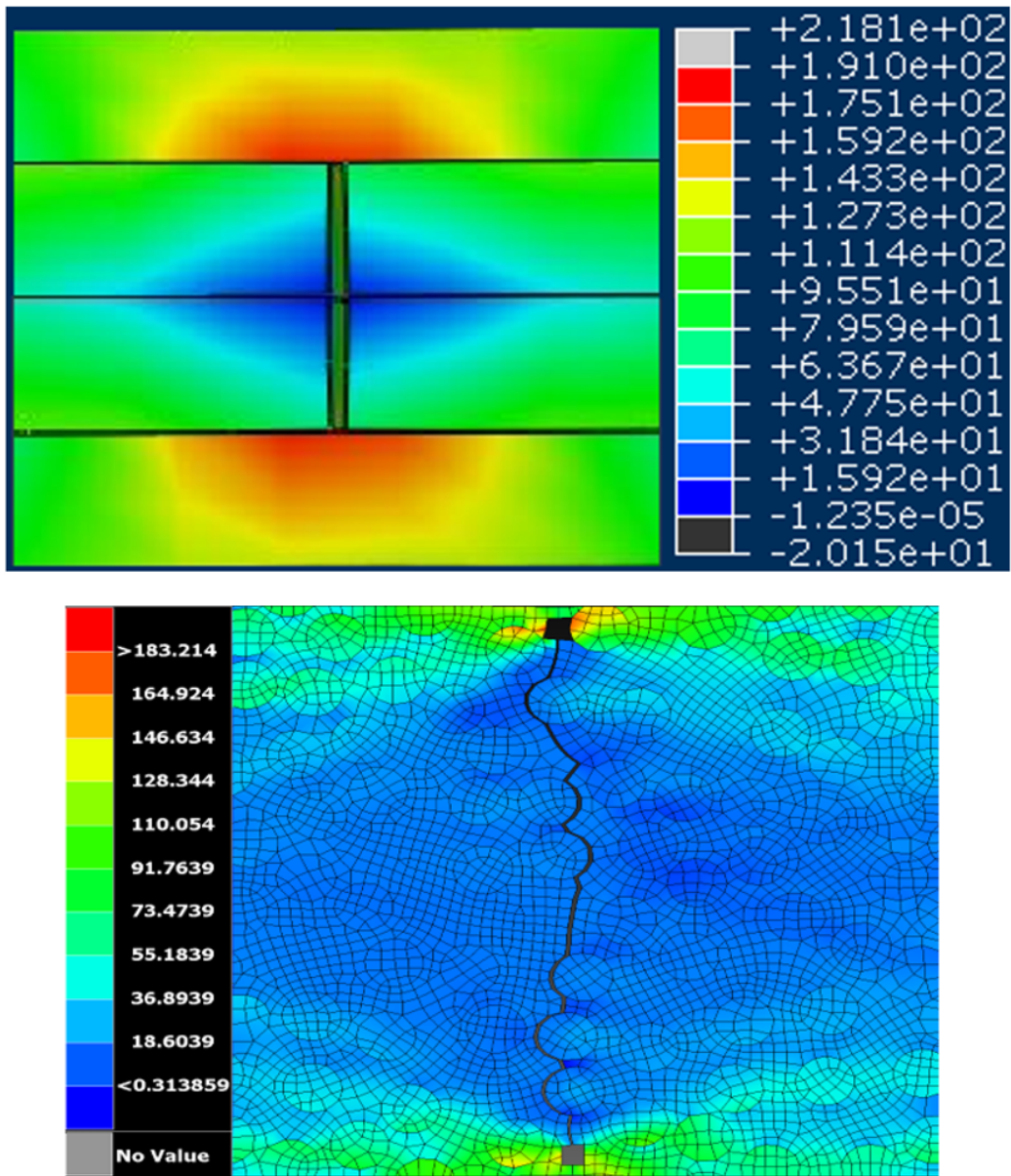


Figure 2.11: Colorbars represent stress values (MPa) around the crack

## 2.7 Conclusions

In this study, a detailed comparison between mean-field approaches and numerical homogenization is performed for both linear elastic and nonlinear elasto-plastic materials. In both cases, the results are in good agreement proving that the mean-field approaches are reliable and efficient to calculate the homogenized response in composite structures.

The FE homogenization is computationally inefficient making its extensive use for the whole domain of a large structure prohibitive even though it is more accurate compared to mean-field approaches. Consequently, mean-field approaches can be applied to the whole material structure in place of the FE method. The fact that the mean-field approaches can be extended to take into account various phenomena involved, such as viscous effects, damage, failure, and healing, makes its use applicable for most of the modern engineering problems, as we will see in detail in the next chapters. Furthermore, the random sequential adsorption method for the generation of periodic microstructures was developed (in-house implementation) and applied. In order for the numerical homogenization method to be applied, a statistically RVE is mandatory combined with the application of the appropriate boundary conditions. The generation of such RVE can be a tedious task adding even more complexity to the application of this method. The stages of pre-processing, solving and postprocessing are avoided using the mean-field homogenization methods. Finally, a stress concentration comparison was made between a meso-scale and a microscale model, using cohesive zone modelling in the first case, and analytical fracture mechanics in the latter case, with correlatable results.

## References

- [1] J. D. Eshelby, “The determination of the elastic field of an ellipsoidal inclusion, and related problems,” *Proceedings of the Royal Society of London. Series A, Mathematical and Physical Sciences*, vol. 241, no. 1226, pp. 376–396, 1957.
- [2] G. Al Kasseem and D. Weichert, “Micromechanical material models for polymer composites through advanced numerical simulation techniques,” *PAMM*, vol. 9, no. 1, pp. 413–414, 2009.
- [3] T. Mori and K. Tanaka, “Average stress in matrix and average elastic energy of materials with misfitting inclusions,” *Acta Metallurgica*, vol. 21, no. 5, pp. 571–574, 1973.
- [4] O. Pierard, C. Friebel, and I. Doghri, “Mean-field homogenization of multi-phase thermo-elastic composites: A general framework and its validation,” *Composites Science and Technology*, vol. 64, pp. 1587–1603, 2004.
- [5] L. Iorga, Y. Pan, and A. Pelegri, “Numerical characterization of material elastic properties for random fiber composites,” *Journal of Mechanics of Materials and Structures*, vol. 3, pp. 1279–1298, 2008.
- [6] S. G. Advani and C. L. Tucker, “The use of tensors to describe and predict fiber orientation in short fiber composites,” *Journal of Rheology*, vol. 31, no. 8, pp. 751–784, 1987.
- [7] T. Mura, *Micromechanics of Defects in Solids*. Martinus Nijhoff Publishers, 1988.
- [8] A. A. Griffith, “The Phenomena of Rupture and Flow in Solids,” *Philosophical Transactions of the Royal Society of London Series A*, vol. 221, pp. 163–198, 1921.
- [9] G. R. Irwin, “Analysis of Stresses and Strains Near the End of a Crack Traversing a Plate,” *Journal of Applied Mechanics*, vol. 24, no. 3, pp. 361–364, 2021.



## **Chapter 3**

### **Crack Growth and Delamination**

### **Analysis in GFRP Composite Materials**

The modeling of the structural behavior of composite materials is an interesting but complex task since the response of the material to loading structural may be difficult to predict, and the failure may be manifested in different forms. In cross-ply fiber-reinforced composites, the major failure mechanisms include: i) the failure of the matrix material (transverse cracking), ii) delamination and iii) the breakage of the fibers. The process of the transverse cracking is a well studied damage mechanism, and can be used in numerical simulations, to study the effects of various parameters on the crack density. In this paper, the finite element modeling of a cross-ply composite under uniaxial loading in tension is performed using ABAQUS software, considering all the potential damage mechanisms. The model takes into account shear-lag effect for the determination of the stress transfer and furthermore it adopts a homogenization procedure for the calculation of elastic and viscoelastic material properties. Stochasticity is introduced by assigning various interfacial strengths that follow a Gaussian distribution, so as to predict the cracking sequence up to saturation in the transverse to the  $0^\circ$  layers. The results are directly compared with available experimental measurements showing reasonable agreement. Finally, a cross-ply RVE model was created and loaded in uniaxial tension and crack propagation is modelled

with Extended Finite Element Method (XFEM). The stress concentration calculations around the crack tips are in agreement with the mesoscale model.

### **3.1 Introduction**

Composite materials are extensively studied numerically and experimentally due to their increasing application in industry. Their behavior can be examined meticulously by incorporating multiscale methods that help achieving an in-depth understanding of the damage mechanisms. The transferring of information between scales allows to extract the response of every material combination that consists the microstructure and proceed with the macroscale analysis taking into account each phase's behavior. Furthermore, mean-field methods are computationally fast methods that allow to obtain the full microstructural information for the entire simulation domain without the need to perform the modeling in such small scales. The combination of multiscale methods with fracture mechanics formulations permits the prediction of any damage mechanism that may appear in laminated composites under realistic constraints providing information with industrial relevance and value.

The mechanism of transverse cracking positions and delaminations in cross-ply composite materials is a well studied problem (1). The scale that the composite material is modeled has a significant role in terms of the accuracy and the type of the damage mechanism that can be simulated. The smaller and more detailed the scale is, the more accurate the model will be and more damage mechanisms may be predicted. The governing damage mechanisms in a cross-ply Glass Fiber Reinforced Plastic (GFRP) loaded in uniaxial tension is the transverse cracking and the delaminations that could occur between the different oriented layers near the crack tips. There are different approaches and theories that can be applied to simulate cracks and delaminations successfully. In this study, a mesoscale and a microscale model are developed. The mesoscale approach is used in a dynamic explicit analysis along with rate dependent materials to predict the saturation of

the transverse cracking and delaminations by using cohesive zone modeling techniques. The microscale approach is used to model the initiation of cracks and their propagation in a 3D cross-ply Representative Volume Element (RVE) using extended finite element method (XFEM) in a quasi static analysis framework. The stress fields at the concentration areas around the crack tips of both methods are compared using strain concentration tensors to link the two scales.

In the existing literature there are models that have been suggested concerning the simulation of interfacial properties. The most common and widely used approach is the XFEM (2). This method allows the modeling of discontinuities existing in the finite elements. Thus, it provides a tool for the insertion of matrix cracks independently of the mesh orientation. Despite the fact that most of the simulations of cracking initiation and propagation are performed using XFEM, this method has a limitation mainly imposed by the chosen analysis which has to follow the Implicit integration framework and not the Explicit. In the present mesoscale model Explicit analysis is adopted where complex dynamic problems with contacts and large deformations can be solved. Another important fact introduced in the present investigation is the use of cohesive interface instead of cohesive elements (3) reducing so the continuum shell elements of the model avoiding the matching restrictions for the mesh of the adjacent layers.

In addition, homogenization theory was used to predict elastic properties for the multiphase materials instead of properties from literature or material databases. Homogenization methods and multi-scale analysis can easily be extended to nonlinear regime (4) for plasticity and damage to get a clear understanding about the inelastic response in the microstructure and observe which component of the composite has conceived damage. This multiscale modeling can be performed using a user defined material through a subroutine UMAT of ABAQUS usually coded in fortran or coupling the solver with another multiscale modeling dedicated software (5). There are also other analytical and numerical homogenization schemes appropriate for continuous fiber reinforced composites such as Aboudi's method of cells (6), and FE-RVE homogenization schemes (7) (8) with compa-

erable results with the homogenization method used in this study (9).

In the present work, a 3D mesoscale model was developed, regarding the layers of the laminate as a homogeneous, transversely isotropic medium and calculating their elastic properties using a two-step mean-field homogenization methodology. The viscous effect of the matrix material during homogenization strategy were taken into account. The interface between the [0/90]<sub>s</sub> layers is modeled with cohesive contacts. A finite number of cracks were placed at the 90° layers of the laminate assuming that their strength followed a Gaussian distribution thus avoiding the development of uniform stress. This approach is different from the work by Fukunaga et al. (10) where a Weibull distribution was used where a brittle behaviour for the 90° is assumed. The adopted methodology was preferred among others for computational stability. Four rows of elements were placed through the thickness of each ply so as to realistically model transverse cracking. By adopting this approach, the stress redistribution and the damage evolution process can be predicted and quantified.

## 3.2 Homogenization Procedure

### 3.2.1 Homogenization method for elastic materials

The elastic properties of the material are obtained using a two step micromechanics homogenization algorithm. Firstly, all of the inclusion families were homogenized separately as a composite material with two phases following Mori-Tanaka homogenization scheme (11). Secondly, all pseudo grains were homogenized to a single composite by adopting Voigt homogenization approach which is schematically depicted in **Figure 3.1** and in mathematical form can be described by  $C_{eff} = \sum_{i=1}^n V_i C_i$  where  $C_{eff}$  is the homogenized stiffness tensor,  $C_i$  is the stiffness tensor of the pseudo grain  $i$  with volume fraction  $V_i$ . In case of a two phase composite material such as glass fiber reinforced polymer (GFRP) with unidirectional long fibers, the two step method coincides with the simple Mori-Tanaka method. The homogenized stiffness tensor is given from the Mori-Tanaka

formula:

$$C_{MT} = C_m + [V_f \langle (C_f - C_m) A_{Eshelby} \rangle] [V_m \mathcal{I} + V_f \langle A_{Eshelby} \rangle]^{-1} \quad (3.1)$$

where  $\langle \rangle$  stands for orientation averaging of fibers orientations which can be ignored for aligned fibers. The quantities  $C_f$ ,  $C_m$  are the stiffness matrices of the epoxy and the glass fibers respectively. The volume fractions of the fiber and the matrix are denoted with  $V_f$  and  $V_m$ . In addition,  $\mathcal{I}$  is the fourth order identity tensor, and  $A_{Eshelby}$  is the strain concentration tensor of the dilute solution defined as:

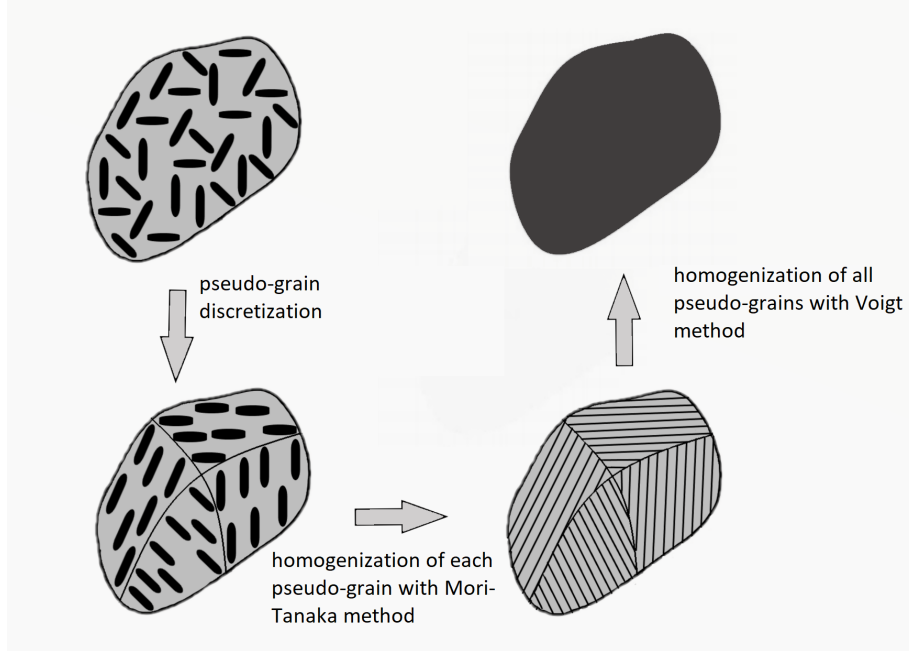


Figure 3.1: Steps used during homogenization procedure: i. pseudo-grain discretization, ii. homogenization of each pseudo-grain, iii. homogenization of all pseudo-grains with Voigt approach

$$A_{Eshelby} = [\mathcal{I} + EC_m^{-1}(C_f - C_m)]^{-1} \quad (3.2)$$

where  $E$  is the Eshelby tensor which depends on the aspect ratio of the inclusion and the properties of the matrix material. The Eshelby tensor can be computed by using analytical solutions that have been developed for certain inclusion geometries and matrix materials. The general solution for inclusions of arbitrary shape embedded in an isotropic matrix is

described as follows

$$E_{ijkl} = \frac{1}{8\pi(1-\nu)} \{ \delta_{ij}\delta_{kl}(2\nu I_i + J_{ik}) + (\delta_{ik}\delta_{jl} + \delta_{jk}\delta_{il}) [(1-\nu)(I_k + I_i) + J_{ij}] \} \quad (3.3)$$

$$I_i = I(\lambda) = 2\pi\alpha_1\alpha_2\alpha_3 \int_{\lambda}^{\infty} \frac{(A_i + s)^{-1}}{\Delta s} ds \quad (3.4)$$

$$J_{ij} = J_{ij}(\lambda) = A_i I_{ij}(\lambda) - I_i(\lambda) \quad (3.5)$$

$$I_{ij} = I_{ij}(\lambda) = 2\pi\alpha_1\alpha_2\alpha_3 \int_{\lambda}^{\infty} \frac{(A_i + s)^{-1}(A_j + s)^{-1}}{\Delta s} ds \quad (3.6)$$

$$\Delta s^2 = (A_1 + s)(A_2 + s)(A_3 + s) \quad (3.7)$$

where

$$A_i = \alpha_i^2 \quad (3.8)$$

The quantities involved are: the Poisson ratio  $\nu$  of the matrix,  $\alpha_1, \alpha_2, \alpha_3$  are the three ellipsoid axes dimensions of the inclusions geometry,  $\delta$  is the Kronecker's delta and the numerical quantities  $I_i, I_{ij}$  which are defined in terms of standard elliptic integrals and details can be found in (11) (12).

The homogenization algorithm, deals with the random orientations by performing orientational averaging using fibers orientation tensor after retrieving fourth order tensor using hybrid closure approximation (13). To calculate the effective properties of a continuous fiber reinforced composite, the ellipsoid principal dimension that corresponds to the fiber's axis is much bigger than the other two axes dimensions:  $\alpha_1 \gg \alpha_2$  and  $\alpha_1 \gg \alpha_3$ .

### 3.2.2 Homogenization of viscoelastic materials

In the present study the viscous effect of the matrix is manifested employing a viscoelastic homogenization scheme which takes into account prony series viscoelasticity. On the other hand, the glass fibers are considered as linear elastic for normal temperatures. The material model of the viscoelastic matrix medium follows the following constitutive equation:

$$\sigma(t) = G(t) : \varepsilon(0) + \int G(t - \tau) : \dot{\varepsilon}^{(ve)}(\tau) d\tau \quad (3.9)$$

$$\varepsilon(0) = \lim_{t \rightarrow 0^+} \varepsilon(t) \quad (3.10)$$

$$G(t) = 2G_R(t) I^{dev} + K_R(t) \hat{I} \otimes \hat{I} \quad (3.11)$$

where the stress ( $\sigma$ ) and strain ( $\varepsilon$ ) second order tensors are invoked,  $G(t)$  is the relaxation tensor,  $\dot{\varepsilon}^{(ve)}$  the viscoelastic (indicated by the ve superscript) strain rate tensor,  $I^{dev}$  is the deviatoric part of the fourth order unit tensor and  $\hat{I}$  is the second order unit tensor. The juxtaposition symbol  $\otimes$  represents the dyadic product. The prony series expression of the bulk and shear modulus are given by:

$$G_R(t) = G(0) \left[ 1 - \sum_{i=1}^n w_i (1 - e^{-t/\tau_i}) \right] \quad (3.12)$$

$$K_R(t) = K(0) \left[ 1 - \sum_{i=1}^{n'} w_i^* (1 - e^{-t/\tau_i^*}) \right] \quad (3.13)$$

where  $w_i, w_i^*$  are the weights for the respective relaxation times  $\tau_i, \tau_i^*$ .

The relation  $\hat{\sigma}(s) = \hat{E}(s)\hat{\varepsilon}(s)$  is the elastic analogous of **Eq. 3.9** for isotropic materials in the Laplace-Carson domain. The quantities invoked  $\hat{\sigma}$ ,  $\hat{E}$  and  $\hat{\varepsilon}$  are the transformed stress, stiffness and strain tensor in the Laplace domain while  $s$  is the complex variable. This leads to a fictitious RVE in the Laplace-Carson domain (14) and the homogenization results are expressed as functions of  $s$ . Inevitably, an inverse Laplace-Carson transformation is required to calculate the results in the time domain (15). The prony series values for the viscoelastic homogenization are taken from the literature (16).

### 3.3 Modeling a cross ply composite material (0/90)s

In the relevant literature several micromechanical (17) (18) or mesoscale (19) (20) (21) (22) (23) (24) (25) approaches have been proposed. In this study, the material at each ply is a transversely isotropic material whose elastic properties were calculated with Mori-Tanaka micromechanical formula based on Eshelby's solution (12) and the structural simulation follows a mesoscale approach. The material properties values used were the Young's modulus of epoxy resin (5.5 GPa), glass fiber (73.1 GPa) and the respective Poisson's ratio values were 0.395 and 0.18. The shape of the glass fibers having  $V_f = 0.63$  is described by their aspect ratio which was 10000 .

The total composite elastic properties after homogenization procedure are reported in **Table 3.1**. The viscous effects contribution of the matrix material to the whole composite with respect to time can be seen in **Figure 3.2**. The strength values, including Interlaminar Shear Strength (ILSS) for the homogenized GFRP material are taken from the literature (26).

Table 3.1: Elastic Properties after elastic and viscoelastic Homogenization

Property	Instantaneous	270 s	Quasi-static
Longitudinal modulus $E_1$ (GPa)	48.1621	46.396	46.386
Transverse modulus $E_2$ (GPa)	18.7977	3.930	3.7541
In plane Poisson ratio $\nu_{12}$	0.252155	0.25029	0.25038
Transverse Poisson ratio $\nu_{23}$	0.485318	0.5658	0.56396
In plane shear modulus $G_{12}$ (GPa)	6.32782	1.255	1.2002
Transverse shear modulus $G_{23}$ (GPa)	6.88076	1.415	1.3505

In order to model the interfaces between the layers cohesive contacts are used, in a nonlinear analysis framework. The adoption of cohesive contacts dominated the alternative options of cohesive elements or XFEM. The cohesive elements approach has two undesirable effects. The first one is the significant increase of the total finite elements number and the second one has to do with the meshing procedure of the different layers which should discretized in a rather restrictive similar manner. As should be stressed, the XFEM approach cannot be used in the dynamic analysis framework with explicit integra-

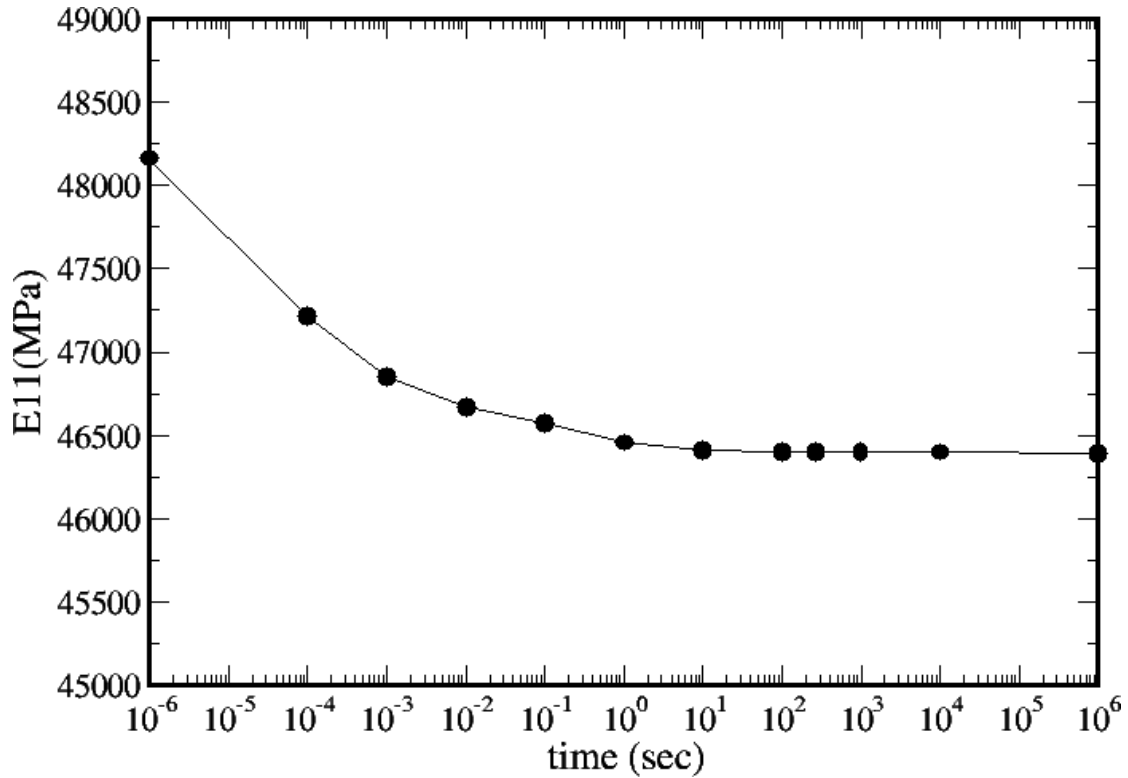


Figure 3.2: Time dependent homogenized axial Young's modulus  $E_{11}$  from viscoelastic homogenization

tion. In the traction-separation model of ABAQUS, a linear elastic behavior is initially assumed followed by the initiation and evolution of damage. The elastic behavior is expressed in terms of an elastic constitutive matrix that relates nominal stresses to nominal strains across the interface. The maximum shear stress criteria are employed to model the failure at the contacts.

The model material geometry is represented by a domain between two adjacent cracks which is undamaged and has a 30 mm length. Every layer has a 0.25 mm thickness value and the composite is loaded uniaxially. Tabular data are employed for the incremental application of the strain up to a total value of 1.5% using a loading duration of 270 seconds. The geometry of the model is depicted in **Figure 4.5**.

For the geometry mesh generation procedure four rows of continuum shell elements along the thickness direction of each laminate were placed for higher accuracy, resulting in a total number of 96000 continuum SC8R type shell elements.

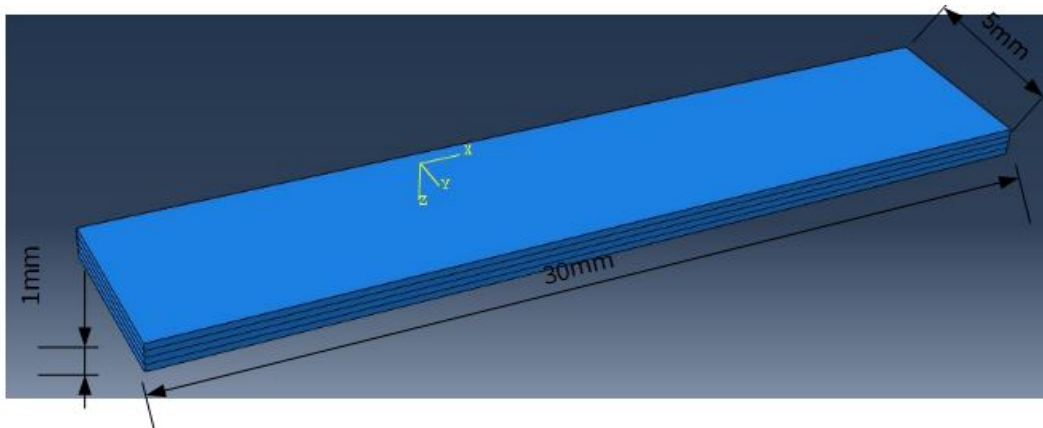


Figure 3.3: Geometry of the cross-ply composite model.

The placement of a high number of potential cracks permits the successful prediction of random matrix cracking (**Figure 3.4**). For every potential crack location different strength values are attributed so as non-uniform stresses are developed as the latter would lead to the simultaneous failure for all interfaces at the cohesion zone. The contacts'

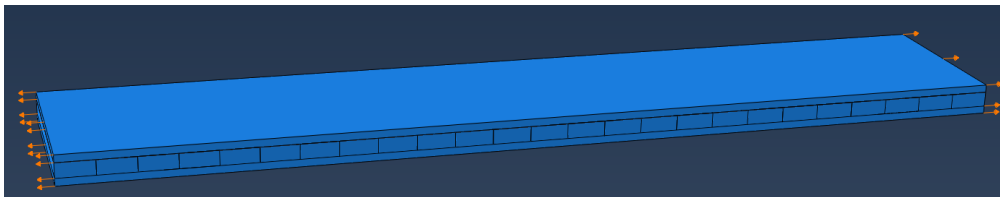


Figure 3.4: Modeling of the possible transverse cracks with cohesive interface

strength, follows a Gaussian distribution with a mean equal to the strength of the matrix and 15% standard deviation .

### 3.4 Results and Discussion

It should be pointed out that all the expected failure mechanisms appear in the present simulation study. Initially, the first transverse cracks are formed. As the loading continues, interfacial delaminations are evident. The existence of a shear lag zone (27) (28) (29) is being revealed. In the sequel the crack density simulation predictions are compared with existing experimental measurements. Finally, it is shown how the ILSS affects the delamination length and the total strength of the total composite material.

### 3.4.1 Delaminations and shear lag zone

Cohesive zone modeling (CZM) provides a simulation pathway to model cohesion for interfaces with zero thickness. In the present study it is used to simulate matrix cracking and delamination. As aforementioned, prior to damage, a linear elastic behavior is assumed in this traction separation model which is valid. The aforementioned behavior is given by the following equation

$$\begin{bmatrix} t_n \\ t_s \\ t_t \end{bmatrix} = \begin{bmatrix} K_{nn} & K_{ns} & K_{nt} \\ K_{ns} & K_{ss} & K_{st} \\ K_{nt} & K_{st} & K_{tt} \end{bmatrix} \begin{bmatrix} \delta_n \\ \delta_s \\ \delta_t \end{bmatrix} \quad (3.14)$$

The quantities involved are the normal ( $t_n$ ), and the two ( $t_s, t_t$ ) shear tractions respectively. The corresponding separations are  $\delta_n, \delta_s, \delta_t$ . It is crucial to underline that the cohesive contact is an interaction and not a material property thus is interpreted differently from cohesive elements. Additionally, CZM necessitates a geometrical nonlinear analysis.

In **Figure 3.5**, the calculated quantity  $CSQUADSCRT = (t_n/t_0^n)^2 + (t_s/t_0^s)^2 + (t_t/t_0^t)^2$  denotes the criterion for damage initiation for the quadratic contact stress. If  $CSQUADSCRT = 1$  the criterion is fulfilled. It should be noted that  $CSQUADSCRT$  value cannot exceed 1 so as to specify damage evolution. For CZM, damage progression is manifested by the reduction of stiffness of the cohesive contacts, whereby, in the case of cohesive elements, damage propagation corresponds to stiffness degradation for the material itself. The present work adopts based on energy criteria, following the analytical forms proposed by Benzeggagh-Kenane (30). The aforementioned forms are useful in cases where the critical energies become equal during separation along the two shear directions ( $G_s^C = G_t^C$ ) and

$$G_n^C + (G_{shear}/G_T)^\eta (G_s^C - G_n^C) = G^C \quad (3.15)$$

$$G_{shear} = G_s + G_t \quad (3.16)$$

$$G_T = G_n + G_{shear} \quad (3.17)$$

with the quantities involved being the cohesive property parameter  $\eta$  and  $G_n^C, G_s^C, G_t^C$  are respectively the required critical fracture energies for failure at the normal, the first and the second direction.

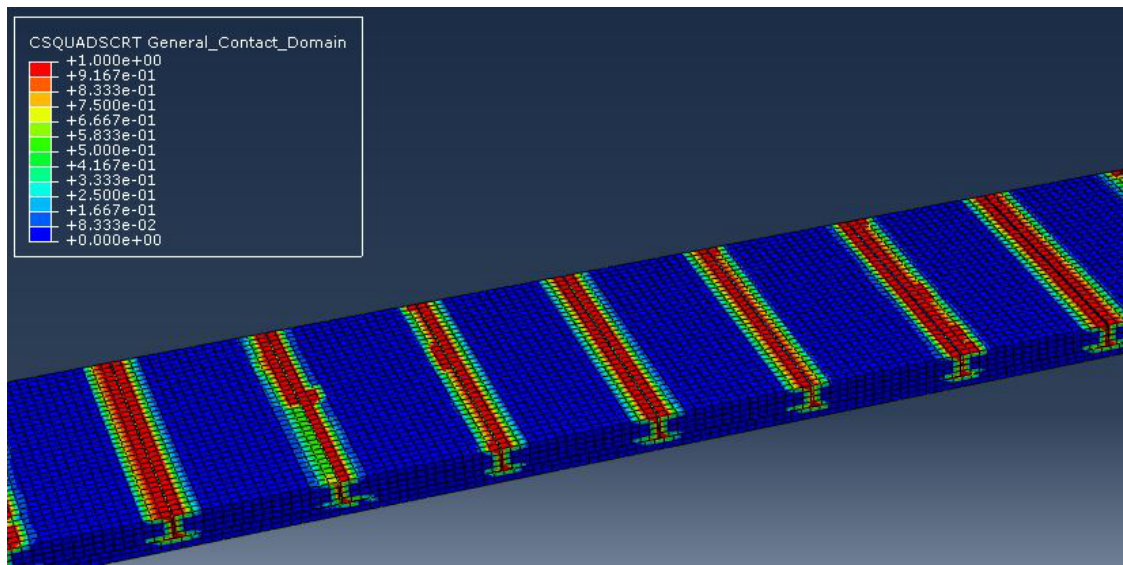


Figure 3.5: Modeling of the possible transverse cracks with cohesive interface. The existence of the shear lag zone is apparent. The upper layer is hidden to get a more clear image of the cracks and the delamination area. Values of *CSQUADSCRT* quantity are given in the colorbar

As the first cracks appear and the loading continues, almost immediately delaminations (31) are initiated too. At the area over and under the tip of the cracks stress concentration is observed. The cracked composite material and the extension of the delamination area around the cracks, are depicted in **Figure 3.5**.

The shear lag zone is apparent. In this zone the normal tensile stresses are almost zero, while the shear stresses at the interface are high and this constitutes the main reason for delamination appearance. As we move away from that zone the exact opposite seems to happen, as the normal stresses are high the next cracks of the composite will be far enough

from an existing crack. The zone's size strongly depends on the: i) layer thickness, ii) stiffness of the outer layers and iii) value of the interlaminar shear strength.

### **3.4.2 Comparison with Experiments**

In the present section comparisons with available experimental measurements (32) are given. Due to strength stochasticity of the  $90^\circ$  layers, there is a continuous transverse matrix cracking. Some representative screenshots during the analysis are presented in **Figure 3.6**. Simulation predictions included in a crack density versus strain diagram are compared with experimental data and depicted in **Figure 3.7**.

The initial cracking and cracking saturation occur for similar axial strain values for both experimental and simulation data. The standard deviation value of the distribution plays a significant role in the cracking density because it can lead to weaker or stronger contacts affecting so the final crack density. It is worth mentioning that in the simulation protocol, the load was applied at constant strain rate through tabular data describing the strain values at the corresponding time of the analysis. Finally, from the two simulation curves of **Figure 3.7** it can be observed that the increase of the composite's stiffness increases the crack density too.

For a strain value around 0.4% the first crack develops and subsequently more cracks appear. In **Figure 3.6** where the second and third time steps are depicted the total axial strain values are 0.5% and 0.8% respectively while for axial strain around 1.2% saturation of crack density takes place.

### **3.4.3 Mesh sensitivity analysis**

In the framework of continuum mechanics, the stress-strain relations of a material define the constitutive model. In case of strain softening behavior of a material strain localizations can appear, resulting in strong mesh dependency of the solution. As a result, mesh refinement can decrease the energy dissipation. To alleviate mesh dependency ABAQUS solver introduces a characteristic length in the formulations that is related to the size of

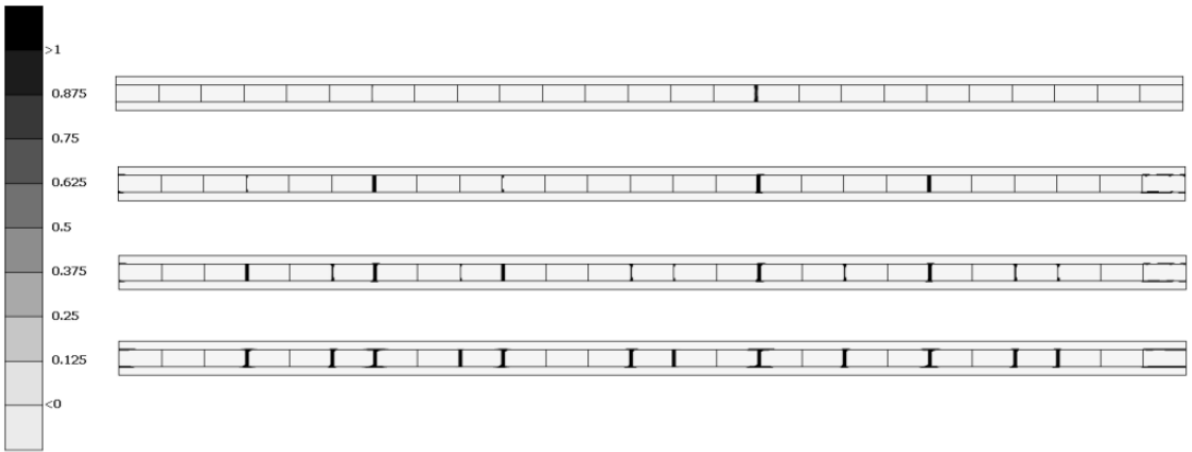


Figure 3.6: Middle layer transverse cracks at different time steps

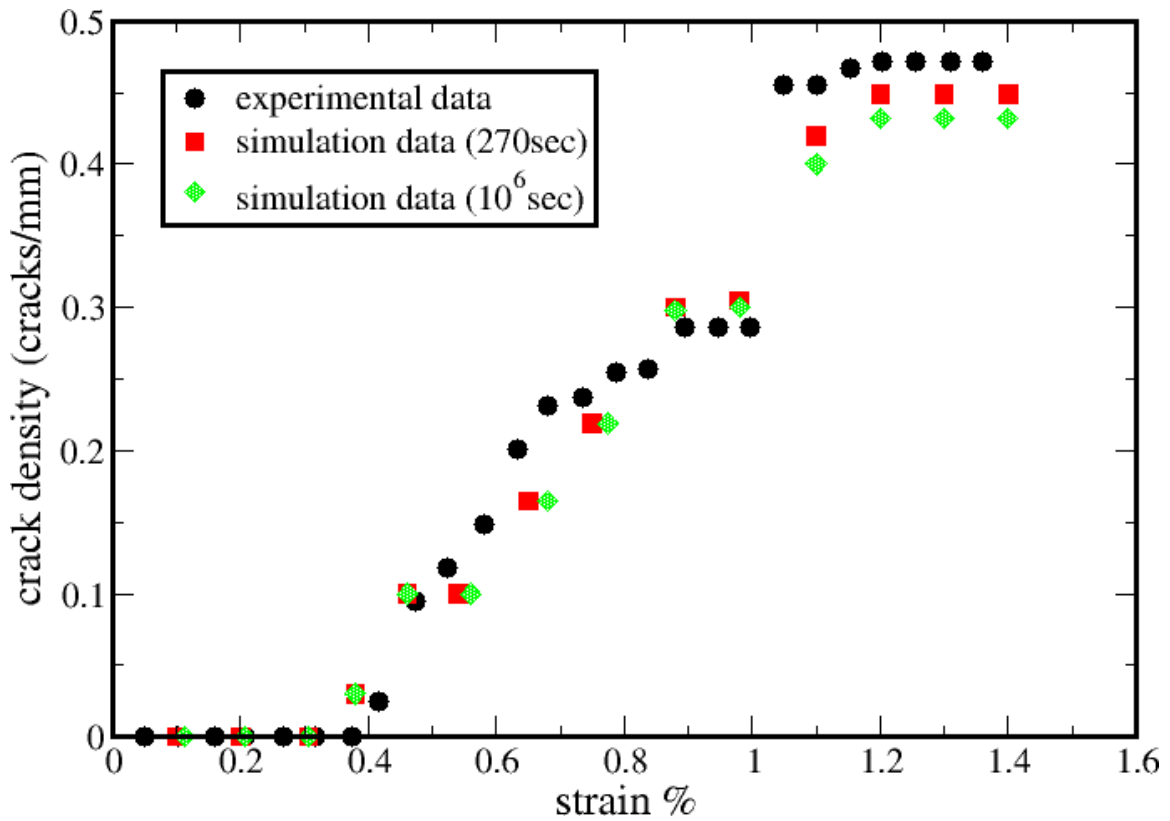


Figure 3.7: Crack density as a function of strain for experiment data (reproduced with permission from (32)) and simulation model data for quasi-static loading and for total loading time about 270 sec

the element and expresses the strain softening part as a stress displacement relation. Thus, the dissipated energy during damage is given per unit area and not per unit volume and is treated as a material property that is used to calculate the critical displacement for damage

initiation. The above method, is also consistent with the fracture mechanics concept of critical energy release rate where it is also treated as a material parameter (33).

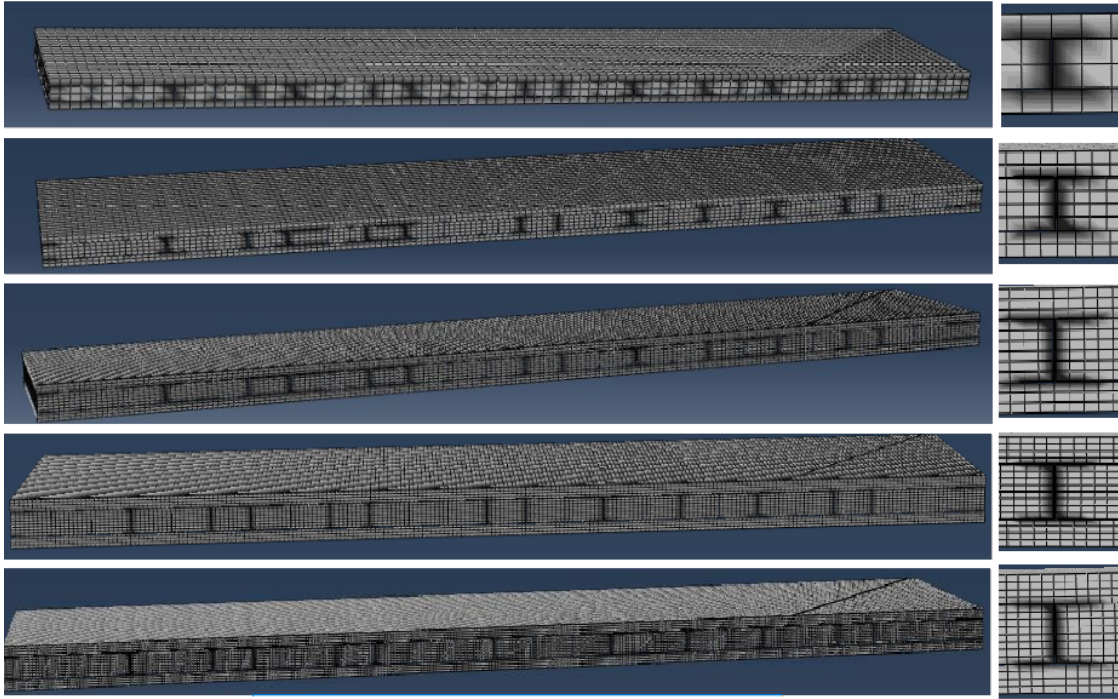


Figure 3.8: Final cracking at the model material geometry for five different meshes for quasi-static loading. At the right corner a magnified local domain encapsulating crack is also given for each of the five different meshes

The cross-ply composite model was solved for five different meshes to examine the mesh dependency having 8000, 45144, 96000, 208306 and 352688 continuum shell elements, respectively, and the results are shown in **Figure 3.8**. It can be concluded for all four models the cracking saturation occurs with the same number of cracks. The only result that significantly differentiates in coarse meshes and seems to stabilize as the mesh gets finer is the mean delamination length (**Figure 3.9**). This result is calculated as an average value from the sum of the delamination length of each crack divided by the number of cracks.

This can be attributed to the small number of elements which translates to a small number of integration points. Inevitably, the results are extrapolated to a larger but unnecessary area. This phenomenon disappears by using an adequate number of elements which was higher than 45000 elements for the specific geometry of the presented model.

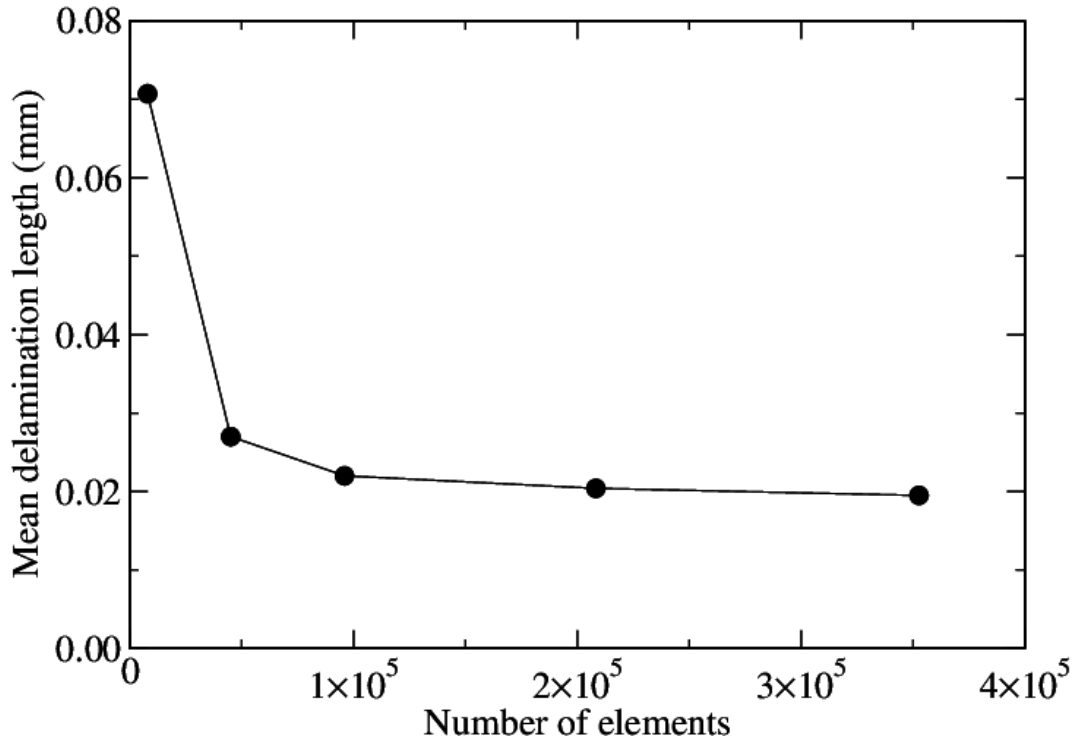


Figure 3.9: Mean delamination length as a function of the number of finite elements

It should be stressed out that for the consistent and successful simulation of the crack profile, more than one rows of elements are needed per layer of the composite material.

### 3.5 Crack growth in microscale using fracture mechanics

As mentioned, XFEM is a popular method for the solution of quasi-static problems containing cracks and interfaces that are mesh independent. The solution is attainable with the enrichment of elements which are intersected by the discontinuity, using special shape functions to handle the singularities and local discontinuities around the crack.

In **Figure 3.10**, a cross-ply composite RVE model (with characteristics as mentioned in section 3.3) is constructed and loaded in uniaxial tension that is applied through Dirichlet-type boundary conditions by using the strain results of the macroscale model. The crack-ing propagation simulated with XFEM is shown as the loading increases. In particular, as the crack propagates the stress in the middle layer reduces while stress concentration in the crack tips is evident, in agreement with the macroscale model. In **Figure 3.11** the

stress concentration values at the crack tips are compared against the simulation predictions of microscale and macroscale models.

However, the stress profiles cannot be directly compared due to the different representation scale. The macro model refers to the stress concentration upon a homogenized material and the micro model refers to the stress concentration upon the fiber. For their direct comparison, the stress in macro model needs to be localized using the stress concentration tensor of Hill's (34) theories which invoke the following equations

$$\sigma_f = B_f : \sigma \quad (3.18)$$

$$B_f = (M - M_m) / [V_f(M_f - M_m)] \quad (3.19)$$

The quantities involved are the compliance tensors of the fiber ( $M_f$ ), the matrix ( $M_m$ ) and the homogenized composite material  $M$ ,  $V_f$  is the volume fraction of the fiber and  $B_f$  is the Hill's fiber stress concentration tensor. The stress concentration tensor connects the stress tensor of a constituent with that of the composite, making possible the direct comparison of the two models.

The maximum stress tensor of the homogenized material in the stress concentration area that occurred from the macro scale analysis in Voigt notation is  $\sigma = [1833.04 \ -51.04 \ -53.82 \ 1.71 \ 0.56 \ -8]$ . The von Mises stress of the fiber that occurred from the stress localization is 2958.3 Mpa which is close to the prediction of the XFEM model around 2894 Mpa.

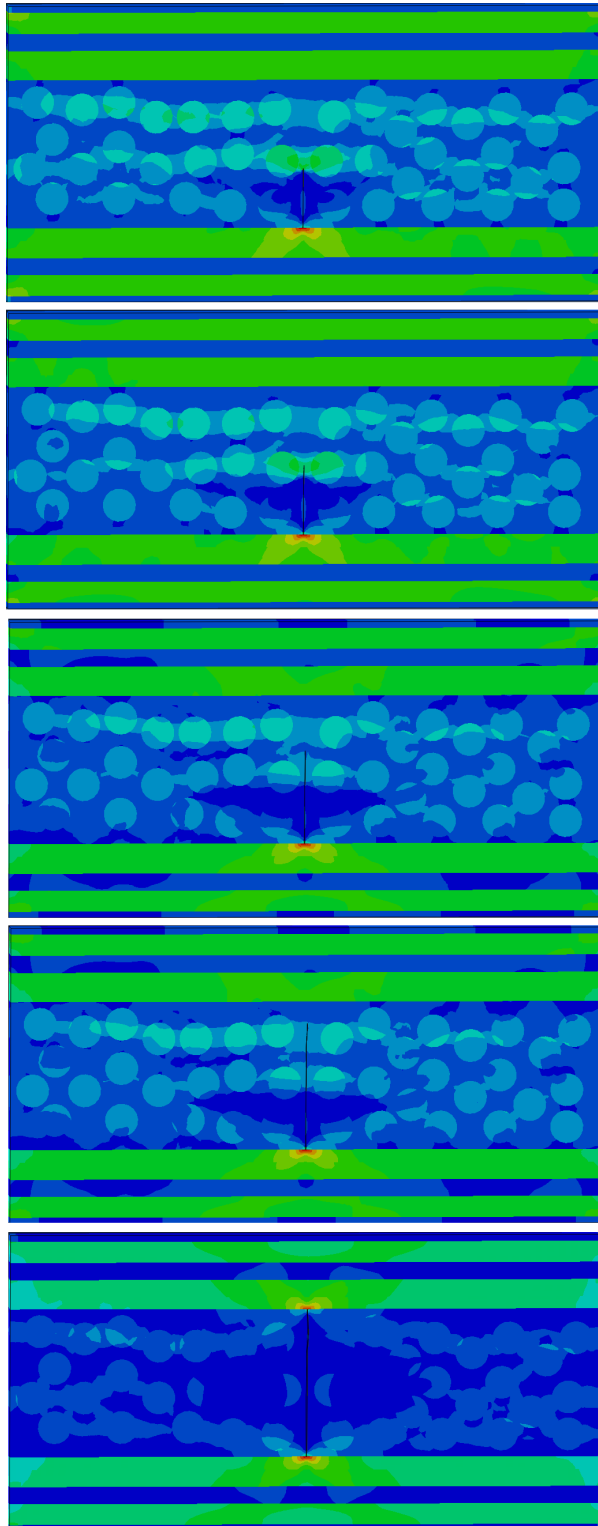


Figure 3.10: Crack growth in a cross-ply RVE using XFEM

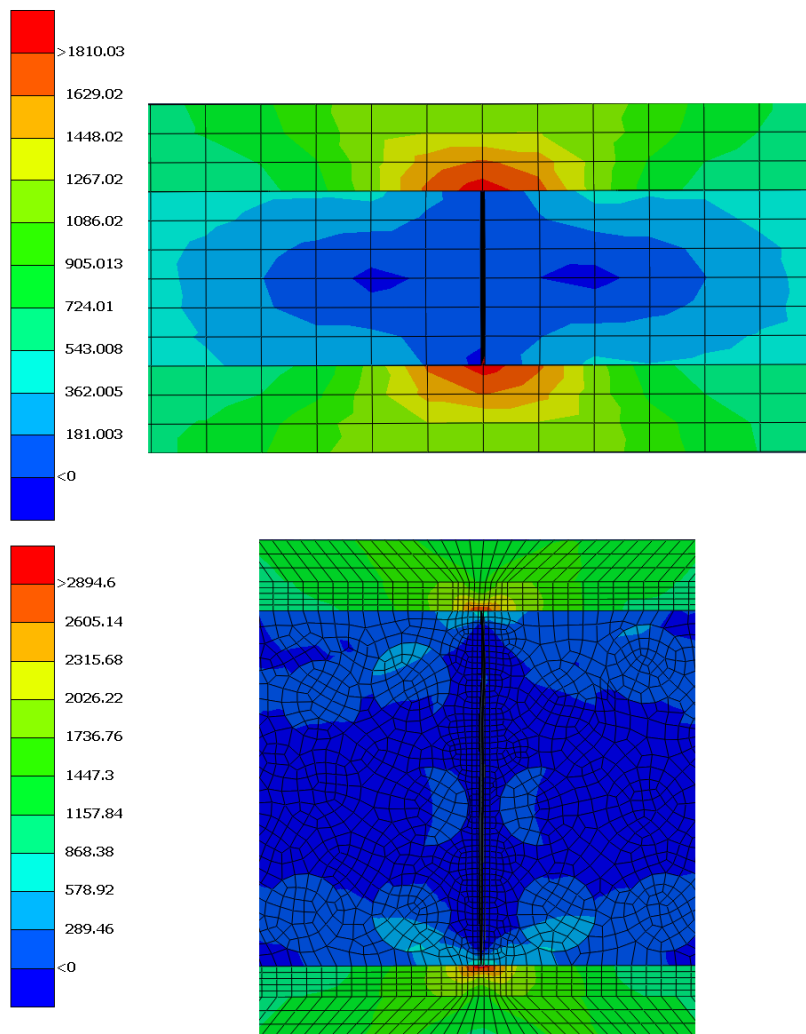


Figure 3.11: Stress concentration comparison between micro and macro models. Color-bars depict stresses in MPa

## 3.6 Conclusions

In this study, a model is proposed for the simulation of damage in cross-ply composite materials. The model incorporates shear-lag effect for the determination of the stress transfer and furthermore it adopts a semi-analytical homogenization procedure for the calculation of elastic and viscoelastic material properties based on the Mori-Tanaka and Voigt approaches. The homogenization algorithm can take into account random orientations by performing orientational averaging using fibers' orientation tensor. Random matrix cracking was simulated by placing a large number of possible cracks with their strength following a normal distribution and is modeled with CZM technique. Mesh sensitivity analysis has been performed showing that cracking saturation occurs with the same number of cracks guaranteeing the consistency of computations. The production simulations revealed that all the anticipated damage mechanisms are evident. Initially transverse cracks appeared and almost simultaneously made their presence clear delaminations at the interfaces near the crack tip. After the cracking initiation, stress redistributions were apparent. Overlapping stress field may be observed too, in the case where two adjacent cracks are in close proximity. Simulation predictions for the crack density as a function of strain are compared with available experimental data showing reasonable agreement. Finally, a cross-ply RVE model was created and loaded in uniaxial tension in a crack propagation analysis with XFEM. The stress concentrations around the crack tips are in agreement with the mesoscale model.

The proposed methodology with the proper modifications and additional development can be used towards the simulation of self-healing of materials and the authors work in that direction.

## References

- [1] F. C. J.M.Berthelot, “A model for transverse cracking and delamination in cross-ply laminates,” *Composites Science and Technology*, vol. 60, no. 7, pp. 1055 – 1066, 2000.
- [2] N. Moes, J. Dolbow, and T. Belytschko, “A finite element method for crack growth without remeshing,” *International Journal for Numerical Methods in Engineering*, vol. 46, no. 1, pp. 131–150, 1999.
- [3] Y. Shi, C. Pinna, and C. Soutis, “Interface cohesive elements to model matrix crack evolution in composite laminates,” *Applied Composite Materials*, vol. 21, pp. 57–70, 2014.
- [4] W. Ogierman and G. Kokot, “Homogenization of inelastic composites with misaligned inclusions by using the optimal pseudo-grain discretization,” *International Journal of Solids and Structures*, vol. 113-114, pp. 230–240, 2017.
- [5] E. Tsivolas, L. N. Gergidis, and A. S. Paipetis, “Prediction of damage mechanisms of cross-ply composite materials using novel non-linear multiscale methodologies,” *Modelling and Simulation in Materials Science and Engineering*, vol. 29, no. 8, p. 085015, 2021.
- [6] J. Aboudi, “Micromechanical analysis of composites by the method of cells,” *Applied Mechanics Reviews*, vol. 42, no. 7, pp. 193–221, 1989.
- [7] G. Kassem and D. Weichert, “Micromechanical material models for polymer composites through advanced numerical simulation techniques,” *PAMM*, vol. 9, pp. 413 – 414, 2009.
- [8] E. Tsivolas, L. N. Gergidis, and A. S. Paipetis, “Computational multi-scale modelling of fiber-reinforced composite materials,” in *Advances in Fracture and Dam-*

*age Mechanics XVIII*, vol. 827 of *Key Engineering Materials*, pp. 263–268, Trans Tech Publications Ltd, 2020.

- [9] O. Pierard, C. Friebel, and I. Doghri, “Mean-field homogenization of multi-phase thermo-elastic composites: A general framework and its validation,” *Composites Science and Technology*, vol. 64, pp. 1587–1603, 2004.
- [10] H. Fukunaga, T.-W. Chou, P. Peters, and K. Schulte, “Probabilistic failure strength analyses of graphite/epoxy cross-ply laminates,” *Journal of Composite Materials*, vol. 18, no. 4, pp. 339–356, 1984.
- [11] T. Mura, *Micromechanics of Defects in Solids*. Martinus Nijhoff Publishers, 1988.
- [12] J. D. Eshelby, “The Determination of the Elastic Field of an Ellipsoidal Inclusion, and Related Problems,” *Proceedings of the Royal Society of London Series A*, vol. 241, pp. 376–396, 1957.
- [13] S. G. Advani and C. L. Tucker, “The use of tensors to describe and predict fiber orientation in short fiber composites,” *Journal of Rheology*, vol. 31, no. 8, pp. 751–784, 1987.
- [14] C. Friebel, I. Doghri, and V. Legat, “General mean-field homogenization schemes for viscoelastic composites containing multiple phases of coated inclusions,” *International Journal of Solids and Structures*, vol. 43, no. 9, pp. 2513–2541, 2006.
- [15] R. Schapery, “A simple collocation method for fitting viscoelastic models to experimental data,” *GALCIT SM 61-32A California Institute of Technology, Pasadena CA*, 1962.
- [16] L. Galuppi and G. Royer-Carfagni, “Laminated beams with viscoelastic interlayer,” *International Journal of Solids and Structures*, vol. 49, no. 18, pp. 2637–2645, 2012.

- [17] Z. Xia, Y. Chen, and F. Ellyin, “A meso/micro-mechanical model for damage progression in glass-fiber/epoxy cross-ply laminates by finite-element analysis,” *Composites Science and Technology*, vol. 60, pp. 1171–1179, 2000.
- [18] D. Mora, C. Gonzalez, C. Lopes, F. Naya, and J. Llorca, “Analysis of transverse cracking in unidirectional composite plies by means of computational micromechanics,” *16th European Conference on Composite Materials, ECCM 2014*, 2014.
- [19] S. Lim and C. Hong, “Prediction of transverse cracking and stiffness reduction in cross-ply laminated composites,” *Journal of Composite Materials*, vol. 23, no. 7, pp. 695–713, 1989.
- [20] M. Ghayour, H. Hosseini-Toudeshky, M. Jalalvand, and E. J. Barbero, “Micro/macro approach for prediction of matrix cracking evolution in laminated composites,” *Journal of Composite Materials*, vol. 50, no. 19, pp. 2647–2659, 2016.
- [21] T. Gorris, P.-É. Bernard, and L. Stainier, “A study of transverse cracking in laminates by the Thick Level Set approach,” *Mechanics of Materials*, vol. 90, pp. 118–130, 2015.
- [22] D. Mortell, D. Tanner, and C. McCarthy, “In-situ sem study of transverse cracking and delamination in laminated composite materials,” *Composites Science and Technology*, vol. 105, pp. 118–126, 2014.
- [23] L. R. Dharani, J. Wei, F. S. Ji, and J. H. Zhao, “Saturation of transverse cracking with delamination in polymer cross-ply composite laminates,” *International Journal of Damage Mechanics*, vol. 12, no. 2, pp. 89–114, 2003.
- [24] Z. R. Khokhar, I. Ashcroft, and V. Silberschmidt, “Interaction of matrix cracking and delamination in cross-ply laminates: Simulations with stochastic cohesive zone elements,” *Applied Composite Materials*, vol. 18, pp. 3–16, 2011.

- [25] I. Garcia, V. Mantic, A. Blazquez, and F. Paris, “Transverse crack onset and growth in cross-ply [0/90]s laminates under tension. application of a coupled stress and energy criterion,” *International Journal of Solids and Structures*, vol. 51, no. 23, pp. 3844 – 3856, 2014.
- [26] A. Kaddour, M. Hinton, P. Smith, and S. Li, “Mechanical properties and details of composite laminates for the test cases used in the third world-wide failure exercise,” *Journal of Composite Materials*, vol. 47, no. 20-21, pp. 2427–2442, 2013.
- [27] J. Nairn and S. Hu, “Micromechanics of damage: a case study of matrix microcracking,” in *Damage mechanics of composite materials* (R. Talreja, ed.), pp. 117–138, The Netherlands: Elsevier, 1994.
- [28] J. Nairn, “On the use of shear-lag methods for analysis of stress transfer in unidirectional composites,” *Mechanics of Materials*, vol. 26, no. 2, pp. 63 – 80, 1997.
- [29] J. Nairn, “Matrix microcracking in composites,” in *Polymer Matrix Composites, Comprehensive Composite Materials* (R. Talreja and J. Manson, eds.), pp. 403–432, Amsterdam: Elsevier Science, 2000.
- [30] M. Benzeggagh and M. Kenane, “Measurement of mixed-mode delamination fracture toughness of unidirectional glass/epoxy composites with mixed-mode bending apparatus,” *Composites Science and Technology*, vol. 56, no. 4, pp. 439–449, 1996.
- [31] P. A. Carraro, E. Novello, M. Quaresimin, and M. Zappalorto, “Delamination onset in symmetric cross-ply laminates under static loads: Theory, numerics and experiments,” *Composite Structures*, vol. 176, pp. 420 – 432, 2017.
- [32] D. T. G. Katerelos, A. Paipetis, T. Loutas, G. Sotiriadis, V. Kostopoulos, and S. L. Ogin, “In situ damage monitoring of cross-ply laminates using acoustic emission,” *Plastics, Rubber and Composites*, vol. 38, no. 6, pp. 229–234, 2009.
- [33] abaqus, *ABAQUS/CAE user’s manual*. Pawtucket, RI : ABAQUS.

- [34] R. Hill, “Theory of mechanical properties of fibre-strengthened materials: I. elastic behavior,” *Journal of the Mechanics and Physics of Solids*, vol. 12, pp. 199–212, 1964.



## **Chapter 4**

# **Prediction of Damage Mechanisms of Cross-ply Composite Materials Using Novel Nonlinear Multiscale Methodologies**

In the present work, a novel multiscale material methodology is applied to a Finite Element mesh of a cross-ply composite material in tension in order to study the progressive damage and failure of the material at multiple scales by combining damage evolution models and failure criteria in microscale and cohesive zone modeling in macroscale. The micromechanics user material (Umat) developed follows a nonlinear version of the Mori-Tanaka theory and is coupled with mesoscale damage model. The concept of this user material is to dehomogenize-localize the strain tensor at each integration point for each time increment using Eshelby's theories and strain concentration tensors. This material implementation allows the researcher to analyze results at two scales in the post processing stage, both for the composite material and the constituents for each time increment. It is observed that in the multiscale model the results are closer to the experimental measurements and even more damage mechanisms can be predicted, such as matrix damage

and fiber failure. The developed multiscale methodology is advantageous since the constituents can follow different material models, with many failure criteria. It is also capable of predicting stresses, strains, plastic strains and more analysis variables not only in the macroscale-homogeneous level but also in microscale constituent-wise level.

## 4.1 Introduction

Composite materials are chosen for components in various industries such as automotive, aerospace, civil infrastructure and marine among others since they combine low weight with high stiffness and strength. Their actual structural response can be unpredictable and the damage may occur in various forms by different mechanisms such as matrix cracking, delaminations, fiber pullout, fiber cracking. For that reason multiscale modelling becomes more and more popular, aiming the clarification of complex structural response mechanisms.

The damage mechanisms appearing in a cross-ply composite material loaded in tension have been studied and simulated extensively. Matrix cracking usually is the first observed form of damage. Although transverse cracks alone cannot cause structural failure they could be responsible for stiffness degradation that leads to more severe forms of damage (1) (2) (3) (4) (5) (6) (7) (8) (9). It is found that after a specific value of strain the first cracks are initiated, and the cracking continues as the loading increases. Simultaneously, delaminations at the crack tips in the interface between the  $0^\circ$  and  $90^\circ$  layers appear. As the cracking continues, stress redistribution at the uncracked portions of the  $90^\circ$  layers takes place to relieve some of the concentrated stress in the cracks. Finally, as the crack density reaches its threshold, cracking saturation is achieved and no more cracks are opening. At this moment all the tension is handled from the  $0^\circ$  layers until their maximum stress capacity is reached signaling the analysis termination.

The aforementioned procedure which includes cracking initiation, cracking propagation with delaminations and finally saturation has been simulated successfully using

various damage methodologies such as XFEM, VCCT, cohesive elements or cohesive zone modelling among others (10) (11) (12) (13) (14) (15) (16). The cohesive zone model (CZM) is a fast computational approach which allows the connection of differently meshed surfaces. By the adoption of CZM the crack interfaces and the interfaces between the layers are simulated using cohesive contacts. The aforementioned method allows different mesh sizes between the layers which can be easily used with explicit dynamic analysis. Petrov et al. (13) used a linear cohesive law within XFEM for intra-ply damage, to study the initiation, development and saturation of transverse cracks. Lee (17) performed a 2D finite element simulation of a cross-ply composite in a uniaxial tension and pure bending, modeling the potential cracks and the interface between the layers of the composite using cohesive elements. In that case the elliptical profile of the transverse cracking was simulated successfully but no delaminations were triggered. Van der Meer and Dávila (15) used an XFEM approach with a single element per ply in a 2D analysis to study the transverse cracking effect. Also in the same study a 3D analysis was performed using cohesive zone model to simulate transverse cracks and delaminations. Eftekhari et al. (18) performed a simulation with XFEM to predict the macromodel's cracking characteristics accompanied by a sequential multiscale approach in three scales to predict the material properties. It should be mentioned that our present proposed methodology uses a real time scale transition using Umat subroutine where non-linear semi analytical methods are developed and the linking between scales is performed with localization tensors. In the research works (19) (20) (21) (22) the general context of numerical FE2 real time scale transition method is used to link the two scales where both micro and macro models are simulated with FE discretizations. The method is very accurate removing certain limitations of the semi analytical methods but is significantly slower compared to mean-field (semi-analytical) solutions especially for complex non-linear materials.

In the present study, a cross-ply epoxy-glass fiber reinforced composite material is simulated in tension, to predict all the damage mechanisms using multiscale methodologies. There are several structural finite element solvers that offer advanced numerical

material models for composites. Most of them consider composite materials as homogeneous and some other adopt micromechanical theories. However, the most accurate is to take advantage of a multiscale model technique to account for all the material's inhomogeneities. This implies that the composite material's properties are not known in the homogeneous level. Instead, only the individual linear and nonlinear properties of the constituents are known. This capability is offered by developing a user material code coupled with a finite element solver (23).

The micromechanics user material developed for the needs of the present study follows a nonlinear version of the Mori-Tanaka theory(24). The user material developed in house as a Vumat subroutine in C++ programming language, and linked with Abaqus/Explicit 2019 (25), a commercial finite element solver. The novelty of this attempt to solve a widely studied problem is the prediction of the damage and failure mechanisms in multiple scales with the combination of damage evolution models and failure criteria in microscale and cohesive zone modeling in macroscale, while taking into account all the material nonlinearities, without the need to model the whole specimen in the microscale that would result in enormous computational times. Most of the already published works treat the layer as homogeneous ignoring the particular mechanical characteristics of each constituent unlike the proposed method. Several multiscale solutions (24) (26) (27) (28) (29) have been proposed to account for the heterogeneities while detouring the FE simulation in microscale. The modified Mori-Tanaka theory that accounts for non linearities is similar to other micromechanics methods such as the self-consistent (SC) solution since the concentration tensors are calculated from the instantaneous properties of the matrix material and are used to estimate the instantaneous overall properties of the non linear composite material. Even though the SC model can be applied to general composite materials and to materials without a matrix phase such as polycrystals, for composites having constituents with different material properties the SC model usually leads to too stiff predictions. For that reason Mori-Tanaka theory was chosen.

The concept of this user material is to dehomogenize the strain tensor at each integra-

tion point for each time increment using Eshelby's theories (30) and strain concentration tensors. Therefore, knowing the strain tensor of each constituent (fiber and matrix) one is able to apply different material model for the fiber and the matrix and also failure criteria for each constituent separately. It should be noted that the solver's convergence to the desired solution necessitates the calculation of the homogenized material's Jacobian inside the subroutine before moving to the next time step. This Jacobian is the consistent tangent stiffness matrix of the composite material that helps the solver achieving quadratic convergence. The above formulation encloses several difficulties. For example, the more advanced the individual material models are the more difficult is the numerical calculation of the homogenized tangent stiffness matrix. This can be avoided using a dynamic explicit analysis where such calculations are not needed. In general, explicit integration methodologies do not require consistent tangent stiffness calculations for the material since convergence is not checked at the end of each time increment due to the use of very small timesteps. An update of the homogenized stresses at each integration point is adequate for the solver to proceed to the next time step, which is trivial when using incremental formulations linearizing the behavior between the time steps, for example by using the volume average of the matrix and fiber stresses. This material implementation allows the researcher to obtain results at two scales in the post processing stage, both for the composite material and the constituents for each time step. The material in this study is a cross-ply fiber reinforced composite material that is solved in a dynamic explicit analysis. A visco-elasto-plastic material model with high damage evolution rate for the epoxy resin is developed.

## 4.2 Multiscale analysis algorithm

Using Eshelby's theory (31) of strain concentration tensors the composite's strain at a single integration point can be dehomogenized in matrix strain  $\varepsilon_m$  and fiber strain  $\varepsilon_f$  for linear elastic materials. Correspondingly, the homogenization can be performed using the

Mori-Tanaka theory (32). The same applies for the strain increment in non-linear materials using the incremental formulation. The strain increment that the solver provides is referred to an integration point of the whole microstructure and not for a specific constituent. In order to be able to apply different material models for the fiber and the matrix, the dehomogenization of the strain increment should be performed. The strain increment averages per phase are related by a strain concentration tensor  $\mathbf{B}^\varepsilon$  as follows:

$$\langle \Delta \varepsilon \rangle_m = [V_f \mathbf{B}^\varepsilon + (1 - V_f) \mathbf{I}]^{-1} : \langle \Delta \varepsilon \rangle \quad (4.1)$$

$$\langle \Delta \varepsilon \rangle_f = \mathbf{B}^\varepsilon : \langle \Delta \varepsilon \rangle_m = \mathbf{B}^\varepsilon : [V_f \mathbf{B}^\varepsilon + (1 - V_f) \mathbf{I}]^{-1} : \langle \Delta \varepsilon \rangle \quad (4.2)$$

with  $\mathbf{B}^\varepsilon$  given by

$$\mathbf{B}^\varepsilon = [\mathbf{I} + \mathbf{E} : (\mathbf{C}_m^{-1} : \mathbf{C}_f - \mathbf{I})]^{-1}, \quad (4.3)$$

where  $\mathbf{I}$  is the fourth order unit tensor,  $\mathbf{E}$  is the Eshelby's tensor,  $\mathbf{C}_m$ ,  $\mathbf{C}_f$  the stiffness tensor for matrix and fiber respectively and  $V_f$  the fiber's volume fraction. After obtaining the individual strain increments the respective material models for each constituent can be applied. This procedure is repeated for every integration point of the model for each time increment and updates the history variables of the material model of each constituent. At every iteration all integration points are examined for possible failure. If the integration point belongs to the outer layers where the fibers are aligned to the loading then the most possible failure mechanism is the fiber failure. On the contrary, if the integration point belongs to the middle layers the most possible failure mechanism is the matrix failure that can either happen by deleting elements when the damage value overcomes the critical damage or by failure of transverse contacts which is the most usual. In **Figure 5.2** the flow chart of multiscale material implementation is presented. In A a comparison with a numerically solved representative volume element is performed for verification purposes.

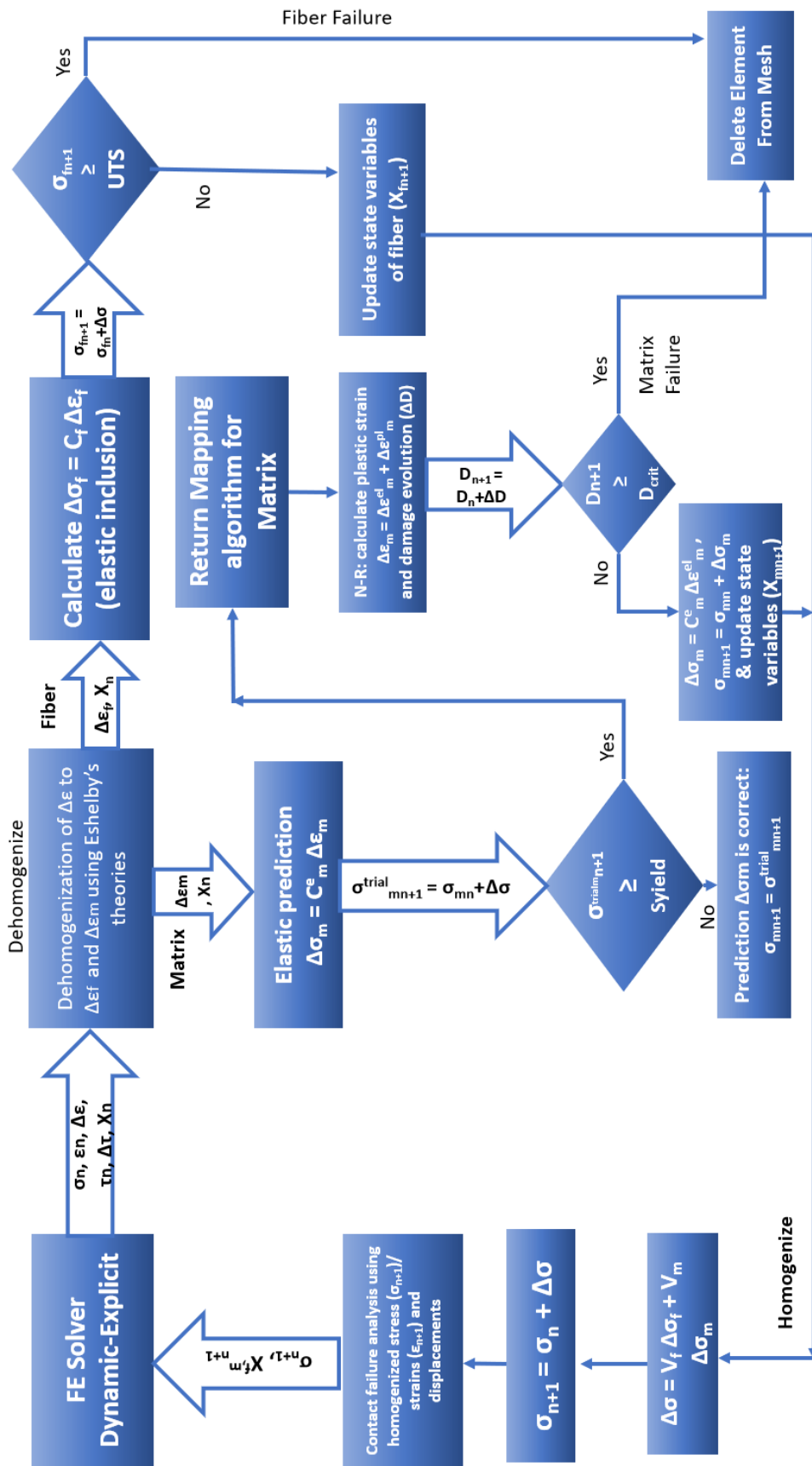


Figure 4.1: Flow chart of multiscale material implementation

## 4.3 Material modelling

### 4.3.1 Matrix material

As mentioned earlier for the glass epoxy material, a prony series viscoelastic material with isotropic hardening plasticity and Chaboche damage with high evolution rate is used. In this model, the matrix stiffness is reduced in time due to viscous effects and once the plasticity and damage is initiated, the matrix stiffness degrades further due to softening that occurs with damage evolution. Using multiscale techniques it is possible to predict the properties' degradation that the material exhibits as the time passes and the loading continues. A damage parameter is calculated through time and accumulates with increasing strain. When the aforementioned parameter exceeds a critical value the material fails and the element can be deleted. The matrix strain can be decomposed (33) to viscoelastic and plastic parts:  $\varepsilon_m = \varepsilon_m^{ve} + \varepsilon_m^{pl}$ .

### 4.3.2 Homogenization of viscoelastic materials

It is commonly known that the loading rate in some materials such as plastics greatly affects the mechanical response due to viscous effects. In those cases a variation of the strain rate can have great impact on the final stiffness of the composite material. To capture those effects various viscoelastic material models have been developed (29). In order to have a clear picture about the viscous effects the total strain can be decomposed in one instantaneous part which is the elastic strain and in a second part that describes a delay in time which is the viscous behavior. In general, viscous effects can be described as a result of the time left to the material to conform with a new configuration at molecular level having minimum energy. In plastics at very low strain rate (quasi-static) the molecular chains have adequate time to align themselves with respect to the load. In higher strain rates this time becomes smaller and as a result the material exhibits stiffer behavior. At this study this behavior is captured using a viscoelastic homogenization scheme taking advantage of the prony series viscoelasticity for the matrix material. The glass fibers can

be considered as linear elastic at room temperature. The following equation describes the viscoelastic material model:

$$\sigma(t) = G(t) : \varepsilon(0) + \int G(t - \tau) : \dot{\varepsilon}^{(ve)}(\tau) d\tau \quad (4.4)$$

with

$$\varepsilon(0) = \lim_{t \rightarrow 0^+} \varepsilon(t) \quad (4.5)$$

and

$$G(t) = 2G_R(t) I^{dev} + K_R(t) \hat{I} \otimes \hat{I} \quad (4.6)$$

where  $\sigma, \varepsilon$  the stress and strain second order tensors,  $G(t)$  is the relaxation tensor,  $\dot{\varepsilon}^{(ve)}$  the viscoelastic (ve) strain rate tensor,  $I^{dev}$  is the deviatoric part of the fourth (4th) order identity tensor and  $\hat{I}$  is the second order identity tensor with  $\otimes$  being the juxtaposition symbol for the dyadic product. The time dependent bulk and shear modulus can be expressed using prony series described by the following equations:

$$G_R(t) = G(0) \left[ 1 - \sum_{i=1}^n w_i (1 - e^{-t/\tau_i}) \right] \quad (4.7)$$

$$K_R(t) = K(0) \left[ 1 - \sum_{i=1}^{n'} w_i^* (1 - e^{-t/\tau_i^*}) \right] \quad (4.8)$$

where  $\tau_i, \tau_i^*$  are the relaxation times and  $w_i, w_i^*$  the respective weights of each relaxation time.

The above linear viscoelastic stress-strain relation (**Eq. 4.4**) for isotropic materials can be transformed to an elastic analogous  $\hat{\sigma}(s) = \hat{E}(s)\hat{\varepsilon}(s)$  formulation in the Laplace-Carson domain ((29; 34)) applying the transformation in the time domain for all the involved equations (constitutive equations, boundary conditions etc.), where  $\hat{\sigma}, \hat{E}$  and  $\hat{\varepsilon}$  are the transformed stress, stiffness and strain tensor in Laplace domain and  $s$  is a complex variable. The result is a fictitious RVE in the complex domain (29). In order to get the homogenization results back in time domain the inverse Laplace-Carson transformation

is required. One of the most computationally efficient methods to perform the inversion is the collocation method (35). Prony series values are given in **Table 4.1** and are used to perform viscoelastic homogenization.

### 4.3.3 Homogenization of materials in plastic region

Once the stress has exceeded the yield stress and the yield condition is satisfied then the material is in the non-linear region. Using the Hooke's law in rate form it is possible to linearize the behavior. In the following formulation the values are referring to the matrix while the index  $m$  is omitted for simplicity:

$$\dot{\sigma} = C^{ep} : \dot{\varepsilon} \quad (4.9)$$

where  $C^{ep}$  is the elasto-plastic tangent modulus (or material Jacobian). The discretization of the above rate equation in time provides the following framework which can be used in the incremental formulation of the material between two consecutive time increments.

$$\delta\sigma_{n+1} = C^{alg} : \delta\varepsilon_{n+1} \quad (4.10)$$

In the above formulation  $C^{alg}$  is the consistent numerical tangent modulus of the material that relates the stress increment with the strain increment and helps the solver to achieve quadratic convergence in implicit analysis. As mentioned earlier the material that was used to simulate the matrix of the composite in the non-linear region is a plastic material with isotropic hardening that follows the von Mises (J2) plasticity theory. The constitutive equations for plasticity can be seen in equations (12)-(17):

$$\sigma = C^{el} : (\varepsilon - \varepsilon^{pl}) \quad (4.11)$$

$$f = \sigma_{eq} - R(p) - \sigma_Y \leq 0 \quad (4.12)$$

$$\dot{\varepsilon}^p = \dot{p}N \quad (4.13)$$

$$\dot{p} \geq 0 \quad (4.14)$$

$$\dot{p}f = 0 \quad (4.15)$$

$$N = \frac{\partial f}{\partial \sigma} = \frac{3dev(\sigma)}{2\sigma_{eq}} \quad (4.16)$$

where  $\sigma_Y$  is the initial yield stress of the material,  $p$  is the accumulated plastic strain of the matrix,  $R(p)$  is the hardening stress, and  $\sigma_{eq}$  is the von Mises measure of the Cauchy's stress tensor, and  $dev(\sigma)$  describes the deviatoric part of stress  $\sigma$  tensor. In order to calculate plastic strain increment from equation (14), the calculation of accumulated plastic strain increment from the following equation has to be preceded (26). This is a nonlinear equation if the hardening function  $R(p)$  is non-linear and can be solved using the Newton-Raphson algorithm

$$3G\Delta_p + R(p) + \sigma_y - \sigma_{eq}^{trial} = 0 \quad (4.17)$$

Finally,  $N$  is the vector, normal to the yield surface of the examined material. For completeness reasons, the tangent stiffness moduli are mentioned here, since they are not needed in explicit integration analysis.

$$C^{ep} = C^{el} - \frac{(2\mu)^2}{h} N \otimes N \quad (4.18)$$

$$h = 3\mu + \frac{dR}{dp} > 0 \quad (4.19)$$

$$C^{alg} = C^{ep} - (2\mu)^2(\Delta p) \frac{\sigma_{eq}}{\sigma_{eq}^{tr}} \frac{\partial N}{\partial \sigma} \quad (4.20)$$

$$\frac{\partial N}{\partial \sigma} = \frac{1}{\sigma_{eq}} \left( \frac{3}{2} I^{dev} - N \otimes N \right) \quad (4.21)$$

#### 4.3.4 Chaboche ductile damage model

Although a fourth rank tensor should be used to describe the damage states on the stiffness tensor, it is very common for practical reasons and simplicity to adopt scalar damage models in meso- and micro-plasticity (36). In the model developed in this study, the usual assumption is adopted where the strain observed in the actual body and in its undamaged form are equivalent, and the average effective stress is defined as (37)(38)(39)

$$\hat{\sigma} = \sigma / (1 - D) \quad (4.22)$$

where  $0 \leq D \leq 1$  is the damage variable. From the von Mises yield criterion, if  $f < 0$  then the behavior remains elastic. No plastic strain or damage evolution for the specific strain increment is occurring. On the other hand, if  $f = 0$ , then evolution of the plastic strain takes place as can be derived from the constitutive equations of the von Mises isotropic plasticity. After the calculation of the plastic strain increment the stress increment in plasticity can be calculated as

$$\delta \hat{\sigma} = C^{el} (\delta \varepsilon - \delta \varepsilon^{pl}). \quad (4.23)$$

When the material enters the plastic region the damage initiation law is evaluated to determine if damage starts. Usually the damage initiation law depends on a value of the accumulated plastic strain ( $p$ ) and if a particular value of plastic strain ( $p_c$ ) is exceeded then damage has started. Once the damage has started the damage evolution law is evaluated. In this study the damage evolution law is

$$\dot{D} = \begin{cases} 0 & p \leq p_c \\ (\frac{Y}{S_0})^s \dot{p} & p > p_c \end{cases} \quad (4.24)$$

where  $Y$  is the strain energy release rate and is calculated as

$$Y = \frac{1}{2} \varepsilon^{el} : C^{el} : \varepsilon^{el} \quad (4.25)$$

Damage variable ( $D$ ) is calculated by using the summation of the damage evolution law in each time increment and finally the updated stress is

$$\sigma = C^{el}(\varepsilon - \varepsilon^{pl})(1 - D) \quad (4.26)$$

### 4.3.5 Algorithm for calculation of matrix stress increment

The formulation that updates the matrix stress increment in this multiscale model consists of the following steps:

1. Dehomogenization of the total strain increment of the composite material that is provided by the solver is performed using the Eshelby's strain concentration tensors resulting to matrix strain increment and fiber strain increment.

2. Viscoelastic stiffness calculation with prony series for the current time step of the analysis. The whole matrix strain increment is considered viscoelastic:  $\Delta\sigma_m^{trial} = C_m^{ve} \Delta\varepsilon_m$

3. von Mises criterion application: if matrix stress is lower than the matrix yield stress then the trial stress calculated in the previous step is correct. In any other case calculate the plastic strain increment  $\Delta\varepsilon_m^{pl}$  such as  $\Delta\varepsilon_m = \Delta\varepsilon_m^{ve} + \Delta\varepsilon_m^{pl}$

4. Recalculation of the stress increment such as  $\Delta\sigma_m = \Delta\sigma_m^{trial} - C_m^{ve} \Delta\varepsilon_m^{pl}$

5. The total matrix stress is updated as  $\sigma_m^{n+1} = \sigma_m^n + \Delta\sigma_m$

6. Application of damage initiation criterion: if damage has been initiated calculate new stress reduction due to damage using the damage factor value for the current incre-

ment.

7. Application of failure criterion: if the damage factor reaches a critical value (usually is specified as unity) then the element fails and is deleted.

## 4.4 Fiber material

For the glass fiber material, as the experimental measurements show (40), the glass fibers exhibit linear response until failure. This can be modeled as a linear elastic material with constant properties over time with an ultimate tensile stress failure criterion. Therefore, when the strain is dehomogenized, a comparison of the current stress with the ultimate tensile strength (UTS) can be performed to decide if the material point can still be used in the calculations. When the stress is higher or equal to the UTS the element can be deleted. As the simulation findings in the sequel show, this happens after cracking saturation, where the stresses are concentrated at the crack tips and the fiber failure starts to take place. The fiber stress update at the multiscale material takes place as follows:

1. The fiber stress increment is calculated as  $\Delta\sigma_f = C_f^{el} \Delta\varepsilon_f$
2. The total fiber stress at the current increment is  $\sigma_f^{n+1} = \sigma_f^n + \Delta\sigma_f$
3. Finally, if  $\sigma_f^{n+1} > UTS_f$  the element is deleted.

## 4.5 Composite material

The response of the total composite material can be calculated from the volume average responses (41) of the individual constituents and the behaviour can be predicted for an integration point throughout the analysis from the Voigt assumption which incorporates the relations  $\Delta\sigma_c = V_f \Delta\sigma_f + V_m \Delta\sigma_m$  and  $\sigma_c^{n+1} = \sigma_c^n + \Delta\sigma_c$ . This homogenized response for a specific integration point is given in **Figure 5.14**. As this solution is provided from explicit integration, the consistent tangent modulus is not needed by the solver in order to converge and to proceed with the next step.

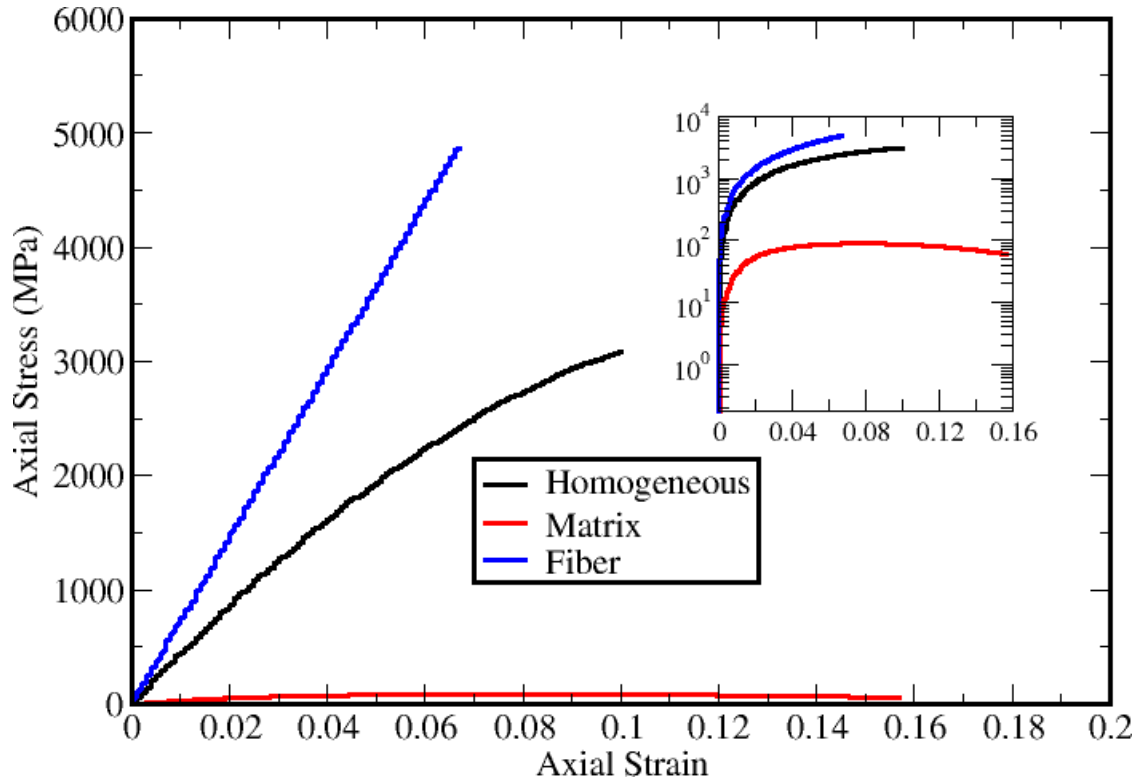


Figure 4.2: Axial stress vs. axial strain of elastic glass fibers, visco-elasto-plastic with damage matrix and of the homogenized response (Not enabled failure). The inset figure represents the values of axial stress in logarithmic scale for clarity

It should be noted that the element deletion can be controlled by any criterion which invokes solution variables relative to physical quantities such as stresses, strains and plastic strains. For instance for the homogeneous material the Tsai-Wu and Hashin criteria can be applied while for the composite material's constituents the ultimate strength criterion could be adopted. In addition, element deletion controls the fibers breakage and the matrix failure in the bulk material between the pre-positioned cracks if needed.

## 4.6 Cohesive zone modelling

The damage mechanisms that correspond to matrix cracking and delaminations are simulated using surface based cohesive contacts. Surface based cohesive behavior provides a way to model cohesive connection with negligibly small interfacial thickness and in this study it was successfully used to model both composite material delamination and matrix

cracking. The particular traction separation model assumes linear elastic behavior until the initiation and propagation of damage. The elastic behavior is described in terms of a constitutive matrix that relates the stresses to the separations across the interface through the following equation

$$\begin{bmatrix} t_n \\ t_s \\ t_t \end{bmatrix} = \begin{bmatrix} K_{nn} & K_{ns} & K_{nt} \\ K_{ns} & K_{ss} & K_{st} \\ K_{nt} & K_{st} & K_{tt} \end{bmatrix} \begin{bmatrix} \delta_n \\ \delta_s \\ \delta_t \end{bmatrix} \quad (4.27)$$

where  $t_n, t_s, t_t$  are the normal and the two shear tractions respectively and  $\delta_n, \delta_s, \delta_t$  are the corresponding separations. Also, this modeling type demands a geometrically nonlinear analysis.

In **Figure 4.3**, the variable  $(t_n/t_0^n)^2 + (t_s/t_0^s)^2 + (t_t/t_0^t)^2$  (depicted in the colorbar) indicates whether the quadratic contact stress damage initiation criterion has been satisfied at a contact point. If its value is equal to 1 the criterion has been fulfilled and if damage evolution is specified for this criterion, the maximum value of this variable does not exceed 1. When the damage initiation is triggered, damage can occur following a specified damage evolution law. For this modeling technique the damage evolution describes the stiffness degradation of cohesive contacts, in contrast to cohesive elements where the damage evolution describes the material stiffness degradation. An analytical energy based damage evolution law was adopted as proposed by Benzeggagh-Kenane (42) which is particularly useful when the critical energies during separation exclusively along the first and second shear directions are the same ( $G_s^C = G_t^C$ )

$$G_n^C + (G_s^C - G_n^C)(G_{shear}/G_t)^n = G^C \quad (4.28)$$

$$G_{shear} = G_s + G_t \quad (4.29)$$

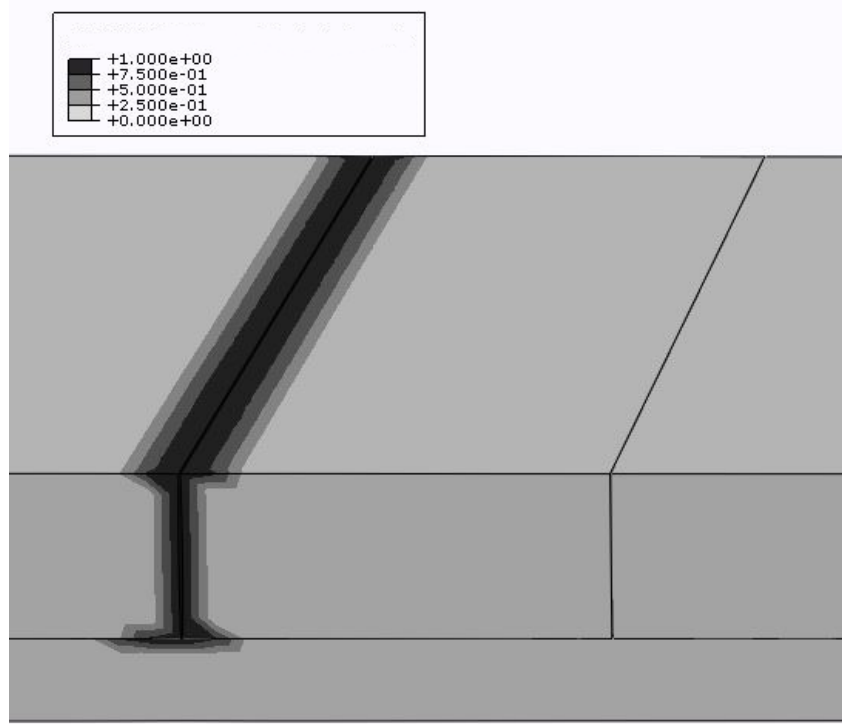


Figure 4.3: Crack and delamination using cohesive zone modeling. Color bar represents contact failure

$$G_T = G_n + G_{shear} \quad (4.30)$$

where  $n$  is a cohesive property parameter and  $G_n^C, G_s^C, G_t^C$  refer to the critical fracture energies required to cause failure at the normal, first and second directions, respectively.

## 4.7 Finite Element Model description

The above multiscale formulation was applied to a cross-ply (0/90)s fiber reinforced composite in order to examine the damage and failure mechanisms that were observed in the experimental procedure (43). An important feature of the multiscale modelling is the micromechanics considerations that take place allowing to apply a different material model for each constituent but also predict the homogeneous behavior of the total composite in an incremental form following the solver's time steps. The constituents are the epoxy resin matrix reinforced with long glass fibers at a volume fraction of 63%. Their proper-

ties can be seen in **Table 4.1**. The footnote in **Table 4.1** refers to the response of the matrix material after 270 seconds of loading. The non-linear material response can be captured by the aforementioned multiscale algorithm.

Table 4.1: Elastic Properties

Property	Epoxy resin	Glass fiber
Young's modulus (GPa)	3*	73.1
Poisson's ratio	0.395	0.18
Volume fraction	0.37	0.63

\*Visco-elastic response at 270 seconds

In **Table 4.2** the prony series relaxation times and weights for the matrix material can be seen.

Table 4.2: Relaxation modulus prony series relaxation times  $\tau_i$  and weights  $w_i$  obtained from (44)

$\tau_i$ (sec)	$w_i$
$4.949 \times 10^{-8}$	$7.878 \times 10^{-2}$
$7.243 \times 10^{-8}$	0.2912
$9.864 \times 10^{-6}$	$7.115 \times 10^{-2}$
$2.800 \times 10^{-3}$	0.2688
0.1644	$8.96 \times 10^{-2}$
2.265	$3.018 \times 10^{-2}$
35.36	$7.606 \times 10^{-3}$
9368	$9.634 \times 10^{-4}$
641400	$4.059 \times 10^{-3}$

The non-linear properties of the matrix material has calibrated from the corresponding experimental values as can be seen in **Figure 4.4**. The calibration was performed using a non-linear programming optimization algorithm for one integration point at the non-linear regime giving the following values of **Table 4.3**. The failure values for matrix cracking, fiber failure and interlaminar shear strength can be seen in Table 4.4. The interface between the layers is modeled with cohesive contacts, in a non-linear analysis framework after examining the alternative options which can be cohesive elements or XFEM. The use of cohesive elements increases significantly the number of the total finite elements and in

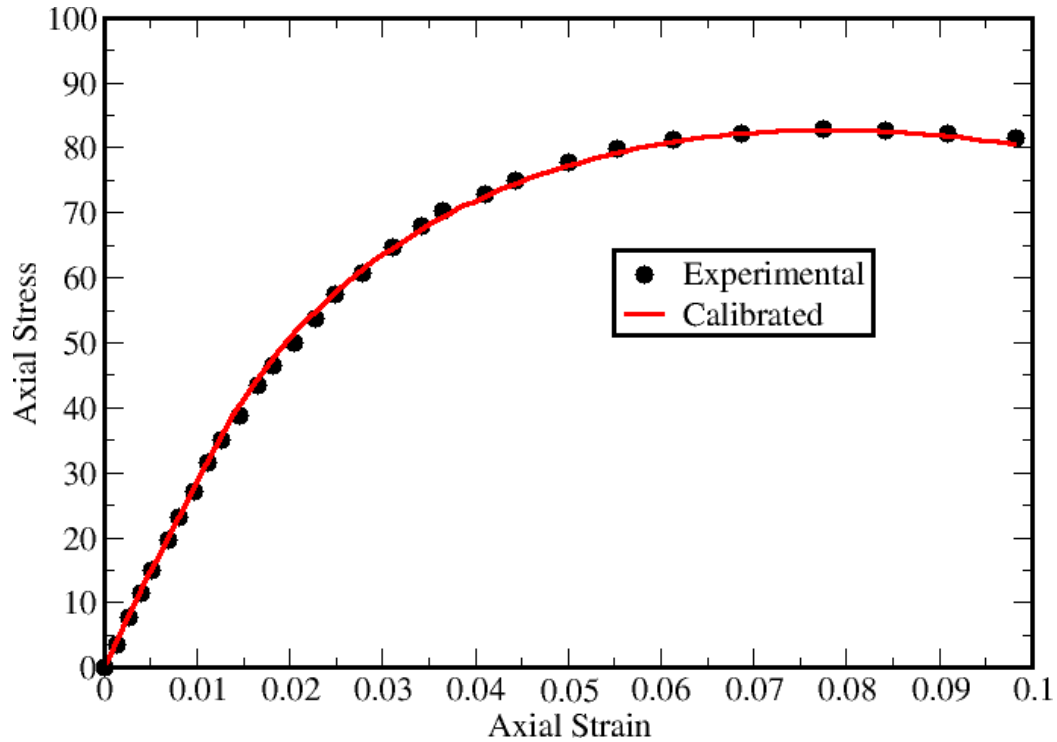


Figure 4.4: Experimental (45) vs. calibrated response of a visco-elasto-plastic with damage non-linear material

Table 4.3: Plastic and damage properties of matrix

Yield stress (MPa)	10
Hardening Modulus (MPa)	206
Hardening Exponent	0.28
Damage Rate Factor	2.8
Damage Exponent	1
Damage Initiation	0

addition demands all the layers to be similarly discretized. For the second option the applicability and the accuracy of the XFEM are debatable and this method can only be used with implicit integration. The available traction-separation model assumes initially linear elastic behavior followed by the initiation and evolution of damage. The elastic behavior is written in terms of an elastic constitutive matrix that relates the nominal stresses to the nominal strains across the interface. The failure of the contacts follow the maximum shear stress criteria.

Matrix Cracking (MPa)	60
ILSS (MPa)	50
Fracture energy Mode I(J/m <sup>2</sup> ) matrix cracking	500
Fracture energy mode II, III matrix cracking(J/m <sup>2</sup> )	1540
Fracture energy mode I for delamination (J/m <sup>2</sup> )	500
Fracture energy mode II, III for delamination (J/m <sup>2</sup> )	800
Ultimate tensile strength of Glass fibers (MPa)	800

### 4.7.1 Geometry

The model represents an undamaged part between two adjacent cracks with total length of 30 mm. Each laminate has 0.25 mm thickness. In the geometry discretization procedure four rows of three dimensional solid elements in the thickness direction of each shell laminates were placed with a total number of 96000 elements. The elements that were used are first order hexahedral elements with reduced integration of type C3D8R. The prediction of random matrix cracking was succeeded by setting a large number of possible cracks with cohesive interface across the 90° layers. The number of the potential cracks that were inserted is double compared to the number of the experimental ones. The aforementioned selection ensures that there will not be any underestimation of the final crack density. In every possible crack different strength values were assigned in order to avoid the development of a uniform stress field leading in a simultaneous failure of all cohesive interfaces. The geometry of the cross-ply composite material model can be seen in **Figure 4.5**.

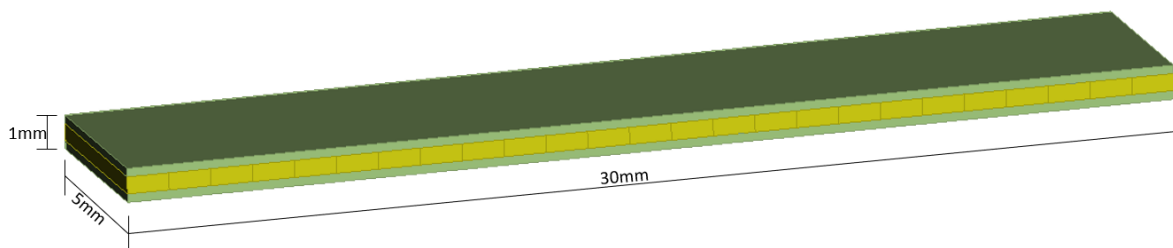


Figure 4.5: Geometry of cross-ply composite material model

### 4.7.2 Boundary conditions

The total composite model is loaded with uniaxial tension. The total strain (1.5%) is applied incrementally through tabular data and the total duration of the loading is 270 seconds which is equivalent to 1500 time steps. Each strain increment is 0.001% and each time increment of the given data is 0.18 seconds. The initial time increment was calculated as  $\Delta t = L/c_d$  where  $L$  is the dimension of the smallest element and  $c_d$  is the dilational wave speed. However the stable time increment was calculated internally by Abaqus (25). This means that ABAQUS/Explicit monitors the finite element model throughout the analysis to determine a stable time increment which may be even smaller than the initial. Finally the stable time increment can be increased by using appropriate mass scaling. It is worth mentioning here that the strain rate is kept constant at 0.00555% per second. The strength of the contacts that may fail, follows a normal distribution with mean value the strength of the matrix material and standard deviation value equal to 15%.

## 4.8 Results

In this section the results of the simulation are presented and compared with experimental measurements. All failure mechanisms matrix cracking, delaminations and fiber cracking are predicted successfully. In **Figure 4.6** the cracking of the composite can be seen from the beginning of the analysis to cracking saturation and finally the total failure of the composite with fiber cracking, when the fibers above a crack tip reach their tensile capacity. The total composite failure takes place above and below a crack tip where the stress concentration is apparent. The crack that causes the total failure depends on the distribution of the matrix predefined crack strength. As fiber bundles around the crack tips interact with the delaminations, a crucial parameter that defines the total composite strength is the interlaminar shear strength.

It should be noted that **Figure 4.7** shows the stress strain curve of the composite material at an integration point of an element above the crack tip in  $0^\circ$  layer, where the

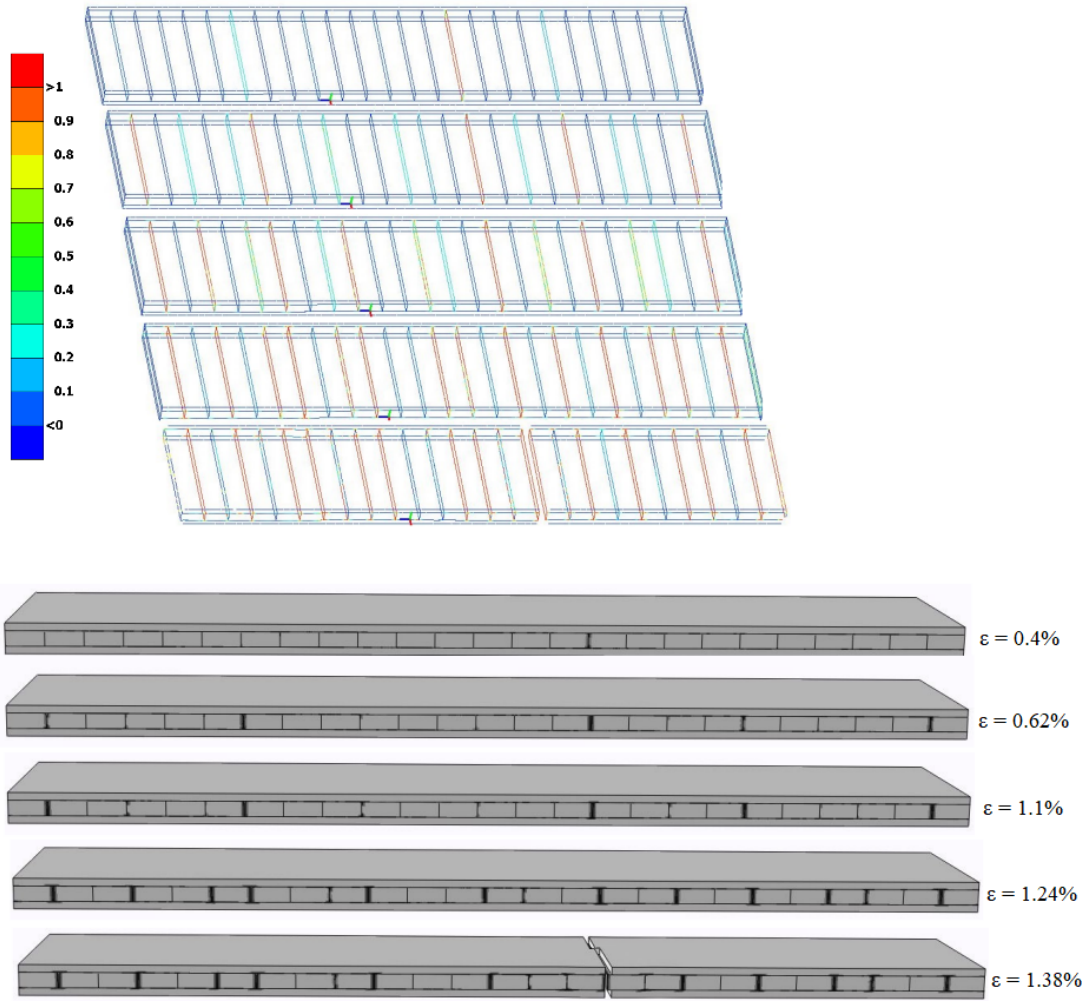


Figure 4.6: Progressive failure of the composite material. The colored lines represent the potential cracks. Blue color represents fully bonded parts and red color total debonding, i.e the satisfaction of the failure criterion. The axial strain is also depicted

total failure occurs (fiber cracking in **Figure 4.7** for  $\epsilon = 1.38\%$ ). The curve is close to the linear case because at this location the fiber is parallel to the loading direction and in conjunction with the high aspect ratio and high volume fraction the elastic material of the fiber dominates the homogenization result producing a material almost linear until failure. The ultimate tensile strength of the  $0^\circ$  layer is observed at approximately 450 MPa.

The averaged stress strain for the whole specimen is calculated in the post processing stage using a script that performs a volume averaging over all elements for all the timesteps of the axial stresses  $\sum_{e=1}^{N_e} V_e \sigma_e / \sum_{e=1}^{N_e} V_e$  and strains  $\sum_{e=1}^{N_e} V_e \epsilon_e / \sum_{e=1}^{N_e} V_e$  where

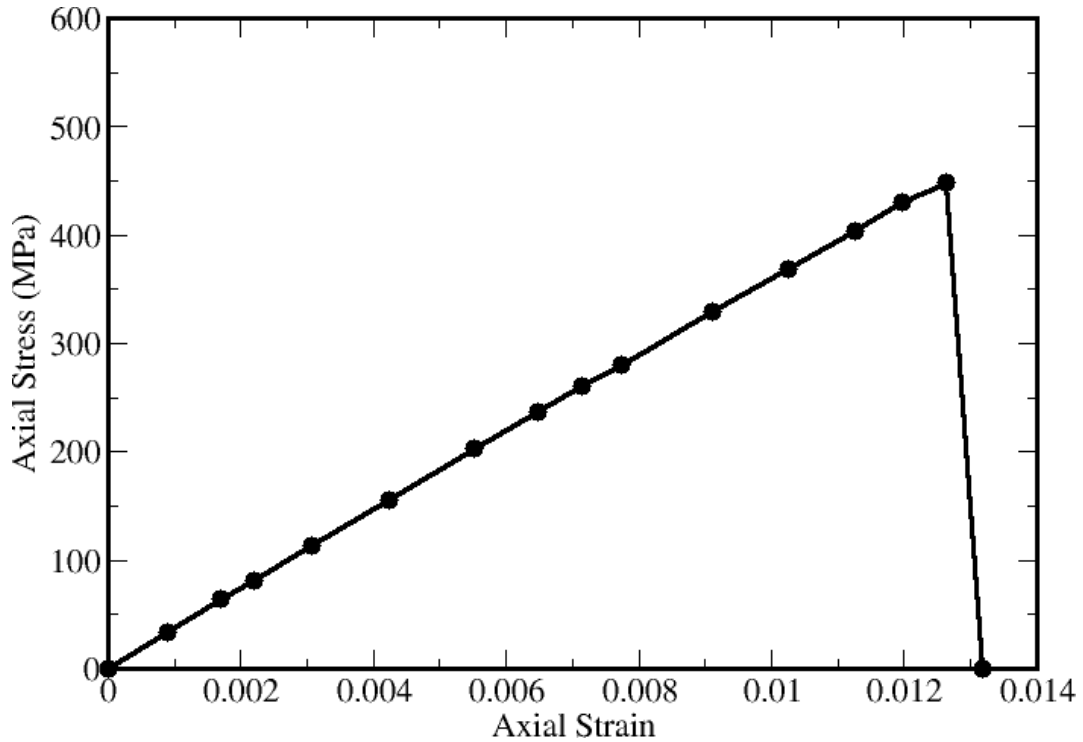


Figure 4.7: Stress vs. strain plot of a solid above the crack tip that fails due to fiber failure at strain around 0.013

$N_e$  is the number of elements. The depicted stiffness degradation for the whole specimen which is presented in **Figure 4.8** is due to the cracking (contacts failure where elements around the crack are unstressed) and the damage evolution of the matrix.

In **Figure 4.9** the results of crack density (already defined as the number of cracks normalised by the length of the specimen) versus strain are compared to available experimental measurements from the Composite and Smart Materials Laboratory of the University of Ioannina (43). The results are also compared with a similar but simpler model also developed in the present study where the homogeneous material of each layer has been originated from visco-elastic homogenization and the behavior is considered as linear until failure. It is obvious that the multiscale methodology provides better predictions of the crack density and the saturated crack density closely follows the experimental measurements.

From **Figure 4.9** can be observed that the cracking starts earlier for the visco-elastic material model due to the stiffer prediction of the matrix material. In the current formu-

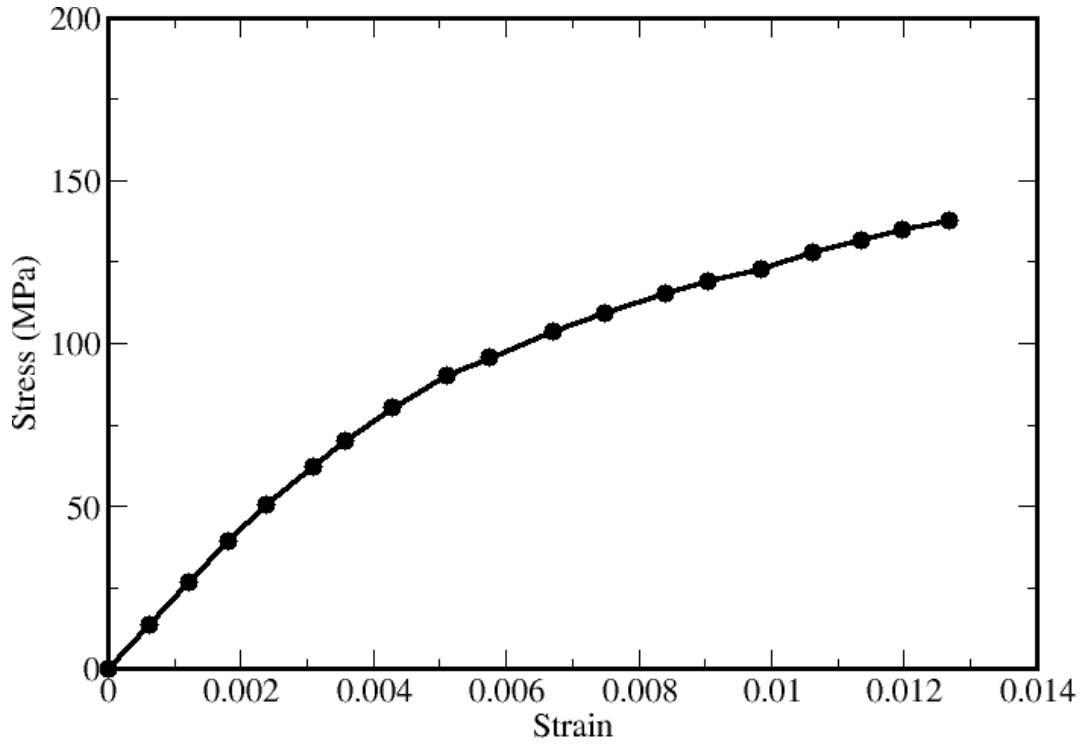


Figure 4.8: Stress vs. strain plot for the whole composite material

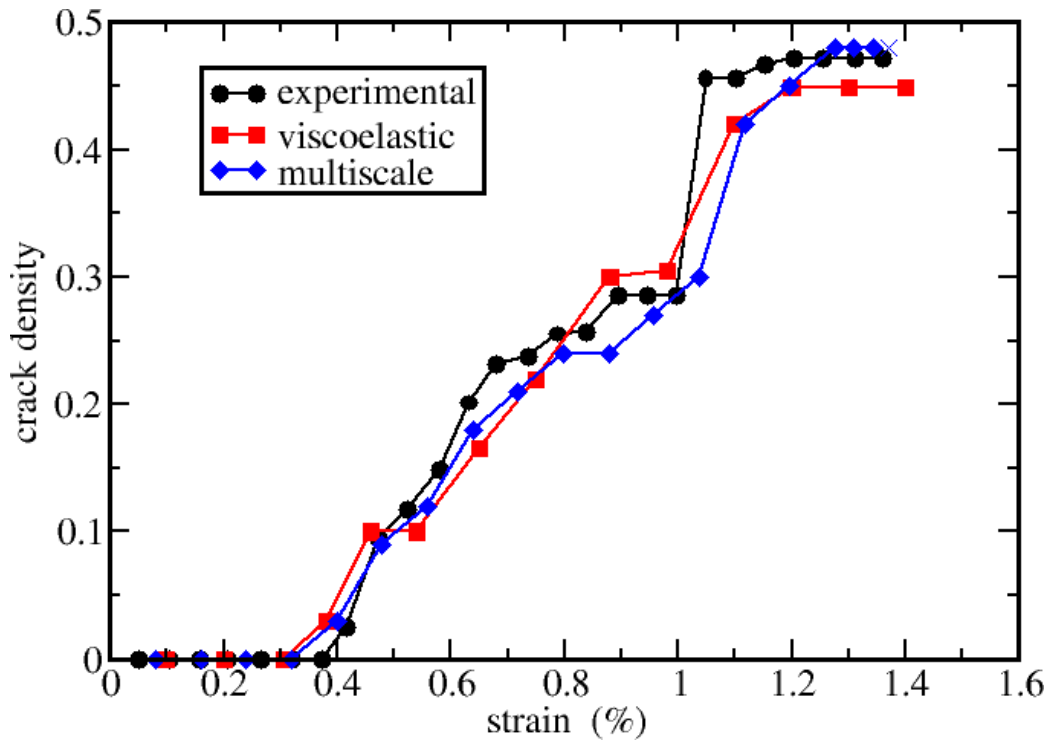


Figure 4.9: Comparison of multiscale algorithm with simple visco-elastic model and experimental results

lation which combines visco-elasto-plasticity with damage, the matrix material enters its nonlinear region, degrades the stiffness more, and as a result the stresses are not as high as in the linear visco-elastic model. For that reason, the first cracks appear for higher strain values, approaching better the experimental results.

Under the framework of comparisons of the results obtained by the multiscale model with the simpler homogeneous viscoelastic model representative timings of the actual production run took place in order to have a detailed information about the computational cost of the proposed methodology. One personal computer equipped with Intel 8th generation 6-core i5 processor and 32GB of memory has been used. The full multiscale analysis needed 1 hour and 54 minutes while the simpler homogeneous viscoelastic model needed 32 minutes both in parallel execution. The memory requirements of the multiscale methodology were below 15 GB RAM.

#### **4.8.1 Mesh Dependency-Sensitivity Analysis**

The developed user material follows a local damage model to predict the damage evolution for the matrix material and for that reason, mesh dependency is expected. Therefore a mesh dependency analysis has been performed. The newly proposed methodology is developed aiming to the prediction of the cracking saturation which is intimately related to the crack density. Crack density is defined as the number of cracks normalised by the length of the specimen. Therefore, the crack density was compared between the differently discretized specimens. Four different discretizations with 8000, 45144, 96000 and 208306 elements were solved. The boundary conditions, and the material properties were identical for the different discretizations. The algorithm that distributes the strength over the cohesive surfaces was applied for every model. As a result, potential cracks at the same positions may not have the same strength between different mesh sizes. The **Figures 4.10, 4.11** show that after exceeding a critical number of elements (approximately 50000) the results converge.

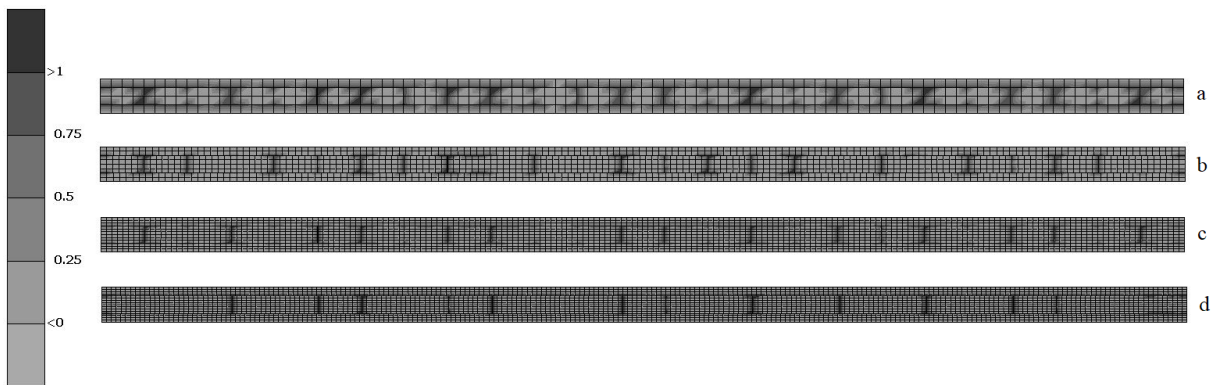


Figure 4.10: Cracking saturation state for the different discretizations used: a. 8000, b. 45144, c. 96000 and d. 208306 elements. Colorbar represents contact failure value

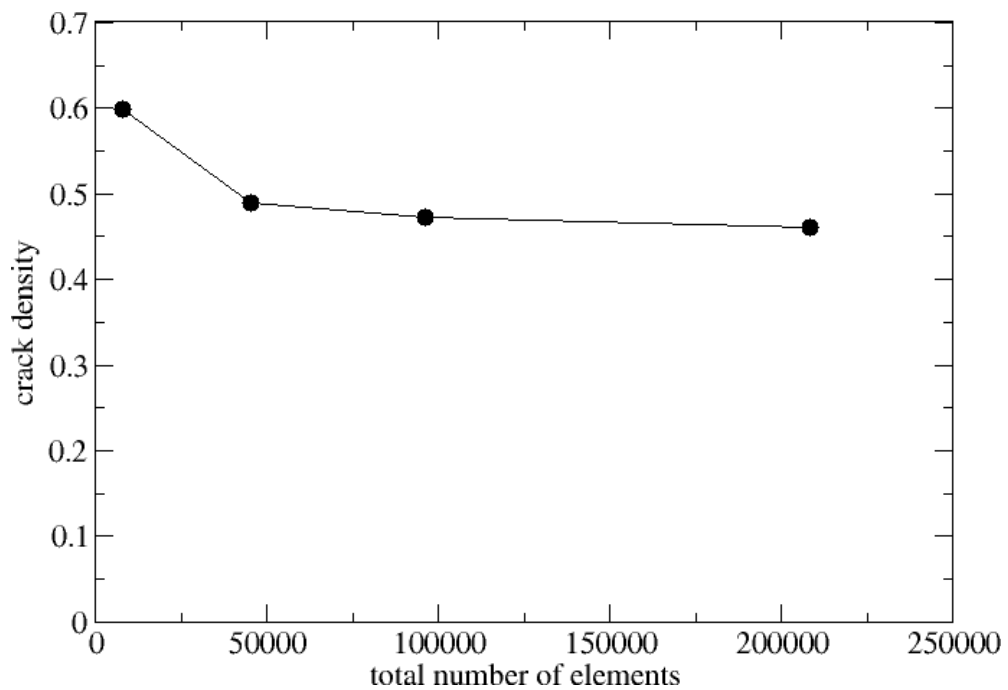


Figure 4.11: Crack density as a function of the total number of elements

## 4.9 Conclusions

A novel multiscale material model is proposed and applied to a cross-ply composite material loaded in uniaxial tension in a dynamic analysis procedure. The proposed new multiscale methodology is based on the Eshelby's single inclusion problem solution to dehomogenize the strain increments and applies a different material model for each constituent. For the matrix a visco-elasto-plastic material model with isotropic damage is adopted while for the fiber an elastic material with known failure properties is used. In order to examine the random transverse cracking, a number of possible cracks were placed in the  $90^\circ$  layers whose strength follows a normal distribution. The possible cracks and the interface between the layers were modeled using cohesive contacts. All the expected damage mechanisms appeared and the actual crack density with respect to strain was compared to experimental measurements and to a simpler meso-scale simulation approach where the layers are modeled as linear visco-elastic. It is observed that in the multiscale model the results are closer to the experimental measurements and more damage mechanisms such as matrix damage and fiber failure can be predicted. Even though the multiscale methodology is more computationally demanding, its most important advantage is that the constituents can follow different material models, with many failure criteria and predict stresses, strains, plastic strains and more analysis variables not only in the homogeneous level (macroscale) but also constituent-wise (microscale) while the solver does not have any information about the microstructure as the multiscale formulation is performed in the user material subroutine. Those per phase analysis variables are used to observe if the fibers or matrix on specific integration points have failed and enables the control of the element failure.

## References

- [1] J. Nairn and H. S., “Damage mechanics of composite materials,” *Composite materials series*, vol. 9, pp. 187–244, 1994.
- [2] S. Liu and J. A. Nairn, “The formation and propagation of matrix microcracks in cross-ply laminates during static loading,” *Journal of Reinforced Plastics and Composites*, vol. 11, no. 2, pp. 158–178, 1992.
- [3] J. A. Nairn, “The strain energy release rate of composite microcracking: A variational approach,” *Journal of Composite Materials*, vol. 23, no. 11, pp. 1106–1129, 1989.
- [4] J. Nairn, “Microcracking, microcrack-induced delamination, and longitudinal splitting of advanced composite structures,” *NASA Contractor Report 4472*, pp. 1–166, 1992.
- [5] J. Nairn, “Applications of finite fracture mechanics for predicting fracture events in composites,” in *5th Int. Conf. on Deform. and Fract. of Comp.*, (London, UK), pp. 1–10, 1999.
- [6] J. Nairn and D. Mendels, “On the use of planar shear-lag methods for stress-transfer analysis of multilayered composites,” *Mechanics of Materials*, vol. 33, no. 6, pp. 335 – 362, 2001.
- [7] C. Herakovich, J. Aboudi, S. Lee, and E. Strauss, “Damage in composite laminates: Effects of transverse cracks,” *Mechanics of Materials*, vol. 7, no. 2, pp. 91 – 107, 1988.
- [8] C. Fu and X. Wang, “Micro-mechanical analysis of matrix crack-induced delamination in cross-ply laminates in tension,” *Composite Structures*, vol. 243, pp. 112202–, 2020.

- [9] Y. Yuan, X. Li, Q. Zhang, P. Liu, and Z. Zhang, “Dependence of damage modes on the ply-thickness of ultra-thin-ply composites,” *Composites Part C: Open Access*, vol. 4, pp. 100105–, 2021.
- [10] J. L. Curiel-Sosa, R. Brighenti, M. C. S. Moreno, and E. Barbieri, “8 - computational techniques for simulation of damage and failure in composite materials,” in *Structural Integrity and Durability of Advanced Composites* (P. Beaumont, C. Soutis, and A. Hodzic, eds.), pp. 199 – 219, Woodhead Publishing, 2015.
- [11] L. Zhao, J. Zhi, J. Zhang, Z. Liu, and N. Hu, “Xfem simulation of delamination in composite laminates,” *Composites Part A: Applied Science and Manufacturing*, vol. 80, pp. 61–71, 2016.
- [12] J. Curiel-Sosa, B. Tafazzolimoghaddam, and C. Zhang, “Modelling fracture and delamination in composite laminates: Energy release rate and interface stress,” *Composite Structures*, vol. 189, pp. 641 – 647, 2018.
- [13] N. A. Petrov, L. Gorbatikh, and S. V. Lomov, “Xfem modelling of transverse cracking in fiber reinforced composites,” in *21st International Conference on Composite Materials, Xian, China, 2017*.
- [14] Z. R. Khokhar, I. Ashcroft, and V. Silberschmidt, “Interaction of matrix cracking and delamination in cross-ply laminates: Simulations with stochastic cohesive zone elements,” *Applied Composite Materials*, vol. 18, pp. 3–16, 2011.
- [15] F. P. van der Meer and C. G. Dávila, “Cohesive modeling of transverse cracking in laminates under in-plane loading with a single layer of elements per ply,” *International Journal of Solids and Structures*, vol. 50, no. 20, pp. 3308 – 3318, 2013.
- [16] R. Krueger, “Virtual crack closure technique: History, approach, and applications ,” *Applied Mechanics Reviews*, vol. 57, no. 2, pp. 109–143, 2004.

- [17] H. Lee, “Damage modelling for composite structures,” *PHD research thesis. School of Mechanical, Aerospace and Civil Engineering, University of Manchester*, 2015.
- [18] M. Eftekhari, S. H. Ardakani, and S. Mohammadi, “An XFEM multiscale approach for fracture analysis of carbon nanotube reinforced concrete,” *Theoretical and Applied Fracture Mechanics*, vol. 72, pp. 64–75, 2014.
- [19] R. Xu, C. Bouby, H. Zahrouni, T. Ben Zineb, H. Hu, and M. Potier-Ferry, “3D modeling of shape memory alloy fiber reinforced composites by multiscale finite element method,” *Composite Structures*, vol. 200, pp. 408–419, 2018.
- [20] Y. Hui, R. Xu, G. Giunta, G. De Pietro, H. Hu, S. Belouettar, and E. Carrera, “Multiscale CUF-FE2 nonlinear analysis of composite beam structures,” *Computers and Structures*, vol. 221, pp. 28–43, 2019.
- [21] G. Chatzigeorgiou, Y. Chemisky, and F. Meraghni, “Computational micro to macro transitions for shape memory alloy composites using periodic homogenization,” *Smart Materials and Structures*, vol. 24, no. 3, p. 035009, 2015.
- [22] P. Fatemi Dehaghani, S. Hatefi Ardakani, H. Bayesteh, and S. Mohammadi, “3D hierarchical multiscale analysis of heterogeneous sma based materials,” *International Journal of Solids and Structures*, vol. 118-119, pp. 24–40, 2017.
- [23] E. Barbero, *Finite Element Analysis of Composite Materials*. CRC Press Taylor and Francis group, 2008.
- [24] I. Doghri and A. Ouair, “Homogenization of two-phase elasto-plastic composite materials and structures: Study of tangent operators, cyclic plasticity and numerical algorithms,” *International Journal of Solids and Structures*, vol. 40, no. 7, pp. 1681 – 1712, 2003.
- [25] abaqus, *ABAQUS/CAE user’s manual*. Pawtucket, RI : ABAQUS.

- [26] I. Doghri, *Mechanics of Deformable Solids: Linear, Nonlinear, Analytical and Computational Aspects*, pp. 301–327. Springer, Berlin, Heidelberg, 2000.
- [27] J. Michel and P. Suquet, “Nonuniform transformation field analysis,” *International Journal of Solids and Structures*, vol. 40, no. 25, pp. 6937–6955, 2003.
- [28] C. Oskay and J. Fish, “Eigendeformation-based reduced order homogenization for failure analysis of heterogeneous materials. computer methods in applied mechanics and engineering, 196, 1216-1243,” *Computer Methods in Applied Mechanics and Engineering*, vol. 196, pp. 1216–1243, 2007.
- [29] C. Friebel, I. Doghri, and V. Legat, “General mean-field homogenization schemes for viscoelastic composites containing multiple phases of coated inclusions,” *International Journal of Solids and Structures*, vol. 43, no. 9, pp. 2513–2541, 2006.
- [30] J. D. Eshelby, “The Determination of the Elastic Field of an Ellipsoidal Inclusion, and Related Problems,” *Proceedings of the Royal Society of London Series A*, vol. 241, pp. 376–396, 1957.
- [31] T. Mura, *Micromechanics of Defects in Solids*. Martinus Nijhoff Publishers, 1988.
- [32] T. Mori and K. Tanaka, “Average stress in matrix and average elastic energy of materials with misfitting inclusions,” *Acta Metallurgica*, vol. 21, no. 5, pp. 571 – 574, 1973.
- [33] B. Miled, I. Doghri, L. Brassart, and L. Delannay, “Micromechanical modeling of coupled viscoelastic–viscoplastic composites based on an incrementally affine formulation,” *International Journal of Solids and Structures*, vol. 50, no. 10, pp. 1755 – 1769, 2013.
- [34] O. Cruz-González, R. Rodríguez-Ramos, J. Otero, A. Ramírez-Torres, R. Penta, and F. Lebon, “On the effective behavior of viscoelastic composites in three dimensions,” *International Journal of Engineering Science*, vol. 157, pp. 103377–, 2020.

- [35] R. Schapery, "A simple collocation method for fitting viscoelastic models to experimental data," *GALCIT SM 61-32A California Institute of Technology, Pasadena CA*, 1962.
- [36] J. Lemaitre and R. Desmorat, *Engineering Damage Mechanics. Ductile, Creep, Fatigue and Brittle Failure*. Springer, Berlin, Heidelberg, 2005.
- [37] J. Lemaitre and J.-L. Chaboche, *Mechanics of Solid Materials*. Cambridge University Press, 1990.
- [38] J. Lemaitre, "Coupled elasto-plasticity and damage constitutive equations," *Computer Methods in Applied Mechanics and Engineering*, vol. 51, no. 1, pp. 31 – 49, 1985.
- [39] M. Mashayekhi, S. Ziaei-Rad, J. Parvizian, K. Nikbin, and H. Hadavinia, "Numerical analysis of damage evolution in ductile solids," *SID Structural Integrity and Durability*, vol. 1, pp. 67–82, 2005.
- [40] K. K. Mahato, M. Biswal, D. K. Rathore, R. K. Prusty, K. Dutta, and B. C. Ray, "Effect of loading rate on tensile properties and failure behavior of glass fibre/epoxy composite," *IOP Conference Series: Materials Science and Engineering*, vol. 115, pp. 012–017, 2016.
- [41] E. Barbero, F. Cosso, and F. Campo, "Benchmark solution for degradation of elastic properties due to transverse matrix cracking in laminated composites," *Composite Structures*, vol. 98, pp. 242 – 252, 2013.
- [42] M. Benzeggagh and M. Kenane, "Measurement of mixed-mode delamination fracture toughness of unidirectional glass/epoxy composites with mixed-mode bending apparatus," *Composites Science and Technology*, vol. 56, no. 4, pp. 439–449, 1996.
- [43] D. T. G. Katerelos, A. Paipetis, T. Loutas, G. Sotiriadis, V. Kostopoulos, and S. L.

- Ogin, “In situ damage monitoring of cross-ply laminates using acoustic emission,” *Plastics, Rubber and Composites*, vol. 38, no. 6, pp. 229–234, 2009.
- [44] L. Galuppi and G. Royer-Carfagni, “Laminated beams with viscoelastic interlayer,” *International Journal of Solids and Structures*, vol. 49, no. 18, pp. 2637–2645, 2012.
- [45] J. M. Müller, N. Rozo Lopez, E. A. Klein, and C. Hopmann, “Predicting the damage development in epoxy resins using an anisotropic damage model,” *Polymer Engineering & Science*, vol. 60, no. 6, pp. 1324–1332, 2020.
- [46] A. Kaddour, M. Hinton, P. Smith, and S. Li, “Mechanical properties and details of composite laminates for the test cases used in the third world-wide failure exercise,” *Journal of Composite Materials*, vol. 47, no. 20-21, pp. 2427–2442, 2013.



## **Chapter 5**

# **Multiscale Modelling of Extrinsic Self Healing GFRP Materials**

In this study, a novel multiscale material model is proposed to simulate the elasto-plastic damage-healing behavior of an epoxy matrix in a composite material. This framework combines the non-linear mean-field homogenization methodologies with the continuum damage-healing mechanics (CDHM) to achieve the healing process in a coupled manner along with the damage. The model is able to predict the time dependent healing effect combined with damage propagation. In the proposed multiscale model, the healing depends on the current damage of the matrix, the available time that the healing can evolve and the rate of healing. A parametric study with respect to the rate of healing and a time dependency analysis were performed to examine the sensitivity of the model. In addition, a microscale method to calculate the healing initiation and healing efficiency is proposed using a representative volume element (RVE) of an epoxy matrix with healing microcapsules. The microscale simulation showed that with 7.5 % volume fraction of microcapsules 40 % of the structural integrity can be recovered.

## 5.1 Introduction

The structural behavior of composite materials is dominated by irreversible damage phenomena that reduce their integrity. This structural degradation of stiffness and strength is due to the evolution of internal defects, usually micro-cracks or voids. In order for this phenomenon to be simulated correctly, continuum damage mechanics (CDM) theories have been developed. These theories provide a macroscopic representation of the voids and micro-cracks that lead to stiffness and strength reduction. A common assumption that is made in the CDM theories is that the damage variable is cumulative and can only be increased. In other words, the damage process is irreversible. However, contrary to degradation phenomena, experiments (1) (2) prove that polymer composites can be healed and therefore recover the whole or a part of their degraded mechanical properties (3). Healing can occur by physical or chemical processes that progressively eliminate the internal defects to a certain extent and can be considered as a procedure opposite to damage.

The self-healing of materials has been extensively studied experimentally and most of the numerical investigations of such kind of materials focus on homogeneous behaviors. Many healing laws in the continuous damage healing mechanics (CDHM) framework have been proposed for different material types including asphalt mixes (4), for cementitious materials (5) (6) and for polymer matrix composites (7). Voyadjis and Kattan (8) proposed the modeling of anisotropic self-healing materials and superhealing. Darabi et al. (9) proposed the extension of the concept of the effective configuration and effective stress to the healing configuration. Subramanian and Mulay (10) introduced a secondary damage variable in the CDHM framework with its own evolution law in order to allow the healed area undergo damage again after healing. Barbero and Ford (11), Privman et al. (12), and Sanada et al. (13) also contributed to the investigation by simulating the self-healing behavior of fiber-reinforced polymer composites. Zemskov et al. (14) investigated the effects of self-healing polymers in an analytical manner. Furthermore, thermo-dynamic constitutive models were developed by Schimmel and Remmers (15), Yagimli and Lion (16), Voyiadjis et al. (17), Wool and O'Connor (18) and Maiti et al. (19) focused

on the molecular level simulation. Mergheim and Steinmann (20) also took into account damage and healing variables, whereas Henson (21) (22) developed a model based on the mixture theory. In addition, Zhelyazov and Ivanov (23) developed a model that takes into account the healing of cement based materials coupled with damage, and Shahsavari et al. (24) applied a viscoelastic–viscoplastic constitutive model for self-healing materials. Limited research efforts can be found regarding multiscale methods combined with damage healing mechanics. Smojver et al. (25) proposed a micromechanical material model with uncoupled healing with damage of a composite material using the rule of mixtures to predict the laminate’s healing behavior in an explicit integration analysis with cyclic loading.

In the framework of CDHM, the healing is usually incorporated into the model with the coupled and uncoupled healing mechanisms. The first is the uncoupled or non-autonomic mechanism, where healing is activated by external triggering. The second is the coupled or autonomic mechanism in which extensive and progressive damage triggers the healing procedure. The coupled healing system applies on composite materials enhanced with microcapsules, it is more direct but lacks repeatability after the first round of healing and the uncoupled system assumes that damage and healing occur in different stages of material’s lifecycle. While numerical models have been developed for plasticity and damage evolution, in terms of healing usually phenomenological laws are used that depend on experimental observations. The procedure of damage takes place in the microscale with micro-cracks or micro-voids reducing the structural integrity. The same applies for the healing procedure. With the use of multiscale modeling the different phases of the material are distinguishable. Thus, important information of microscale is transferred to the macroscale assisting not only on the better understanding of the phenomena but also to more accurate predictions of the material’s behavior.

In the present work, a multiscale approach is introduced for the simulation of a glass fiber reinforced polymer material taking into account the elasto-plastic micro-damage-healing behavior of the matrix. The healing is incorporated into the suggested model in a

coupled healing mechanism. The mean-field methods have been successfully applied in the CDM framework before (25)(26) but to the authors' knowledge, there is no published work that incorporates a multiscale modeling procedure based on the Eshelby's theory for strain localization and applied in a coupled healing mechanism.

## 5.2 Proposed multiscale algorithm

In the context of continuum damage healing mechanics the following configurations (presented in **Figure 5.1**) are usually adopted as far as the material's cross section is concerned. The nominal configuration where the cross section  $A$  includes pure material, damaged and healed parts. The healing configuration cross section  $\bar{\bar{A}}$  contains only pure material and healed damage parts. Finally, the effective configuration with cross section  $\bar{A}$  which is consisted only by pure material ( $A > \bar{\bar{A}} > \bar{A}$ ).

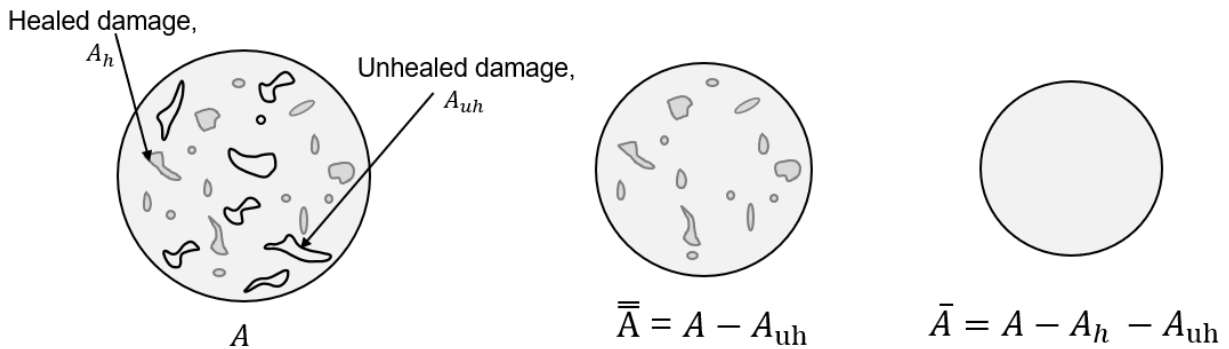


Figure 5.1: A.Damaged (nominal) configuration B.Healing Configuration C.Effective (undamaged) configuration

The strain and stress tensors in damaged and healing configurations are related with the strain equivalence hypothesis which states that the total strain and strain rate for these two configurations are equal. The coupling of plasticity, damage and healing is performed in the healing configuration where the unhealed damage is removed and the cross section contains only undamaged (pure) material and healed damage.

The proposed multiscale algorithm which is shown in **Figure 5.2** is applied in the healing configuration.

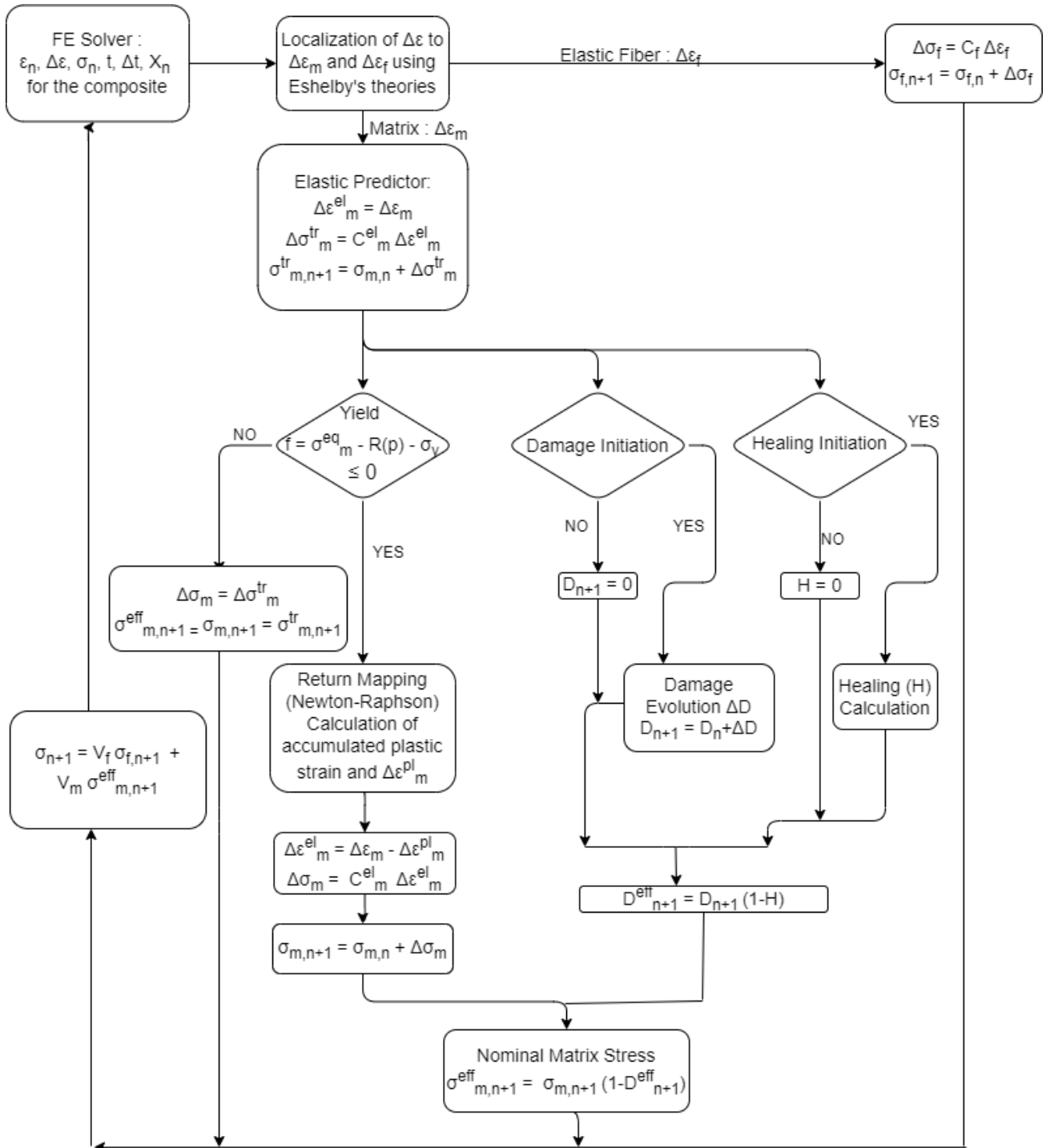


Figure 5.2: Flow chart of multiscale material implementation

To elaborate on the algorithm, for every integration point of the macroscale model, the composite material's stress, strain increment and history variables from the previous time step are known. The aim of this user material is to calculate the stress tensor values of the next time step. Initially, the macroscale strain increment is dehomogenized to

the individual strain increment of the matrix and of the fiber using strain concentration tensors in order to be able to apply the corresponding material model for each constituent. Regarding the fibers, linear elasticity is considered, so the updated stresses are calculated from Hooke's law. For the matrix material, the trial stresses are calculated from Hooke's law. The value of the yield function is obtained using the trial stress to observe if the material has entered the plastic region. If the value does not exceed zero, then the trial stresses are the correct stresses and the material is in its elastic region. A homogenization of the matrix and fiber stresses is performed and the homogenized stresses are provided to the solver to proceed with the next time step. If the material enters the plastic region, then with a Newton-Raphson iterative procedure, the accumulated plastic strain is calculated (reference Equation) in order to correct the stresses and return to the yield surface. As the material enters the plastic region, the damage and healing initiation criteria are checked, in order to calculate the effective damage variable to further correct the matrix stresses according to the healing and damage that has been developed. Once the matrix material stresses are calculated and the history variables are accordingly updated, homogenization of the stresses is performed.

Using Eshelby's theories (27) the composite's strain rate at a material point can be separated to matrix strain increment  $\Delta\varepsilon_m$  and fiber strain increment  $\Delta\varepsilon_f$  in a nonlinear analysis framework with incremental formulation. The strain increment provided by the solver refers to an integration point of the whole (homogenized) composite. Dehomogenization of the aforementioned strain increment is necessary in order to be able to apply an elasto-plastic-damage with healing for the matrix material and elasticity for the material of the fibers. Regarding the strain increment dehomogenization, the use of strain concentration tensors produces more accurate results compared to other phenomenological models (Reuss, Voigt, Rule of Mixtures) since it takes into account not only the volume fraction and the direction of the fibers, but also the fiber geometry and the matrix material. In addition, it can handle random fiber orientations by incorporating the appropriate orientation tensors. The strain increment averages per phase are related to a strain

concentration tensor  $B^\varepsilon$  as follows:

$$\Delta\varepsilon_m = [V_f \mathbf{B}^\varepsilon + (1 - V_f) \mathbf{I}]^{-1} : \Delta\varepsilon \quad (5.1)$$

$$\Delta\varepsilon_f = \mathbf{B}^\varepsilon : \Delta\varepsilon_m = \mathbf{B}^\varepsilon : [V_f \mathbf{B}^\varepsilon + (1 - V_f) \mathbf{I}]^{-1} : \Delta\varepsilon \quad (5.2)$$

with  $\mathbf{B}^\varepsilon$  given by

$$\mathbf{B}^\varepsilon = [\mathbf{I} + \mathbf{E} : (\mathbf{C}_m^{-1} : \mathbf{C}_f - \mathbf{I})]^{-1}, \quad (5.3)$$

The quantities involved are: the fourth order unit tensor  $\mathbf{I}$ , the Eshelby's tensor  $\mathbf{E}$ ,  $\mathbf{C}_m$ ,  $\mathbf{C}_f$  the stiffness tensor for matrix and fiber respectively and the fiber's volume fraction  $V_f$ . The proposed multiscale algorithm is developed in a VUMAT subroutine in an explicit analysis and runs for every integration point of the model in order to update the history variables for each constituent. At every iteration all integration points are examined for initiation of plasticity, damage and healing to calculate the effective stress in the appropriate configuration and provide it to the solver.

### 5.3 Matrix material

The epoxy material of the matrix uses an elasto-plastic material with isotropic hardening plasticity and isotropic damage coupled with healing. As the material enters the plasticity region a return mapping procedure is adopted to correct the predicted stresses and return the stress state to the yield surface. After entering the plastic region the damage initiation criteria are checked in order to account for the cumulative damage. If the material point has undergone damage then it is also checked for healing initiation in order to calculate the partial recovery of the mechanical integrity that is reduced due to damage.

### 5.3.1 Homogenization of materials in plastic region

When the equivalent stress exceeds the yield stress of the material and the yield criterion is satisfied, the material enters the plastic region. The plasticity in most cases is handled by linearizing the plastic behavior, using a rate form of Hooke's law. All the equations regarding the plasticity are applied for the matrix material of the microstructure. However, for simplicity, the index  $m$  is omitted.

The Hooke's law in rate form is presented in eq. (5.4)

$$\dot{\sigma} = C^{ep} : \dot{\varepsilon} \quad (5.4)$$

where  $C^{ep}$  is the tangent stiffness modulus for the elasto-plastic material (or material Jacobian). Time discretization of the rate equation, following the incremental formulation framework, leads to **Eq.(5.5)**

$$\delta\sigma_{n+1} = C^{alg} : \delta\varepsilon_{n+1} \quad (5.5)$$

In the above formulation  $C^{alg}$  is the consistent numerical tangent (or algorithmic) modulus of the material that relates the stress increment with the strain increment. In an implicit integration framework, the algorithmic modulus is necessary to be calculated in order to achieve quadratic convergence. On the other hand, in case of explicit integration which applies in this study, the calculation of the tangent stiffness is not mandatory, since the nature of this method is to perform numerous small increments. The **Eq.(5.6)** **Eq.(5.7)** can be used instead of **Eq.(5.5)**. The plasticity model that is used to simulate the behavior of the matrix material, follows the von Mises (J2) plasticity theory with isotropic hardening and invokes the following equations

$$\sigma = C^{el} : (\varepsilon - \varepsilon^{pl}) \quad (5.6)$$

$$\delta\sigma_{n+1} = C^{el} : \delta\varepsilon_{n+1}^{el} \quad (5.7)$$

$$f = \sigma_{eq} - R(p) - \sigma_Y \leq 0 \quad (5.8)$$

$$\dot{\varepsilon}^p = \dot{p}N \quad (5.9)$$

$$\dot{p} \geq 0 \quad (5.10)$$

$$\dot{p}f = 0 \quad (5.11)$$

$$N = \frac{\partial f}{\partial \sigma} = \frac{3dev(\sigma)}{2\sigma_{eq}} \quad (5.12)$$

The quantities involved in the aforementioned **Eqs. (5.6 - 5.12)** are: the yield stress  $\sigma_Y$ , the accumulated plastic strain  $p$ ,  $R(p)$  is the plastic stress obtained from eq.(5.14), and  $\sigma_{eq}$  is the von Mises measure of the Cauchy's stress tensor,  $dev(\sigma)$  describes the deviatoric part of stress  $\sigma$  tensor and  $N$  is the vector, normal to the yield surface of the examined material. In order to calculate plastic strain increment, the calculation of accumulated plastic strain increment from the following equation has to be preceded (28). If the hardening function  $R(p)$  is non-linear, then **Eq.(5.13)** is nonlinear too

$$3G\Delta_p + R(p) + \sigma_y - \sigma_{eq}^{trial} = 0 \quad (5.13)$$

and can be solved using an iterative Newton-Raphson scheme.

In this study  $R(p)$  is the power law plasticity and is defined as in eq.(5.14)

$$R(p) = Kp^n \quad (5.14)$$

where  $K$  is the hardening modulus and  $n$  is the hardening exponent, and are usually calibrated from experimental measurements.

### 5.3.2 Continuum damage mechanics

In classic CDM as introduced by Kachanov (29), the stresses in the fictitious configuration without damage, are related with the stresses in the damaged (nominal) configuration with the following formula:

$$\sigma = \hat{\sigma}(1 - D) \quad (5.15)$$

where  $0 \leq D \leq 1$  is the damage variable. For  $D = 0$  the nominal and damaged configurations are equal and for  $D = 1$  complete failure of the material is considered. The damage evolution law is often described as an increasing function of time, and for that reason, damage initially was considered an irreversible phenomenon. However, some materials combined with healing mechanisms have the potential to recover a portion of the mechanical properties and hence, heal. In order to model this procedure, the CDM framework must be appropriately extended to capture the changes in the material's microstructure during the healing process. The damage evolution law used in this study is the classic Chaboche damage model (30). The damage variable for isotropic damage is scalar, while in case of anisotropic damage is a higher order tensor. Without loss of generality and for simplicity, isotropic damage is considered.

After damage initiation the damage evolution is evaluated as:

$$\dot{D} = \begin{cases} 0 & p \leq p_c \\ \left(\frac{Y}{S_0}\right)^s \dot{p} & p > p_c \end{cases} \quad (5.16)$$

where  $s$  is the damage exponent,  $S_0^{-1}$  is the damage rate factor,  $p_c$  is the damage initiation threshold and  $Y$  is the strain energy release rate and is calculated as

$$Y = \frac{1}{2} \varepsilon^{el} : C^{el} : \varepsilon^{el} \quad (5.17)$$

In equation 5.16 where the damage evolution law is presented, the damage initiation criterion depends on the value of a critical accumulated plastic strain  $p_c$ . In this study the damage initiation criterion is set to zero ( $p_c = 0$ ), meaning that the damage starts to evolve the moment the material enters the plastic region. Damage factor ( $D$ ) is the sum of the damage evolution law in each time increment and finally the updated stress in the damaged configuration is

$$\sigma = C^{el}(\varepsilon - \varepsilon^{pl})(1 - D). \quad (5.18)$$

### 5.3.3 Healing

The healing mechanisms are usually reflected by the coupled and uncoupled healing systems. In case of uncoupled healing systems, damage and healing are independent of each other. Healing and damage cannot occur simultaneously which means that damage can evolve when healing is constant, and when damage is constant healing can take place (usually during the unloading phase or in a constant loading condition). It is obvious that this is not the case for extrinsic self-healing polymers such as polymers enriched with microcapsules or micro-vascular systems. In this case as damage propagates (i.e micro-cracks or micro-voids) a capsule may break and release the containing uncured resin in the crack. As a result, part of the mechanical properties are recovered. This procedure is best described by a coupled healing law, that allows damage and healing evolve at the same time, where healing is activated during damage evolution. **Eq.(5.18)** should be modified to account for healing when calculating the stresses in the healing configuration

$$\sigma = C^{el}(\varepsilon - \varepsilon^{pl})(1 - D(1 - h)). \quad (5.19)$$

When  $h$  is set to 0 the healing mechanism has not been initiated, and a value of 1

means fully healed damage or complete recovery of the mechanical properties. A value of  $0 < h < 1$  denotes a partial recovery of the structural integrity. The same applies for healing as in case of damage. For anisotropic healing the healing variable is described by a higher order tensor. In this study, as in the case of damage, the healing is considered isotropic and the healing variable is scalar. Usually the healing function or evolution law is based either on experimental measurements or phenomenological models. In the present study the following healing function is adopted (5):

$$h(t) = \begin{cases} 0 & D \leq D_{crit} \\ (1 - e^{[-gD(t_{hf}-t_{hi})]}) & D \geq D_{crit} \text{ (or } \varepsilon_m \geq \varepsilon_{m,crit}), \dot{D} > 0 \end{cases} \quad (5.20)$$

where  $D$  is the damage variable,  $t_{hf}$  is the time of healing,  $t_{hi}$  is the time of healing initiation and  $g$  is a material parameter calibrated from experiments. When the healing initiation criterion is met for the first time, the current analysis time is assigned to the healing initiation time. The healing characteristics of the material are defined numerically using the parameter  $g$ . In real world, this parameter specifies how fast the healing process evolves. Micromechanically speaking, it may depend on the total volume of the capsules, the strength of the healing agent, the capsule shell thickness among others. After the initiation of the healing process, the material gradually recovers its original stiffness and the mechanical response tends to become similar to the response of the original material. It is worth mentioning that the coded material law is modular allowing any healing evolution law to be used in order to best describe the material each time.

## 5.4 Composite material

As mentioned earlier the material of the fibers exhibits linear elastic response. The homogenized material behavior can be predicted from the volume average responses (31) of each constituent from the Voigt assumption  $\Delta\sigma_c = V_f\Delta\sigma_f + V_m\Delta\sigma_m$  and  $\sigma_c^{n+1} =$

$$\sigma_c^n + \Delta\sigma_c.$$

The implemented algorithm is applied in an explicit integration scheme where only the update of the homogeneous stress need to be calculated in numerous small increments in contrast with the implicit integration where a consistent tangent stiffness is required for quadratic convergence of large strain increments.

## 5.5 Results

For evaluation of the proposed multiscale material model, several virtual tests have been performed including three point bending tests using 3d solid elements. The results of the continuum damage healing material of the matrix was compared against the results of a multiscale material with pure elasto-plastic matrix and of a matrix material with elasto-plastic-damage without healing (32) in order to demonstrate the healing effect.

	<b>Matrix</b>	<b>Fiber</b>
Young's modulus (MPa)	5500	73100
Poisson ratio	0.398	0.18
Volume fraction	0.7	0.3
Aspect ratio	-	10
Yield stress (MPa)	30	-
Hardening modulus(MPa)	100	-
Hardening exponent	0.4	-
Damage rate factor	20	-
Damage exponent	0.7	-
Damage initiation	0.	-
Healing parameter	0.01	-

Table 5.1: Matrix and fiber material properties, for elasticity, plasticity, damage and healing

### 5.5.1 Three point bending test

In the case of the three point bending test a specimen with dimensions of 100 mm x 15 mm x 3 mm is used (**Figure 5.3**). The material properties are given in **Table 5.1**. The radius of the loading nodes and the supports was 5 mm. The total loading nose displacement

is 9 mm and is applied in an explicit analysis that lasts 1 second. Since only the healing model is time dependent, the time was scaled inside the user subroutine when taking into account the healing effect.

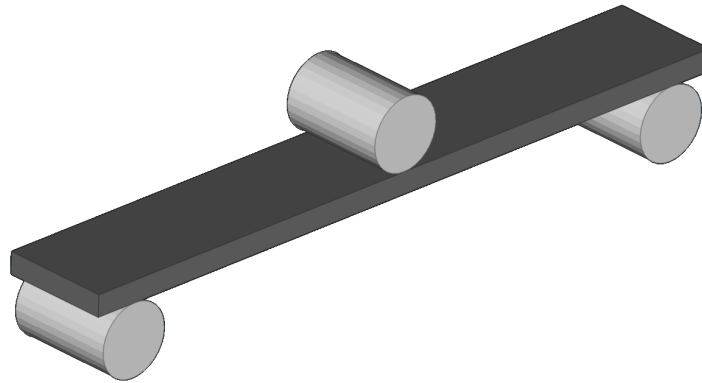


Figure 5.3: Three point bending setup

The same setup was solved with a pure elasto-plastic matrix material, with an elasto-plastic-damage matrix material, and for elasto-plastic-damage with coupled healing matrix material with total times of 200 s and 600 s. The fibers remained elastic during the analysis.

It is known that in Continuum Damage Mechanics computations, strain localization occurs over a damaged band of finite width. This phenomenon tends to minimize when non local damage laws are used, in order for the damage to be mesh independent, but even in this case, the damage will depend on a characteristic element length.

In **Figure 5.4** it can be observed that in the case of damage without healing the damage variable reaches a high value and as a result the damage tends to localize in the middle of the specimen. This damage localization can cause the failure of the specimen if the imposed strain reaches a slightly higher value. On the other hand, when healing is taken into account the damage localization is less intense, so that the specimen can withstand higher strains as the damage tends to expand in a larger area but with smaller values. This happens due to the fact that the healing is analogous to the damage, so that areas with more damage can heal more. It is clear in **Figure 5.4** that having more time available for healing, the damage localization reduces, and the developed stresses are higher.

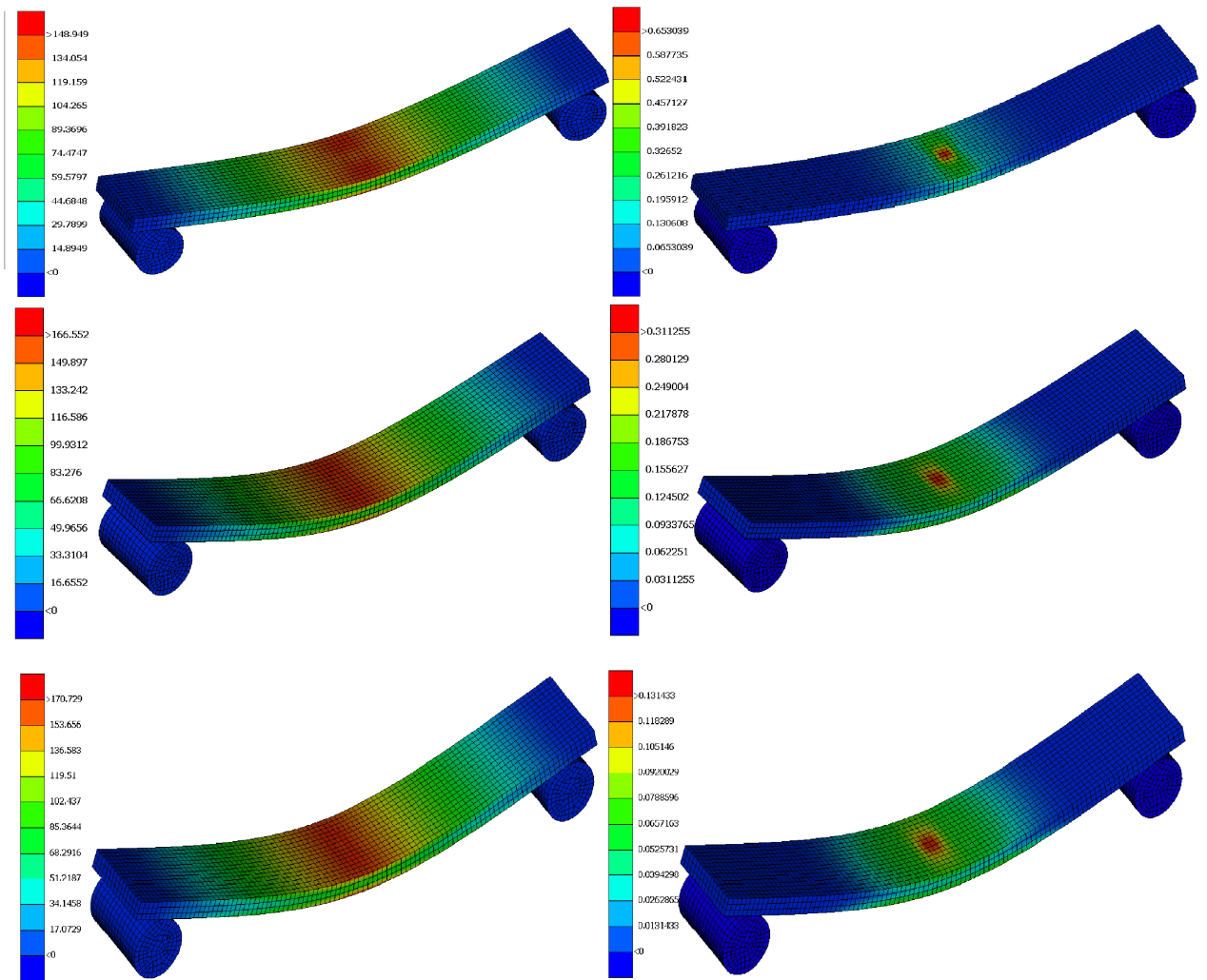


Figure 5.4: Virtual three point bending experiment. **Top Left:** Matrix stress without healing. **Top right:** Matrix damage parameter without healing. **Middle left:** Matrix stress with 200 s healing. **Middle right:** Matrix damage parameter with 200 s healing. **Bottom left:** Matrix stress with 600 s healing. **Bottom right:** Matrix damage parameter with 600 s healing. Stress values depicted in the left colorbars are in MPa while the right side colorbars represent the dimensionless matrix damage parameter values

In the following plots axial stress vs axial strain curves for the matrix, fibre and homogenized response (**Figures 5.5, 5.6, 5.7**) for four different cases, i.e. elasto-plasticity without damage, elasto-plasticity with damage without healing, elasto-plasticity with damage and healing with 200 s and 600 s available healing time.

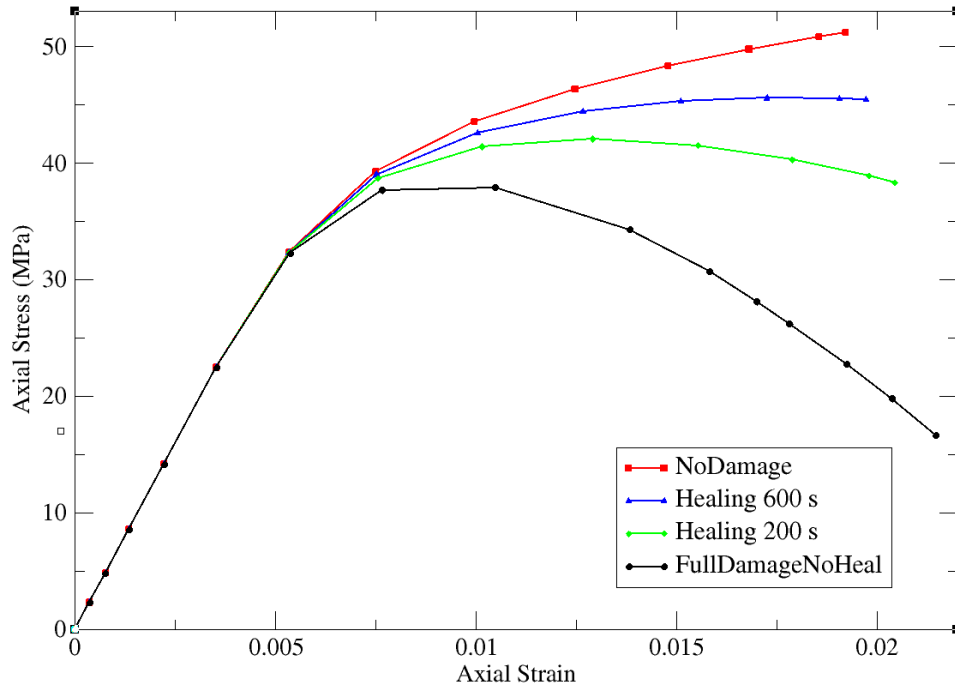


Figure 5.5: Matrix response for variable healing times

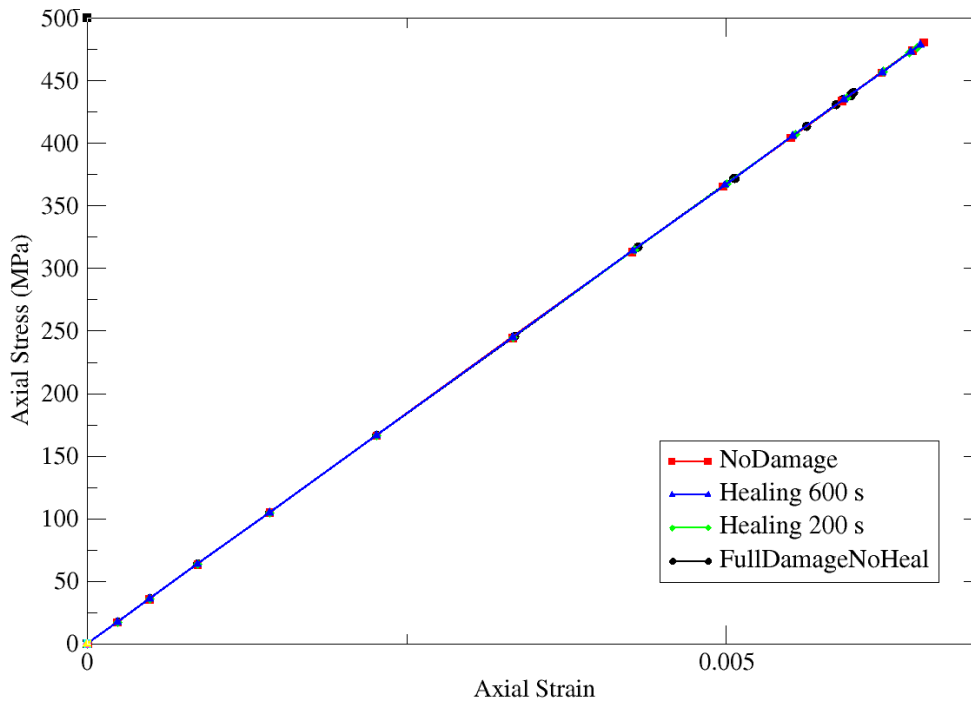


Figure 5.6: Fiber response for variable healing times

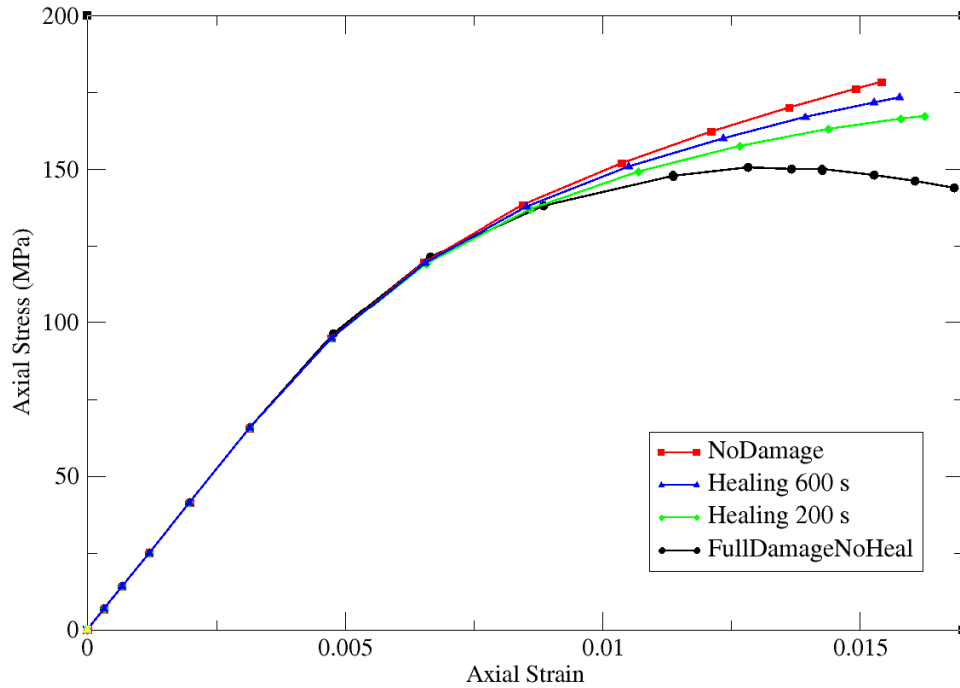


Figure 5.7: Homogenized response for variable healing times

In the graphical representations the axial stress vs. axial strain curves for the matrix, fiber and homogenized response (**Figure 5.5**) of the element in the middle of the specimen (**Figure 5.4**) and at the bottom side where the axial stresses are tensile (positive), are presented. The actual value of axial strain is adopted (avoiding its alternative % numerical representation) throughout the chapter. As can be observed, increasing the total analysis time results in a significant increase of healing in the matrix material and by extension, in the composite material after homogenization takes place. As the fibers remain elastic during the analysis, the stress/strain relationship for the fibers is similar for all analyses. Small differences between the analyses occur in the total strain that corresponds to the fibers. Comparing the final stresses in the matrix material it is shown that in the material without healing a total of  $D = 68\%$  of loading carrying capacity has been lost. In case of healing in the 200 s analysis the damage has been partially recovered and is equal to 29% and in the 600 s analysis the effective damage is equal to 11%.

## 5.5.2 Parametric study

The healing law as described in previous section, depends on the available time for healing, on the magnitude of damage and on the parameter  $g$ , that defines the rate of damage recovery. In this section it is shown how this parameter affects the stiffness recover and the role of the available healing time. It is worth mentioning that since all the material models are time independent except healing, the time was scaled inside the VUMAT subroutine only when calculating the healing effect. Also, the healing initiation criterion was calculated in microscale and occurred that the first microcapsules started breaking at strain value equal to 0.009.

## 5.5.3 Parametric study of $g$ parameter

In this study a coupled healing law is used, in order for the healing to take place along with damage evolution. The healing variable in **Eq.(5.20)** refers to the healing that is activated as damage continues to evolve, agreeing with the mechanism that describes the autonomous self-healing process. In case of capsule based healing, increase of damage means evolution of the micro-cracks that may break a capsule. Consequently, the healing agent released from the capsule reacts with the catalyst, forming a solid material that can fill the cracks. A critical number of micro-cracks is needed in order for the healing to start, a fact that is taken into account in the healing initiation criterion. The amount of healing largely depends of the dispersion of the capsules and the magnitude of damage. With appropriate capsule distribution and magnitude of damage a large part of the material can be healed. The rate of healing is represented by the parameter  $g$  combined with the current damage at each time step of the analysis, in the applied healing law.

In order to examine the affect of the matrix material characteristics in this multiscale damage - healing framework, different values of the parameter  $g$  in the matrix material were adopted in a simple tensile test, keeping the total time of the analysis constant, as can be seen in **Figure 5.8**. From **Figure 5.8** it is clear that for low values of  $g$ , a small

amount of properties can be recovered while for higher values of  $g$  (e.g. 0.1) complete recovery of the damage can be achieved in small amount of time.

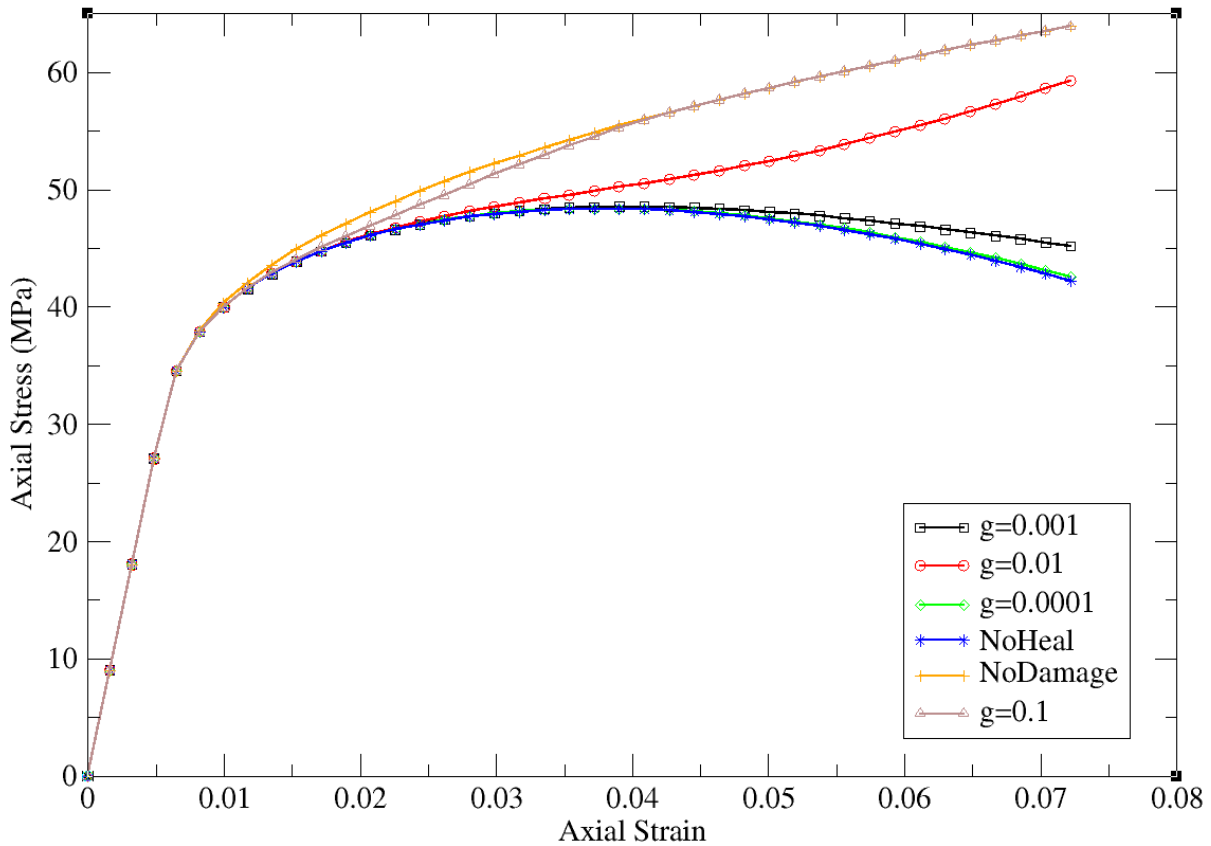


Figure 5.8: Effect of parameter  $g$  in matrix axial stress vs. axial strain in tensile test at 4000 s )

In **Figures 5.9 and 5.10** the healing and damage evolution with respect to time are presented. It is clear that changing the order of magnitude in the characteristic parameter  $g$ , greatly affects the increase rate of healing and subsequently the effective damage rate of reduction. Since this analytical healing law is sensitive to this material parameter it is important to be correctly calibrated using experimental measurements to achieve a realistic healing evolution rate.

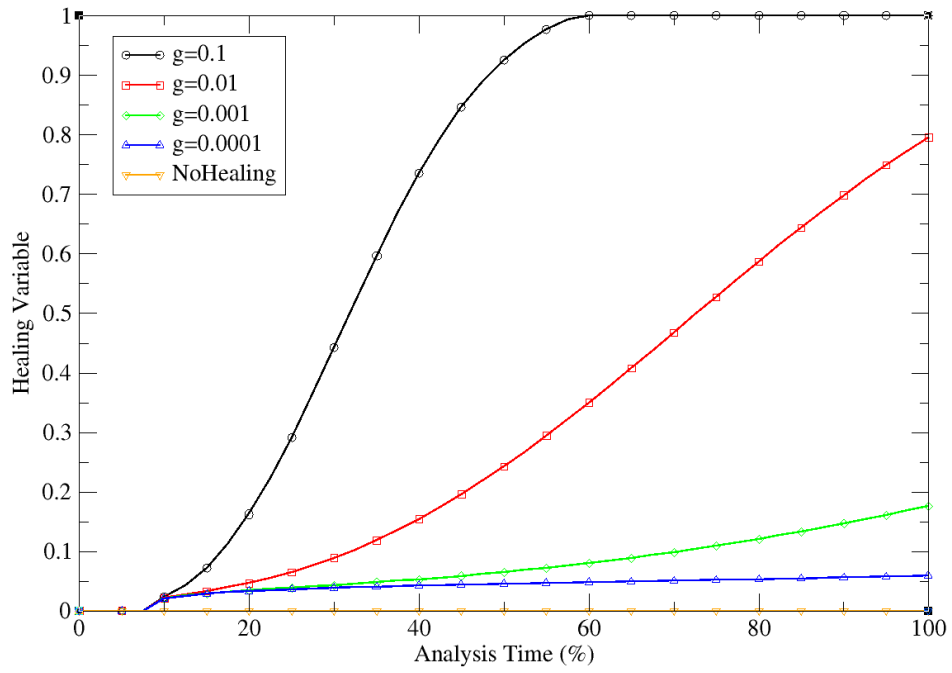


Figure 5.9: Healing variable evolution vs analysis time

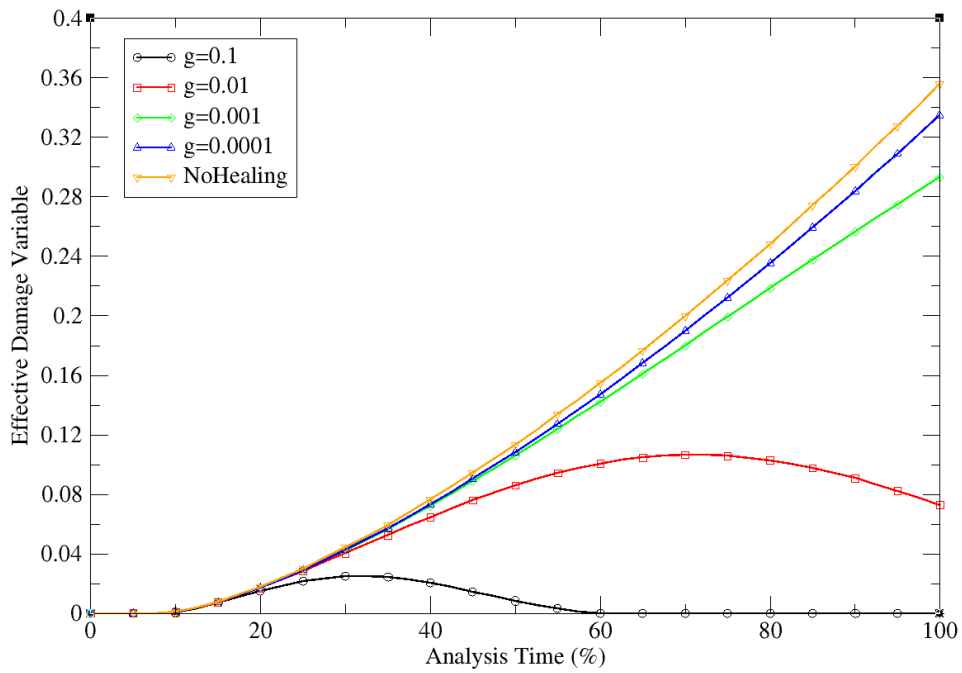


Figure 5.10: Effective damage evolution vs analysis time

### 5.5.4 Time dependency analysis

To examine the time dependency of the proposed damage-healing formulation, a similar procedure was adopted, running the same analysis for different loading times keeping the healing parameter  $g$  constant and equal to 0.01 and for available healing times of 200, 400, 600 and 1200 seconds. All of the material parameters corresponding to elasticity, plasticity damage and healing remain constant throughout the different analyses.

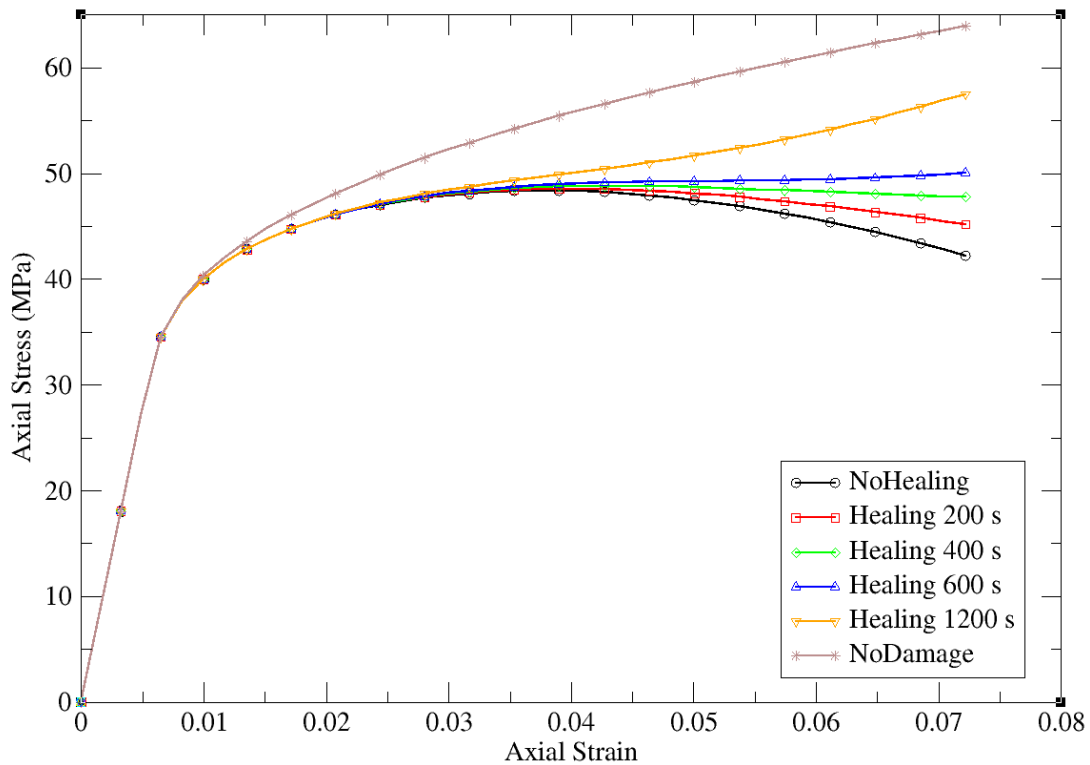


Figure 5.11: Time dependency analysis

From **Figure 5.11** becomes obvious that increasing the available time for healing the material can regain a larger part of the initial structural integrity. For low healing times, such as 200 s, the stiffness recovery is not significant, and the damage evolution rate is higher than the healing rate. As a result, the material enters a softening region as in the case without healing, but at slightly higher strain. For healing times larger than 400 s, the healing has adequate time to evolve and at a higher rate than the damage, which is strain dependent and not time dependent. This means that the material will enter a hardening

regime instead of softening and with adequate healing time the stress can reach the values as in the case without damage which implies full recovery.

## 5.6 Microscale modelling

In order to predict the healing initiation and healing efficiency of the microcapsule based polymer, a RVE was generated containing the matrix material and microcapsules at 7.5% (33) volume fraction, that was solved and homogenized numerically (34). The microcapsules were dispersed randomly and in a periodic manner with Random Sequential Adsorption (RSA) method. The size of the RVE  $L$  was selected according to the convergence of the maximum tensile stress ( $L \geq 4R$ ), where  $R$  is the microcapsules diameter. A minimized RVE size was selected (as  $L = 4R$ ) to increase the computational efficiency (35) (36). The RVE is meshed using first order linear tetrahedral elements and Periodic boundary conditions were applied (37).

The aim is to obtain the maximum tensile stress of the undamaged and healed specimen, and finally calculate the healing efficiency of the microstructure. The model is numerically executed in a loading-unloading-reloading procedure, combined with two user defined subroutines, for user defined fields (VUSDFLD) and user defined material behavior (VUMAT). The letter V denotes that the analysis is performed in an explicit framework. The VUMAT subroutine was used to define the matrix and capsule material behaviors that are modeled as elastic with maximum stress criteria for failure. Also in the unloading step the matrix elements can be healed according to a criterion defined in the VUSDFLD subroutine. The second subroutine was used to check for failed microcapsules and mark the matrix elements inside a specified distance around those failed microcapsules in order to be healed in the unloading phase.

It is worth mentioning that in order to simulate this loading/unloading procedure in an explicit integration analysis a smooth loading curve was used (**Figure 5.12**). Following this way, it is guaranteed that only a small amount of acceleration changes between

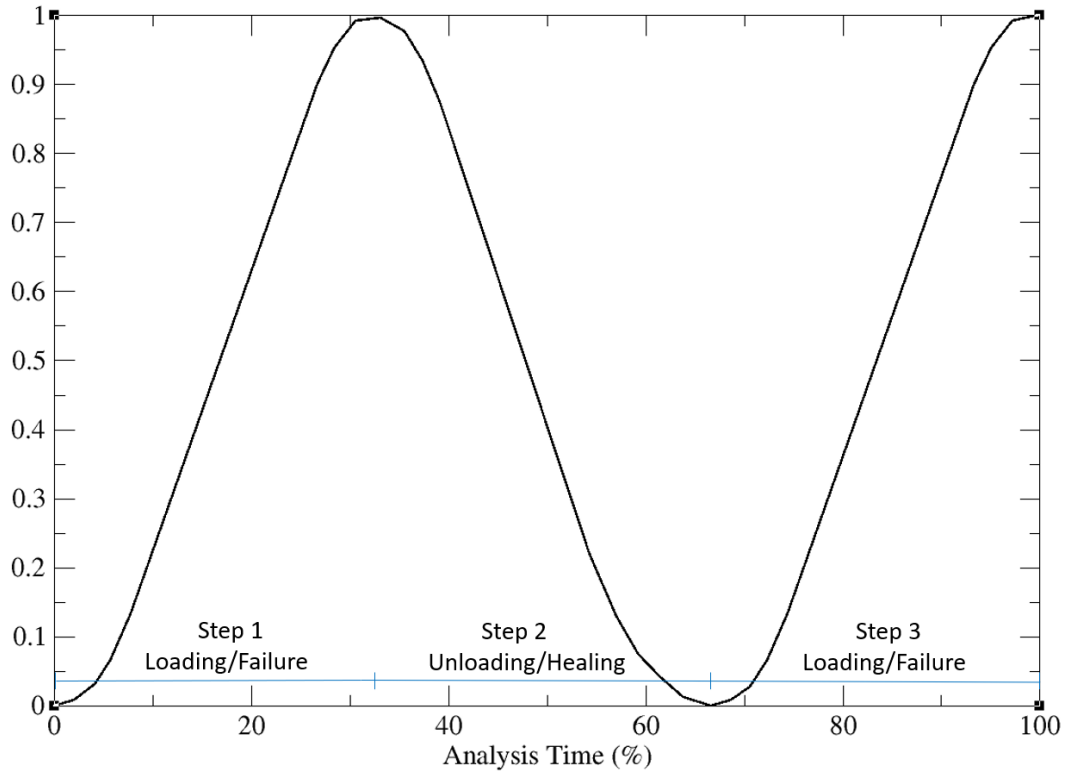


Figure 5.12: Loading scale factor vs analysis time

consecutive timesteps takes place. Sudden changes of acceleration can cause stress waves leading to inaccurate solutions with erroneously massive element deletion.

The aim of this method is to collect the failed elements that lie in the surrounding volume of failed micro-capsules. The specified distance was selected having as the main criterion the volume of each micro-capsule. In other words, the surrounding volume should be close to the volume of the micro-capsule increased with a factor to account for the mesh size, since for coarse mesh sizes and microcapsules with small diameter, few or no elements will be found inside the aforementioned range. It should be noted that any distance can be selected for this criterion relied depending on different observations. In other words all failed elements whose center of gravity is in range of  $[0, R\sqrt[3]{2\pi}]$  the center of the capsule, are healed in the unloading phase.

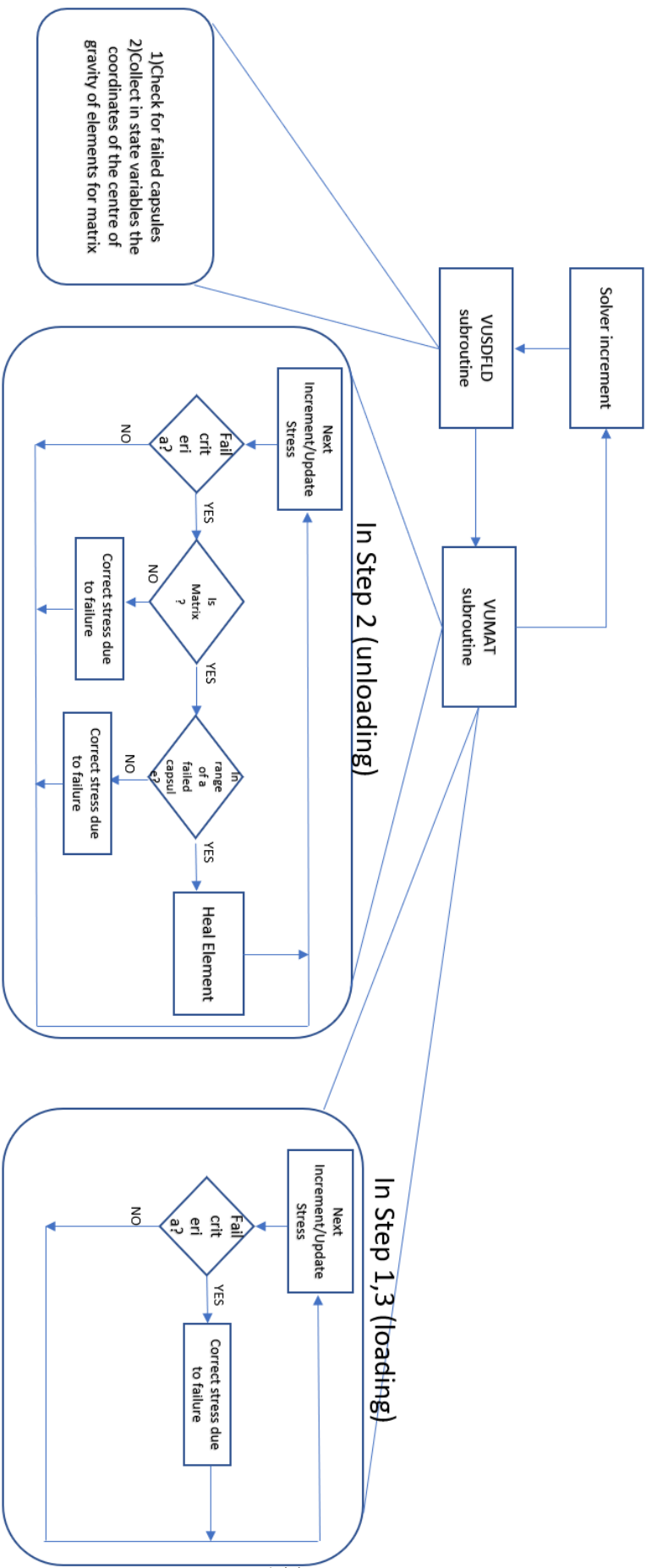


Figure 5.13: Algorithm for failure and heal of materials around failed capsules

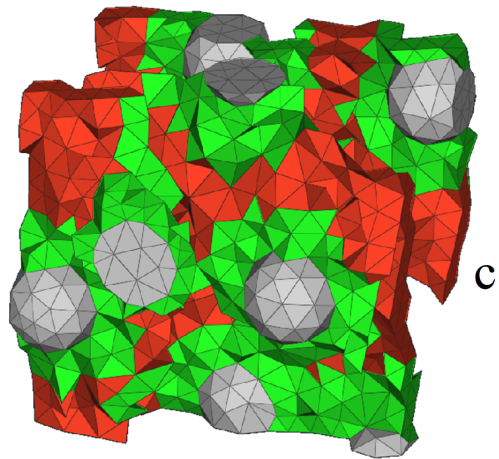
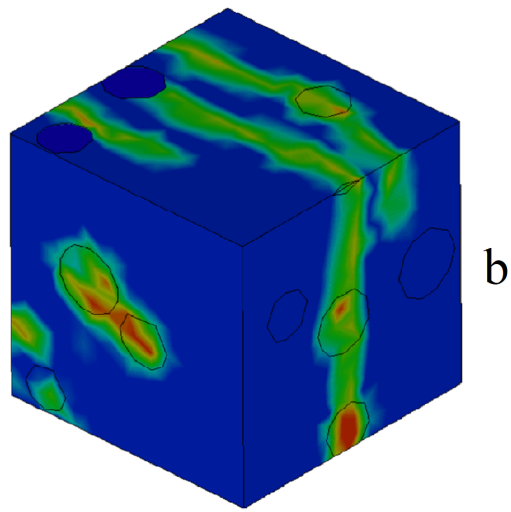
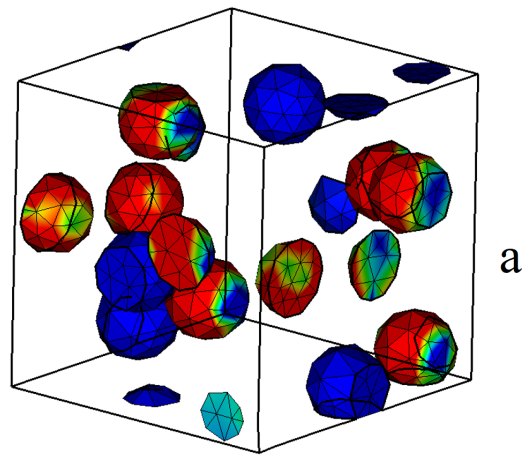


Figure 5.14: **a**: Failed capsules in red **b**: Microcracks in RVE **c**: Isolated failed elements, while in green color are the healed elements

The algorithm for failure and heal of materials around failed capsules is given in **Figure 5.13**. In addition, representative configurations with failed capsules, microcracks in RVE and isolated failed elements are depicted in **Figure 5.14**.

The average stresses and strains of the RVE is calculated using the rule of mixture for each time step of the analysis, by considering the analysis results of each element.

$$\hat{\sigma}_{ij} = \frac{1}{V} \int_V \sigma_{ij} dV = \frac{1}{V} \sum_{k=1}^N \sigma_{ij}^k V^k \quad (5.21)$$

$$\hat{\varepsilon}_{ij} = \frac{1}{V} \int_V \varepsilon_{ij} dV = \frac{1}{V} \sum_{k=1}^N \varepsilon_{ij}^k V^k \quad (5.22)$$

where  $\hat{\sigma}_{ij}$ ,  $\hat{\varepsilon}_{ij}$  is the average stress and strain,  $\sigma_{ij}$ ,  $\varepsilon_{ij}$  are the element stress and strain,  $V$ ,  $V^k$  are the total RVE volume and the volume of element k and N are the total number of elements.

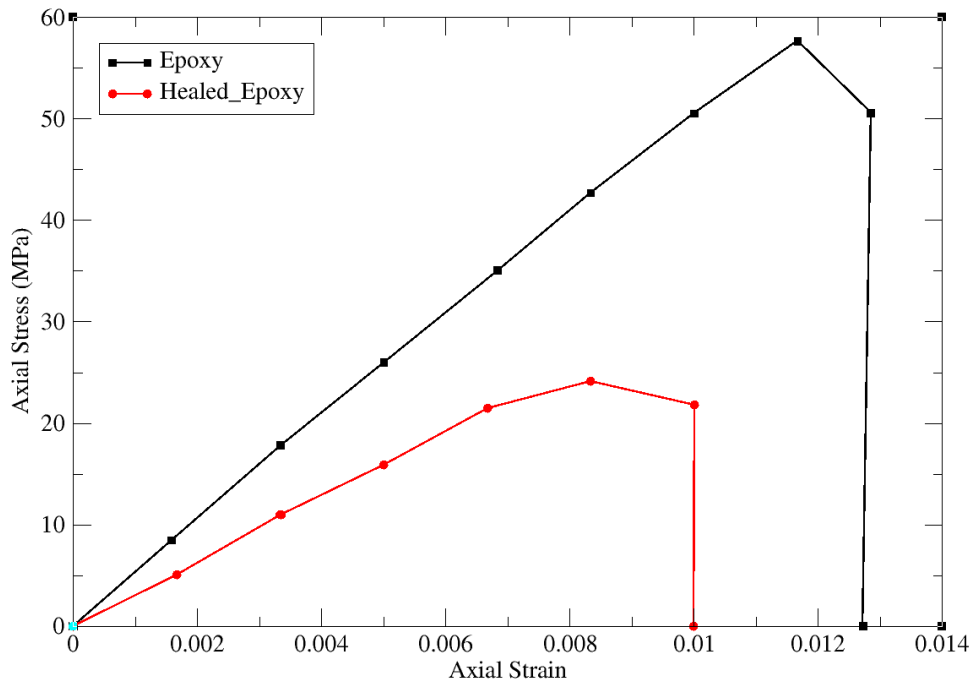


Figure 5.15: Average stresses - average strains relation obtained from the RVE tensile test for the undamaged epoxy material at the first loading cycle, and healed material at the second loading cycle.

From **Figure 5.15** that presents the ultimate stress of the initial material occurred from the first loading cycle, and the ultimate stress of the healed material occurred from the second loading cycle, the healing efficiency (as defined in (38)) is calculated approximately at 40%

$$h = \frac{\sigma_{heal}^{ult}}{\sigma_{init}^{ult}} \quad (5.23)$$

## 5.7 Conclusions

A novel multiscale material model is proposed that takes into account the damage and healing procedures that occur in the matrix material of the composite microstructure. In contrast to the existing mean-field multiscale methods in the CDHM framework (25)(26) for Fiber Reinforced Plastic (FRP) where the healing takes place in an uncoupled healing mechanism and the strain localization uses the Voigt and Reuss iso-strain and iso-stress approximation, the proposed methodology is based on the Eshelby's solution. Eshelby's solution incorporates strain concentration tensors and tends to produce more accurate results for the strain increment dehomogenization for matrix and fiber strain increment. Another major difference of the proposed multiscale approach compared to existing methods is that is applied in a coupled mechanism and the healing can take place simultaneously with the damage propagation. For the matrix an elasto-plastic material model with isotropic damage coupled with isotropic healing is adopted while the fibers are considered elastic during the whole analysis. The most important advantage of this methodology is that the constituents can follow different material models, taking into account damage and healing phenomena in the matrix material and predict a homogeneous response by averaging the response of each constituent of the microstructure. The proposed method is modular in that different damage and healing laws can be applied easily in the coded subroutine. Finally, a micromechanics methodology is proposed using a self-healing RVE with microcapsules combined with VUSDFLD and VUMAT subroutines in an explicit integration framework in order to calculate the healing efficiency of the composite material

used. The RVE with the embedded microcapsules is initially loaded until failure. In the sequence, in the unloading phase, uncoupled healing takes place in the elements around the failed microcapsules by utilizing the VUSDFLD subroutine. Finally, reloading of the RVE takes place, again until failure and by comparing the ultimate stresses, the healing efficiency is calculated.

## References

- [1] M. Kosarli, D. G. Bekas, K. Tsirka, D. Baltzis, D. . Vaimakis-Tsogkas, S. Orfanidis, G. Papavassiliou, and A. S. Paipetis, “Microcapsule-based self-healing materials: Healing efficiency and toughness reduction vs. capsule size,” *Composites Part B: Engineering*, vol. 171, pp. 78–86, 2019.
- [2] L. Zhang, X. Tian, M. H. Malakooti, and H. A. Sodano, “Novel self-healing cfrp composites with high glass transition temperatures,” *Composites Science and Technology*, vol. 168, pp. 96–103, 2018.
- [3] M. K. Darabi, R. K. Abu Al-Rub, E. A. Masad, and D. N. Little, “Constitutive modeling of fatigue damage response of asphalt concrete materials with consideration of micro-damage healing,” *International Journal of Solids and Structures*, vol. 50, no. 19, pp. 2901–2913, 2013.
- [4] R. K. Abu Al-Rub, M. K. Darabi, D. N. Little, and E. A. Masad, “A micro-damage healing model that improves prediction of fatigue life in asphalt mixes,” *International Journal of Engineering Science*, vol. 48, no. 11, pp. 966–990, 2010.
- [5] C. Oucif, G. Z. Voyiadjis, and T. Rabczuk, “Modeling of damage-healing and nonlinear self-healing concrete behavior: Application to coupled and uncoupled self-healing mechanisms,” *Theoretical and Applied Fracture Mechanics*, vol. 96, pp. 216–230, 2018.
- [6] T. Zhelyazov, “Numerical simulation of the response of concrete structural elements containing a self-healing agent,” *Materials*, vol. 15, no. 3, p. 1233, 2022.
- [7] E. J. Barbero, F. Greco, and P. Lonetti, “Continuum damage-healing mechanics with application to self-healing composites,” *International Journal of Damage Mechanics*, vol. 14, no. 1, pp. 51–81, 2005.

- [8] G. Z. Voyiadjis and P. I. Kattan, “Healing and super healing in continuum damage mechanics,” *International Journal of Damage Mechanics*, vol. 23, no. 2, pp. 245–260, 2014.
- [9] M. K. Darabi, R. K. Abu Al-Rub, and D. N. Little, “A continuum damage mechanics framework for modeling micro-damage healing,” *International Journal of Solids and Structures*, vol. 49, no. 3, pp. 492–513, 2012.
- [10] H. Subramanian and S. S. Mulay, “On the constitutive modelling of elasto-plastic self-healing materials,” *International Journal of Solids and Structures*, vol. 234-235, pp. 111289–, 2022.
- [11] E. Barbero and K. Ford, “Characterization of self-healing fiber-reinforced polymer-matrix composite with distributed damage,” *Journal of Advanced Materials*, vol. 39, pp. 20–27, 10 2007.
- [12] V. Privman, A. Dementsov, and I. Sokolov, “Modeling of self-healing polymer composites reinforced with nanoporous glass fibers,” *Journal of Computational and Theoretical Nanoscience*, vol. 4, pp. 190–193, 02 2007.
- [13] K. Sanada, N. Itaya, and Y. Shindo, “Self-healing of interfacial debonding in fiber-reinforced polymers and effect of microstructure on strength recovery,” *The Open Mechanical Engineering Journal*, vol. 2, pp. 97–103, 10 2008.
- [14] S. V. Zemskov, H. M. Jonkers, and F. J. Vermolen, “Two analytical models for the probability characteristics of a crack hitting encapsulated particles: Application to self-healing materials,” *Computational Materials Science*, vol. 50, no. 12, pp. 3323–3333, 2011.
- [15] E. Schimmel and J. Remmers, “Development of a constitutive model for self-healing materials.” <http://resolver.tudelft.nl/uuid:6ad6ebfd-aa1c-46f1-a9d5-c17109b8a423>, 01 2006. Report DACS-06-003.

- [16] B. Yagimli and A. Lion, “Experimental investigations and material modelling of curing processes under small deformations,” *ZAMM - Journal of Applied Mathematics and Mechanics / Zeitschrift für Angewandte Mathematik und Mechanik*, vol. 91, no. 5, pp. 342–359, 2011.
- [17] G. Z. Voyiadjis, A. Shojaei, and G. Li, “A thermodynamic consistent damage and healing model for self healing materials,” *International Journal of Plasticity*, vol. 27, no. 7, pp. 1025–1044, 2011.
- [18] R. P. Wool and K. M. O’ Connor, “A theory crack healing in polymers,” *Journal of Applied Physics*, vol. 52, no. 10, pp. 5953–5963, 1981.
- [19] S. Maiti, C. Shankar, P. Geubelle, and J. Kieffer, “Continuum and molecular-level modeling of fatigue crack retardation in self-healing polymers,” *Journal of Engineering Materials and Technology*, vol. 128, pp. 595–602, 10 2006.
- [20] J. Mergheim and P. Steinmann, “Phenomenological modelling of self-healing polymers based on integrated healing agents,” *Computational Mechanics*, vol. 52, pp. 681–692, 2013.
- [21] G. M. Henson, “Engineering models for synthetic microvascular materials with interphase mass, momentum and energy transfer,” *International Journal of Solids and Structures*, vol. 50, no. 14, pp. 2371–2382, 2013.
- [22] G. Henson, “Continuum modeling of synthetic microvascular materials,” in *Collection of Technical Papers - AIAA/ASME/ASCE/AHS/ASC Structures, Structural Dynamics and Materials Conference*, 2012.
- [23] T. Zhelyazov and R. Ivanov, “Numerical investigation of the mechanical behaviour of a structural element containing a self-healing agent,” *IOP Conference Series: Materials Science and Engineering*, vol. 1002, pp. 012–015, dec 2020.

- [24] H. Shahsavari, R. Naghdabadi, M. Baghani, and S. Sohrabpour, “A finite deformation viscoelastic–viscoplastic constitutive model for self-healing materials,” *Smart Materials and Structures*, vol. 25, pp. 125027–, nov 2016.
- [25] I. Smojver, D. Ivančević, and D. Brezetić, “Modelling of micro-damage and intrinsic self-healing in unidirectional cfrp composite structures,” *Composite Structures*, vol. 286, pp. 115266–, 2022.
- [26] I. Smojver, D. Brezetić, and D. Ivančević, “Explicit multi-scale modelling of intrinsic self-healing after low-velocity impact in gfrp composites,” *Composite Structures*, vol. 302, pp. 116213–, 2022.
- [27] T. Mura, *Micromechanics of Defects in Solids*. Martinus Nijhoff Publishers, 1988.
- [28] I. Doghri, *Mechanics of Deformable Solids: Linear, Nonlinear, Analytical and Computational Aspects*, pp. 301–327. Springer, Berlin, Heidelberg, 2000.
- [29] L. M. Kachanov, “Introduction to continuum damage mechanics,” Martinus Nijhoff Publishers, 1986.
- [30] J. L. Chaboche and P. M. Lesne, “A non-linear continuous fatigue damage model,” *Fatigue & Fracture of Engineering Materials & Structures*, vol. 11, no. 1, pp. 1–17, 1988.
- [31] E. Barbero, F. Cosso, and F. Campo, “Benchmark solution for degradation of elastic properties due to transverse matrix cracking in laminated composites,” *Composite Structures*, vol. 98, pp. 242 – 252, 2013.
- [32] E. Tsivolas, L. N. Gergidis, and A. S. Paipetis, “Prediction of damage mechanisms of cross-ply composite materials using novel non-linear multiscale methodologies,” *Modelling and Simulation in Materials Science and Engineering*, vol. 29, pp. 085015–, nov 2021.

- [33] A. Teimouri, R. B. Isfahani, S. Saber-Samandari, and M. Salehi, “Experimental and numerical investigation on the effect of core-shell microcapsule sizes on mechanical properties of microcapsule-based polymers,” *Journal of Composite Materials*, vol. 56, no. 18, pp. 2879–2894, 2022.
- [34] M. G. D. Geers, E. W. C. Coenen, and V. G. Kouznetsova, “Multi-scale computational homogenization of structured thin sheets,” *Modelling and Simulation in Materials Science and Engineering*, vol. 15, pp. 393–404, may 2007.
- [35] L. Qi, W. Tian, and J. Zhou, “Numerical evaluation of effective elastic properties of composites reinforced by spatially randomly distributed short fibers with certain aspect ratio,” *Composite Structures*, vol. 131, pp. 843–851, 2015.
- [36] X. Chao, L. Qi, J. Cheng, W. Tian, S. Zhang, and H. Li, “Numerical evaluation of the effect of pores on effective elastic properties of carbon/carbon composites,” *Composite Structures*, vol. 196, pp. 108–116, 2018.
- [37] W. Tian, L. Qi, X. Chao, J. Liang, and M. Fu, “Periodic boundary condition and its numerical implementation algorithm for the evaluation of effective mechanical properties of the composites with complicated micro-structures,” *Composites Part B: Engineering*, vol. 162, pp. 1–10, 2019.
- [38] X. Tsimigkris, D. Bekas, M. Kosarli, S. Tsantalis, A. Paipetis, and V. Kostopoulos, “Mechanical properties assessment of low-content capsule-based self-healing structural composites,” *Applied Sciences*, vol. 10, no. 17, 2020.



# Chapter 6

## General Conclusions and Future Work

### 6.1 General Conclusions

In the current thesis novel multiscale material models for the prediction of the behavior and damage mechanisms of composite materials were presented. After the 1st chapter's preliminaries, the 2nd chapter contained comparisons between mean-field and full-field multiscale methods. Although full-field methods can predict accurately the stress and strain fields in a microstructure it is known that they are computationally inefficient especially when compared with the mean-field methods. The main goal was to compare the most common mean-field method of Mori-Tanaka with the finite element method. In the same chapter, the comparison was performed for linear elastic materials having different material symmetries (isotropic, transversely isotropic, orthotropic). The results showed agreement between the two methods with a difference to the predicted homogenized material properties in most cases around 6%. These differences can be attributed to the type of boundary conditions, the quality of the discretization of the microstructure and the inherent limitations of the mean-field methods. The mean-field method was extended to account for plasticity and the same comparison was performed revealing that the predicted stress strain fields and the homogenized properties produced by the two methods are in good agreement.

Due to their computational efficiency the mean-field methods can be applied to real world engineering problems and structures and are capable of providing accurate results not only in macroscale but also in microscale. On the other hand, full-field methods such as the finite elements for solving the BVP in the RVE, are proved to be more accurate, but the solution time of their application in large structures can be prohibitive. Furthermore, the RVE generation is necessary in order to solve the BVP in the discretized domain. The aforementioned RVE generation can be a tedious task and in many cases there are limitations regarding the volume fractions or the geometry of the inclusions. Discretized microstructures have been used extensively in this thesis for validation purposes of the novel multiscale models. The implemented algorithm for the generation of RVEs based on Random Sequential Adsorption method was also presented.

In chapters 3 and 4, numerical models were developed to predict the damage mechanisms appearing in a cross-ply composite material in uniaxial tension. By adopting fracture mechanics techniques such as cohesive zone modelling it was possible to simulate the cracks and delaminations and in addition, continuum mechanics principles for the prediction of material's behavior proved to be reliable and accurate when compared with available experimental observations and measurements. Two different material models were developed in order to predict the homogeneous behavior of the heterogeneous multilayered material under investigation. The first material model originates from the mean-field homogenization method applied to viscoelastic matrix and elastic inclusions. Since all the material models involved are linear, the model could be set in the preprocessing stage of a dynamic analysis. The second material model takes into account the visco-elasto-plastic behavior with damage response of the matrix and elastic response of the fibers and was used for the simulation of the same experimental system. In addition, failure criteria were assigned to predict the total failure of the composite material. Since the aforementioned material model is nonlinear and hence loading path dependent, it is necessary to transfer the response to the solver for each integration point of each time step. The coded subroutines that predict the homogenized response were linked with the finite element solver by

using the dynamic linked library (dll) protocol. It was observed that this material model demonstrated the higher accuracy when compared with a simple viscoelastic material model. The results of the cracking density and saturation are closer to the experiments and the predicted failure strain also agreed with experimental observations.

In order to validate this novel multiscale material model a microstructure with continuous fibers was generated. The matrix material followed a visco-elasto-plastic material with damage and the fibers remained elastic. After solving the RVE problem, the homogenized stress strain response was retrieved by using the volume average of the fields for each phase. The results of the mean-field methods were very close to the numerical results of the RVE problem that was solved with the finite element approach. Furthermore, a comparison of the stress concentration at the crack tips of the macroscale model with the stress concentration of the microscale model was performed. In case of microscale two different approaches were used. The first one followed analytical fracture mechanics relationships to calculate the stress concentration using stress intensity factors. In the second case, the cracking propagation was simulated in a cross-ply microstructure with XFEM. Then, by using the stress concentration tensors in the macroscale model, the homogenized stress response in the crack tips was localized/dehomogenized to matrix stress and fiber stress. The comparison of the microfields between the results of the two scales showed good agreement. Consequently, the proposed model, can accurately predict the cracking initiation, cracking propagation, delaminations, matrix damage (softening), cracking saturation, total failure of the composite specimen and stress concentrations at the crack tips.

In chapter 5, the multiscale material developed previously, was properly extended in order to study the self-healing of a damaged material. In previous chapters and simulation campaigns, the damage procedure which is a cumulative phenomenon, was considered irreversible. However, it has been experimentally proved that materials having microcracks and microvoids can be healed. The simulation study was aiming to describe the extrinsic self-healing of composite materials using self-healing microcapsules. A self-healing

algorithm was presented along with the necessary numerical information relative to the novel material model development and implementation. As in the case of damage, a healing initiation criterion and a healing propagation law is needed. In the proposed model, the healing depends on the magnitude of the accumulated damage, the available healing time and a parameter that represents the rate of healing. The model can simulate the response of extrinsic self-healing composites, where the healing procedure is triggered by the damage propagation and can predict the recovery of the material's structural integrity depending on the healing rate and the available time for healing.

Furthermore, an algorithm that can be applied in microscale is presented, that offers the ability to predict the healing efficiency and healing initiation of RVEs embedded with microcapsules. Those values can be used in the multiscale material model as thresholds for the healing procedure.

All the in-house developed code that was initially designed to work as external library with Abaqus solver, was integrated under a unified windows platform application with graphical user interface. This application can perform multiscale analysis using both mean-field and finite element approaches using the in-house nonlinear finite element solver, generate microstructures, apply boundary conditions and visualize the results.

## **6.2 Future work**

In the context of this research the novel material models were able to describe accurately the behavior of composite materials when the experimental procedures were simulated. However, all the multiscale material models are developed under the framework of infinitesimal strain theory. Their application in various engineering simulations used in the industry such as sheet metal forming simulations or crash tests presupposes their extension to the finite strain framework in order to be able to deal with large deformations and large rotations taking into account the deformation gradient in the calculations. Material models such as hyperelasticity for elastomers and superplasticity for alloys can be used in

a similar mean-field multiscale manner, provided that the already developed models are extended in the finite strain framework.

A lot of research effort should be given in the simulation of self-healing materials. The autonomous self-healing was successfully predicted, however it is interesting to investigate the performance of multiscale models in non autonomous systems. In case the material system is thermodynamically stable, external stimuli need to be provided in order for the healing to take place. This covers a different self-healing system and can be combined with the developed material in cyclic loading simulations where the autonomous healing can take place in the loading phases, and the non autonomous healing can take place in the unloading phase using a different healing law.

Another interesting field that gains increasing attention is the artificial intelligence. The numerical tools that were developed in the context of this PHD thesis can be used to generate training data sets for artificial neural networks (ANNs). An automated procedure with scripting can be set to generate and solve discretized microstructures and collect them in a noise free sampling set. The trained ANN can be used to predict the response of more complex behaviors than elastoplasticity, such as damage and healing without solving the BVP of the discretized domain.

Finally, the developed models that can predict the damage and failure mechanisms can be combined with the simulation of non-destructive testing (NDT) methodologies, such as ultrasound and thermography. A full workflow of damaging a specimen under the designed external loading and recognizing the internal damage using simulations can be proved valuable in the process of designing a new structure or a product.



# Appendices



## A Multiscale material model verification

A representative volume element (**Figure A.1**) of one layer with continuous fibers has been created and loaded in uniaxial tension (**Figure A.2**) in order to compare the per phase results and the homogeneous behaviour between the developed material model and the numerical solution. The total axial strain was 0.063 and applied incrementally for 270 seconds. Perfect interface between fiber and matrix is assumed.

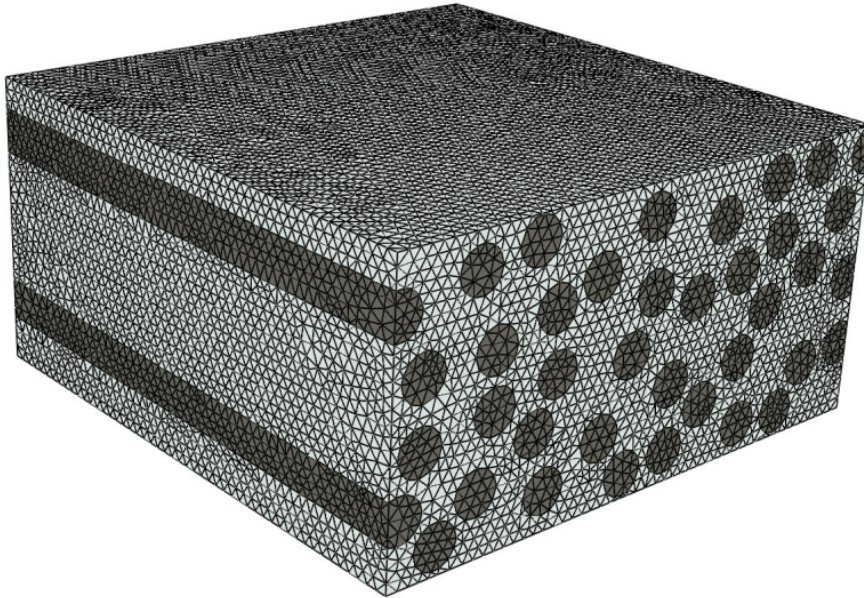


Figure A.1: Representation of 1-layer RVE with volume fraction  $V_f \approx 0.4$

The matrix material follows a visco-elasto-plastic with isotropic damage model and the glass fibers are considered to be elastic. The material properties have been described in **Section 4.7**. No failure criteria are applied in this verification procedure. In order for the stress strain plots to be generated it is necessary to calculate the volume averages of the micro variables (stress, strain) for each phase for every time step of the analysis (**Eq. A.1**). In a micro-marco approach each macro point  $\hat{x}$  can be viewed in the micro level as a center of a RVE with domain  $\omega$  and boundary  $\partial\omega$ . It should be noted that in micro,macro approaches an RVE represents an integration point of the macroscale. The developed multiscale model (Umat) result is the direct solution of the algorithm for one integration point with strain tensor provided. The RVE result is the result of the same strain tensor

applied in the representative volume element (RVE) and homogenized numerically. This calculation takes place in the post processing stage and the average micro variables can be calculated by

$$\langle f \rangle_{\omega_i} = \frac{1}{V_i} \int_{\omega_i} f(\hat{x}, x) dV_i \quad (\text{A.1})$$

with  $i = 0, 1$  where 0 represents the matrix phase and 1 the fiber phase,  $\omega_i$  is the domain of each phase,  $V_i$  is the total volume of each phase,  $f$  represents the micro variable (stress or strain), and  $x$  the micro coordinates. The homogenized averages over  $\omega$  (the whole RVE domain) is given by

$$\langle f \rangle_{\omega} = u_1 \langle f \rangle_{\omega_1} + (1 - u_1) \langle f \rangle_{\omega_0} \quad (\text{A.2})$$

where  $u_1 = V_1/V$  is the volume fraction of the fibers (1).

In case of the developed material model, since the calculations are performed in the macroscale, the micro variables are provided by the localization procedure using the strain concentration tensors from **Section 5.2**. Finally the non-linear plots for each phase and for the homogeneous behaviour (**Figures A.3, A.4, A.5**) are created for direct comparisons between the micro model (RVE) and the developed multiscale model.

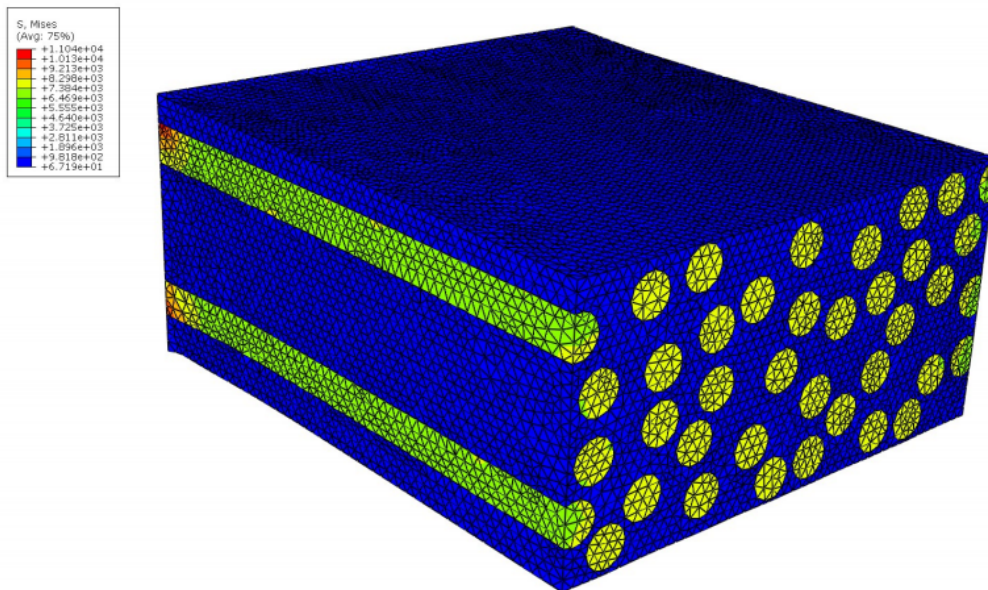


Figure A.2: von Mises stress distribution in RVE

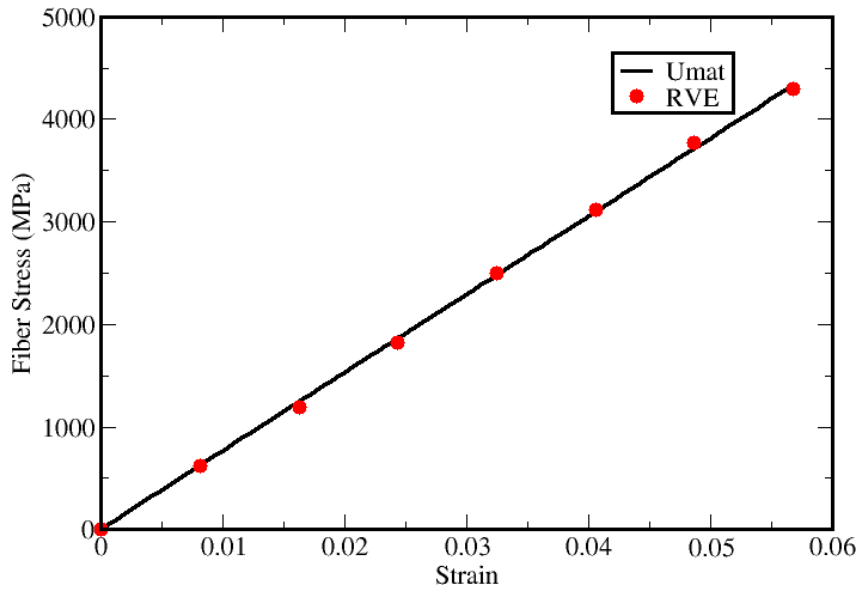


Figure A.3: Fiber stress-strain diagram for direct comparison between the micro model (RVE) and the developed multiscale model (Umat)

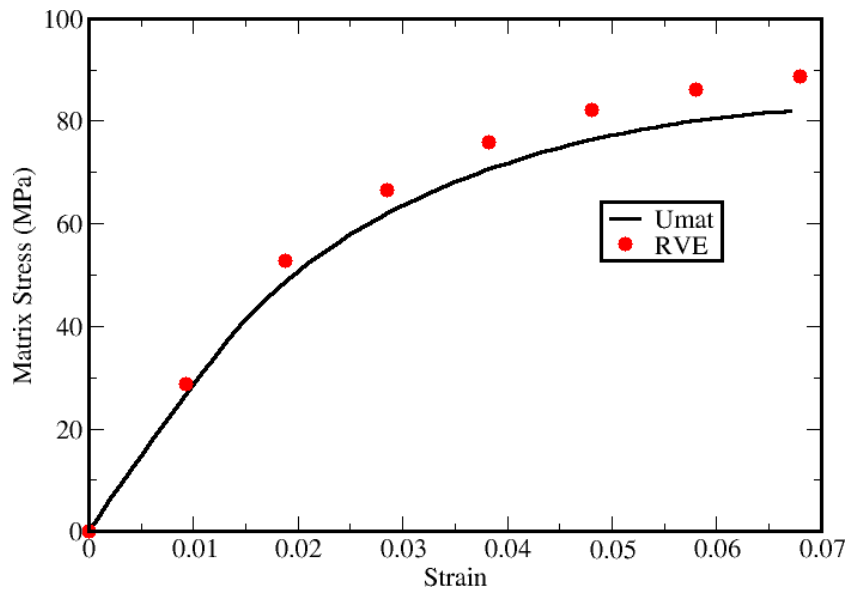


Figure A.4: Matrix stress-strain diagram for direct comparison between the micro model (RVE) and the developed multiscale model (Umat)

The two modelling approaches are in close agreement and the small deviations can be attributed to the nature of the mean-field approaches and their assumptions which do not take into account the interactions between the nearest inclusions and neglect the randomness of the inclusions positions.

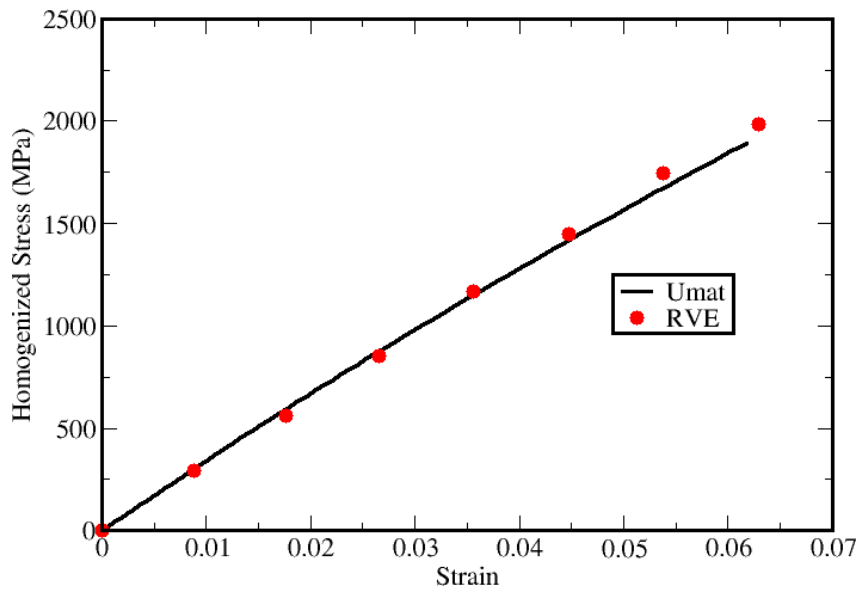


Figure A.5: Homogenized stress-strain diagram for direct comparison between the micro model (RVE) and the developed multiscale model (Umat)

## B Periodic Boundary Conditions

In this section the application of the appropriate periodic boundary conditions (2)(PBC), (3) in pre-processing stage is presented, in order to evaluate the mechanical properties of a periodic microstructure. This step is mandatory to perform homogenization using a discretized microstructure with finite elements.

### B.1 PBC formulation

Existing investigations have shown that FE homogenization procedure produces better approximation when PBC are applied instead of uniform displacement. A periodic RVE of a composite material with domain  $\omega$  and boundaries  $\partial\omega$ , those boundaries are decomposed to two opposing faces  $\partial\omega_+$  and  $\partial\omega_-$ . Every  $x_+$  point on boundary  $\partial\omega_+$  corresponds to a unique  $x_-$  point on boundary  $\partial\omega_-$  either directly through the nodes of similarly discretized hedras or in case of non matching mesh through the nodes of similarly discretized surfaces that are in contact with the opposing hedras.

The macroscopic strain  $\varepsilon_{ij}$  of the RVE can be expressed with the displacement field  $u_i$  as :

$$u_i(x_1, x_2, x_3) = \varepsilon_{ij}^0 x_j + u_i^*(x_1, x_2, x_3) \quad (\text{B.1})$$

where  $\varepsilon_{ij}^0 x_j$  is the linear displacement field and the term  $u_i^*(x_1, x_2, x_3)$  is the periodic part of the displacement field on the boundary surfaces. Formula B.1 cannot be directly applied to the RVE since the periodic part is unknown. In any periodic RVE the opposing hedras contain pairs of points and the displacement of those pairs can be written as

$$u_i^{k+} = \varepsilon_{ij}^0 x_j^{k+} + u_i^* \quad (\text{B.2})$$

$$u_i^{k-} = \varepsilon_{ij}^0 x_j^{k-} + u_i^* \quad (\text{B.3})$$

where  $k^-$  and  $k^+$  is a pair of points in the opposite parallel boundary surfaces.  $u_i^*$  is identical in both equations B.2 and B.3 due to periodicity. By subtraction of B.2 and B.3

$$u_i^{k^+} - u_i^{k^-} = \varepsilon_{ij}^0(x_j^{k^+} - x_j^{k^-}) = \varepsilon_{ij}^0(\Delta x_j^k) \quad (\text{B.4})$$

For each pair of points  $(\Delta x_j^k)$  is constant, so the term  $\varepsilon_{ij}^0(\Delta x_j^k)$  is also constant with a specified macro strain  $\varepsilon_{ij}^0$  and can be implemented in the finite element model using displacement constraints.

## B.2 Implementation in the FE model

The PBCs are generated in the preprocessing stage of the FE analysis, and can be applied on the surface nodes of the RVE hedras through linear multi point constraints (MPC). MPC requires that a linear combination of displacements is zero such that:

$$a_1 u_i^P + \dots + a_n u_k^R = 0 \quad (\text{B.5})$$

where  $u_i^P$  is displacement field of defree of freedom  $i$  of point P, and  $a_n$  are the coefficients that define the relative motion of nodes. The displacements on the boundaries are applied with the help of a reference point (RP). This point is not a part of the RVE discretization but is used as a driver node, unconnected from the mesh of the RVE, to provide the necessary degrees of freedom to control the response of the RVE. The system of equation used in the PBC is described by the following equation:

$$u_i^{k^+} - u_i^{k^-} = u^{RP} \quad (\text{B.6})$$

where  $u^{RP}$  is the displacement field of the reference point. This equation is applied to all node pairs of opposite faces. Corner nodes and edge nodes must be excluded from the inner hedra nodes to avoid overconstraint of the same nodes, which causes errors to most of the FE solvers.

- Corner nodes: A,B,C,D,A',B',C',D'
- Edges : AA',BB',CC',DD',CD,AB,AD,BC,A'B',C'D',B'C',A'D'
- Faces : Top [ABCD], Bottom [A'B'C'D'], Front [AA'B'B], Rear [DD'C'C], Left [BB'C'C], Right [AA'D'D]

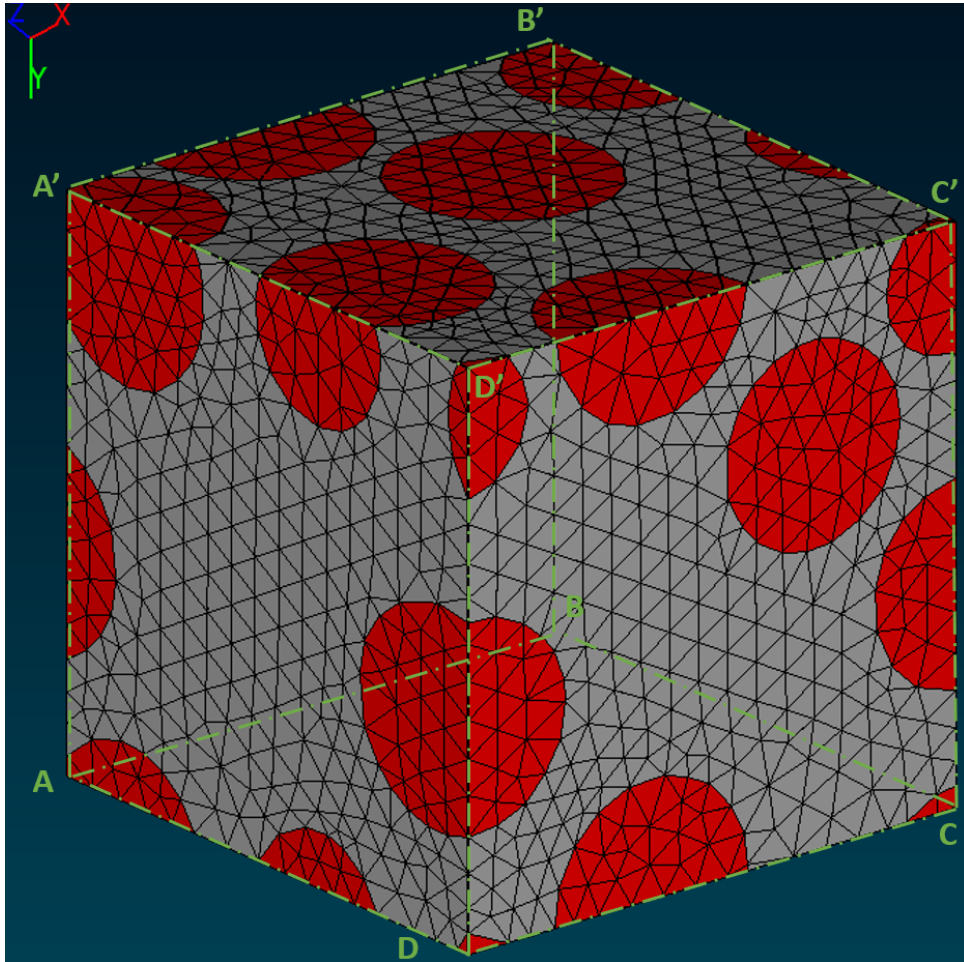


Figure B.1: RVE and corresponding node numbering

To calculate the effective elastic properties of an orthotropic material six different load cases need to be applied. Three tensile loading conditions (one for each tensile direction 11,22,33) and three for the shear deformation. Three reference points are needed. The first two are used to apply the three shear loading conditions and the 3rd, to apply 3 tensile loading conditions.

For the case of axial loading in  $x$ -direction the system of equations are as follows:

$$\begin{aligned}
u_1^{RP3} &= \varepsilon_{11}, \\
u_2^{RP3} &= 0, \\
u_3^{RP3} &= 0, \\
u_i^{RP1} &= 0, \\
u_i^{RP2} &= 0, \\
i &= 1, 2, 3
\end{aligned}
\tag{B.7}$$

and for the case of shear loading in  $xy$  plane :

$$\begin{aligned}
u_1^{RP1} &= \varepsilon_{12}/2, \\
u_2^{RP1} &= 0, \\
u_3^{RP1} &= 0, \\
u_1^{RP2} &= 0, \\
u_2^{RP2} &= 0, \\
u_3^{RP2} &= 0, \\
u_i^{RP3} &= 0, \\
i &= 1, 2, 3
\end{aligned}
\tag{B.8}$$

The rest of the tensile and shear conditions can easily be retrieved by modifying the equations (B.7, B.8)

## C The GUI of Multiscale Modeller

All of the aforementioned developed methods are embedded in a windows platform application that can perform mutliscale analysis using both mean-field and FE approaches. The formulations are developed in C++ language, and initially designed to work as a user material ((V)UMAT) in conjunction with Abaqus solver (4). In the sequence, the code was embedded under a GUI (Graphical User Interface) application that can work both with Abaqus and the inhouse nonlinear finite element solver.

### C.1 User Inteface

The user interface was created using the Qt creator capabilities for building a GUI program combined with OpenGL (5) as graphics engine in conjunction with GLSL coded shaders for realistic 3D model representation using the graphics processing unit (GPU). At the beginning of the program the user can select between the micromechanics mode or the finite element mode.

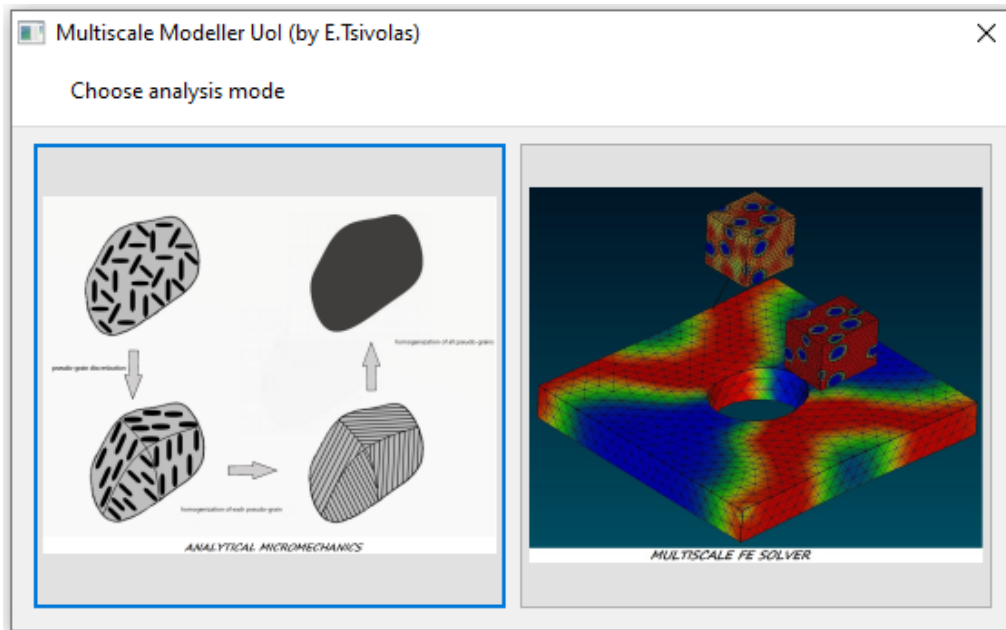


Figure C.1: Multiscale Modeller modes

## Micromechanics mode

The first mode can predict linear (elastic and visco-elastic) and non linear (elasto-plastic, visco-elasto-plastic, elasto-plastic-damage, elasto-plastic-damage-healing) response of a microstructure using the mean-field approaches as described in chapters 3,4 and 5 (Figure C.2).

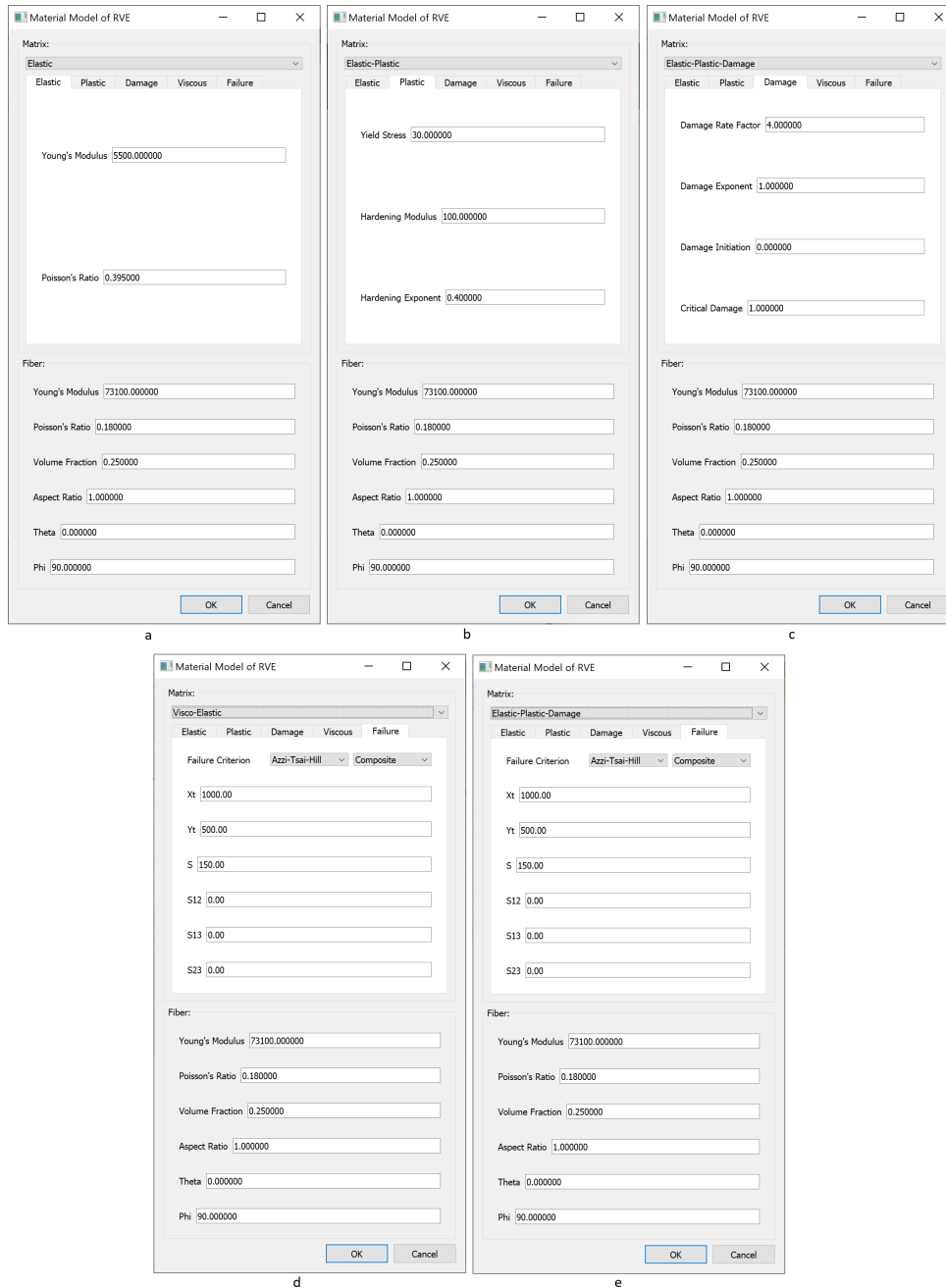


Figure C.2: Examples of definition of multiscale material model parameters. **a**: Elasticity **b**: Elasto-plasticity **c**:Elasto-plasticity with damage **d**: Visco-elasticity **e**: Assignment of failure indicator

The user has to define the material of each constituent, the volume fraction, geometric characteristics of the fiber and an applied strain. The program creates the stress/strain curves for each constituent and the composite, and calculates the homogenized composite properties. Also an RVE representation of the fictitious composite is created in order to show the response of each constituent graphically as shown in **Figure C.3**.

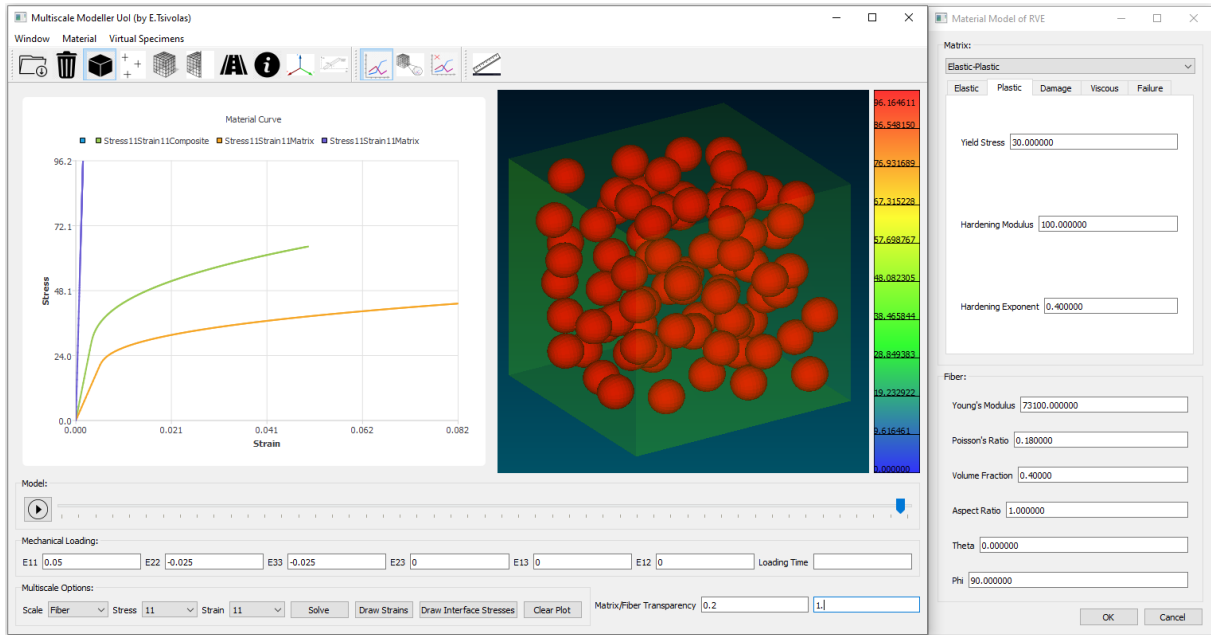


Figure C.3: Micromechanics mode with stress/strain curves of each constituent, the homogenized response and the representation of the fictitious RVE

## Finite element mode

The finite element mode includes the inhouse developed finite element solver that uses the Eigen library (6) for sparse matrix representation and the solution of linear systems of equations combined with a Newton-Raphson formulation to solve non linear problems with implicit formulation. This mode can perform three different tasks:

- a) It can apply boundary conditions in a RVE (Dirichlet, PBC) and perform homogenization to predict the average response of the composite (**Figure C.4**).

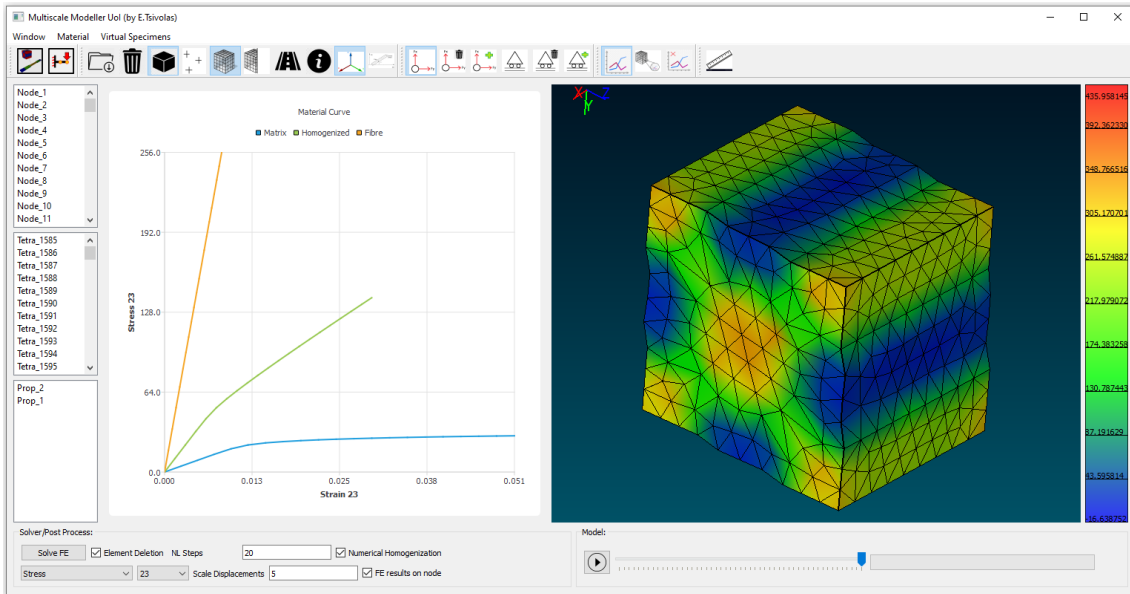


Figure C.4: Finite element mode example with boundary condition application of shear in yz and numerical homogenization of RVE

b) The second task, is the ability to solve a finite element model at multiple scales. In this task, the code of the micromechanics mode can be called for each integration point of the macroscale model, to perform a multiscale analysis of a specimen or a complete structure (**Figure C.5**).

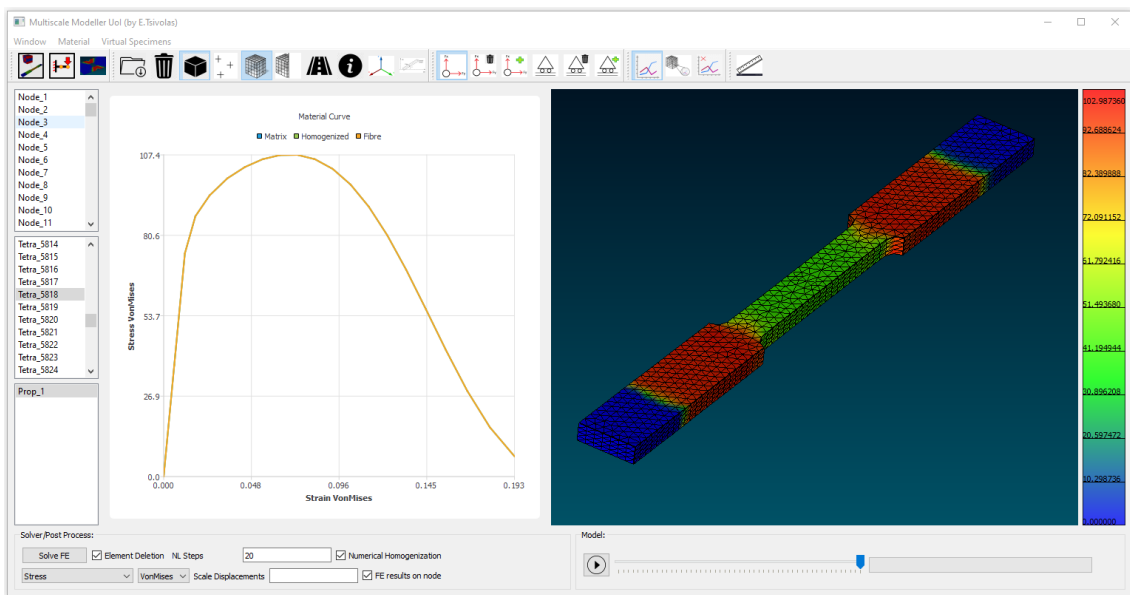


Figure C.5: Finite element mode example with mean-field homogenization for each integration point

c) Finally the FE2 method is implemented where a microstructure is solved at the same time with a FE model for each integration point and drives the material response at the macroscale (**Figure C.7**) viewing the results at both macro-level and micro-level at selected integration points (**Figure C.6**). In this mode, it is necessary to define a RVE for each material of the macro model and also assign a material law for each constituent of the RVE. Next, for every time step, the strain increment of each integration point is converted to boundary conditions for the RVE. Then, by solving the RVE problem, homogenized stresses and stiffness of the composite is calculated and provided to the solver that handles the macro model to continue with the solution. Despite the fact that this method is very accurate it should be noted that is the least efficient for simulating large structures. Consequently, is not analyzed in detail or further adopted. It is only used for verification purposes.

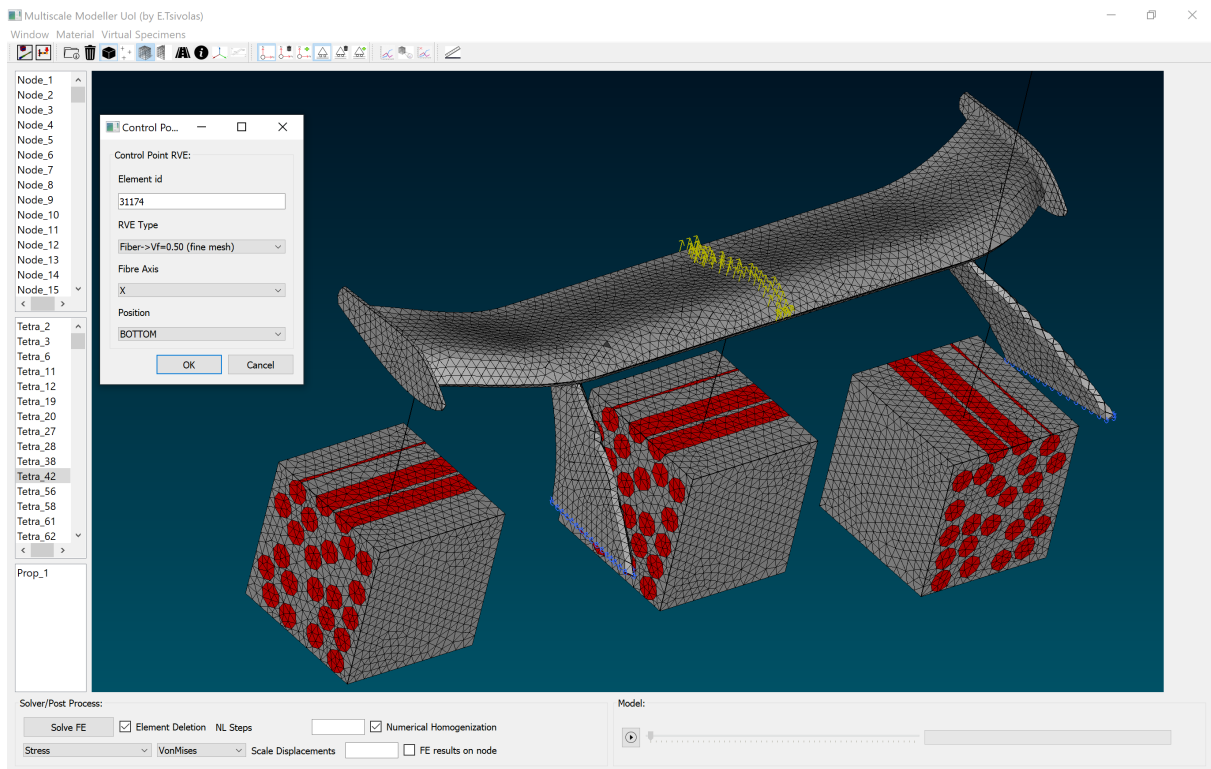


Figure C.6: Setting up control points to visualize the microstructures' response for specified material points, after the completion of FE2 method

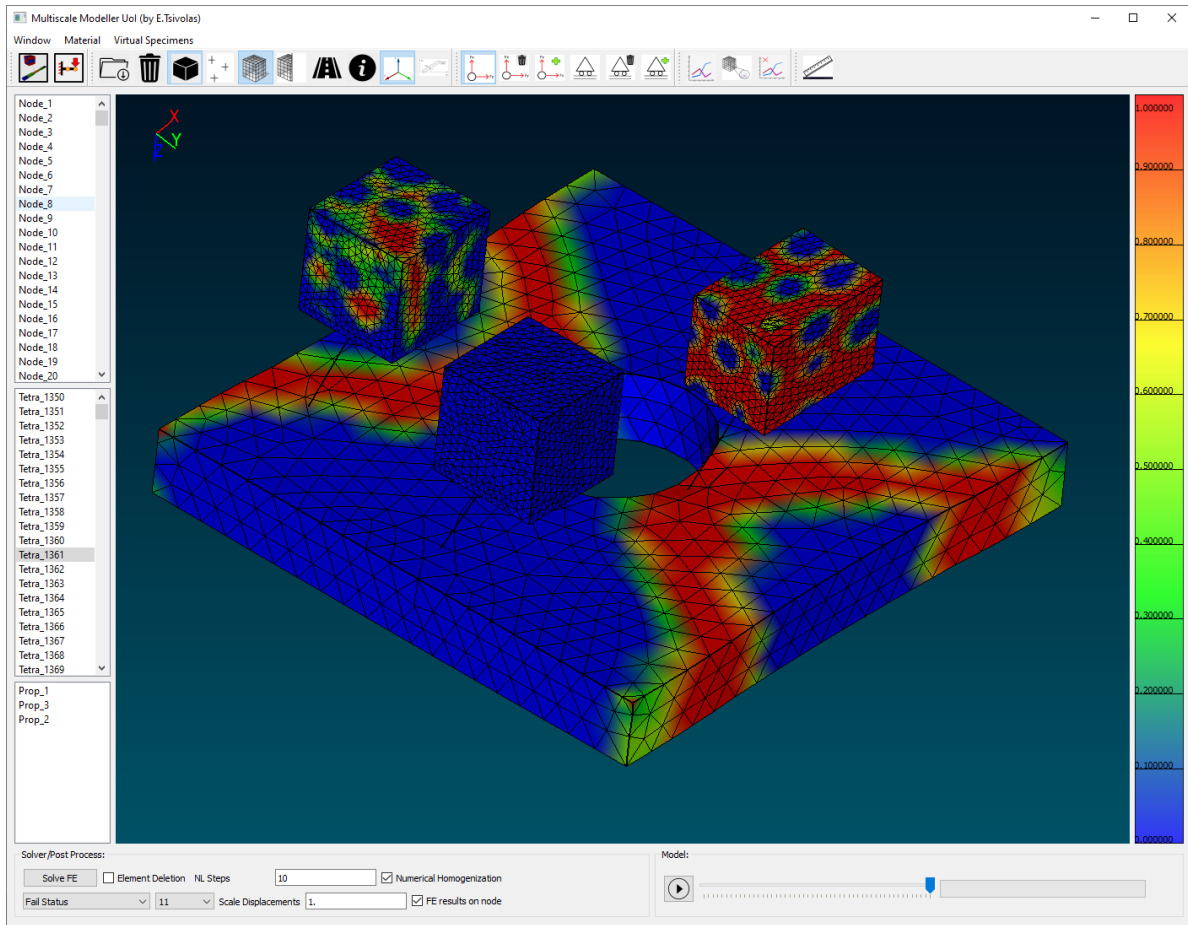


Figure C.7: Finite element mode example with FE2 method and visualization of failure status

For all of the above cases, basic pre-processing tasks such as 3D meshing of triangular meshed models using the TetGen library(7), applying boundary conditions (nodal forces, displacements) by selecting nodes from the screen and model manipulation tasks such as measurements, and various geometric queries can be handled. Also vital post-processing capabilities were added such as element deletion, fringe plots of displacements, stresses, strains, plastic strains, damage variable, failure criteria index and export plots for specified elements among others, offering the ability to visualize and export the results for every time step of the analysis.

## References

- [1] E. Tsvolas, L. N. Gergidis, and A. S. Paipetis, “Computational multi-scale modelling of fiber-reinforced composite materials,” in *Advances in Fracture and Damage Mechanics XVIII*, vol. 827 of *Key Engineering Materials*, pp. 263–268, Trans Tech Publications Ltd, 2020.
- [2] D. Garoz, F. Gilabert, R. Sevenois, S. Spronk, and W. Van Paepegem, “Consistent application of periodic boundary conditions in implicit and explicit finite element simulations of damage in composites,” *Composites Part B: Engineering*, vol. 168, pp. 254–266, 2019.
- [3] W. Tian, L. Qi, X. Chao, J. Liang, and M. Fu, “Periodic boundary condition and its numerical implementation algorithm for the evaluation of effective mechanical properties of the composites with complicated micro-structures,” *Composites Part B: Engineering*, vol. 162, pp. 1–10, 2019.
- [4] M. Smith, *ABAQUS/Standard User’s Manual, Version 6.9*. United States: Dassault Systèmes Simulia Corp, 2009.
- [5] M. Woo, J. Neider, T. Davis, and D. Shreiner, *OpenGL programming guide: the official guide to learning OpenGL, version 1.2*. Addison-Wesley Longman Publishing Co., Inc., 1999.
- [6] G. Guennebaud, B. Jacob, *et al.*, “Eigen v3.” <http://eigen.tuxfamily.org>, 2010.
- [7] H. Si, “Tetgen, a delaunay-based quality tetrahedral mesh generator,” *ACM Trans. Math. Softw.*, vol. 41, no. 2, pp. 1–36, 2015.



# **Curriculum vitae**

# Tsivolas Eleftherios

Experienced Civil Engineer with a demonstrated history of working in the computer software development. Skilled in programming languages C++, Python, Fortran, experienced in Advanced Materials, multiscale modelling of Composites, and several simulation software. Professional Engineer with MSc focused on Materials Engineering from University of Ioannina, and a PhD candidate since 2019.



Thermi, Thessaloniki  
Greece



lioutsiv8@gmail.com



28.08.1990



Eleftherios Tsivolas

## PUBLICATIONS

- Crack growth and delamination analysis in GRFP composite materials, E. Tsivolas, L.N. Gergidis, A.S. Paipetis, *Applied Sciences*, 2022
- Simulation study of damage mechanisms appearing in cross ply composite material loaded in uniaxial tension, E. Tsivolas, L.N. Gergidis, A.S. Paipetis, *MATEC web of conferences*, 2021
- Prediction of damage mechanisms of cross-ply composite materials using novel non-linear multiscale methodologies, E. Tsivolas, L.N. Gergidis, A.S. Paipetis, *Modelling and Simulation in Materials Science and Engineering*, 2021
- Computational multi-scale modelling of fiber-reinforced composited materials, E. Tsivolas, L.N. Gergidis, A.S. Paipetis, *Key Engineering Materials*, 2019
- Multiscale modelling of extrinsic self-healing GFRP materials, E. Tsivolas, L.N. Gergidis, A.S. Paipetis, submitted to *Modelling and Simulation in Materials Science and Engineering*, 2022

## CERTIFICATES

- Materials data sciences and informatics [Georgia Institute of Technology]
- Mechanical Behaviour of Materials, Stress Transformations, Beams, Columns, and Cellular Solids [MIT]
- Elements of Structures [MIT]

## Education

- February 2019 – Present  
PhD Materials' Science and Engineering  
University of Ioannina  
(Materials Science and Engineering Department)  
**Dissertation:** Study of structural behaviour and damage mechanisms appearing in composite materials with the use of numerical simulations
- October 2015 –April 2018  
MSc. Advanced Materials  
University of Ioannina  
(Materials Science and Engineering Department)  
Degree Grade: 8.40/10.00  
**Thesis:** Study and simulation of failure of cross-ply composite materials in uniaxial tension
- October 2008 – January 2014  
MEng. Civil Engineering (5-year course Diploma)  
University of Patras (Civil Engineering Department)  
Degree Grade: 7.04/10.00  
**Thesis:** Laboratory investigation of hydraulic jump in a closed duct of rectangular cross section
- September 2005– June 2008  
2<sup>nd</sup> High School of Arta, Greece  
Graduated with an Apolyterion of an average of 19.10/20.00  
Honorary awards and prizes from the Hellenic Ministry of Education for outstanding academic performance throughout all school years

## Work Experience

- June 2016 – Present [*Beta CAE Systems SA*]

## Coding and Computer Skills

- Programming Languages  
C, C++, Python, Fortran, R
- Simulation Software (CAE)  
Ansa, Meta, Abaqus, Nastran, Marc, Ansys, Digimat

## PERSONAL SKILLS

---

- Analytical way of thinking and with problem solving capability
- Noteworthy team-leading and managerial skills gained during various projects
- Excellent organization skills with great attention to detail
- Team working & communication

## LANGUAGES

---

### English

Full professional proficiency

### German

Elementary proficiency

### Greek

Native language

## Coding and Computer Skills

- Operating Systems  
Windows, Linux
- Software development packages  
Qt Creator, Visual Studio, R Studio, Dev C++
- Design Software (CAD)  
AutoCAD, SolidWorks
- Project Management Packages  
Microsoft Project, Jira
- Other  
Wolfram Mathematica, Office Suite, TeX Studio, OpenGL

## Conferences

- June 2021  
International Conference of Engineering Against Failure (ICEAF 2021, Virtual)  
Presentation of Simulation Study of the Damage Mechanisms Appearing in a Cross Ply Composite Material Loaded in Uniaxial Tension
- June 2020  
Conference of Advanced Analysis and Simulation (CAASE 20, NAFEMS (Beta CAE Systems SA))  
Presentation : Capturing multiscale response of composites with homogenization techniques
- September 2019  
International conference of fracture and damage mechanics (FDM 2019, Rhodes Island)  
Presentation of Computational multi-scale modelling

## Other

- Development of an in-house multiscale simulation software (Multiscale Modeller) for the needs of PhD Research